COATINGS ON STAINLESS STEEL FOR SOLID OXIDE FUEL CELL INTERCONNECTS

Richard Clarke

A Thesis Submitted for the Degree of PhD
at the
University of St Andrews

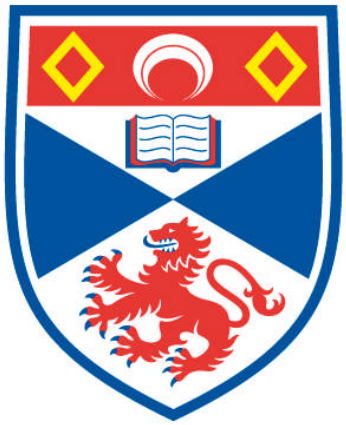

2012

Coatings on Stainless Steel For Solid Oxide Fuel Cell Interconnects

A thesis presented for examination for the title of Ph.D

by

RICHARD CLARKE

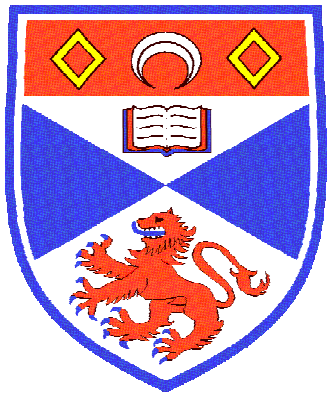

University of St. Andrews

April 2012

SUBMISSION OF PHD AND MPHIL THESES REQUIRED DECLARATIONS

1. Candidate's declarations:

I, Richard J. Clarke, hereby certify that this thesis, which is approximately 38,000 words in length, has been written by me, that it is the record of work carried out by me and that it has not been submitted in any previous application for a higher degree.

I was admitted as a research student in November, 2005 and as a candidate for the degree of Doctor of Philosophy in February, 2007; the higher study for which this is a record was carried out in the University of St Andrews between 2005 and 2012.

I, Richard J. Clarke, received assistance in the writing of this thesis in respect of grammar, spelling and, which was provided by Dr. Stephen Gamble

2. Supervisor's declaration:

I hereby certify that the candidate has fulfilled the conditions of the Resolution and Regulations appropriate for the degree of Doctor of Philosophy in the University of St Andrews and that the candidate is qualified to submit this thesis in application for that degree.

3. Permission for electronic publication:

In submitting this thesis to the University of St Andrews I understand that I am giving permission for it to be made available for use in accordance with the regulations of the university Library for the time being in force, subject to any copyright vested in the work not being affected thereby. I also understand that the title and the abstract will be published, and that a copy of the work may be made and supplied to any bona fide library or research worker, that my thesis will be electronically accessible for personal or research use unless exempt by award of an embargo as requested below, and that the library has the right to migrate my thesis into new electronic forms as required to ensure continued access to the thesis. I have obtained any third-party copyright permissions that may be required in order to allow such access and migration, or have requested the appropriate embargo below.

The following is an agreed request by candidate and supervisor regarding the electronic publication of this thesis: Embargo on both part of printed copy and electronic copy for the same fixed period of 5 years. Publication would be commercially damaging to the researcher and the supervisor and University.

Acknowledgements

Without the help of many individuals for insight, inspiration, and sometimes, brute force, it would not have been possible.

At the top of the list would have to be Prof. J.T.S. Irvine, for his undying patience, and because no matter how annoying I was as a student, he believed I could achieve this based on an initial half an hour interview.
I would also like to thank all the past and present members of the JTSI research group, friends all, particularly Cristian Savaniu for his assistance with sol-gel preparation, Deep Pakrash for listening and happily engaging with my philosophical debates, Gael Corre for too many things to list, Steve Gamble, for sitting next to me and helping to proof read, and everyone in the group for listening to me and giving me fantastic feedback, or being honest enough to tell me when I was full of it.

Thanks also go to the technical staff at St. Andrews who are always able to make the most impossible gear, and then keep it running.

I would like to thank the university for assessing me as a home student after another reputable learning institution insisted I was a foreigner who somehow had a UK passport.

I would like to thank the Student Advice Centre for coming through for me twice when we were so broke it does not bare thinking about, and for finding me a place to live when my home life went, lets just say, a wee bit more than “a bit wobbly.”

Last but not least I would like to thank my family;

My children for putting up with my absences, moods when things were not going well, for putting up with moving too many times to count, lack of money,

and vehicular breakdowns in the middle of nowhere with incredible grace, all as if it were all just part of the fun.

I would like to thank my wife for taking the kids whilst I was working late and weekends, for encouragement, undying love, and all that she has done for so very, very long.

I would also like to thank my parents for believing that I could do this and for taking care of my affairs when I was not available to do so, and for all their encouragement and assistance in so many different areas that they can not be listed.

I would like to also dedicate this work to all the mature students in the world, most especially to one of my oldest friends Dr. Canyon Steinzig, who foolishly like me, started his Ph.D in his late 30's and who has completed his work in pain and addiction less than a week of me completing this work. Without his long distance advice and shoulder to cry on, without knowing that there was another crazy old parent daring to complete a thesis, I would have been completely alone.

To all of you, for all of your help, thanks for making this possible.

Table of Contents

List of Figures

ABSTRACT

Enabling inexpensive and ubiquitous steels for use as solid oxide fuel cell interconnects has two major hurdles to overcome. Firstly, corrosion must be limited such that the interconnect can have longevity. Secondly, the evaporation of chromium from the corrosion layer must also be limited such that the fuel cell can have longevity.

The evaporation of chromium from chromia, titanium doped chromia, and chromium cobalt spinels was studied and characterized. Spinels lost the least amount of mass during evaporation experiments, and changed the least after experimental conditions were imposed on them that. Chromium titanate samples retained a significant amount of chrome that would have evaporated had the sample been chromium oxide alone. This was due to local changes at the surface with titanium becoming enriched and blocking loss of further chromium.

Various methods of depositing titanium doped chromia on the surface of SS430 were investigated. Sol-gel was attempted, but proved problematic. Evaporation of elemental titanium onto SS430 followed by conversion to rutile by heating followed by the evaporation of chromium into the rutile layer was investigated at length. These layers are nanoscale when evaporated and about 10 times thicker after oxidation. Characterization of the resulting Ti layers showed that at low temperatures a thick dense layer of rutile could be observed. At higher oxidation temperatures, the titanium was difficult to find.

Evaporation of cobalt onto SS430 created thin films when oxidized. The films were shown to control the evaporation of chromium by production of spinels. These layers were characterized with X-Ray Diffraction and scanning electron microscopy and impedance spectroscopy. They were shown to be quite conductive compared to the titanium coatings

1 INTRODUCTION

Since the last great extinction of carbon based life on our planet 65 million years ago, geological forces and micro-organisms have been working together to strip our atmosphere of carbon and store it in vast carbon reserves as coal, oil, natural gas and methanates. Fig.1.1 shows this carbon cycle[1].

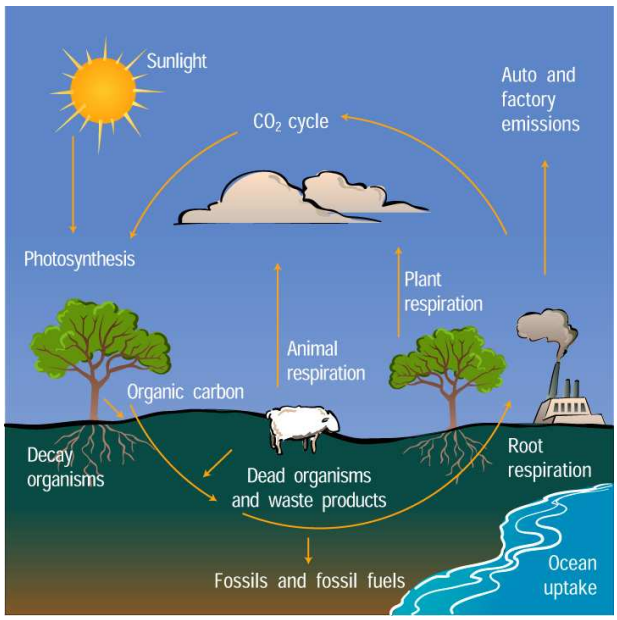

Fig.1.1: The carbon cycle From http://www.windows2universe.org/earth/Water/co2_cycle.html

These are the world's oldest and slowest turnover renewable fuels. Since the industrial revolution, we have managed to liberate a staggering amount of those reserves, with little or no intention of replacing them, whilst preventing and endangering the processes that capture those resources. The mismatch in production/consumption produces increased levels of carbon in our atmosphere, shown in fig.1.2. This change is happening at a rate not seen since the Cretaceous-Tertiary extinction.

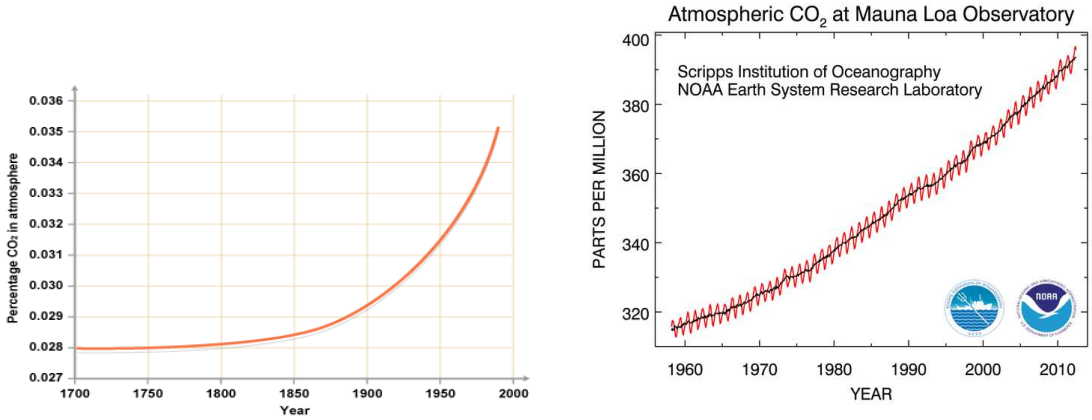

Fig.1.2 and 1.3: Graphs of Carbon Dioxide in the Atmosphere (Keeling curves) By The BBC (left)[2]and US Department of Commerce National Oceanic and Atmospheric Administration[3]

Even with solar, wind, tidal and nuclear production rates increasing, fossil fuels are not likely to decrease in importance for the foreseeable future, as shown in fig.1.4. With little chance of convincing people to use less power, and with demand increasing from developing nations that are dependent on coal and oil, more efficient power systems need to be developed.

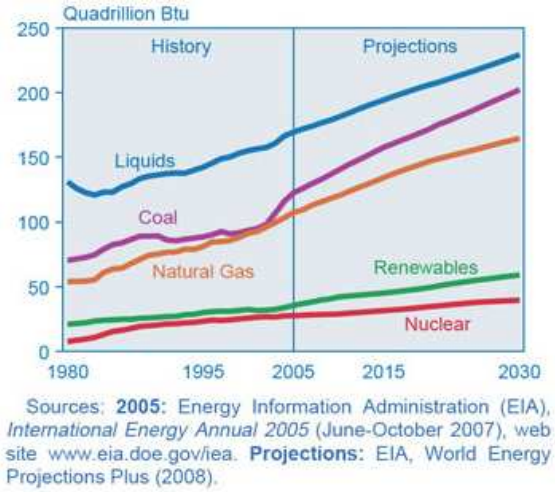

Fig.1.4: History and projected energy consumption by type From US DOE [4]

1.2 BACKGROUND ON ENERGY CONVERSION

The conventional conversion of fossil fuel from chemical potential energy to electrical and heat energy requires, 3 steps, at minimum, and more for reciprocating engines. Energy is converted from chemical to thermal and pressure energy, from thermal and pressure to kinetic and from kinetic to electrical. For instance, if the electricity is produced from coal, the coal is burned to make steam (chemical to thermal and pressure energy), the steam will be

passed through a turbine (pressure and to kinetic) and the kinetic rotational energy is then converted to electricity with a generator (kinetic to electrical energy) [5].

Fig.1.5: Hackney Power station, Showing one of Parsons 40,000 HP steam turbines from Wonders of World Engineering [6]

Traditionally, this conversion happens at centralized national or regional power stations, such as Hackney power station, in fig.1.5. The centralized distribution of power guarantees additional transmission losses. As much as 70% of energy is lost between the carbon stores and a typical home in losses incurred by energy conversion and transmission. By comparison, fuel cells offer direct conversion of chemical energy to electrical energy, skipping at least two conversion steps, greatly reducing the losses. Additionally, domestic localized production of energy can produce power on site, removing all transmission losses.

1.3 OBSTACLES

So why doesn't everyone have a fuel cell in their house? Clearly this would be the most sensible choice for heat and power, and each unit could be fed with existing gas distribution networks to most homes. Unfortunately, even though they have been around longer than the internal combustion engine, fuel cells still face difficult processing and materials

challenges before they can be deployed with the reliability, longevity and low cost exhibited by existing power systems.

As with many integrated system devices, if any integral part fails, so does the system. Often there will be one component that is taken for granted, seemingly insignificant, or forgotten, and its failure will be catastrophic. In the case of a motor car, it could be argued that the pivotal items would be the pistons, but equally important and perhaps less obvious at first are the tyres: No rubber contact equates to no traction. In a DC motor, magnets, windings etc. are important, but just as crucial are the carbon brushes. In the case of fuel cells, obvious choices would be anodes, cathodes and electrolytes but the less obvious choice would be the interconnects, which, like brushes, are the interface to the wires. With the best chemistry, materials, process engineering and energy conversion rates in the world, without an inexpensive and reliable electrical connection to the outside world fuel cells will be limited in their applications.

1.4 FUEL CELL OVERVIEW

All fuel cells and batteries work by similar principles. Two substances (gases, fluids, solids, or any combination) in opposite states of reduction/oxidation are reacted whilst forcing the electrons to perform work. Oxygen and hydrogen, for example, or ethanol and oxygen are typical combinations used for fuel cells. In detail, the principle is to bring together a compound in an energy state that is ready to donate electrons (hydrogen, methanol, metals, etc.) with a species that is willing to accept electrons (oxygen) whilst making these electrons do work before equalizing the charge states. In order for electrons to pass through the electrical load from one side to the other, there must be a equivalent charge that will transfer in the opposite direction. In most cases this is achieved by allowing oxygen ions to the anode or protons to the cathode through an electronically resistant but ionically conductive membrane.

Fig. 1.6 shows a schematic representation of a fuel cell.

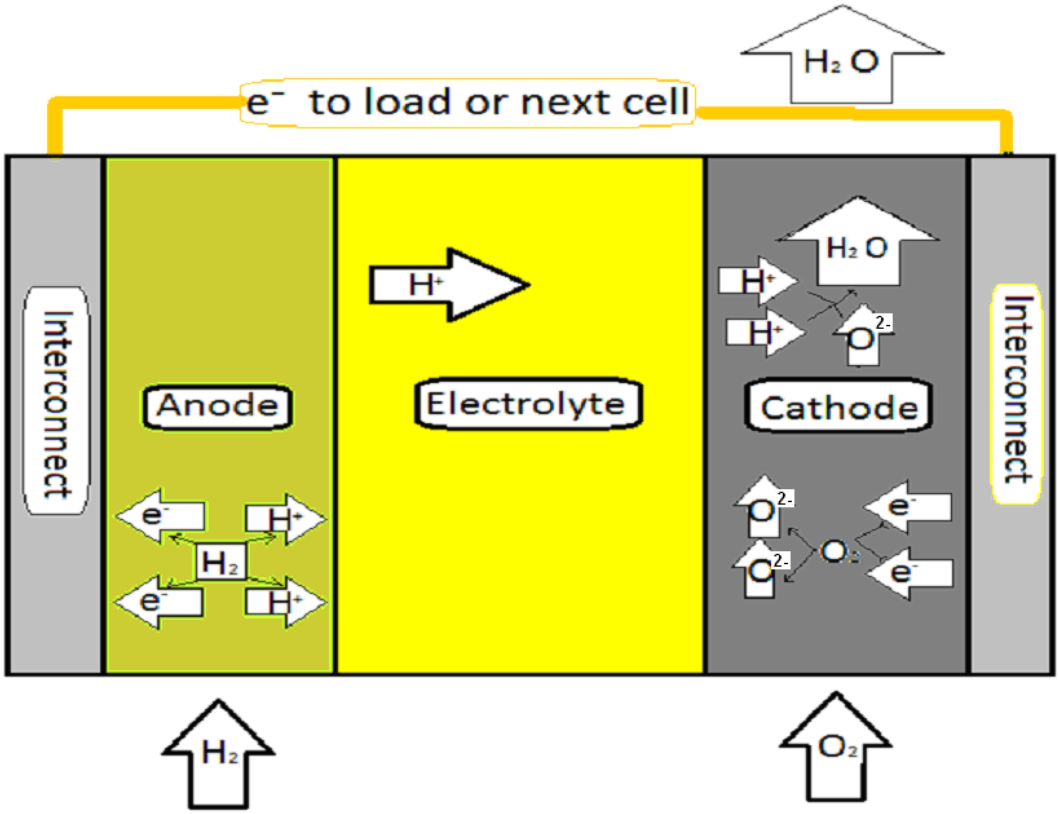

Fig.1.6: Schematic and processes inside a typical proton conducting electrolyte fuel cell

This forces electrons to take a separate path through an electrical load. A key difference between fuel cells and batteries is the change in mass: With batteries, the power is a function of the stored energy at the electrodes or in their electrolytes. With a fuel cell, the chemical potential energy is stored outside the reactor, and as long as it is supplied, energy can be converted. Fuel cells are, in this way, much like internal combustion engines or gas turbines, converting the mass of fuels and air to energy, water and CO_2 and releasing it. With a battery there is no loss of mass after reaction: the spent reactants are retained, and performance will always decrease exponentially as spent products impede fresh reactants.

1.5 FUEL CELL BASICS

Fuel enters on one side of an ion transfer media and oxygen (or other oxidizer) on the other. The ion transfer media is chosen to allow either protons from the fuel side or oxide ions from the oxidizer side, but in either case no electrons. For polymer electrolyte membrane fuel cells (PEMFCs), the ion transfer media is usually a poly-sulfonated plastic, such as Nafion. This type of material allows protons and surrounding water through, but does not allow other ions through in the reverse direction, and is electronically insulating.

For solid oxide fuel cells (SOFC), the ion permeable media is a ceramic that allows oxygen ions through. Fig.1.7 shows a schematic of the typical SOFC. Oxygen molecules enter the cathode side of the fuel cell. Electrons are added from the electrode as oxygen ions radicalize into atoms and travel through the exchange membrane, taking 2 electrons each.

When they meet the fuel the electrons are released as the oxygen combines with the fuel to create water in the case of hydrogen fuel, and/or other oxidation products.

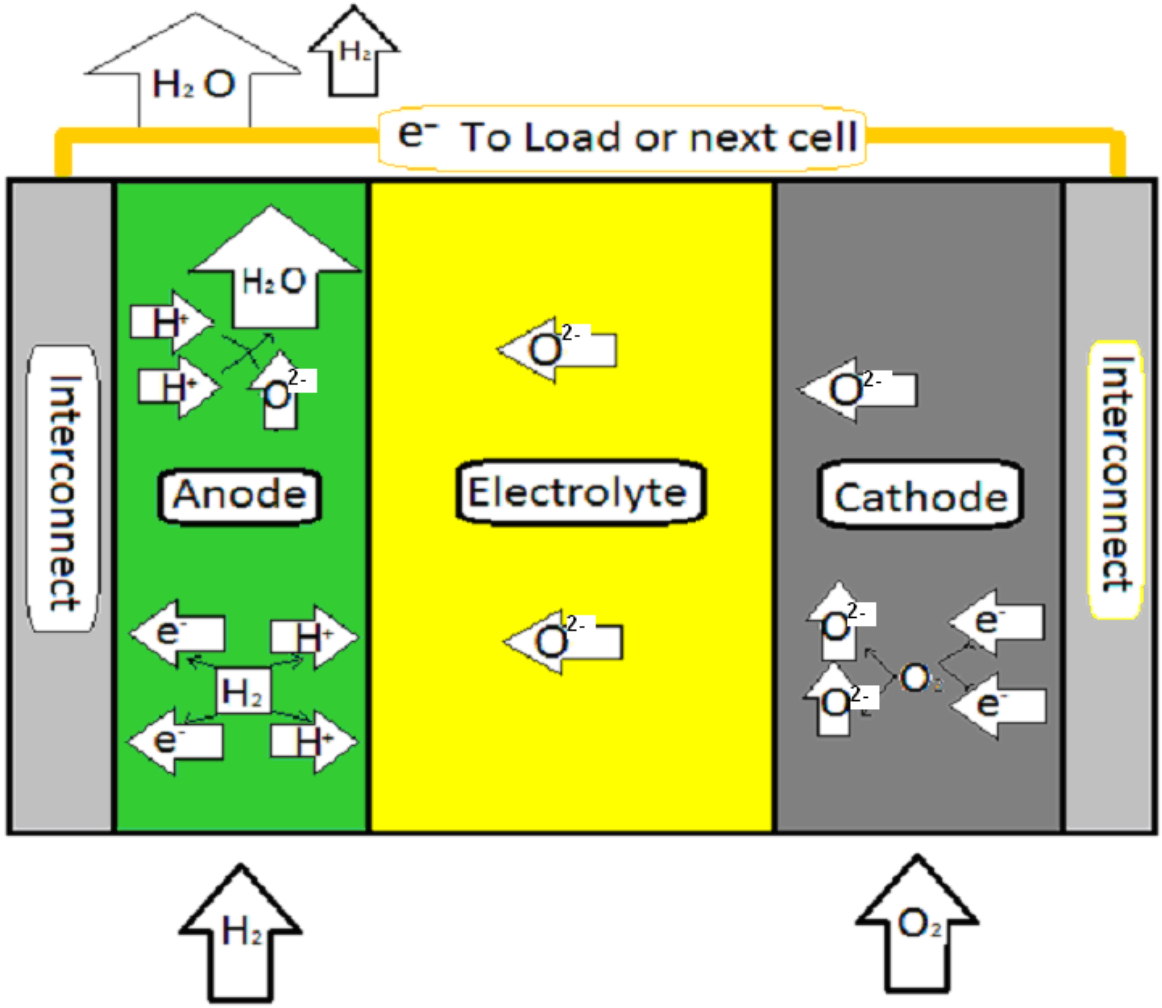

Fig.1.7: Typical oxide ion electrolyte type fuel cell schematic.

1.6 TYPES OF FUEL CELL

Fuel cells are categorized by operating temperature range, electrolyte type, fuel type and other defining characters. All electrochemical devices have an anode and a cathode, which are the electrodes of the device, one or more electrolyte, and current collectors. All fuel cells take fuel at the anode and air or O_2 at the cathode[7].

1.6.1 CLASSIFICATION BY ELECTROLYTE

Fuel cells can be categorized by electrolyte charge carrier type, such as proton conducting and oxygen ion conducting. Further sub-classification could be based on electrolyte construction such as polymer, ceramic, or molten salt. Still further sub-division can be made, such as liquid carbonate or phosphoric for the salt type which would encompass one of each from proton and oxygen ion conducting.

Proton conduction in its simplest form has the benefit of adding exhaust materials to air, the less expensive and more abundant reactant. This can translate to higher fuel utilization rates as no fuel reprocessing step is needed. However, exhaust water is produced at the cathode for these fuel cells and at high conversion rates can block the uptake of oxygen at the cathode triple phase boundary. For oxygen ion conduction, exhaust is produced at the anode which means that spent materials will crowd the triple phase boundary, impeding the kinetics of the anode reactions. Additionally, clean fuel is mixed with exhaust, translating to lower utilization rates and possibly the need for separation processes. Fuel cells of this type are somewhat analogous to 2 stroke internal combustion engines (ICEs). Both major oxygen ion conducting electrolyte systems, molten carbonate and solid oxide, operate at higher temperatures where the oxygen ion conductivity is higher through those media.

1.6.1.1 PEMFC

Polymer Electrolyte Fuel Cells (PEMFC) use a fluorinated sulfonic polymer membrane such as Nafion as the electrolyte which is a proton conductor. However, because the protons generally take water with them these electrolytes don't work if dried out, meaning PEMS can't be operated above 100°C. Unlike 4 stroke internal combustion engines, all fuel cells must release their exhaust into either the fuel or the air, and in the case of PEMS running on hydrogen, water production occurs at the cathode. However, there is no exhaust entering fresh fuel or being expelled with it. Because the fuel is more valuable than the air this must be a benefit.

1.6.1.2 MCFC

Molten Carbonate Fuel cells use CO_2 to transport oxygen as CO_3^{2-} from the cathode to the anode at high temperature. [8] They operate at higher temperatures where carbonate salts are liquid using a mixture of KCO_3 and $NaCO_3$ as the transport salts. The higher temperature and other factors mean that MCFCs can operate on hydrocarbons and also carbon and coal.

1.6.1.3 SOFC

Solid oxide fuel cells use ceramic materials as the majority of the components. These ceramics generally have poor operating properties at lower temperatures and so SOFCs typically operate between 600°C and 1000°C. Most SOFC systems utilize an oxygen ion conducting material as opposed to PEMS which use proton conductors, and so the net flow of matter tends toward the anode and not the cathode. This is advantageous as the net flow

of water to the anode combined with the higher operating temperature allows in situ steam reformation of longer chain hydrocarbons to more usable forms like CO and H_2 as a fuel. However, as with all fuel cells that utilize oxygen migration to the anode, there is fuel dilution where exhaust is constantly entering the fuel compartment and prohibiting conversion to electricity and for high conversion rates an additional separation step is required.

1.7 ADVANTAGES OF SOFC

All fuel cells work at extremes including chemical potential between the electrodes, extremes of electrical potential across interconnects, and in the case of SOFC's extremes of temperature between running and shut down states. This heat, in conjunction with the exhaust water that is expelled into the fuel compartment of SOFCs can give the advantage of using internal steam reformation to utilize fuels that are long chain hydrocarbons. Additionally, excess heat from SOFCs can be utilized as a second power source for home and industrial Combined Heat and Power (CHP), where waste heat is used for other purposes like central heating or process heating.

1.8 FUEL CELL PARTS

All fuel cells and batteries have similar components, shown in fig.1.8. These are anode, cathode, electrolyte and current collectors. In fuel cells that are stacked, the interconnect also serves to stop anode and cathode gases from mixing in addition to passing current from one anode to the next cathode. In other electrochemical applications these arrangements would be called bipole plates. This section will focus on SOFC specifically.

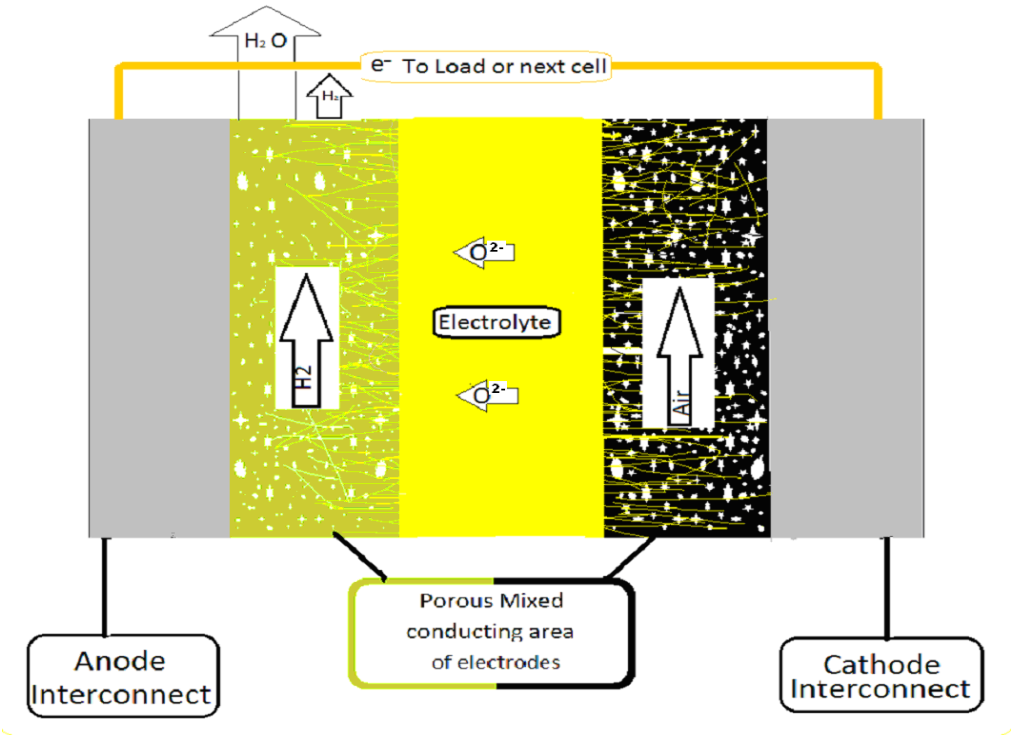

Fig.1.8: Parts of SOFC

1.8.1 ANODES

Anodes oxidize fuel and recover electrons that are liberated and conduct them to the electrical load. Materials for anodes must be mixed ionic and electronic conductors. Where the gas phases, anode and electrolyte meet is called a triple phase boundary. The three phases are gas (fuel), electrode and electrolyte. The exhaust and inlet gases are not generally differentiated and the exhaust gases are often not included in the mathematical models. [9] For SOFC anodes the materials are generally metal ceramic mixtures (cermet) however investigation into purely ceramic anodes is ongoing. Currently NiO/Ni are mixed with YSZ or other oxygen conducting electrolytes. Unfortunately, this oxygen conduit can lead to further oxidation of the anodes on shutdown if reducing gasses are not supplied. The cycling of oxidation and reduction can cause large surface area anodes to agglomerate into lumps of metal.

1.8.2 ELECTROLYTE

For most SOFC, this is an oxygen ion or proton conducting ceramic. The state of the art is currently yttrium doped zirconia and gadolinium doped ceria. In order for conduction to take place, the temperature is elevated as these materials are poor ionic conductors at low temperatures. The electrolyte allows the ionic transfer of ionic species (H^+, O^{2-} or other ionic species such as CO_3^{2-}).

1.8.3 CATHODE

Cathodes receive the oxidizing material and allow electrons into the oxidizing material from the load. As in anodes, cathodes must have mixed conduction, and state of the art cathodes utilize a mixture of electrolyte and electrode to increase the triple phase boundary surface area and provide ionic and electronic conductivity. Lanthanum Strontium Manganate is one of the ceramics of choice.

1.8.4 CURRENT COLLECTOR

These components attach to or are cast as part of the electrodes and allow electrons to travel to the interconnect. For current state of the art SOFC's this is usually electrode material that has no electrolyte material added and sits next to the interconnect.

1.8.5 INTERCONNECT

Interconnects connect the current collectors of each fuel cell to either the next cell or to the electrical load, and are analogous to the "brushes" in a motor For scientific (non commercial) purposes, gold, silver and platinum have been used. However, for SOFC to become ubiquitous, cost will be a major factor and large quantities of expensive elements would be prohibitive. As improvements in ionic conductivity have made operating temperatures lower, inexpensive alloys are being considered for interconnects. Some alloys have most of the desired properties. The oldest ceramic interconnect is lanthanum

chromate, which is a semiconductor. High temperatures are required to make this material conductive at the desired level.

1.9 GEOMETRIC LIMITATIONS

There are two main types of solid oxide fuel cells: planar and tubular. However, in most other continuous chemical processors, be it high speed batch of a reciprocating engine, plug flow or a series of continuously stirred reaction tanks, there are generally two ports: one input and one output. This is the case even if there are multiple reactant inputs or phases in multiple positions. For all ICEs and gas turbines, fuel is mixed with air in a single port into the reactor and ejected through the other. Matter coming out is multiphase -gas, liquid and nano-particulate (soot). Even though it may be a multiphase stream, it is considered single and for the most part does not need additional treatment steps or separation.

Because of these factors, many chemical processes can be modeled as a pipe. For many of these pipe models, efficiency is somewhat proportional to stream velocity and pressure. For instance, with steam turbines, increases in steam pressure or velocity bring increases in efficiency. In a fuel cell the two reactants must be kept separate throughout the reactor. No matter the type of fuel cell, the electrolyte forces a reactor geometry that is planar due to the two dimensional diffusion barrier, the electrolyte. Devices that contain diffusion membranes that separate two reactants throughout the reactor can't be modeled as pipes because the two ports available at either end of a pipe are already used.

From a reactor engineering point of view, even with tubular cells, the reactor is essentially planar. There are only 2 ports, one on either side of the diffusion membrane. Therefore, whatever comes out as exhaust has to come out into either the fuel or the air. Whichever side it comes out at will inevitably choke that electrode's triple phase boundary. Increasing the current load increases the production of exhaust, which drives up the resistance, making the fuel cell's efficiency inversely proportional to operating output. This is clearly seen in any Nernst polarization curves. Increasing the microstructure area increases the operating range but does not invert the performance curve.

From this point of view, it's clear that 100% conversion to products at maximum flow rate and current load in a fuel cell that exhausts into the anode in a single pass is neither possible nor desirable. When we look at the definition of the triple phase boundary being where the electrolyte and oxygen meet in a cathode where electrons are stripped and oxygen ions are transported into the electrolyte, then surely for an SOFC the anode area must be a quadruple phase boundary. This is where the anode, the electrolyte, the electrons, oxygen ions and fuel meet and where exhaust is produced. Due to the dimensional constraint of all fuel cells imposed by the planar nature of the electrolyte, there is no third port to blow out the 4^{th} phase.

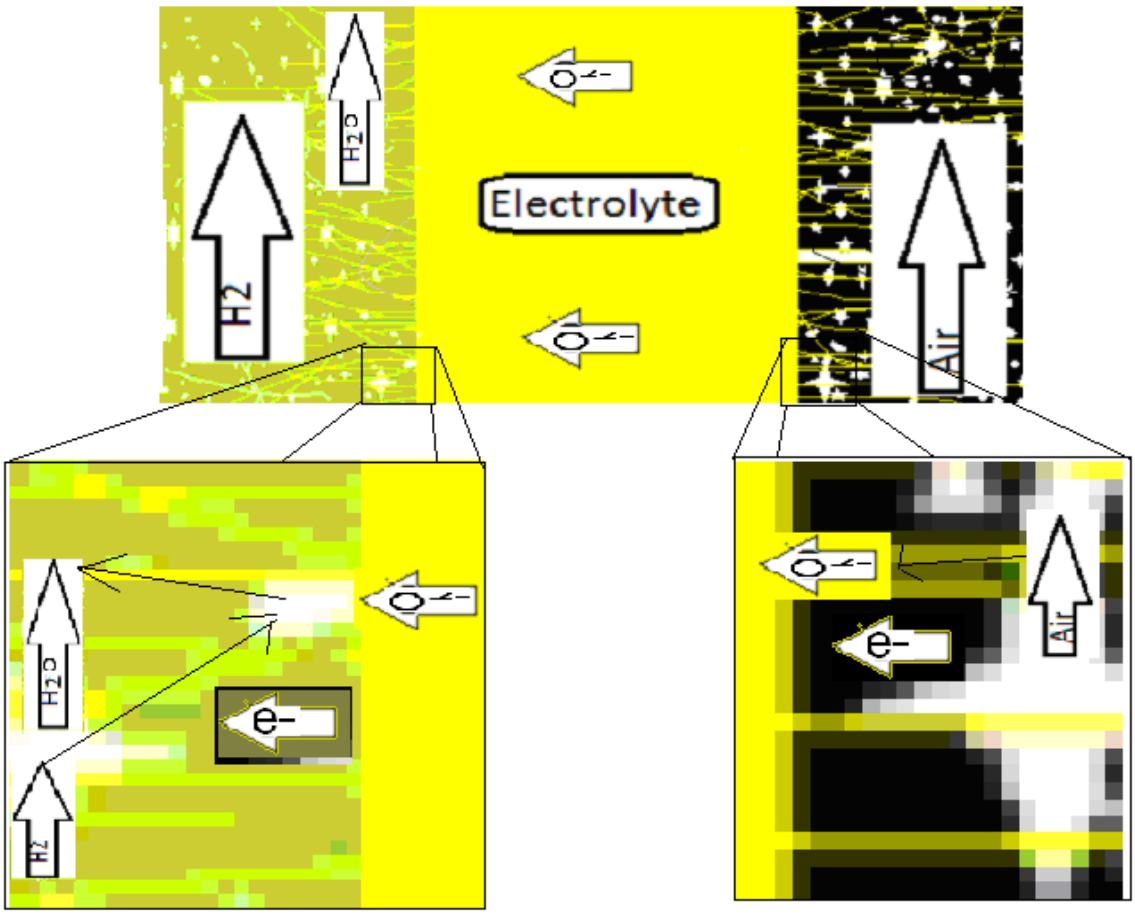

Fig.1.9: The multi phase boundaries of SOFC microstructure

Fig 1.9 shows that the half cell reactions occur in the pores of the microstructure. For the anode, fuel is oxidized when 2 hydrogen atoms meet 1 O^{2-} ion, whilst releasing 2 electrons. Water is produced, making this the most complicated interface in the SOFC with 2 solid phases, electrons and oxide ions meeting, and 2 gas phases getting in each other's way. In the cathode side, only air or oxygen is going in, and nothing should be impeding its uptake as there is no exhaust.

The consequence is that fuel cells have to be optimized for specific operating conditions as the high conversion rate performance is poor due to the concentration polarization. Although the internal combustion engines (ICEs) have generally poor efficiency, especially at low load, it can run from 5% to 100% load and change to anywhere in that range with increasing efficiencies at higher outputs as modeled by the Carnot efficiency. With fuel cells increasing loads create lower efficiencies. Others have claimed the inverse, which is, ICEs and gas turbines (GTs) have poor performance in the mid and low range and only operate best at 100% throttle. This would be an equally valid claim. The truth of the matter is that ICEs and GTs have peak power and peak efficiency in generally the same place, due to the Carnot efficiency. FCs have peak efficiency at lowest load, and considerably lower efficiency at peak power. At maximum current a fuel cell is approaching diminishing returns. When quoting power and efficiency FC and battery sales personal often neglect to point out that peak efficiency cannot be attained at peak power, something ICE and GT sales personal don't have to worry about because peak power and efficiency are in the same place.

Nernst's and Fick's equations explicitly state that this function of the geometry of the reactor will be the same for any chemical reactor that requires a diffusion barrier to separate two reactants and where a reactant and a product are traveling in opposite directions. All reactors of this type will have the same performance limitations, be it in the metals recovery industry, fuel cells, or chlor-alkali as is demonstrated. This is clearly demonstrated by the polarization curves of all electrochemical processes that use membranes. It also partly explains the exponential decay curve of all batteries, and high OVC and low performance at high current. This is why so few of these types of reactors are run in single pass mode: you can't get all the energy out efficiently. However, single pass is what we would prefer to reduce balance of plant. For SOFC, some heat is required to keep the cell hot, so there is the option of burning the unused fuel for that purpose.

The biggest advantage of SOFC is the ability to use this high quality heat for another process such as heating a home or process fluid or to drive steam reformation of hydrocarbons into usable fuels.

1.9.1 PLANAR SOFC

In the planar SOFC anodes, cathodes and electrolytes are cast into sheets of unsintered ceramic, assembled and sintered. Different types of planar system may have different assembly and sintering procedures. The completed cell sheets are then assembled in stacks with an alloy interconnect separating each cell. Although this means that they have a high reaction surface area and very high power packing density, there are problems associated with the heat transfer, fuel distribution, fuel utilization, and manifolding, and expansion properties amongst others. These issues are common to most stacked or plate and frame type systems such as filter presses, chlor-alkali cells, and metals recovery systems that employ diffusion membranes. [10] [11] Because of the high packing density, planar systems have a very high but not necessarily constant thermal profile with respect to position which means it can take a long time to heat them up and cool them down. Because ceramics are strong in compression but not tension [12] , mismatches in thermal expansion rates of the materials lead to shear stresses parallel to the plates of the device during cooling or heating depending on which component has the higher coefficient of thermal expansion (CTE).

However one huge advantage with any plate and frame type system is the ability to change sealing and contact pressure whilst operating. With most plate and frame type devices, sealing pressure can be increased either by increasing a screw or hydraulic ram pressure or by increasing the mass. Solid oxide fuel cells that do not have integrated electrode and current carrier usually require some pressure to decrease contact resistance between the current carrying interconnect and the ceramic electrode. Assuming that other pieces in the SOFC are strong and flexible enough to survive this additional pressure, it can be adjusted in planar units.

Interconnects in planar solid oxide fuel cells are generally sheets of alloy.[13] In most planar systems, the interconnect acts as a bi-pole between a cathode and the next adjacent anode. Because of this, planar SOFC interconnect materials have to be stable in both reducing and oxidizing conditions as both anode and cathode connectors.

1.9.2 TUBULAR SOFC

With tubular units the electrodes and electrolytes are cast into tubes. In most engineering applications tubes can be easy to seal and adjust. This is not always the case for ceramic tubes which show higher strength when compressed on the outside in than they do from the inside out. [12] Multitudes of tubes do not pack as densely as sheets or planes and there is no way of generating extra pressure on the contact or seal during operation without adjustable compression sleeves, and this would mean a pipe connecting on the outside of the tubular fuel cell. Interconnects for tubular cells usually consist of an alloy pipe that is inserted into the anode ceramic and a wire wrapped around the outside of the fuel cell for the cathode. Inserting pipes inside ceramic tubes puts the stresses in the hoop tension direction where ceramic tubes are the weakest. As discussed earlier, ceramic tubes perform better when compressed from the outside in than the inside out, just as eggs are strong in compression but easy for birds and reptiles to gain exit from. This translates to less damage when sealing to the outside of a ceramic tube, but makes connection to the inner electrode difficult. Interconnects for Tubular systems also serve as fuel or air delivery conduits. This is why sealing is so important for these systems, and so difficult to achieve on the inside. One great advantage is reducing the chemical and electrical potential as the interconnect tube can't be a bipole. This may translate into less corrosion load.

1.10 INTERCONNECTS FOR SOFC

As mentioned above, different configurations of SOFC put different requirements on interconnects. The term interconnect is more specific to SOFC systems operated in flat stacked series model. In this configuration the interconnects are essentially bi-poles and act as gas barriers separating the fuel in the anode of one fuel cell the air in the cathode of the next. Unfortunately this configuration puts the maximum chemical potential across the interconnect as there is a reducing fuel on one side and oxygen the other [13].

At higher temperatures of 800℃ and above, only expe nsive ceramics or superalloys are suitable for the interconnect application, but as operating temperatures have come down steel has been considered due to its low cost. Most steels are optimized for lower operating temperatures than SOFC applications.

According to the Jülich Institut für Energie und Klimaforschung[13] the criteria for interconnect selection are:

- High electronic conductivity with low ionic conductivity
- Chemical stability in both fuel and air
- Thermal expansion match to other components
- High mechanical strength
- High thermal conductivity
- Chemical stability with regard to other cell components
- Low cost

1.11 INTERCONNECT MATERIALS

As mentioned above there are two types of current collector: ceramic and metallic. The most successful types of ceramic conductors are doped lanthanum chromates, perovskite p-type semiconductors that are already fully oxidized and show strong reduction resistance for anode work. However, the conductivity of these materials is a function of temperature and so they function best at temperatures above 900°C. A further problem is the evaporation of chromium which deposits in the triple phase boundary of the cathode halting SOFC operation [14. Currently much research in SOFC's is focused around lowering operating temperatures which opens the door to cheaper but less chemically resistant materials. Work is focused on steels that can be used as current collectors. Chromium containing steels also lose chromium into the system for the same reasons. For longer chain hydrocarbons the lower limit of operating temperature is the minimum temperature for steam reformation, around 750°C. The performance of the ceramics balanced with longevity of interconnect due to metal corrosion is also of concern. If reformation is not a desire, then the lower bound of the operating temperature is governed by the performance of the ceramics used. Currently an accepted lower value for low temperature SOFC is 600°C [15].

1.11.1 METALS

Metals are a major engineering material range. Included in this term are the soft metals, light metals, etc. Metals can be glassy, or crystalline depending on treatment strategies. Mixtures of metals can have many different properties. Metals and their mixtures can be heat or force treated to bring about other properties.

There are several sub groups of metals. One major categorizing factor is mixtures or alloys. Metal mixtures or alloys are different in their behavior to pure elemental metals due to the behavior and solubility of the alloying atoms, bonds, charge, and size of the alloying elements interfering with the structure of the material. If the alloying element atom is of similar size then it is likely to substitute for an atom of the base material. If it is much smaller, then the alloying atoms can go between the base metal atoms.

1.11.1.1 SOLUBILITY

A good case of solubility of one element into another would be carbon into iron. Iron has been used for a long time by humans, but alone has relatively poor performance. The first alloying element of consequence is carbon.[16] Alloys of carbon and iron are generally called steel. Carbon has an atomic radius of 70 pm, where as irons is 140 pm, meaning carbon will be mostly interstitial or in between iron atoms. Adding carbon to iron in large enough quantities (about 41/2 weight%) forms a eutectic with a melting point of about 1150°C compared to 1550°C for iron, however the solubility of carbon at 0°C is 0.008% and increases to 0.02% at 723°C. The eutectic of 4.3% carbon in iron is actually a two phase material consisting of fully saturated iron and Fe_3C [16]. This is because there is a solubility limit to the amount of carbon iron can contain in solution before there becomes a second phase. The dual phase eutectic properties form the basis for the cast irons as the lower melting point makes it possible to pour moulds at lower temperatures. Without heat

treatment, these mixtures are generally ferritic. Upon cooling, this mixture usually has lots of carbon deposits, which is why cast irons look grey when cut or shattered.

1.11.1.2 STEELS

1.11.1.2.1 HEAT TREATING

If mild steels are heated above about 910^{o}C they change phase from BCC to FCC and lose their magnetic properties. At this point they become Austenitic [12].

1.11.1.2.2 COOLING RATES

If high carbon content austenitic steel is cooled slowly, much of the carbon will come out of solution and form carbon deposits as in the cast iron. This is not the case if the cooling rate if very fast. The lowest rate at which the solution can be cooled yet stay supersaturated is called the critical cooling rate. This is the basis for tempered steel. These steels are very strong but very brittle, and also known as martenistic.

1.11.1.2.3 AGING

Over time, carbon can come out of solution from these super saturated solid state solutions giving rise to fine carbon deposits. Elevated temperatures can hasten this effect and weaken the steel. However, if the steel is lightly heated for extended periods then properties of both mild steel and tempered steel can exist in the same material such as hardness, ductility and yield strength. These properties are effects of the microstructure of the steel. The steel can also be “worked” where its shape can be changed by rolling, pressing or elongating. This type of treatment changes the microstructure by elongating the carbon deposits and grain boundaries into sheets and disks instead of spheres and blobs.

1.11.2 STEEL TYPES

The above properties of steel are generally classed as Marten site, Austenite and Ferrite.

1.11.2.1 FERRITE

Ferrite is the most basic form of iron and steel. Its crystal structure is BCC or body centered cubic. Most carbon steels are ferrite. These steels are magnetic, easily machined and shaped, can be strengthened by working or rolling and are ductile.

1.11.2.2 AUSTENITE

Unlike ferrite, austenite has a FCC or face centered cubic crystal structure. It is paramagnetic, not ferromagnetic, but considerably stronger than ferrite.

1.11.2.3 MARTENSITE

Martetnsites are steels with mixture elements and post mixing treatment that force body centered tetragonal crystallographic structure. This is accomplished by rapid cooling of austenite. The rapid cooling traps dissolved carbon in solution before it can form cementite or carbon deposits.

1.11.3 OTHER ALLOY ELEMENTS

Adding other elements to iron can change other properties. All alloying manufacturers have to adhere to the international standards for amounts of each element added to the alloys. Most publish a comprehensive list of alloying elements and their purposes. The following list is taken from Chase alloys in Staffordshire [17]. The list is as follows:

Carbon, as discussed above can change the strength, hardness, and melting point of steel due to solubility. Heat treatments can further manipulate strength, hardness, and ductility as well as other properties

Manganese can change the high temperature working properties and increase strength, toughness and hardening of steel. Unfortunately, Mn is one of the more volatile elements that can be included in steel.

Oxygen is always somewhat dissolved in steel mixtures unless processing is done under a gas blanket or in a vacuum. Unfortunately, it can combine with carbon to make carbon monoxide which can bubble from the steel during cooling. It can be deliberately added to some alloys to form oxide dispersion alloys which have other interesting properties such as machinability and heat resistance. This technique is often used for turbine blades

Chromium is primarily used to increase oxidation resistance by forming Chromia on the surface of the steel. Chromium is added in amounts between 10 and 20%, with higher amounts of chromium accounting for higher oxidation resistance. Chromium and Iron have similar atomic radii, meaning chromium will be substitution in the alloy and not interstitial as in the case of carbon. This is the reason why there is no limit of solubility for chromium in iron.

Nickel is added in amounts of 8% and higher to form high temperature steels and with chromium to form high temperature stainless steels which are austenitic. These steels are tougher than chromium only stainless steels and also more resistant to oxidation

Molybdenum improves corrosion pitting by chlorides and sulphides in stainless steels. Without chromium it improves high temperature strength and hardness.

Titanium stabilizes carbon by forming titanium carbides. These form preferentially to chromium carbides which allows chromium to be free for corrosion resistance in stainless steels. Titanium can also preferentially oxidize, also known as “killing”

Phosphorus and **Sulphur** are usually added together and improve mach inability in low chromium steels. By its self phosphorus increases strength and corrosion resistance in non stainless steel, but can make welds brittle

Selenium is added to improve machinability

Niobium is added to stabilize carbon by preferentially oxidizing, and also strengthens steels used for high temperature applications.

Nitrogen increases austenitic stability in stainless steel. Like nickel it helps form austenite, and improves yield strength

Silicon is used as a killing agent, and also as a cast releasing agent. Most steels contain a small amount of silicon. It contributes to the hardening of the ferritic phase and silicon killed steels are harder and stiffer than aluminium killed steels. However, silicon forms oxides on the surface of steel which are poor electronic conductors.

Aluminium is uses as a killing agent, and can be used with nickel alloys to form oxide dispersion strengthened alloys. It can also be used to form oxide layers on the surface of steel that are non conductive and protect the steel from corrosion.

Cobalt can become radioactive when used in steels used in nuclear power plants. However, it's difficult to separate cobalt from nickel and steels containing nickel usually have some cobalt by default.

Tantalum is similar to niobium chemically, and is used for similar effects.

Copper is usually present in most stainless steels as a residual element that cannot be removed, however it is deliberately added to a few alloys to produced precipitation hardening properties.

1.11. STEEL PROTECTION STRATEGIES

There are two general strategies for steel protection. The first is alloying, which consists of adding elements to the alloy that will modify the corrosion layer as it grows. The second is to coat the steel with a coating that will block oxidation of the steel (such as paint or powder coating, or cladding with another material or metal or sputtering). Coatings that are to go on or grow on steel for SOFC purposes need to conform to the Jülich criteria, as mentioned before.

1.11.5 ALLOYS AS INTERCONNECTS

Many metals and alloys have been examined for SOFC interconnect service with a few that are notable for key properties such as thermal expansion coefficient. [18] Superalloys have been tried but their corrosion layers are often poor conductors of electrons, (which is why

they are so good at protecting the superalloys at high temperature. See next chapter). [19] [20] In the steel family SS316(or marine grade stainless) has been tried, but has a significantly higher coefficient of thermal expansion at 17 $x10^{-6}$ than the ceramics used in SOFCs. SS430 is of great interest due to its low thermal expansion coefficient of 10 $x10^{-6}$ [21]. However, due to its lower chromium content its high temperature corrosion is rapid. It also has poor chromium retention at higher temperature in the presence of water, as does SS316.

For SOFCs it should be noted that the alloy itself does not make the electrical or physical contact to the ceramics in the cell. The bulk alloy provides an intermediate storage of elements used for the further synthesis of the functional layer, and provides metallic conduction and connection to the wires or rest of the cell. With the exception of platinum, all metal interconnects corrode to form an additional oxide material that connects to both the alloy and the SOFC ceramic components. All of the above listed criteria apply to the alloy as they did to ceramic interconnects, and to the resulting functional corrosion layer.

There are additional considerations. The corrosion layer must have low ionic permeability. If the corrosion layer is oxygen ion permeable then the corrosion layer will continue to grow and form more oxides at the interface between the corrosion layer and the alloy. If the corrosion layer is permeable for alloy elements, corrosion products form on the outer part of the corrosion layer and react with the atmosphere and ceramics. For instance, if the corrosion layer is chromium permeable, chromium will deposit in the triple phase boundary. The functional layer or corrosion layer is discussed in detail in the next chapter.

REFERENCES

[1] T.-H. P. Wilfred M. Post, William R. Emanuel, Anthony King, Virginia H. Dale Donland L DeAngelis, *http://www.as.wvu.edu/biology/bio463/globalcarbon.pdf* **1990**.

[2] T. BBC in *50 years of the Keeling curve*, (Ed. H. Briggs), **2007**.

[3] N. O. A. A. E. S. R. L. DOC in *Trends in CO2 at Mauna Loa Observatory*, (Ed. U. D. o. Commerce), **2012**.

[4] DOE in *International Energy Outlook may 2009*,. (Ed. U. D. o. Energy), Department of Energy, Washington DC, USA, **2009**.

[5] Serway, R, Beichner, R, *Physics for Scientists and Engineers*, **2000**, Saunders College Publishing, Orlando, florida

[6] Winchester, C, *Wonders of World Engineering*, **1937**, The Amalgamated Press, againalble at **http://en.wikipedia.org/wiki/Hackney_Power_Station**

[7] A. D. James Larminie, *Fuel Cell Systems Explained*, John Wiley and Sons, Chichester, **2003**

[8] K. Adamson, *Stationary Fuel Cells (an overview)*, Elsevier, Amsterdam, **2007**, p.

[9] D. M. B. Ryan O'Hayre, Fritz B. Prinz, *journal of the Electrochemical Socieny* **2005**, *152*, a439 a444.

[10] R. H. Perry, *Chemical Engineers' Handbook*, McGraw-Hill, **1997**, p. Perry, R.H.; Green, D.W. (1997). Perry's Chemical Engineers' Handbook (1997th Edition). McGraw-Hill.

Online version available at:

http://www.knovel.com/knovel1992/Toc.jsp?BookID=1948&VerticalID=1990.

[11] J. M. R. Coulson, J. F., *Chemical Engineering*, Butterworth Heinman, Oxford, **1999**, p. thousands.

[12] M. F. J. Ashby, D.R.H., Engineering Materials 1, An Introduction to their Properties and Applications, Butterworth-Heinenmann, Oxford, **1980**, p. 275.

[13] F. Tietz in Solid Oxide Fuel Cells: Interconnct Materials, Vol. Limnos, Greece, **2006**.

[14] E. M. Konysheva, J.; Penkalla, H.; Singheiser, L.; Hilpert, K., *Journal of The Electrochemical Society* **2007**, *154*, B1252-B1264.

[15] I.P.F.T.H.E SOFC600, *SOFC600 Project Summary*, **2007**.

[16] W. F. Hosford, *Iron and Steel*, Cambridge University Press, **2012**.

[17] Chase Alloys in Effects of alloying elements in steel, **2010**. available at http://www.chasealloys.co.uk/steel/alloying-elements-in-steel/

[18] W. J. P.-A. Quadakkers, J.; Shemet, V., *Materials Research* **2004**, *7*, 203-208.

[19] a) S. J. Geng, *Solid State Ionics* **2006,** ; b) J. H. Zhu, Journal of Hydrogen Energy **2006**.

[20] S. J. Z. Geng, J. H.; Lu, Z. G., *Scripta Materialia* **2006**, *55*, 239-242.

[21] P. E. Gannon, V. I. Gorokhovsky, M. C. Deibert, R. J. Smith, A. Kayani, P. T. White, S. Sofie, Z. Yang, D. McCready, S. Visco, C. Jacobson and H. Kurokawa, *International Journal of Hydrogen Energy* **2007**, *32*, 3672-3681.

2 CORROSION OF METALS

INTRODUCTION

In SOFC scientists and engineers have looked at ceramic interconnects, alloy interconnects, and combinations. All systems have limitations. Ceramics are expensive to process, alloys need to corrode a little for their corrosion resistance to become apparent, and combinations are difficult to manage. The fact that alloys need to corrode to a degree to prevent further corrosion may seem counter intuitive. However, for corrosion resistance of alloys to take place, thermodynamics must be favorable for a corrosion layer to be formed. For the layer to be limited in its thickness, the kinetics of this corrosion layer's growth will need to be slow. The two processes that govern the corrosion layers progress are the transfer of electrons and the transfer of oxygen or metal ions. Very few alloys chosen for corrosion resistance are particularly good at conducting electrons through their corrosion layer as this is their protection mechanism. For interconnects a corrosion layer is needed that has poor oxygen transfer so that the base metal can be protected from oxidation, but excellent electron transfer so power can be recovered from the fuel cell. These parameters tend to highlight chromia forming alloys as the only option.

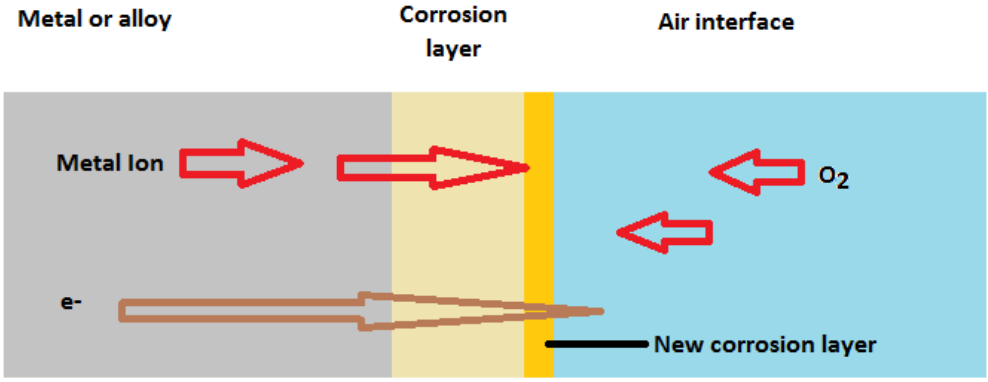

Corrosion by metal ion migration through corrosion layer. Limited by kinetics of metal ion. Electrically conductive, poor oxygen kinetics.

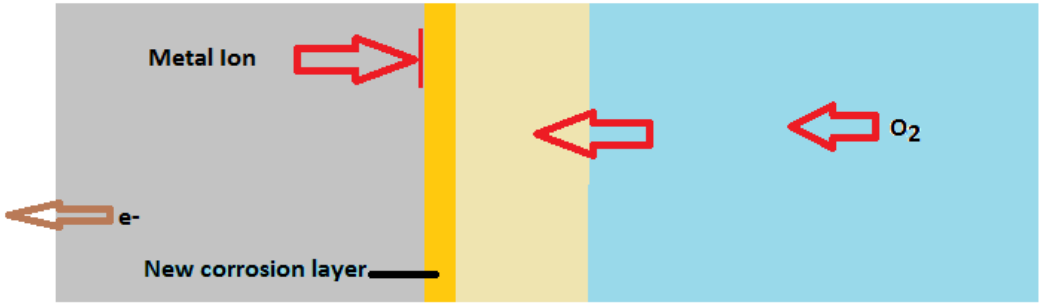

Corrosion by oxygen ion migration through corrosion layer. Limited by kinitics of oxygen and/ or electrons through corrosion layer. Poor electronic conductivity = good corrosion protection.

Fig.2.1: Corrosion mechanisms

One way to help SOFC scientists to think of corrosion is to consider it as a fuel cell. Zinc air batteries are a type of fuel cell where metal is consumed instead of hydrogen. If we consider

a fuel cell where the interconnect is actually an electrode and a fuel source, then the problem will become more apparent. If the metal is corroding, then in some cases, the product is an electrolyte (for metals like Zr, Al, Ti) or a mixed conductor for metals like iron and chromium. There are no metals at SOFC operating temperatures for which a purely electronic layer is the product. If there were a purely conducting layer as a product, it would be impossible to produce a corrosion layer as no oxygen would be transported to the triple phase boundary, between the metal and the corrosion layer, or no metals would be transported out toward the oxygen. With a purely electronic conducting product layer we have the most desirable but impossible case scenario. It is the optimization of the worst case scenario – mixed conduction – that all metallic interconnect specialists must be concerned. And it is because of the mixed conduction that all metallic interconnects are doomed to fail at some point in their lifetime, and why we must forever optimize the kinetics of this product layer.

2.1 CORROSION OF METALS

Metals can be categorized by several criteria, but oxidation performance is the obvious starting point for SOFC's. According to Evans, metals should be first segregated between metals that form films and those that do not. This is based on the work of Pilling and Bedworth in the 1920's[1]. Non film forming metals do not oxidize or form volatile species and include Pt, Mo. The vast majority of all other metals form films, and should be segregated between those that form oxides that occupy less volume than the metal they replace, and those that occupy more volume than those they replace. Smaller volume film producers are Mg and Ca and it has been shown that surprisingly, these films are protective to further oxidation in dry environments[2-4]. This comes as a surprise to most as these metals are known for combusting in air. S.J. Gregg and W.B. Jepson showed that Calcium heated in dry air below 475^{o}C did not oxidize, but that the oxidation became measurable above 500^{o}C. Their experiments showed that the presence of water greatly accelerated the oxidation at lower temperatures.

2.2 CORROSION MECHANISMS

2.2.1 DRY CORROSION

At room temperature dry corrosion is possible if the products have a lower Gibbs free energy than the reactants (metal and oxygen)[5]. Dry corrosion starts with chemisorption of oxygen onto the surface of the metal, ionization of the metal, and the oxygen. Oxidation starts at nucleation points and grows laterally and joins up. For gold, platinum and silver at room temperature, oxidation is not favourable.

2.2.2 FILM GROWTH

All corrosion is electrochemical in nature. For corrosion to occur, there must be an anode, cathode, oxidation and reduction. If considered as a fuel cell or battery, the metal would be the fuel. However, more like a battery, spent materials, or products do not leave the reaction

site but instead build up. As film growth progresses, after initial oxidation the film will continue to grow. For further growth to occur metals and oxygen must meet and electron transfer must take place. In the production of films this means oxygen and/or metals must travel thought the film. For chromium, metal ions travel through the oxide film and create oxidation products at the interface between the film and the atmosphere. For zirconium, aluminum and titanium, the film is grown at the interface between the film and the metal. High oxygen ion conductivity makes zirconia suitable for SOFC electrolytes. In either case, as the film grows, concentration gradients occur across the film of metals in increasing oxidation states. At the metal/film interface metals will be less oxidized than those at film/atmosphere interface. For instance, titanium oxide film progresses as Ti in the bulk, TiO close to the bulk, Ti_2O_3 in the film and finally TiO_2 at the outer crust. It is important to note if thermodynamically and kinetically possible the corrosion process will remain dynamic and will continue until one reactant is consumed. The driving force is oxidation potential across the film from metal on one side to the atmosphere on the other. As Evans pointed out, [1] "(the) distinction between corrosion velocity and corrosion probability has served to clear up several of the apparent contradictions which puzzled earlier investigators." Corrosion may be thermodynamically favorable, and kinetically slow. If it is thermodynamically inevitable, then corrosion will always continue, but it may be take centuries or more. If it were not, there would be no film at all. Controlling the kinetics of film growth are the migration of ions and equivalent charge transfer through the film. If oxygen or metal ion transport is very slow, layer growth will be slow. If electron transfer is slow, growth will be slow. If both are fast, as in the case if iron oxides, then corrosion will be inevitable and fast.

Several corrosion models have been proposed throughout the years with each successive version becoming more sophisticated. [6] Early models were empirical in nature, such as the Tammann, Pilling and Bedworth theory of oxidation. They found that oxidation for many metals was proportional to the square root of time. Their assumptions were that growth occurs by uncharged particles, diffusion is independent of concentration, that the concentrations at the interface regions were independent of film thickness, and that film growth was steady state.

Later as these assumptions proved invalid and as the models failed to fit film growth observations, more sophisticated models were devised. Wagner's theory of oxidation was based on the assumption that corrosion continues by the transfer of charged particles, which was based on the theories of Debye and Nernst.

Later the Cabrera Mott theory, which uses the assumptions that electrons can pass freely from metal to oxide surface and ionize oxygen atoms. The consequence is a uniform field within the oxide which can change the Fermi level of the oxide. Although this model is far more accurate, it is also more intensive, and requires more independent measurement of variables. It also does not take into account other processes that influence macroscopic growth of oxide films, and therefore may not be useful for predicting growth of complex or doped oxide growth, as in corrosion of alloys.

2.2.3 DRY CORROSION MODELS

Dry corrosion rate models for oxidation of metals all follow the exponential corrosion law first proposed by Wagner. Although Wagner's theory of oxidation can also be used for wet, and electrical influence corrosion, the dry case is the starting point. The chemical reaction is broken into half reactions. Eq1 describes electrons leaving metals and the metals becoming ionic and is as follows.

eq 1 $M_{(s)} > M^{x+} + xe^{-}$

Here M is any metal, s denotes solid (or in the case of mercury, liquid and would be denoted as l) , x is the charge of the metal as electrons leave and also the coefficient of the amount of electrons liberated. The second part of the reaction is the changes in oxygen.

eq 2 $O_{2(g)} + 4e^{-} > 2O^{2-}$

where O_2 is oxygen, e^- are electrons, and O^{2-} are oxygen radicals. Combining these two reactions results in

eq 3 $M_{(s)} + (x/4)O_{2(g)} > MO_{x/2(s)}$

where O^{2-} and M^{x+} have combined to from the metal oxide.
At first the film growth rate will not be governed by the thickness of the film but by other factors such adsorption rate of oxide onto surface or rate of ionization of the metal or oxygen which will remain constant throughout the oxidation. As the film thickens it prohibits further film growth so the rate will be proportional to film thickness. [5]This can be described as

eq 4 $\frac{dy}{dt} = k1/(k2 + k3y)$

where y is thickness, t is time, and k's are constants which separates to

eq 5 $k1dt = (k2 + k3y)dy$

Integrating both sides,

eq6 $Kt = \frac{1}{2}k3\, y^2 + K2y$

When t is small ky dominates and as it thickens y^2 dominates. Films that are more permeable will become linear if film growth is not impeded by the film. More protective oxides will show parabolic behaviour. This is governed by mass transport of either metal ions out or oxygen in and charge transfer. The stability of the film is not predicted in this simple model. Internal stresses caused by differences in density from the bulk can create tension in films with densities higher than the metal and compression in films with lower densities. Both cases cause cracks when the film has reached a critical thickness when the

yield strength is lower than the stress created. Upon film cracking oxidation accelerates at crack sites and under the film causing graphs with several humps at higher resolutions. Dry corrosion is faster at higher temperatures.

2.3 WET CORROSION

Like fuel cell operation, wet corrosion is an electrochemical process, and like dry corrosion, the products have to have a lower Gibbs free energy for the corrosion to take place. At higher temperatures the Gibbs free energy is lowered for corrosion products. For wet corrosion there has to be an anode, a cathode, an electrical connection between them, and an electrolyte to allow equivalent charge transfer. Because wet corrosion cells are electrochemical cells they follow the model set by Nernst [7] which equates performance to mass transfer, diffusion layers, concentration gradients by

eq7 $E = E^0 - \left(\frac{RT}{ZF}\right) lnQ$

where E is the cell potential, E^0 is the standard potential at the given temperature T, R is the universal gas constant, z is the number of moles of electrons transferred and F is Faraday constant. Q represents the reaction quotient which is the concentrations of reactants divided by concentrations of products, each to the power of their coefficient in a balanced chemical equation. The Nernst equation can be derived from Gibbs free energy and relates the potential of a cell to the thermodynamics of the reaction.

2.3.1 WET CORROSION MODELS

Wet corrosion can be further classified into electrochemical action with or without applied EMF.

2.3.2 CORROSION WITHOUT APPLIED EMF

If there are no external applied currents corrosion will be caused by chemical attack, a corrosion cell caused by dissimilar metals in contact with each other and an electrolyte, oxygen concentration gradients across the metal, dissimilarities in the metal at local areas and/or cracks in the oxidation film. In the corrosion cell, oxidation happens at the anode. Other corrosion effects are changes in oxygen concentration due to cavitation of fluids, changes due to stagnation between metal plates, and microbial attack. The corrosion current is a function of the size of the corrosion electrodes, and the electronic and ionic resistance of the corrosion cell as per the Nernst equation.

2.3.3 CORROSION WITH APPLIED EMF

When imposing an EMF on a corrosion system we create electrochemical reactor. Depending on the species, pH of the solutions, and current available, different products will be formed consuming different reactants. In pure water when imposing an EMF of small

magnitude in the direction of ambient corrosion the anode will become consumed and the cathode will be protected In acidic conditions Corrosion rates with applied EMF can be higher than ambient corrosion depending on EMF polarity and can be halted by reversal of the ambient corrosion current. At higher current densities with the imposed current at the same polarity as ambient corrosion, H^+ will be formed at the anode and OH^- will be formed at the cathode. However, at some point the potential will be high enough that dissolution of metals and transfer of electrons will be too slow so support the high current and at this point dense and non conductive metal hydroxides and oxides will be produced and corrosion and imposed current will stop. This is called passivity. Although an interesting phenomenon, it's not much use for fuel cell interconnects[8].

Without imposed EMF's, these processes can be stopped or slowed by reversing the corrosion current, choosing metals that are noble enough for the electrode, or adding a third electrode that is less noble for sacrifice.

2.3.4 WET CORROSION RATES

In both cases, corrosion rate is a function of the corrosion current which is itself a function of the voltage and resistance of the corrosion cell, the area of the electrodes and other factors. This general case does not take into account other factors like void formation or crack and heal cycles due to stresses in the oxide layer which can give cyclical rates depending on the rate of crack and heal.

2.4 HIGH TEMPERATURE CORROSION

Corrosion at high temperature is more thermodynamically possible due to the temperature dependence of Gibbs free energy for creation of oxidation products. For the purposes of this work, high temperature oxidation will be the focus. Ellingham Richardson diagrams are useful for determining metal oxide compositions with temperature and pO_2 on one axis and ΔG along the y[9].

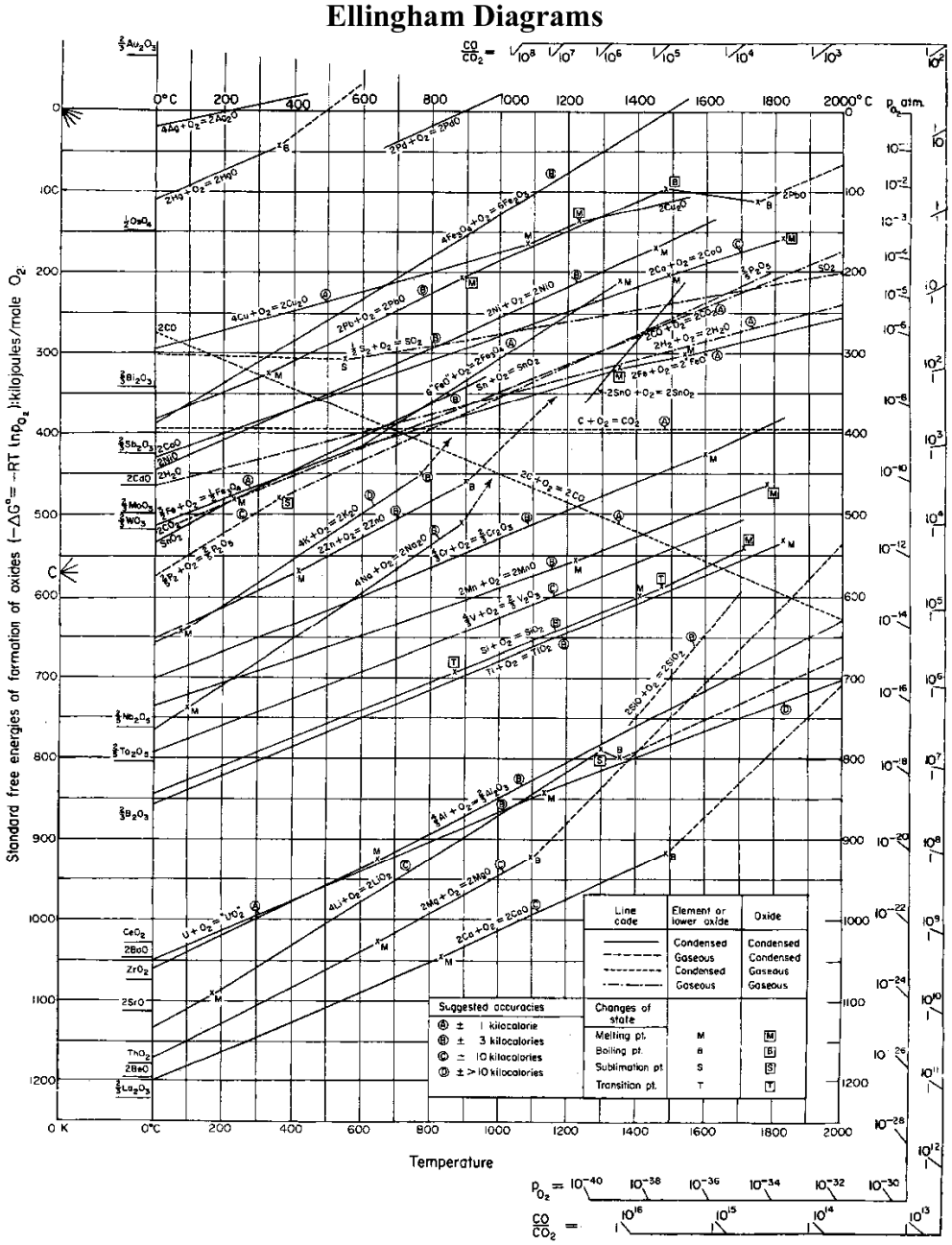

Fig.2.2: Ellingham Richardson Diagram from Kofstads High Temperature Corrosion[9]

Unfortunately, as can be seen from the above Ellingham-Richardson diagram, chromium is only represented with one oxide, Cr^{3+}. Any thermodynamic data recovered from the Ellingham-Richardson diagram will not describe the evaporation of chromium to Cr^{6+} as only the +3 oxide is shown. Even though gaseous metals and oxides are discussed, Chromium 6 and gaseous chromium 6 are ignored. This is possibly due to historical precedent, as chromium evaporation only became known in the 1960's. However, it's more likely that the conditions for evaporation are so many that it simply can't be graphed in 2 dimensions or

even 3. The parameters to consider are temperature, water content, pH, and electrical potential.

With no other influence, high temperature corrosion wet or dry follows the same rate models set forth for dry corrosion because water is no longer an electrolyte but a gas. For corrosion to progress elemental metal and oxygen need to meet. The solid state diffusion of oxygen or metal can take many paths including lattice diffusion and along grain boundaries. As the scale grows other further phenomena will influence corrosion such as porosity or cavities which will affect the corrosion rate[9] [10]. Oxygen pressure plays a large role on oxidation rates of metals at high temperatures. Two possible processes can be rate determining for oxidation; Rate of dissociative adsorption of oxygen and the solid state diffusion of oxygen or metal ions through the scale. In either case, charge must be balanced by transfer of electrons at some point.

Temperature dependence of oxidation follows the Arrhenius equation of

eq8 $K = K^o \exp(-\frac{Q}{RT})$

where Q is activation energy, R is gas constant and T is temperature in Kelvin[9].

2.4.1 WAGNER'S OXIDATION THEORY REVISITED

Wagner's oxidation theory assumes that lattice diffusion of reacting atoms, ions or electrons through the scales determines the rate of oxidation. Lattice diffusion is assumed to be possible by point defects and the migrating species may constitute lattice and electronic defects such as vacancies, interstitial ions or electrons, and electron holes.

Because the diffusion is slow through the bulk, reactions at the interfaces on either side of the scale are comparatively fast. Therefore, metal oxide and oxygen are in equilibrium at the outside interface, and metal and metal-oxide are in equilibrium at the inner interface.
The driving force for oxidation is the oxygen partial pressure gradient between the two interfaces. The model for corrosion in these conditions is the same as discussed in section dry oxidation.

The equations that model corrosion layer growth are explained in detail, with one of the better mathematical derivations in Per Kofstads “High Temperature Corrosion” starting in chapter 6[9].

2.5 ELECTROCHEMICAL HIGH TEMPERATURE OXIDATION

Although EMF and corrosion are widely discussed, very little information is available on the effects of EMF with high temperature oxidation. Information that does exist shows different behaviors for positively, negatively and uncharged interconnects, similar to dual gas studies[11]. The vast majority of metal oxidation and corrosion in reducing gas studies are in relation to engines, gas turbines and furnaces. The demands on these devices is not

generally electrical or electrochemical in nature, but purely mechanical, except for furnace wire which acts as a conduit for electrons through the metal bulk only and not through an oxidation layer. Although Kofstad discusses the difference between the models of oxides that are predominantly electronic and ionic, he does not discuss the effects of corrosion in an applied EMF on these layers. Literature searches of electrochemical corrosion in SOFC's mostly bring information regarding chromium evaporation and re-deposition in SOFC cathodes, even though this is not a strictly a corrosion process. Corrosion in electric fields is discussed in detail by Evans in chapter 11 of “An Introduction To Metallic Corrosion” [1] but he does not discuss high temperature corrosion in electric fields.

There are a few basic facts that can be surmised about high temperature electrochemical corrosion. Higher temperatures affect both thermodynamics and kinetics. In the first case, we can say with a high degree of certainty that more different types of reactions will be taking place. I the second case, they will be happening faster.

Hexavalent chromium evaporation would fall into the category of oxidation products that do not form films, and therefore offer no protection. Although Cr_2O_3 is the predominant species in dry air, high temperature, high humidity air leads to formation of CrO_3 and CrO_2OH species. [12] Oxygen partial pressure gradients and water content drive the evaporation of hexavalent chromium, and or applied EMF's have been shown to drive deposition and conversion of these species at the triple phase boundary between cathode and electrolyte EMF [13] or oxygen partial pressures [14].

2.5.1 OXYGEN CONCENTRATION GRADIENT EFFECTS ON CORROSION OF STEELS

Alloys that are predominantly iron in their makeup are steels. Iron is a very abundant, cheap and easy to manipulate element, however, its corrosion resistance is very poor due to the high ionic and electronic conductivity of its oxides. Iron is usually alloyed with aluminum, iron, carbon, nickel, and chromium to improve strength, corrosion resistance, high temperature behavior and wear properties.

For the corrosion of steel interconnects in SOFC there are two phenomenon due to changes in oxygen partial pressure. The first is due to changing operating conditions on a single side of an interconnect. Toward the exit the oxygen partial pressure will be lower than at the inlet. This may set up local corrosion currents within the interconnect. The second effect is due to the different gases on either side of a single interconnect element used in stack mode.

Effects of dual gas on a single interconnect element has been documented by several groups [15] [16] and it has been shown that air contacting interfaces of interconnect metals exposed to a single atmosphere behaved differently than those exposed to fuel on one side and air on the other. The cause for this is proton diffusion through the metal and oxide layers. Protons traveling through the metal and arriving at the air side of the interconnect can cause local production of water and hydroxide species. Yang et.al found that there was also an increase in the iron transport to the cathode side which in turn caused hematite formation in SS430 and increased iron concentrations in spinels on Crofer. Minor

differences between samples exposed to fuel gasses only and fuel side scales of dual gas samples were noted as mostly pitting[16-17]. This may put in doubt the wisdom of using metallic interconnects without separation because although gas tight, they are still proton conducting.

2.6 CORROSION CONSIDERATIONS IN SOFC

2.6.1 OPEN CIRCUIT CORROSION

2.6.1.1 CATHODIC ENVIRONMENTS

At open circuit and low temperatures some dry oxidation of the cathode interconnects will exist if only enough to form an interference coating. If condensation or humidity is high, stagnant conditions where the cell is idle for long periods will generate oxygen gradients in the gas between the electrolyte and the cathode side interconnect. If there are cracks in the oxidation film this can cause localized corrosion currents. At higher temperatures these effects are increased due to increases in Kinetics and changes in thermodynamics.

2.6.1.2 ANODIC ENVIRONMENTS

When hydrogen is supplied to the anode at open circuit there is a much larger chemical potential gradient as oxygen concentration will be lower toward the electrolyte as it is ionized and transported to the electrolyte. At the interconnect we can expect slowed oxidation, reduction of certain elements, and hydrogen embrittlement of the interconnect as well as hydrogen transported to the cathode side. In an SOFC stack that uses metallic bipolar interconnects at open circuit voltage (OCV) there is still a very small fuel cell current but the metal becomes the electrolyte and the electron transfer medium. In the case of silver used as a bipolar interconnect with hydrogen and oxygen on the other the hydrogen and oxygen conduction follow Sevierts law and the formation of water due to hydrogen and oxygen meeting in the bulk causes rapid failure. [15] These issues are not such a factor if not using an interconnect as a bipolar plate with oxygen on one side and hydrogen on the other. It is the chemical potential that causes these problems. The kinetics of this type of degradation are increased at higher temperatures.

2.6.2 CORROSION UNDER LOAD

When chemical potential in the form of fuel cell gasses and load placed across the fuel cell an electro motive force (EMF) opposite to one imposed by external current under electrolysis or ambient corrosion will come into existence. Because there are few hydrogen species at the cathode or oxygen species at the anode depending on humidity, oxygen will be consumed at the cathode to oxygen ions and Hydrogen will be converted to protons at the anode. Oxidation of cathode interconnects is more likely due to presences of oxygen ions and gas at the cathode. Other products may be available by the disassociation of water and production of water at the cathode side such as hydroxides. At operating temperature we can expect a combination of dry oxidation and wet corrosion of the interconnects on the

cathode side and faster migration of ions through the film into or out of the metal depending on film type.

2.7 PROTECTION METHODOLOGY

Although metallic interconnects are not the electrodes in SOFC's, they do carry the current, transfer the current through an interface, and are exposed to gaseous environments. Because the film has resistance, there is a potential difference between metals in the interconnect bulk, oxide film, and electrodes. Because these films are both ionic and electronic conductors, we can assume that there will be a corrosion cell within the interconnect structure between the metal and the fuel cell electrode.

Metals in general can be protected by physically sealing from oxygen and water, or impeding the corrosion cell. As seen above, oxide films can slow further attack. [8] This behavior is seen with titanium and aluminium and can be enhanced electrochemically by increasing the corrosion current to give anodized coatings. These coatings become non conductive and therefore protective. The corrosion cell can be modified to change corrosion potential. Corrosion depends on the electrochemical series [7], so imposing a reversed or neutralizing external current as in cathodic protection [8], or using a metal lower in the electrochemical series as a sacrificial anode can halt corrosion. [18] [8] These measures are not possible at high temperature or inside a functioning electrochemical device.

2.8 CORROSION OF STEEL

Corrosion resistant steels are about 300 years old and come in three main varieties: Austenitic, ferritic, and Martenistic. All three systems incorporate chromium in order to control corrosion and increase strength. There are generally 2 types of high temperature corrosion resistant alloy: those containing aluminium and those containing chromium. [10] Alumina is an oxygen ion conductor and forms at the metal/film interface like titanium, silicon and zirconium oxides. Chromia is generally more electronically conductive than alumina, zirconia and titania at higher temperatures but does not conduct oxide ion.

2.9 SOFC INTERCONNECTS

Throughout the late 80's SOFC workers concentrated on lanthanum chromite interconnects[19] However these materials suffer from high cost and strength in compression only, combined with poor electronic conductivity at lower temperatures. A benefit of ceramic interconnects is their resistance to oxidation. Most of these ceramics are poor hydrogen conductors so secondary cells do not occur. As improvements in the electrolyte and electrodes lessened the need for high temperatures, lanthanum chromite interconnects became less desirable[10]. Kofstad and Bredesen recognized the potential for alloys as SOFC interconnects and correctly identified most of the barriers[10]. Their 1992 paper states that alumina forming alloys are to be avoided due to poor electronic conductivity and predicts chromia forming alloys produce hexavalent chromium, which they did not perceive as a problem. Research progressed into other materials including super alloys [20-21] which due to their suitability for gas turbines show promise as interconnects.

However, super alloys owe their high temp oxidation resistance to poor electronic conductivity by inclusion of alumina titania and zirconium. If SOFC ‘s are to be as ubiquitous as ICE’s and not gas turbines, then the material costs need to be similar to ICE’s and not gas turbines. This pure cost driver brings inexpensive steels into the picture.

2.9.1 PROTECTION METHODOLOGY FOR METALLIC INTERCONNECTS FOR SOFC'S

With all the other influences in fuel cells, an interconnect that is perfectly dimensionally stable and only electronically conducting would be the best option. However, at the operating conditions of SOFC, only platinum would be an option, making cost prohibitive.
For the alloys, there are two approaches to create useful interconnects. The first is to put elements into the alloy that will come out under corrosion conditions to form the desired functional layer. The second is to put something on the alloy as a functional layer.
For the first strategy, two alloys formed specifically as interconnects are Crofer from ThyssenKrupp and the ZMG range from Hitachi[22]. These products have shown excellent improvements over commercially available resistance to oxidation in SOFC environments. However these materials also show ability to evaporate chromium in high temperature high humidity situations.

Many workers have offered somewhat successful solutions to halt the evaporation and re-deposition of chromium compounds at the TPB with perovskites, spinels and other materials[23]. However, these additional treatments can be expensive, time consuming and create layers that are not self healing[24].
2.9.2 Protection methodology of cheap steels for fuel cells

Just as corrosion can be considered very similar to metallic fuel cell, fuel cells can be considered wet corrosion cells. Oxidation of fuel is the goal whilst using the released energy to perform work. Water is not always needed for wet corrosion, however most fuel cells tend to have an abundance of water or steam. In PEM fuel cells, the hydrogen is generally supplied with water so the membrane will stay moist, and water is produced at the cathode, where it is often a problem. In SOFC, water is produced at the anode, whereas at the cathode, there is enough water in the air for corrosion to be considered wet. The air must be moist, or evaporation of chromia would not be a problem. [14]

Corrosion inside SOFC's is clearly high temperature in nature. However, due to other influences inside the fuel cell such as protons and water at the cathode interconnect it cannot be considered strictly high temperature and dry.

High temperatures and electronic requirements prohibit the uses of paints and anodized coatings. Coating the interconnects with fully dense electrode material in a fashion similar to cladding could work but dense electrode material is rarely possible and mixed conductance electrode material may not alleviate oxidation of the interconnect as ionic and electronic conductance is still high. Additionally, matching thermal expansion coefficients would be crucial. Clearly the only choices for protecting steels in SOFC's are conductive coatings or local growth of films. For success this layer would need to be thin, continuous, and have poor ionic conductivity for corrosion kinetics to remain sufficiently slow and excellent

electronic conductivity. If there are any voids in the protective layer a local potential difference between the exposed layer and the protective layer can accelerate the destruction of the exposed metal[1].

2.9.3 Alloying for “corrosion resistance” To form films

The most important benefit of corrosion layers on alloys is the self healing nature. When the oxide layer is damaged, it is repaired by exposure to the atmosphere. However there are two major drawbacks. In more complex alloys micro additions of elements used to solve one problem can create or exacerbate another. In the case of corrosion resistance, adding Al will slow corrosion because it is a poor electronic conductor[20]. The second drawback is the corrosion itself. For the protective functional layer to grow reaction with the atmosphere must take place; it must be thermodynamically favorable. The film growth will slow as the corrosion product thickens but it is never stopped until one of the reactants is completely depleted, either from the atmosphere, or from the bulk. The atmosphere is always replenished in SOFC's so the interconnect will always corrode. For corrosion protection to exist under these circumstances there must be corrosion. [1] For wet corrosion the problem is worsened as both electronic conductivity and ionic conductivity are needed for corrosion to take place. [8] Wagner found alloys that formed oxide layers with poor electrical conductivity were better at resisting corrosion by blocking at least one part of the corrosion circuit [1] and alloys with both poor electronic and ionic conductivity are best. Explained in terms of thermodynamics and kinetics, if you can’t stop it, then you have to slow it down. Unfortunately the best oxidation resistant corrosion layers are usually the worst electronic conductors such as aluminium oxide, titanium oxide, ad silicone oxide.

Since before Kofstad suggested chromia forming steels would be applicable to SOFC interconnects in 1992, research into alloys for SOFC has been ongoing. [21, 25] [25-26] [27] [28]. As mentioned above, there are two alloys specifically for the application, Crofer 22 apu manufactured by Thysenn- Krupp and ZMG232 by Hitatchi. Both of these materials have been successful as anode interconnects where reducing gasses slow formation of oxides. In SOFC anodes, the only supply of oxygen will be from the electrolyte. However, as a true bi-pole interconnect, anodic with hydrogen on one side and cathodic with air on the other, chromium poisoning still exists. [14] Even with their excellent SOFC corrosion resistance these materials must be coated with other materials to stay functional within desired time limits.

These state of the art alloys, have as many as 8 extra elements added after iron and chromium[29]. Balancing all the desired functions of the corrosion layer is difficult. Kosftads treatment of corrosion layer thicknesses using differential equations for each individual element and it’s oxide become unworkable with so many variables.

2.9.4 CORROSION LAYER MANUFACTURING AND TESTING FOR SOFC

A literature review will reveal that most coatings and corrosion layers formed on alloys for SOFC interconnect purposes are rarely tested in true SOFC environments[11, 17, 30-31]. These layers are tested by exposure to single gases at temperature but rarely the

electrochemical forces available in SOFC's or with dual atmospheres. This may account for the large amount of alloys and coatings with favorable test results and few commercial outlets. Proof for this can be found when examining chromium poisoning phenomena. Generally speaking, corrosion layers on alloys cannot be formed that are as elegant as coatings that are specifically manufactured and deposited: We should not expect to rust perovskite functional layers in place to the desired thickness and then expect it to stop and stay that way forever. For the desired layer to evolve, thermodynamics must dictate its production. However, it should be noted that materials coated on to steel will have far better adhesion characteristics if some elements are present in both the steel substrate and the coating.

2.10 COATINGS

Many different coatings have been applied to interconnects with many different techniques with varying success[32] [33] [23-25]. Coatings must bond to and form an impermeable barrier with the existing surface of the alloy or oxide layer. Coatings must also have compatible behavior with the exterior interface (ceramic and atmospheric). Application techniques include tape casting, sol gel deposition, painting, inking, screen printing, impregnation, magnetron sputtering, radio frequency sputtering, EVDP, and so on.

There are some drawbacks to all coatings: There are additional processing steps and related expense, no self healing behavior and in many cases added fragility. Lack of self healing is a problem for all engineering coatings from paint to high tech ceramic coatings. In the oldest case of paint on iron, if the paint is scratched the metal will corrode and continue to corrode under the paint. Imperfections in the paint at application such as pin holes maybe unnoticeable, however corrosion will start at the pinhole and continue under the paint in the surrounding area. In the case of dimensionally stable anode (DSA) for wet electrochemistry applications such as water treatment, ruthenium and rubidium oxide are coated onto titanium. If in initial application there is a pinhole or if the coating is damaged then the electrode at that area will be rendered ineffective. Titanium is chosen as the substrate because of its passivation behavior in most environments, however there are conditions where the titanium will be consumed under the coating and the whole electrode rendered useless.

2.11 HYBRID APPROACH

A hybrid approach could be considered: use a coating on the alloy that adds elements that are not in the bulk alloy to create a functional layer containing elements from the bulk, the coating, and the atmosphere. By adding an element, products may be formed that were not possible by alloying alone, but with better bonding to the oxide layer than coating alone.

The final layer should have all the properties of coatings or films mentioned in previous sections. Additionally, similar to Teflon and poly vinyl di fluoride (PVDF) with respect to fluoride, the coating should be stable or saturated with chromium. This offers chromium as one of the elements available from the metal bulk.

One possible advantage is to adding a single element layer is the fact that final product will have a finite layer thickness, as corrosion of substrate is limited by supply of elements in the coating. Here the thickness of the coating is crucial: too much additional element and the desired functional material may not be formed in a short enough time scale. If the layer is too thin there may not be enough additional element to form a functional layer and instead form a low concentration impurity and not a new material.

Under the right circumstances it may be possible to form the desired corrosion products of a more expensive alloy without the drawbacks of adding these elements to the bulk whilst also limiting the corrosion and chromium evaporation. This could equate to cheap steels retaining their pretreatment machineability, whilst gaining the functionality of more expensive materials post treatment.

2.12 MATERIALS SELECTION

2.12.1 SUBSTRATE SELECTION

SS430 was found to have most of the desired properties with only high temperature corrosion resistance and chromium volatility suppression missing. Many researchers have specifically selected SS430 for study for these reasons and enabling SS430 for interconnects is a major ongoing research goal of the SOFC community.

When selecting materials to protect SS430 it should be noted that its oxidation is of the chromia type For reasons of compatibility, and possible adhesion, final corrosion/coating products of a similar nature to chromia should be of great interest. A major property of SS430 is that its CTE is compatible with SOFC ceramics. [28]. The corrosion film should also have similar CTE.

2.12.2 DESIRED LAYER

2.12.2.1 CHROMIUM TITANATE

A similar material to Cr_2O_3 is Ti-doped chromia. Doping chromium oxide with low percentages of titanium has many advantages and some disadvantages. The general formula is $Cr_{2-x}Ti_xO_3$.

- It is structurally indistinguishable from un-doped chromia using standard laboratory x-ray diffraction. This makes identification by XRD difficult especially when coated onto steel substrates.
- Its CTE is similar to the un-doped chromia.
- It is more stable and less volatile for chromium evaporation than Cr_2O_3 in humid environments. Evidence is provided by the Williams patent[34]. A higher resistance to humidity would also suggest a higher resistance to chromium 6 evaporation, as humidity has been the key to chromium 6 evaporation in SOFC's[14]. In essence, titania stabilizes chromia in wet environments.

- Its resistance to humidity is the reason CTO is used as a commercial gas sensor. Consequently, properties are well studied. It is a P-type semiconductor[35]. Also studied for gas sensors are iron titanates[36-37]. This will have relevance if iron titanates are also corrosion products of steel with micro additions of Ti. There are standard production techniques for depositing CTO and FTO on many different surfaces.

2.12.2.2 CHROMIUM DOPED RUTILE

At the other end of the Chromia/titania phase diagram is chromium doped titania. TiO_2 and reduced titania are well studied materials.

- TiO_2 gives Titanium metal its excellent corrosion resistance and the reason that titanium rates so well on the galvanic scale when it is so readily oxidized. However it is a poor conductor of electrons, which is unfortunately why it is such a good corrosion protection layer[9].

- It has a CTE similar to that of titanium metal (8.6µm/(m^oK) at 25^oC) at 7.14µm/(m^oK) for perpendicular to the xy plane and 9.19µm/(m^oK) for parallel to the xy plane.

- TiO_2 conductance can be improved by reduction of rutile to Magneli phases or doping with other elements such as Niobium or Chromium. Both of these strategies are well studied. Chromium doped titania and chromium and niobium doped titania have been studied as gas sensors and SOFC electrodes because of their stability and conducting behavior [38].

Although Magneli phase titania has been used in wet electrochemistry as anodes and cathodes, it oxidizes readily in high temperature oxidizing environments[39]. Reduction of rutile like coatings or maintenance of reduced coatings by fuel at the anode may stop protonic conduction through the metal halting embrittlement and production of water at the cathode side of the interconnect.

Doped Titania is more resistant to oxidation as it is already at max oxidation. It is orders of magnitude more conductive than TiO2 which is relevant to cathode side of interconnect[40].

Further reduced doped titania has also been studied as electrodes for electrochemistry with favorable results over un-doped Magneli phases. These materials show better oxidation resistance than undoped rutile when reduced and can be cyclically reduced [40].

For all of these materials, chromium can be provided from the SS430 by evaporation. Titanium can be deposited several ways including sol-gel, EVPD or even cladding.

Adding a small amount of Ti to the surface will allow localized production of the desired compounds where additions of Ti to the bulk would make machineability difficult and production expensive. The chances of making pure compounds this way is extremely remote, however, on both ends of the Ti/Cr spectrum there are compounds that might work as electronic conductors and have good chromium retention. Although these might not be the materials that are grown on the surface, the other corrosion products that are possible ,

such as FeTiO have also been researched as gas sensors, and therefore may be conductive enough should the functional layer be thin enough. By limiting the thickness of the Ti layer to a very small thickness we limit the thickness of the produced layer and therefore limit the undesired effects of resistance.

2.12.2.3 CHROMIUM COBALT SPINEL

Although not a terribly good conductor, chromium cobalt spinels have been used by other researchers for the specific purpose of sequestering chromium that would otherwise evaporate from the interconnect and redeposit at the triple phase boundary[41].

2.13 PROJECT GOAL

The aim of this project is to coat SS430 with Titanium or Cobalt to form a barrier layers by corrosion to improve SS430's corrosion properties when used as an interconnect for solid oxide fuel cells. The first objective is to evaluate cobalt chromium spinels and titanium chromium eskolaites for their ability to retain chromium in conditions where evaporation of chromium has been demonstrated as a problem for SOFC interconnects.

The next objective is to form chromium titanium eskolaites on the surface of SS430 and evaluate its performance as an interconnect layer.

The third objective is to use techniques discovered for titanium deposition on SS430 for the production of similar layers and oxide layers containing chromium cobalt spinels.

REFERENCES

1. Evans, U.R., *An Introduction to Metallic Corrosion*. 3rd ed. **1981**, london: Edward Arnold.
2. Mikhail, R.S.G., V. K., *Rate of oxidation of magnesium metal in dry oxygen.* Journal of Applied Chemistry, **1960**. **10**(9): p. 384-388.
3. Gregg, S.J.J., W. B., *148. The oxidation of calcium in dry oxygen.* Journal of the Chemical Society (Resumed), **1960**: p. 712-716.
4. Gregg, S.J.J., W. B., *186. The oxidation of calcium in moist oxygen.* Journal of the Chemical Society (Resumed), **1961**: p. 884-888.
5. Chilton, J.P., *Principals of metallic corrosion*. Monographs for teachers **1973**, Londo: chemical society.
6. Schennach, R. *Theory of metal oxidation*. Available from: http://www.staff.tugraz.at/robert.schennach/Theory_of_Metal_Oxidation.pdf.
7. University of Edinburgh, *Corrosion of metals*, agvailable at *http://www.cmse.ed.ac.uk/MSE3/Topics/MSE3-corrosion.pdf*, U.o. Edinburgh, Editor. 2001-**2002**, University of edinburgh: Edinburgh. p. 9.
8. Evans, U.R., *Mettalic Corrosion, Passivity and Protection*. 1 ed. **1937**, London: Edward Arnold.
9. Kofstad, P., *High temperature corrosion*. **1988**: Elsevier Applied Science, London, newyork.
10. Kofstad, P.B., R., *High temperature corrosion in SOFC environments.* Solid State Ionics, **1992**. **52**(1-3):
11. Li, Y.J., Y.; Wu, J.; Pineault, R.; Gemmenn, R.; Liu, X., *Corrosion Behavior of Ebrite and SS430 in Coal Syngas with Loaded Current.* International Journal of Applied Ceramic Technology, **2010**.
12. Froitzheim, J.H.R., E.; Larsson, L. G.; Johansson, J. E.; Svensson, *Investigation of Chromium Volatilization from FeCr Interconnects by a Denuder Technique.* Journal of The Electrochemical Society, **2010**. **157**(9): p. B1295-B1300.
13. Konysheva, E.P., H.; Wessel, E.; Mertens, J.; Seeling, U.; Singheiser, L.; Hilpert, K., Chromium Poisoning of Perovskite Cathodes by the ODS Alloy Cr5Fe1Y[sub 2]O[sub 3] and the High Chromium Ferritic Steel Crofer22APU. Journal of The Electrochemical Society, **2006**. **153**(4): p. A765-A773.
14. Povoden, E., |Thermodynamic database of the La-Sr-Mn-Cr-O oxide systems and applications to solid oxide fuel cells, in Swiss Federal Institute of Technology, Zurich. **2008**, Swiss Federal Institute of Technology, Zurich: Zurich. p. 188.
15. Singh, P.Y., Z.; Viswanathan, V.; Stevenson, J., *Observations on the structural degradation of silver during simultaneous exposure to oxidizing and reducing environments.* Journal of Materials Engineering and Performance, **2004**. **13**(3): p. 287-294.
16. Yang, Z.W., M.S.; Singh, P.; Stevenson J.W.; Norby, T., *Oxidation Behavior of Ferritic Stainless Steels under SOFC Interconnect Exposure Conditions.* Journal of The Electrochemical Society, **2004**. **151**(12): p. B669-B678.
17. Yang, Z.G.X., G. G.; Stevenson, J. W.; Singh, P., CORROSION BEHAVIOR OF INTERCONNECT CANDIDATE ALLOYS UNDER AIR//SIMULATED REFORMATE DUAL EXPOSURE CONDITIONS, in Advances in Solid Oxide Fuel Cells Iii, N.P. Bansal, Editor. **200**8, Amer Ceramic Soc: Westerville. p. 279-288.

18. Wranglen, G., *An Introduction to Corrosion and Protection of Metals*. **1972**, Stockholm: Institut For Metallskydd.

19. Zhu, W.Z.D., S. C., *Development of interconnect materials for solid oxide fuel cells.* Materials Science and Engineering A, **2003**. **348**(1-2): p. 227-243.

20. Quadakkers, W.J.P.-A., J.; Shemet, V., *Metallic materials in solid oxide fuel cells.* Materials Research, **2004**. **7**: p. 203-208.

21. Zhu, W.Z.D., S. C., Opportunity of metallic interconnects for solid oxide fuel cells: a status on contact resistance. Materials Research Bulletin, **2003**. **38**(6): p. 957-972.

22. Thyssen-Krupp, Crofer 22 APU Material data Sheet no. 4046 **2006**.

23. Chen, X.H., P. Y.; Jacobson, C. P.; Visco, Steven J.; De Jonghe, L. C., *Protective coating on stainless steel interconnect for SOFCs: oxidation kinetics and electrical properties.* Solid State Ionics, **2005**. **176**(5-6): p. 425-433.

24. Konysheva, E.L., J.; Wessel, E.; Tietz, F.; Christiansen, N.; Singheiser, L.; Hilpert, K., *Influence of different perovskite interlayers on the electrical conductivity between La0.65Sr0.3MnO3 and Fe/Cr-based steels.* Solid State Ionics, 2006. **177**(9-10): p. 923-930.

25. Gannon, P.E., et al., Enabling inexpensive metallic alloys as SOFC interconnects: An investigation into hybrid coating technologies to deposit nanocomposite functional coatings on ferritic stainless steels. International Journal of Hydrogen Energy, **2007**. **32**(16): p. 3672-3681.

26. Montero, X.J., N.; Piron-Abellan, J.; Tietz, F.; Stover, D.; Cassir, M.; Villarreal, I., Spinel and Perovskite Protection Layers Between Crofer22APU and La[sub 0.8]Sr[sub 0.2]FeO[sub 3] Cathode Materials for SOFC Interconnects. Journal of The Electrochemical Society, **2009**. **156**(1): p. B188-B196.

27. Geng, S.J.Z., J. H.; Lu, Z. G., *Evaluation of several alloys for solid oxide fuel cell interconnect application.* Scripta Materialia, 2006. **55**(3): p. 239-242.

28. Quadakkers, W.J.P.-A., J.; Shemet, V.; Singheiser, L., *Metallic interconnectors for solid oxide fuel cellsa review.* Materials at High Temperatures, 2003. **20**: p. 115-127.

29. Thyssen-Krupp, *Crofer 22-apu*. 2006.

30. Chen, X.H., P.Y.; Jacobson, C.P.; Visco, S.J.; De Jonghe, L.C., Protective Coating on Stainless Steel interconnect ofr SOFCs. Oxidation kinetics and Electrical Properties. Solid State Ionics, May 2004.

31. Purushotham, K.P.W., L. P.; Brack, N.; Pigram, P. J.; Evans, P.; Noorman, H.; Manory, R. R., *Corrosion behavior of Zr modified CrN coatings using metal vapor vacuum arc ion implantation.* Journal of Vacuum Science & Technology A, 2007. **25**(1): p. 110-116.

32. Quadakkers, W.J.G., H.; Hänsel, M.; Pattanaik, A.; Khanna, A. S.; Malléner, W., *Compatibility of perovskite contact layers between cathode and metallic interconnector plates of SOFCs.* Solid State Ionics, 1996. **91**(1-2): p. 55-67.

33. Brylewski, T.P., K.; Morgiel, J., Microstructure of Fe-25Cr/(La, Ca)CrO3 composite interconnector in solid oxide fuel cell operating conditions. Materials Chemistry and Physics, 2003. **81**(2-3): p. 434-437.

34. Williams, D.E.P., K. F. E, *multi electrode gas sensors and methods of making and using them*, in *http://www.freepatentsonline.com/5918261.pdf*, U.P. office, Editor. 1999: USA.

35. Naisbitt, S.C.P., K. F. E.; Williams, D. E.; Parkin, I. P., A microstructural model of semiconducting gas sensor response: The effects of sintering temperature on the response of chromium titanate (CTO) to carbon monoxide. Sensors and Actuators B: Chemical, 2006. **114**(2): p. 969-977.

36. Luthra, V.P., K. F. E.; Palgrave, R. G.; Williams, D. E.;Tandon, R. P.; Parkin, I. P., *Fabrication and characterization of Fe1.90Ti0.10O3 gas sensitive resistors for carbon monoxide.* Sensors and Actuators B: Chemical, 2009. **135**(2): p. 430-435.

37. Luthra, V.P., K. F. E.; Palgrave, R. G.; Williams, D. E.;Tandon, R. P.; Parkin, I. P., *Gas-sensing properties of Fe2-xTixO3+[gamma] (x = 0-1.4).* Polyhedron, 2010. **29**(4): p. 1225-1230.

38. Lashtabeg, A., Niobium based materials for use as current collectors in the anode of Solid Oxide Fuel Cells, in chemistry. 2004, University of St Andrews: St Andrews. p. 243.

39. Smith, J.R.W., F. C.; Clarke, R. L., *Electrodes based on Magnéli phase titanium oxides: the properties and applications of Ebonex® materials.* Journal of Applied Electrochemistry, 1998. **28**(10): p. 1021-1033.

40. Chen, G.W., C. C.; Cho, H.; Macdonald, D. D.; Mallouka, T. E., *EIS Studies of Porous Oxygen Electrodes with Discrete Particles.* Journal of The Electrochemical Society, 2003. **150**(9): p. E423-E428.

41. Bateni, M.R.W., P.; Deng, X.; Petric, A, *Spinel coatings for UNS 430 stainless steel interconnects.* Surface and Coatings Technology, 2007. **201**(8): p. 4677-4684.

3 EXPERIMENTAL PROCEDURES

3.1 EXPERIMENTAL CLASSIFICATION

Experiments break down into two types: Preparation and evaluation. Preparatory experiments were necessary to find the exact procedure to produce the desired product. For example, there are various sputtering techniques to deposit cobalt or titanium onto stainless steel, and there are various formulations of sol-gel to produce a coating. Not all systems work. Evaluation experiments are used to test produced formulations for effectiveness.

3.2 SAMPLE PREPARATION

Sample preparation breaks down into the sub categories of materials to be coated and materials for coating.

3.2.1 SUBSTRATES

Substrates were prepared by sanding with 600 grit sand paper, cleaning with acetone and drying near 80℃. Some samples were pre-oxidized prior to coating by heating in air at various temperatures ranging from 350 to 450°C. This was to form a rough, chromium rich surface that could react with coatings to form new materials.

Materials to form coatings break down into 3 types: powders, sol-gel, and evaporation targets, slivers of thin metal.

3.2.2 POWDER PREPARATION FOR COATINGS AND SOLIDS

Powders formed by solid state synthesis generally go through the steps of mixing, grinding with mortar and pestle, ball milling, sintering, and repeat[1].

Many of the properties of ceramics formed by solid state reaction depend on preparation techniques. Finer starting powders translate to better mixing, better sintering, and a more homogenous product[2]. This is partly due to the increased solid state diffusion because of shorted diffusion distances.

3.2.2.1 Mixing for solid state synthesis

All materials were weighed using a college balance and mixed with a mortar and pestle for 20 minutes with acetone. After initial grinding, further ball milling was required.

3.2.2.2 BALL MILLING

The mixture from the above step was decanted into a plastic bottle to which zirconia balls were added along with acetone as a lubricant and a dispersing agent. All powders were ball milled for 24 hours at 100 RPM with a custom ball mill.

3.2.2.3 PELLETIZING

After ball milling some samples were pelletized and these pellets were sent for initial sintering. Pelletizing ensures close contact for solid state diffusion of elements throughout the sample.

3.2.2.4 INITIAL SINTERING

Materials were sintered using a Carbolite muffle furnace with ramp rates of 3^{o}C/minute. Samples were held at sintering temperatures for 24 hours. Unless otherwise stated cooling rates were between 3 and 5^{o}C/minute.

Following sintering, samples were crushed, re-ground with a mortar and pestle, ball milled and sintered again at least once. Samples were tested for phase purity with X-Ray diffraction.

3.3 SOL-GEL

The basic sol-gel process generally follows the steps of mixing correct stoichiometric ratios of organometallic complexes, organic fuels and possibly oxidizers and dispersing agents to form a mixture of colloidal metals, solvent and oxidizer[3]. The aim is to from a nano-mixed colloidal suspension, slowly evaporate solvent to a form a super critical gel and combust to rapidly oxidize the nano-colloidal mixture to from super fine powders. Powders made by sol-gel are finer, better mixed and more uniform than powders by solid state synthesis. Processing is faster as there is no need for grind/sinter/repeat cycles used for solid state synthesis[4].

Following synthesis some sol-gels were pelletized and sintered and some were left as powders. All were tested for phase purity.

3.3.1 CTO SOL-GEL 1

Titanium tetrabutoxide was mixed with chromium (111) nitrate, ammonium citrate and propylene glycol to form the sol-gel the mixture. It was heated and mixed using a hot plate until it was thick and viscous. The final product destination dictated the next steps. For some experiments, gel was painted directly onto substrates and heated. For other experiments, the gel was fired to form a powder which was then reground and re sintered and either used as a base for ink or paint or fired into a pellet.

By the nature of their constituents, many sol-gels form aggressive combustion materials. A mixture of hydrocarbon fuel, oxidizer, and metal particles ready to change oxidation state will always have very aggressive kinetics. As can be seen from the above ingredients, ammonium nitrate becomes one of the constituents. For some experimental procedures these materials are combusted in lab beakers on hot plates. However this process is generally not vigorously controlled.

In some cases combustion is so hot that the materials sinter during combustion. Unfortunately the combustion is so fast that a correct peak temperature cannot be read and so hot that it may not be possible to dissipate the heat properly. However, maximum temperatures could be calculated based on the quantities present and the heat transfer characteristics of the beaker.

This is the case with the above mixture for producing CTO. As such, gels with the above recipe were not appropriate for making coatings on steal. There was little to no adhesion from these gels, and all that remained from these samples was ultra fine powders on the surface of the steel.

3.3.2 CTO SOL-GEL 2

The above formula was adjusted to remove the resulting mixture of ammonium nitrate, by the substitution of chromium nitrate for chromium chloride. The remaining steps were the same for this sol-gel[3].

3.3.3 COBALT CHROMIUM SOLGEL

Chromium cobalt spinel was manufactured using the sol-gel method by mixing cobalt carbonate, chromium (111) nitrate, ammonium citrate and propylene glycol in the correct proportions to form the sol-gel the mixture. It was heated and mixed in a beaker on a hot plate until it was thick and viscous, then combusted in the beaker. None of the cobalt containing sol-gel solutions were used for coatings, only for pure materials for the evaporation study.

3.4 EVAPORATION (SPUTTER) COATING

There are several physical deposition techniques for depositing elemental metals onto surfaces[5], however, only evaporation was available. This technique was re-developed in-house due to the poor results of other techniques used to deposit titanium and chromium titanate onto SS430. After much trial and error testing, a way of depositing Ti onto surfaces using an evaporator was found. Materials to be evaporated were cut into 3mm by 25mm strips from 0.01mm thick sheets of Ti acquired from Advent.
These strips were folded in half to form long U shapes and inserted in into the heating elements of the evaporator. The U shape forced a spring connection into the heating coil which performed the dual functions of added heat conductance into the Ti and short circuiting the coil, to which provides additional electro resistive heating through the target.

The evaporator was originally intended for coating epoxy-mounted samples with gold for SEM viewing. The evaporator consists of a rotary vane vacuum pump, a diffusion pump, a variable power supply for the heating elements, hand-wound tungsten heating coils, a control circuit and a glass dome chamber. After the Ti foil targets were placed in the heating coil and a vacuum was drawn of $3x10^{-5}$ bar, the heating elements were energized to melt the

titanium. The evaporation was complete when the Ti disappeared and coated the inside of the dome and the substrate with a durable metallic layer.

Many challenges were encountered before proper titanium sputtering was achieved. If the titanium foil strip was too wide or the power level too low, titanium would fuse to the tungsten and become brittle. Removal of the brittle Ti from the heating element usually resulted in breakage of the element. If the power level was not high enough for sublimation, liquid Ti would fuse with the W heating element, resulting in a metal solution resulting in replacement. Repeated attempts to sputter Ti with contaminated tungsten elements would end with brittle titanium targets stuck to the tungsten. However, repeated experiments of this type still deposited a thin layer of material on the SS430 substrate. This layer usually had a blue or green color.

When using gold with the evaporator, the instructions suggest slowly increasing the power through the heating coils until the gold evaporates. However, with titanium, this method would again result in brittle titanium strips stuck to the heater. Best results were found when maximum current was used at the start so that heat would continue to rise rapidly and flash the titanium away.

The maximum measured current recorded by the evaporator was 13 amps. The resistance of the heating coils was measured at .5 ohms. The voltage was calculated to be 6.5V and the power was calculated to be 85 Watts.

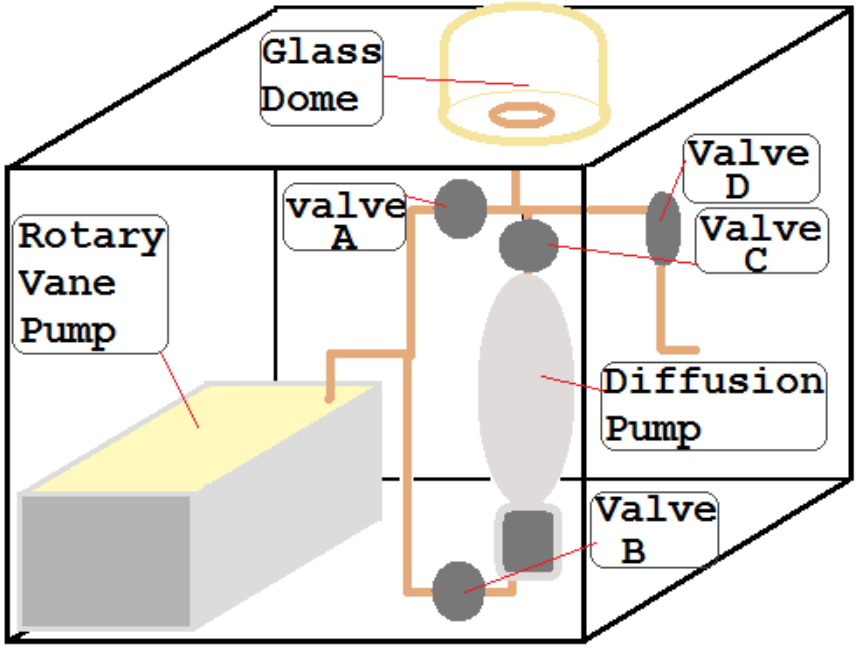

Fig.3.1: The evaporator

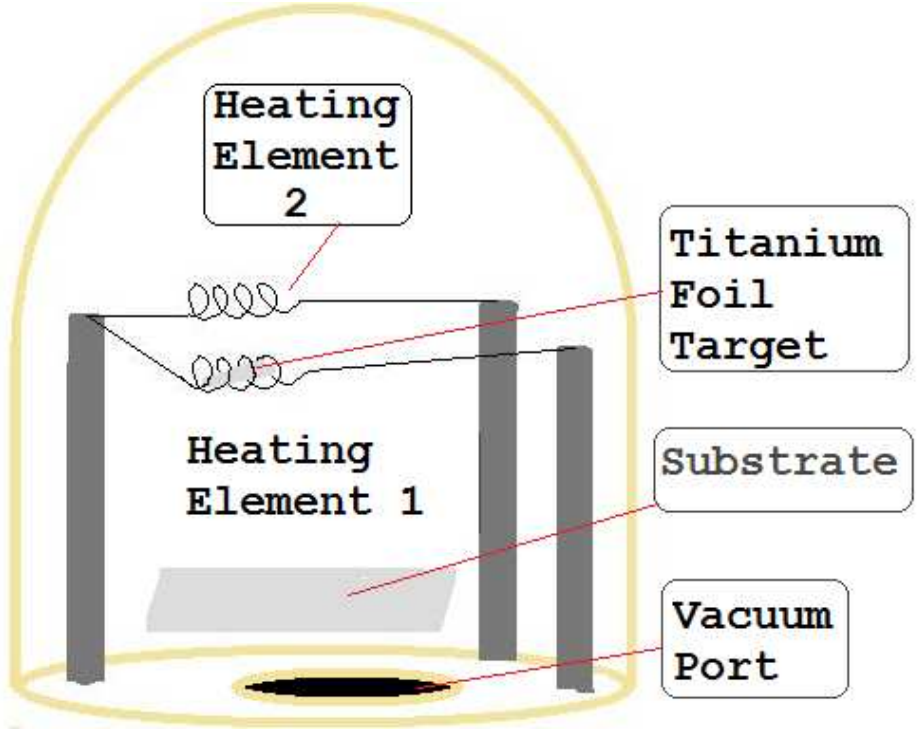

Fig.3.2: Inside the glass dome.

These layers are very thin due to the small mass of material to be spread (target) and the distance of the substrate to the target and the surface area that encompasses. Evaporation is indiscriminate and will coat everything spherically from the centre of the target outward. The equation $T = m/(4\rho * \pi * r^2)$ where *T* is the thickness of the coating, ρ is the density of the target, and r is the distance between the substrate and target describes the thickness of the coating with the input parameters of m for mass of target used, and r which is distance between the target and substrate.

3.5 CORROSION EXPERIMENTS

Corrosion experiments break down into two groups: tests where only heat is applied and symmetrical cell testing where materials were heated with a current load whilst resistance was measured.

3.6 METALS HEATING

Materials that were to be tested were placed in a furnace. Temperatures and ramp rates were chosen based on the materials and desired observations. Ceramics and composite ceramic/metal samples were heated at 2-3 degrees/min and cooled at the same rate to lessen the stresses of CTE mismatch. Metals were heated and cooled at higher rates depending on the corrosion layer and substrate CTE's.

3.7 SYMMETRICAL CELL TESTS

Symmetrical cell tests were performed on materials that showed promise from heating experiments. These tests consisted of treated and untreated interconnects separated by LSM pellets or tapes.

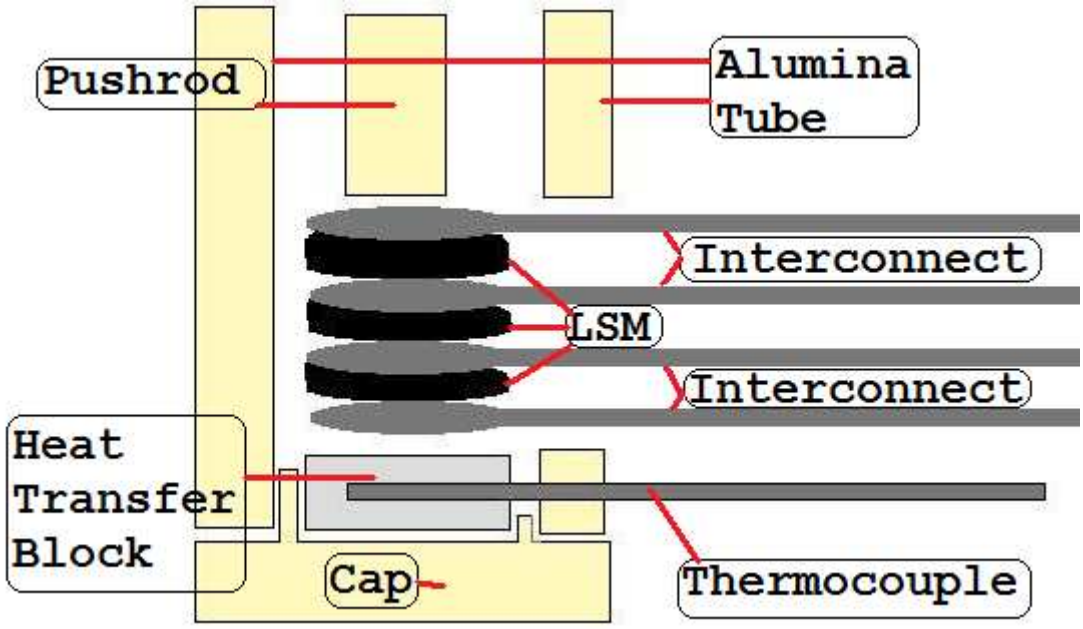

Fig.3.3: Working tip of stack rig

Experiments of this type broke down into tow sub groups: tests that utilized pre-sintered pellets and tests that utilized pellets sintered in place and had pre cast and sintered pellets of LSM. Pre-sintered pellets were manufactured from commercial LSM powder which was pressed to form 10mm by 2mm pellets that were fired at 1400^{o}C then sanded flat with 600 grit silicon carbide sandpaper and washed in acetone, then dried.

3.8 IN SITU SINTERING OF LSM TAPES

Some symmetrical cell experiments used green LSM tapes that were 2 layers thick. The tape was obtained from St Andrews Fuel Cells and was manufactured according to their standards using a tape casting machine. Disks of LSM were cut using a 10mm laboratory cork cutter and two were stacked. Each of these two layer tapes were placed between interconnects in the stack. Initial experiments showed that disks would be displaced with applied pressure and moderate heat. This would cause an electrical short. To alleviate this, the pressure from the rod was not applied until the tapes had been heated in place to 700^{o}C. The usual sintering temperature is much higher. However, removal of the solvents was the primary goal which would avoid displacement of the LSM. After heating for a day, the push rod was tightened and the power was applied.

There are two routes to in situ sintering: the first being direct heating from the furnace and the second being heat added from electro-resistive heating. The heat transfer block and thermocouple were added to measure the in situ temperature of the stack, and was it shown to be 100^{o}C higher than the furnace temperature.

Heat added by electro-resistive heating follows the two equations $P=I^2$ where P is power, I is current and R is resistance and $Q=MC_p(T_{hot}-T_{cold})$ where Q is heat, M is mass, Cp is the heat capacity, and T is temperature. Equating Q to P gives $I^2R=MC_p(T_{hot}-T_{cold})$. T_{cold} is the furnace temperature, so calculating the T_{hot} requires knowledge of current, resistance, the mass to be heated, its heat capacity, and heat transfer losses. Assuming that there are no convective or radiative cooling mechanisms, it may be possible to ignore those heat transfer losses as a first best guess. Finding the heat transfer coefficient *h=(delta Q)/(A*delta T* delta t)* for a composite LSM/SS430 stack would require knowledge of the area *A*, the changes in heat loss, *Q*, change in temperature *T* and the change in t time. The addition of the heat transfer block with thermocouple allowed measurements of the change in temperature due to electro resistive heating. One of the main assumptions for electro resistive heating is that the interfacial area is continuous. However, if the interface surfaces do not contact completely and there are point contacts instead, then the surface area is much lower and, the temperature will be considerably higher locally as the parameter *A* will be smaller for the same heat flux. This implies that even higher temperatures than recorded may be present at the highest resistance areas, namely, the interfaces between LSM and interconnect and the LSM.

3.9 INTERCONNECTS

Interconnects were made from SS430 foils with various coatings installed. After shaping with sharp scissors, the interconnects were flattened using a hydraulic press with 5 metric tonnes of pressure. After flattening, they were lightly sanded with 600 grit, cleaned with acetone, and coated with titanium.

3.10 SAMPLING

As mentioned above, the second sub category of experiments is focused around testing of performance.

3.10.1 X-RAY DIFFRACTOMETRY (XRD)

A Phillips X'pert PW 3020 diffractometer with a Cu radiation source was used to identify compounds and corrosion layers. Powders were ground to a fine powder using a pestle and a mortar. Pellets and plates were sampled directly. Powders were placed on an aluminium plate before being placed into the diffractometer. A typical run was carried out over a period of 1 1/2 hours.

3.10.2 PATTERN COLLECTION

X-ray diffraction is a technique that uses the wave properties of high energy photons to fit between small gaps on a sample at the atomic scale. It relies on the wave property of photons and their constructive or destructive interference when put through small holes. Instead of holes, the gaps between atoms in the sample are used. As the waves pass between the atoms and are diffracted, the intensity of the peak for the corresponding angle is defined. The sample is rotated through a series of angles, each angle generating a

specific peak. The peaks correspond to angles where or x-rays constructively interfere as a function of whole number wavelengths, which in turn informs the positions of atoms in the crystal lattice and the distances between the atoms. From the peaks we can calculate unit cell size and type, position of atoms in the cell, phases present, symmetry and space group of the crystal system.

Most crystalline materials have their own unique X-ray patterns and the technique can be used to identify individual crystal structures. If one or more known materials are present, it can be used to find extra peaks of new materials or deviations of known ones. This is not always the case with materials that are doped with very small amounts of similarly sized atoms.

Monochromatic x-rays are produced when a beam of electrons provided by an electron gun, which consists of heated tungsten filament, is accelerated through a potential difference of 30 – 50 kV to strike a metal target. The incoming electron knocks out an electron from the 1s orbital which has to be filled from an outer orbital, such as 2p or 2s. As a higher energy electron fills the vacant hole, it loses a quantum of energy in the form of a high energy photon, in the frequency range of x-rays. If the higher orbital filling the lower orbital is always the same, then the frequency and wavelength of the photon will also be fixed. In the case of Cu going from 2p to 1s has a fixed wavelength of 1.5418 Å. Undesired frequencies can be filtered out with metal foils and single crystals.

3.10.3 BRAGG'S LAW

Peaks that are recovered and their corresponding transmission angles can be applied to Bragg's law, which states that two monochromatic light beams diffracted by parallel plates are in phase if the total distance traveled is different by whole number wavelengths only. This comes from the mathematical derivation that the extra distance travelled is

$$xy = yz = d\sin\theta$$

$$xyz = 2d\sin\theta$$

$$xyz = \mathrm{n}\lambda$$

Which leads us to Bragg's law given by [6]

$$2d\ \sin\ \theta\ =\ \mathrm{n}\lambda$$

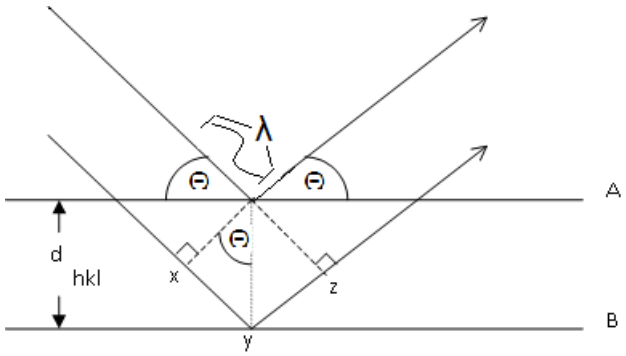

Fig.3.4: Graphical interpretation of Bragg's law

The above graphic shows parallel planes A and B which represent the distance between two planes in a crystal. The fixed frequency parallel X-Rays approach the A and B planes at angle θ with wavelength λ . The extra distance travelled is a function of the angle and the amount of full extra wavelengths travelled. When the light wave peaks arrive at opposite peak hights, no peak is formed. When the peaks coincide the interference is constructive and a peak is generated. This peak is at $n\lambda$, where n is a whole number. Using the diffraction peaks for known angles we can find *d* for all the spaces between the atoms and using furrier transforms the spaces between all the atoms can be calculated.

3.11 SCANNING ELECTRON MICROSCOPY

Scanning electron microscopy is similar to microscopy but instead of light shining on the work piece, it is bombarded with electrons. At the top of the microscope is an electron gun, which is formed by a heated tungsten cathode, and an anode which are both connected to a high voltage dc power supply in order to accelerate the electrons freed from the tungsten, in a similar fashion to the XRD. The electron beam is filtered and focused by coils or plates which are used to scan the beam over the surface of the piece to be viewed in much the same way as a cathode ray tube delivers electrons to phosphorescent dots on a TV picture screen. As each position is sampled the electrons bounce back and are caught by a detector. As the electrons are scanned across the surface, an image is created by combining the individual positions.

Other information can be gathered by the SEM providing it is fitted with other specialized detectors. X-rays gathered from electrons hitting inner valance electrons can give information about the elements hit. Back scatter detectors can be used to gather electrons bounced from the sample elastically, which can give information about the elements in the sample and be used to give an element map.

3.12 ELECTRICAL RESISTANCE

Resistance of coatings can be difficult to measure, especially if the coating is on a highly conductive substrate like steel. Four point probe resistance measurements are not valid when the vast majority of the current is passing through the substrate. Four point resistance measurements are best when applied to a single material, or a coating on an insulator. Because many of the coatings used in this work were manufactured from a single element evaporated onto a steel surface and chromium coming from the steel, surrogate non conductive substrates could not be substituted for steel. The coatings were too thin to be removed from the steel.

The thin and somewhat delicate nature of these coatings also meant that ohmmeter readings were problematic. Pushing too hard with the probes could pierce the coating and measure the resistance of the steel only. Electrical resistance measurements had to be recovered some other way.

3.12.1 IMPEDANCE SPECTROSCOPY

Impedance spectroscopy was employed to measure the resistance and impedance of certain coatings. In the case of Ti coatings, the resistance is a function of the time and temperature of corrosion. For instance, if low temperatures were used, only rutile was produced, which is a known insulator. For longer durations and higher temperatures, more conductive, less capacitive coatings are expected. [7]

Impedance spectroscopy is a technique where an ac load is put on the materials in question. Varying the frequency of the load can determine different characteristics of the materials electrical and physical properties. The data was recovered automatically using a Hewlett Packard impedance analyzer. Frequency range and voltage were adjustable. Analysis was performed in Z-view.

3.12.2 SYMMETRICAL CELL RESISTANCE MEASUREMENTS

The majority of the resistance measurements were taken using the rig from section symmetrical cell testing. In this system, DC power is applied to the end interconnects and voltage is read at the two middle interconnects and at each end interconnect. This way several readings can be obtained from a single electrical source. The contributions to resistance in this system are from the interconnect base material, the LSM, and the interface. This interface is comprised of the outside layer of LSM, where it touched the corrosion layer, the corrosion layer and the area where the corrosion layer touches the steel interconnect.

One drawback of this technique is the assumption that the temperature is constant. Current added to the system will make additional heat in the form of Joule resistive heating. This heat can dramatically change the temperature of the system and also its resistivity.

3.13 THERMOGRAVIMETRIC ANALYSIS (TGA)

TGA analysis can show how much weight is gained in a sample, the temperature at which this occurs and reversibility[8]. It can be used to measure oxidation, or in other atmospheres, other phenomena. In order to characterize the affect of titanium coatings on SS430, TGA was attempted on samples of SS430 that were both coated and un-coated using a TGA 1000+. Unfortunately, the results gathered were not usable due to the magnetic nature of the sample. This would imply that the TGA 100+ does not have a counter-wound furnace. It is essentially a magnetic coil in addition to a heater. It's likely that the switching element of the heating power control circuit is a zero crossing solid state relay. These devices allow power into the heating coils at a specific part of the AC sine wave and turn off as the voltage hits zero. If the control circuit is always starting on the same side of the AC sine wave then a net DC or pulsed DC current is imposed on the coil. In combination, these two factors create a magnetic field inside the TGA furnace, mostly pointing in one direction. This will affect any material that has magnetic properties. For SS430, these magnetic properties stop at the Curie temperature of 700^{o}C

One way of dealing with this would be to turn off the power to the furnace during times when the balance is reading. Another way would be to counter-wind the furnace coils with exactly the same amount of clockwise and counter-clockwise turns to eliminate all electromagnetic forces. Unfortunately neither of these measures seems to have been taken.

One of the most important pieces of information that can be retrieved from the TGA is the temperature at which oxidation starts to increase.

The TGA1000+ was useful for measuring weight gain rates at fixed temperatures above the Curie point.

3.14 ALTERNATIVE TGA

In order to find the changes take place at elevated temperatures for SS430 that is coated with Ti, two samples were prepared of similar size, one of which was coated with Ti by evaporation.

3.14.1 SAMPLE PREPARATION

For some tests, sheets of metal were cut into similarly shaped and sized pieces, treated with a cleaner, dried and coated and weighed. These samples were then heated in the same furnace for a specified time and weighed again. The change in mass was recorded.

3.15 CHROMIUM EVAPORATION

The materials that were selected as coatings for stainless steel were tested for their high temperature chromium volatility[9]. It should be stressed that these materials were not coated onto steel to test their transmittance of chromium, but instead, large cylinders were created to test their emittance.

Materials were manufactured by the steps outlined in sections 3.2 and 3.3, and pelletized into cylinders 13mm across and 13mm high. These cylinders were sintered at various temperatures as outlined in the chromium evaporation chapter. Two cylinders were placed in an alumina boat that was inserted into an alumina reaction tube. Air or oxygen was pumped through a bubbler containing isothermal water at 25^{o}C and then into the reaction tube which was inside a tube furnace. Temperatures for reaction were 1000^{o}C and 1200^{o}C. At the exit of the reaction tube another bubbler was used to catch escaping vapors, and a chiller was used to catch vapours that escaped the first bubbler.

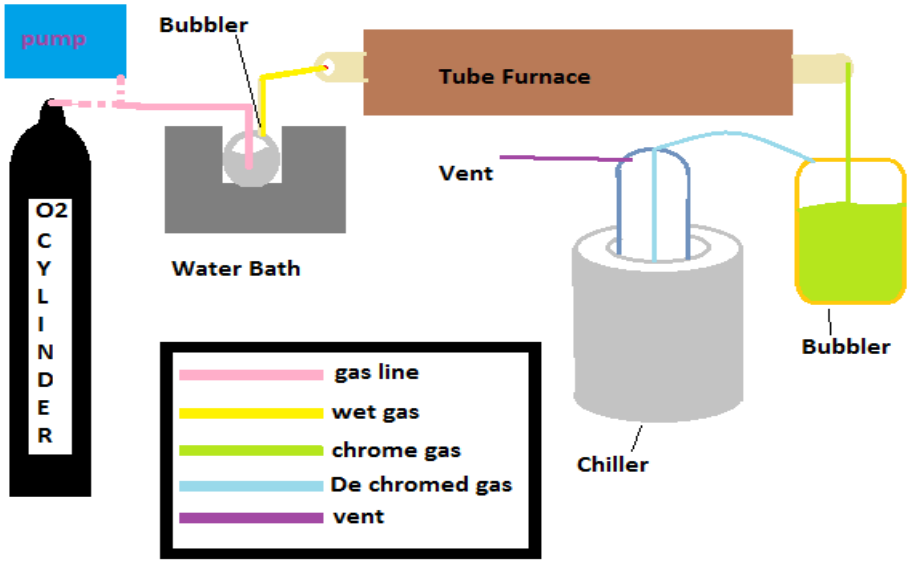

Fig.3.5: Evaporation rig

REFERENCES

[1] H. Fecht, E. Hellstern, Z. Fu and W. Johnson, Metallurgical and Materials Transactions A 1990, 21, 2333-2337.

[2] W. H. Rhodes, Journal of the American Ceramic Society 1981, 64, 19-22.

[3] G. Neri, Journal of European Ceramic Society 2004, 24, 1435-1438.

[4] M. Guglielmi and G. Carturan, Journal of Non-Crystalline Solids 1988, 100, 16-30.

[5] P. M. Martin, Handbook of Deposition Technologies for Films and Coatings: Science, Applications and Technology, Elsevier, 2009, p.

[6] M. M. Woolfson, Frontmatter

An Introduction to X-ray Crystallography, Cambridge University Press, 1997, p.

[7] J. T. S. S. Irvine, D.C.; West, A.R, Advanced Materials 1990, 3, 132 - 138.

[8] R. P. W. Scott in Thermal Analysis, Vol.

[9] D. C. M. Cohen, Journal of the Electrochemical Socieny 1961, 108, 438 442.

4 CHROMIUM RETENTION OF OXIDES AT HIGH TEMPERATURE

4.1 BACKGROUND

Hexavalent chromium is known to evaporate from stainless steels and chromia in the presence of water at high temperatures as demonstrated by Caplan and Cohen in the 60's[1]. Chromium is in steel to protect the iron from rapid corrosion. Much work in SOFC interconnects involving steel has been focussed on preventing chromium evaporation. In the presence of water and at high temperatures Cr_2O_3 is known to oxidize to $CrO_2(OH)_2$[2] (essentially molecular chromic acid, H_2CrO_4) which is then known to re-deposit to form Cr/Mn spinels on the interconnects and Cr_2O_3 a the triple phase boundary[3-7]. In an effort to keep these types of materials away from the triple phase boundary, many groups have attempted to deposit either chrome spinels or elements that will react with chrome to from spinels at the interconnect surface to keep stray chromium from depositing as the oxide at the triple phase boundary. These techniques include but are not limited to electroplating, sputtering, and radio frequency deposition [8].

Although forming these spinels at the interconnect has shown to improve performance of SOFC interconnects and has been shown to stop deposition of Cr_2O_3 and other species at the triple phase boundary, little direct data regarding chromium retention of spinel coatings exists. With this in mind, comparison of evaporation from chromium/cobalt containing spinels, CTO and Cr_2O_3 were compared.

4.1.1 EXPERIMENT DESIGN

The mechanism of chromium evaporation is discussed at length by other researchers[6]. Unfortunately there is little or no thermodynamic data regarding chromium evaporation and as such chromium VI species do not appear in Ellingham Richardson diagrams for chromium oxidation.

There are many parameters to choose from when designing experiments for chromium evaporation in solid oxide fuel cells. Current, water content, inclusion of anode components etc. are at one end of the scale of complication, and just bare coatings are at the other. For example, the presence of hydrogen has been show to have a contributing factor to corrosion of bipole interconnects[9-11], and current has been shown to affect re-deposition of chromium oxides at the triple phase boundary Inclusion of too few parameters can ignore key factors, inclusion of too many can blur results.

It is important to note that these experiments were not intended to show the performance of coating materials when coated onto steel. These experiments were designed to show the performance of the coatings as chromium retainers. One reason to remove the steel from the experiments is to avoid source ambiguity. If a steel/coating sample is to be used and the steel not completely sealed then it would be impossible to distinguish chromium that came from the coating and chromium that came from the steel. It would make sense that if material containing chromium could show poor performance in emitting chromium then it would also probably be also poor at transmitting chromium if placed on the of an infinite well

of chromium like the surface of steel. As such, the work presented in this chapter did not test the materials' performance as barriers over steel, but just their emittance of chromium. A second reason to omit the steel is to compare results to existing data from literature, and as such, the work does show the performance of these materials for chromium retention, and compares well to Caplan and Cohen's study.

4.2 PREPARATION

The materials prepared for this experiment, Cr_2O_3 and $Cr_{1.8}Ti_{0.2}O_3$ (CTO), and Chromium cobalt Cr_2CoO_4 spinel were produced by sol gel, solid state synthesis and in the case of chromia, from existing, reagent grade material from Aldrich. After synthesis, the powders were examined with x-ray diffraction to ensure phase purity, then pressed into 13 mm dies at 5 tonnes and sintered at 1000^{o}C. Details of synthesis techniques are available in the experimental chapter.

Great care was taken to not mix or confuse the CTO and chromia samples as they are the same colour, have very similar XRD patterns and samples had similar shapes. Fortunately post evaporation the samples were easily identifiable. CTO samples were yellow gained a yellow hue, Cr_2O_3 samples became blacker, and spinel samples went very slightly darker or dirty looking.

4.2.1 HIGHER TEMPERATURE SINTERED PELLETS

One group of sol gel samples were further pelletized and sintered at 1400^{o}C. This is the sintering temperature used by Caplan and Cohen in their 1961 study of chromium evaporation[1] however their ramp rates were not published. The ramp rates used for these samples were 3^{o}C/min to 1400^{o}C and 10^{o}Cper minute to room temperature. The aggressive cooling rate was used to save time and was used under the assumption that a slower rate would not affect the sample. However, this assumption was invalid. The higher temperatures were reducing and the rapid cooling quenched in oxygen vacancies. These samples showed additional peaks. After regrinding and reheating the samples returned their pre sintered state both in colour and crystallinity. The additional peaks in these samples were compared to those of reduced samples of Ti/Cr/Nb rutiles as discussed by Lashtabeg et.al[12]. At 1400^{o}C both chromia and CTO have become chemically reduced slightly, which is to be expected at elevated temperatures with fast cooling rates where the changes caused by the slightly reducing atmosphere are frozen in upon cooling. Caplan and Cohen did not discuss the diffraction patterns of their sintered samples, but other differences were apparent such as density. Their density was much higher, meaning that reduction would only have happened at the very surface, and may not have been detectible.

Sol gel CTO powder samples and solid state CTO powders showed similar XRD patterns to chromia as eskolaite, the known pattern for the chromia being used for the hkl values. The unit cells are presented in section 4.7.

4.2.3 MATERIALS ANALYSIS

For visual analysis please see section 4.6

4.2.3.1 XRD OF CHROMIA

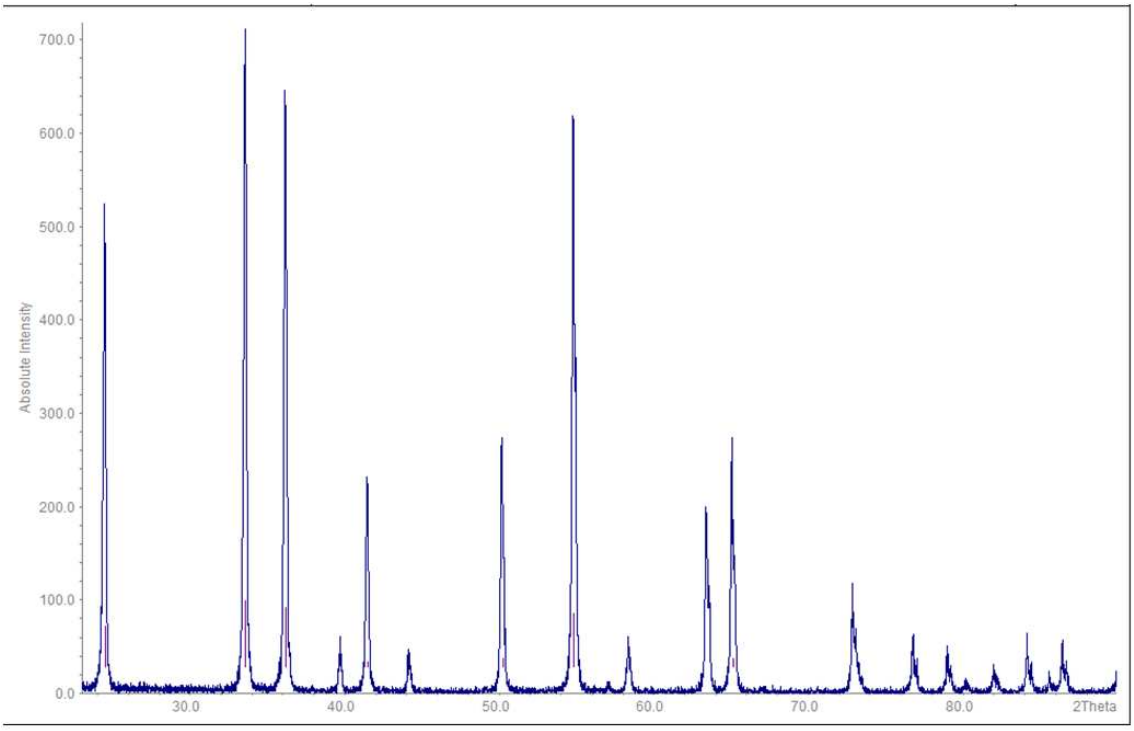

Fig.4.1: chromia from Aldrich source.

As can be seen in fig.4.1 and would be expected, chromia from the Aldrich sample bottle proved to be pure eskolaite. Chromia is in the R-3c space group. The unit cell parameters were a=4.962(4) and c=13.614(7). This compares to the card 38-1479 standard of 4.95876 and 13.5942 respectively.

	Standard	Sample	Diff(%)
A	4.95876	4.962(4)	0.065
C	13.5942	13.614(7)	0.15

Table4.1 :Unit cell parameter of Cr_2O_3 Compared to values from card 38,1479

4.2.3.2 X-RAY DIFFRACTION ANALYSIS OF CTO

As can be seen below and has been discussed in other papers, titanium doped chromia has a very similar X-Ray diffraction pattern to chromia[13-14]. The blue curve below is pelletized CTO that was sintered at high temperatures and cooled quickly at 10^{o}C/min. The purple curve is the same material that has been reground. As can be seen, the powder sample has a similar curve to chromia, the extra peaks in the pellet are due to high temperature reduction of the sample. Please see section 3.7 for analysis of unit cell parameters of before

and after samples. See Chapter 5 for a discussion on changes in unit cell parameters with carious Ti loadings at various temperatures.

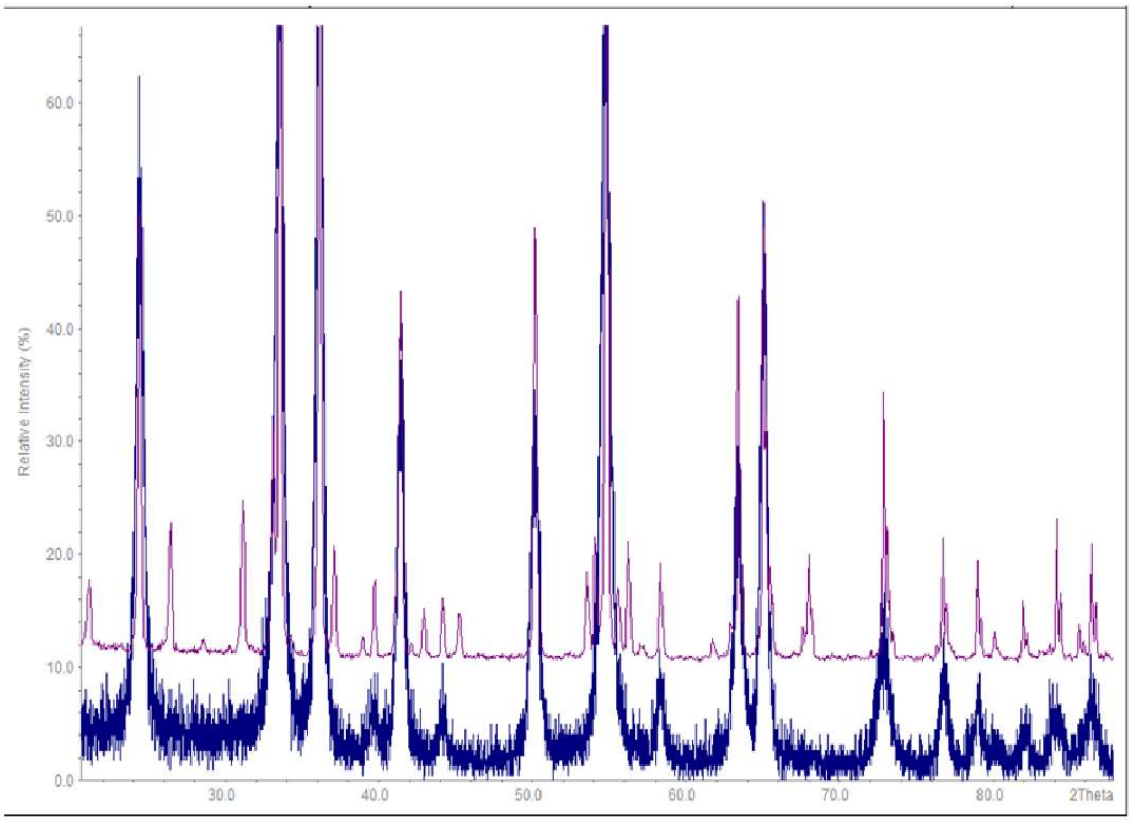

Fig.4.2: X-Ray diffraction pattern of $Cr_{1.8}Ti_{0.2}O_2$ fired at high temperature (purple) and reground (blue)

The additional peaks in fig.4.2 are due to other phases of chromium titanium oxide. *Phase Diagrams For Ceramicists* suggests that other combinations of chromium and titanium. Further phases are suggested at higher temperatures by Somiya although these temperatures were not reached[14].

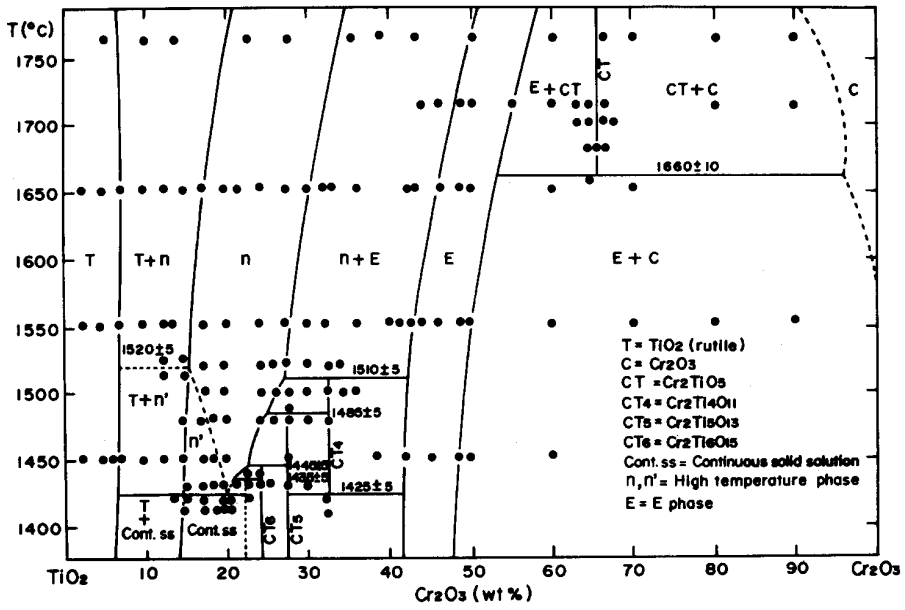

Fig.4.3: Phase diagram for high temperature mixtures of TiO_2 and Cr_2O_3 from Journal of Solid State Chemistry[14]

Although the TiO_2 Cr_2O_3 axis in fig.4.3 shows some defined materials at 1300^oC and these materials were available for comparison in the PDF data base, none of these materials were found in the sample. Further additional materials were found in the PDF database, and these materials were all reduced doped rutiles. Again, no one material matched the extra peaks, however, main peaks from several cards did line up to one or two of the non eskolaite peaks. Three peaks are required for refinement of rutile or eskolaite. It is also possible that contamination from the furnace is producing other phases. The muffle furnace used for this production has been used for cobalt, manganese, and other volatile metals for several years. In order to continue, the CTO material was heated to 1300^oC and cooled at 2^oC/min. After this cooling, additional peaks were minimized. Please see following sections for analysis.

4.2.3.3 XRD COBALT CHROME SPINEL

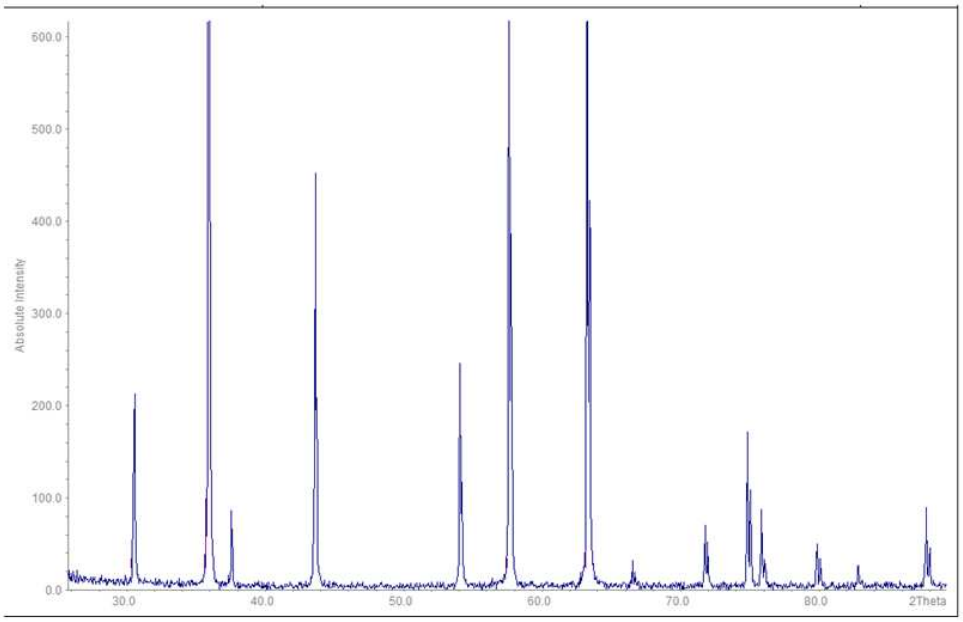

Fig.4.4: X-Ray diffraction pattern of chromium cobalt spinel

As can be seen from fig.4.4, the spinel formed by sol-gel synthesis was phase pure. This particular sample was pelletized and used in the evaporation experiment. Cr_2CoO_4 is in the space group Fd3m. Below is a comparison of the sample compared to the known standard from PDF card 22,1084.

	Standard	Sample	Diff(%)
A	8.3299	8.3366(9)	0.080

Table 4.2:Unit cell parameter of sample of Cr_2CoO_4 compared to standard from card 22.1084

4.3 EVAPORATION IN WET AIR

Following sintering and weighing, samples were heated in a tube furnace with moist flowing air following the procedure used by Caplan and Cohen [1]. For these experiments, air was pumped through an air flow meter followed by a heat transfer coil, followed by a water bubbler at thermostatically controlled at 25^{o}C. With both the air and the water at 25^{o}C the relative humidity can be calculated to be 100%, or 3.1% water vapour by volume based on the vapour pressure of water being 3.189 Kpa and atmospheric pressure being 101.3 KPa. This humid air was then passed into the reaction tube which was set at 1000^{o}C. Exit gases were fed through a second bubbler to catch excess moisture and metal in solution, then through an ice cooled condenser to remove any remaining hexavalent chromium, and a second air flow meter to ensure no leaks. The flow was set to 6l/min which was the maximum flow rate of the pump used. Each experiment ran for 1 week total.

4.4 EVAPORATION IN WET O_2

A second set of experiments were conducted at higher temperatures in flowing O_2 so that results could be compared to Caplan and Cohen. The flow rate was set at 6l/min.

In this series of experiments, the mass of sample and containing boat were recorded at room temperature and humidity using multiple measurements on two balances. The samples were placed into the same alumina tube used for previous experiments. The furnace temperature was set to 1200^{o}C for 1 week. The change in mass of both the sample and the boat were recorded in an effort to detect change in mass by either evaporation or mass transfer to the boat, be it solid state diffusion or re-condensation.

4.5 RESULTS

Figure 4.5 shows the results from this study and those from Caplan and Cohen. The data from Caplan and Cohen has been extrapolated due to the short duration of their experiments.

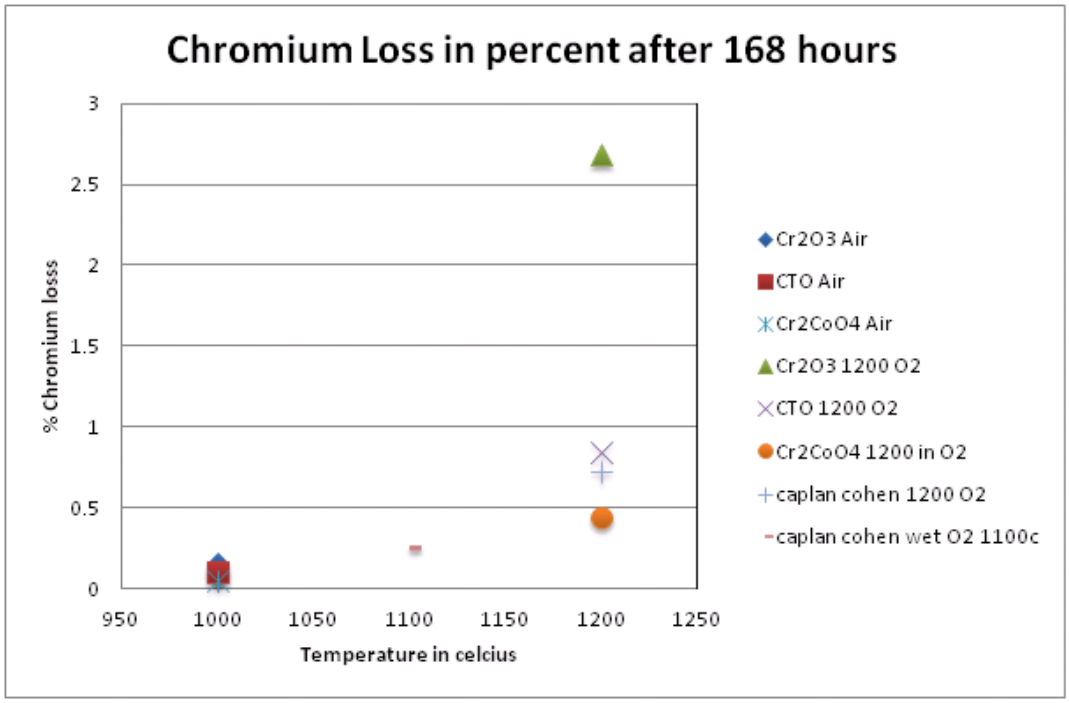

Fig.4.5a: Evaporation results

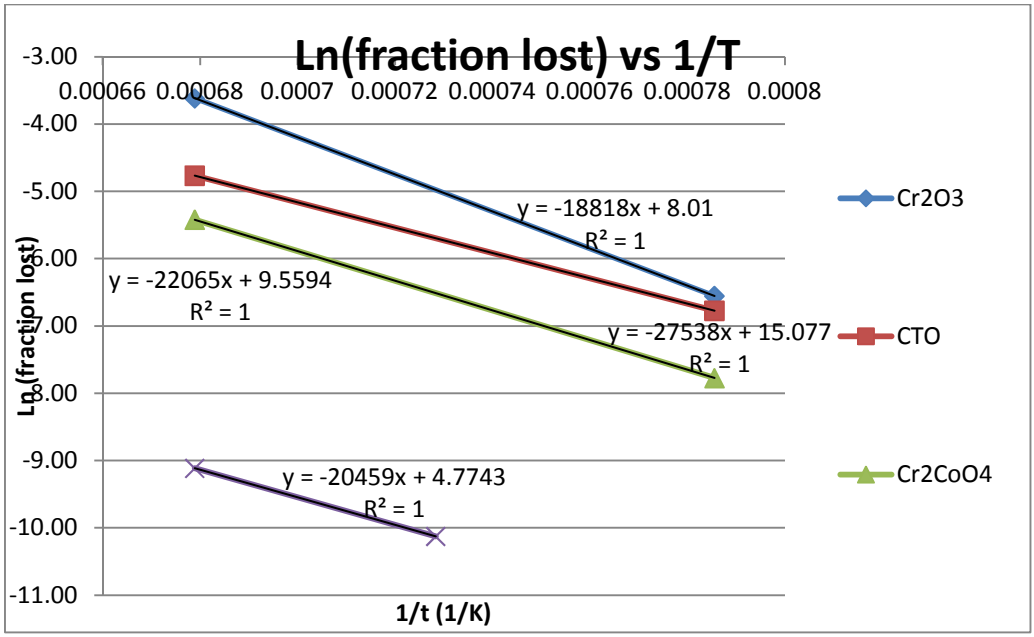

Fig.4.5b: Log (fraction lost)vs 1/temperature

Chromia	Activation energy(KJ/mol)
Cr2O3	2263
CTO	3312
Cr2CoO4	2654
Cr2O3 (C and C)	2461

Table.4.3: Activation energies of evaporation

The data clearly shows that CTO loses less mass than Chromia, and $CoCr_2O_4$ loses even less mass. The high activation energy for CTO is likey due to lack of data points. There are however differences between this study's results and Caplan and Cohen's results. There are several possible explanations for these differences.

- Sample mounting. Caplan and Cohens samples were suspended by wires and not sat in alumina boats. They had no solid state diffusion.
- Sintering program and density. Caplan and Cohen not only sintered at temperatures high enough to reduce the chromia, but also must have pressed the pellets at much higher pressure to attain 98% density. Their ramp rates and durations were not discussed, but if high cooling rates are used samples remain reduced. The pellets used in this study were 60% for chromia and CTO and as low as 47% for spinel. Due to the density of their pellets the surface area must have been comparatively small for similar mass and volume. This would equate to loss of mass only from the first few layers. This is likely the most important factor. High density equates to slower kinetics.
- The sampling. Caplan and Cohen, 20 hours compared to 7 days for this experiment. In order to compare their results to these Caplan and Cohen's results had to be adjusted for time.

Although Caplan and Cohen did perform an experiment at 1000C, it was in still air and the data was not usable as the conditions for this sample were not wet flowing air.

4.5.1 PERCENT CHROMIUM CONTENT CORRECTION

It should be noted that there is a dilution factor with CTO and cobalt/chromium spinel and as such the concentration of Cr per sample will drop. This could mean that apparent evaporation is decreased simply by removing the percentage of Cr in the sample, and reducing the Cr from the surface area where evaporation takes place. In order to correct for this dilution, the percentage mass loss was divided by the mass percentage of chromium in the sample. This calculation assumes that mass loss is due to chromium only and ignores any loss of cobalt, and assumes there will be no loss of titanium by evaporation.

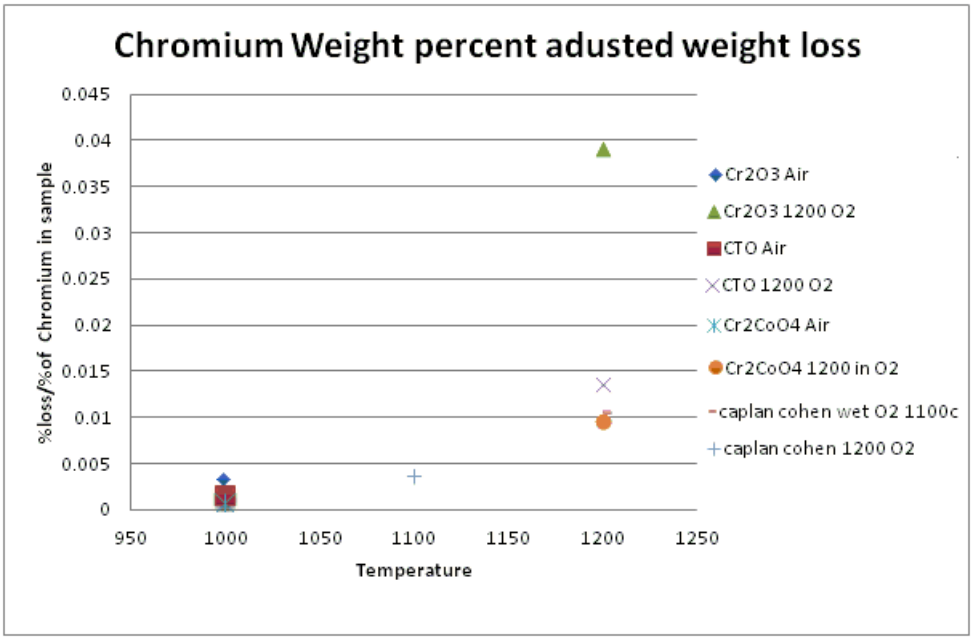

Fig.4.6: Corrected chromium weight percent evaporation result. All data for wet atmospheres

The corrected data agrees with fig.4.5 showing that both titanium doped chromia and chromium cobalt spinel loose less mass than chromia alone, and not just because the chromium is diluted, it must be somehow fixed or protected.

4.6 VISUAL ANALYSIS

After the experiment there were some colour changes to the samples. The CTO sample changed from green to a yellow colour. This is likely due to the relative concentration decrease in chromium at the surface, and higher titanium compounds. Chromia samples went much darker. Spinel samples also darkened but not to the same extent as chromia samples. Discolouration in all the samples was more intense toward the front of the sample in relation to the direction of wet air/O_2 flow, suggesting that the effects of evaporation were more intense at the front or re condensation was possible at the back. The discolouration of all the pellets was so thin that it could not be detected by XRD. This would suggest that

evaporation is only from the very surface of the pellet, and not the bulk, even when samples had considerably lower density than Caplan and Cohens, which in turn points to evaporation being a function of the surface area of the pellet and not the mass{Cohen, 1961 #2}. When chromium evaporates as hexavalent species it takes additional oxygen with it according to the reaction;

$Cr_2O_3 + 2H_2O + 3/2O_2 \rightarrow 2CrO_2(OH)_2$

If the oxygen is not supplied by the atmosphere, then it can be taken directly out of the Cr_3O_3 leaving behind oxygen vacancies. Holt and Kofstad predicted oxygen vacancies at temperatures over 1000^oC [15] Tiny amounts of defects can account for high changes in colour, as in the case of Magnelli phase titanium oxides which with only a tiny amount of oxygen removed goes from pure white to dark blue/jet black due to changes in oxygen of 10% defects in the case of Ti_5O_9. This is likely the cause of the colour change of the chromia sample as the defects would become frozen in as the sample was cooled.

4.6.1 CTO DISCOLOURATION

The CTO sample went a yellowish colour mostly at the front of the sample where concentrations of evaporated chromium would be lowest. This is evident in fig.4.7

Fig.4.7: showing CTO evaporation sample. Flow was from left to right.

4.6.2 CHROMIA DISCOLOURATION

After the evaporation experiment with wet oxygen the chromia sample turned black and stained the boat the same colour. The staining was only on the surface of the pellets, but could not be removed from the alumina boat. This is evident in fig.4.8, as the chromia boat is seen in the top of the image.

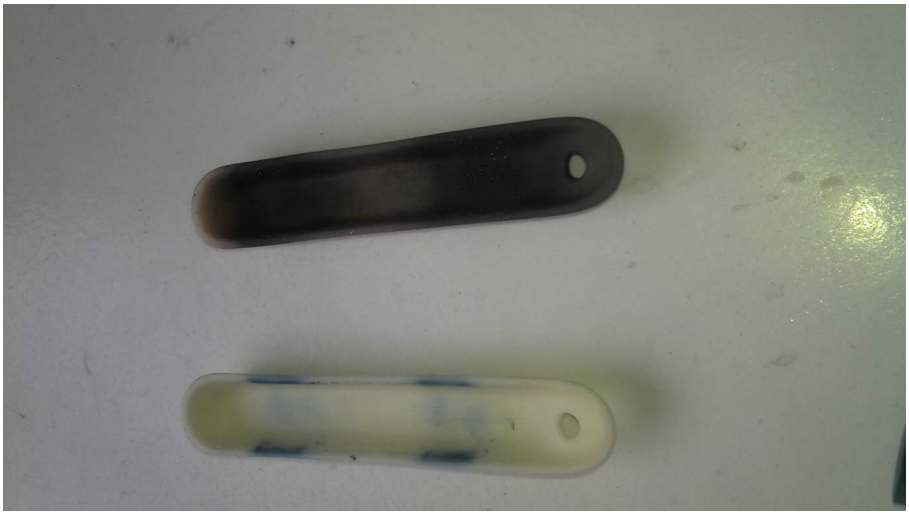

Fig.4.8: Sample boats. Top was Cr_2O_3 in wet O_2 at 1200C, bottom was spinel for same conditions.

Fig.4.9: Pellets colour change: left to right, Spinel, CTO, Cr203. Top row post ox, bottom row pre oxidation

4.6.3 CHROMIUM COBALT SPINEL DISCOLOURATION

Fig.4.8 shows the spinel boat in the bottom of the picture. Both Chromia and cobalt are known to evaporate at these temperatures, cobalt often with a bright royal blue, but as can been seen, chromia alone has stained far more than the chromium cobalt spinel.

As can be seen in fig.4.9, there was only slight difference in the spinel samples colour compared to the change in colour for both chromia and CTO.

4.7 X-RAY ANALYSIS

Post evaporation samples were compared to pre evaporation samples with X-Ray diffractometry. The unit cell parameters were indexed and compared for changes in the samples caused by the experiment.

4.7.1 CHROMIA

Below in fig 4.10 are the before and after patterns for the same chromia pellet.

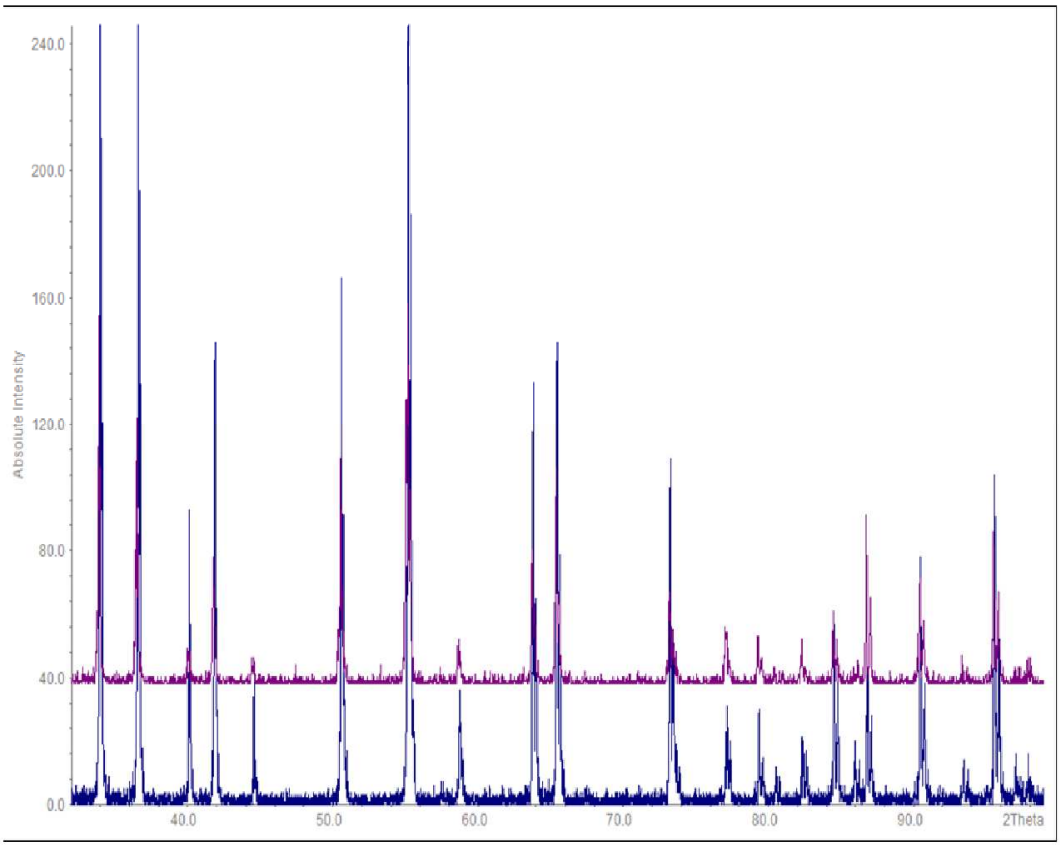

Fig.4.10: Before (Blue) and after (purple) evaporation X-Ray data for Chromia

HKL data from card number 38,1479 were applied to the four main peaks positions in the above patterns prior to refinement using Stoe “Index and Refine” software.

	A	C
Pre	4.9661(13)	13.618(3)
Post	4.9639(18)	13.607(4)
Change	0.04%	0.08%

Table 4.4: Lattice parameters for Chromia pre- and post-evaporation

As can be seen there is very little change in the lattice parameter A or C. These tiny changes could be due to oxygen defects at the surface and reduction of the sample. This would explain the dark discolouration of this sample post experiment. The shift in the patterns from the peak data from the card is due to poor alignment of the pellets in the custom sample holder.

4.7.2 CTO

Below are the before and after x-ray patterns for the same CTO pellet used for mass change experiments.

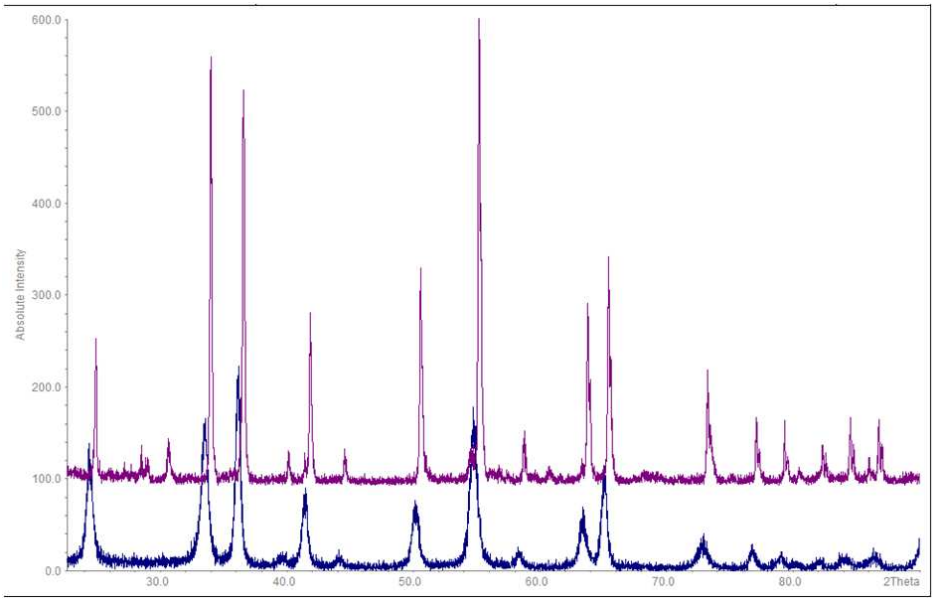

Fig.4.11: X-Ray diffraction patterns for CTO, pre(blue) and post (purple)evaporation

	A	C
Pre	4.974(32)	13.62(6)
Post	4.9654(12)	13.607(3)
Change	0.17%	0.09%

Table 4.5: Lattice parameters for CTO pre- and post-evaporation

Changes in the lattice parameters for CTO are more significant than for chromia, but still quite low. These changes could be explained by changes in local stoichiometry of the sample at the surface which could be supported by the colour change.. However, there are additional peaks on either side of 2 theta =30^{o} and around 60^{o} that appear post evaporation experiment. These peaks were found to be $Cr_{.46}Ti_{.54}O_{1.77}$ as represented by PDF card 30,417, which is a Cr doped and reduced rutile. Unfortunately the HKL values for this material are not currently available and so indexing could not be performed.

4.7.3 CHROMIUM COBALT SPINEL

Below in fig 4.12 are the before and after X-Ray patterns for the spinel pellet.

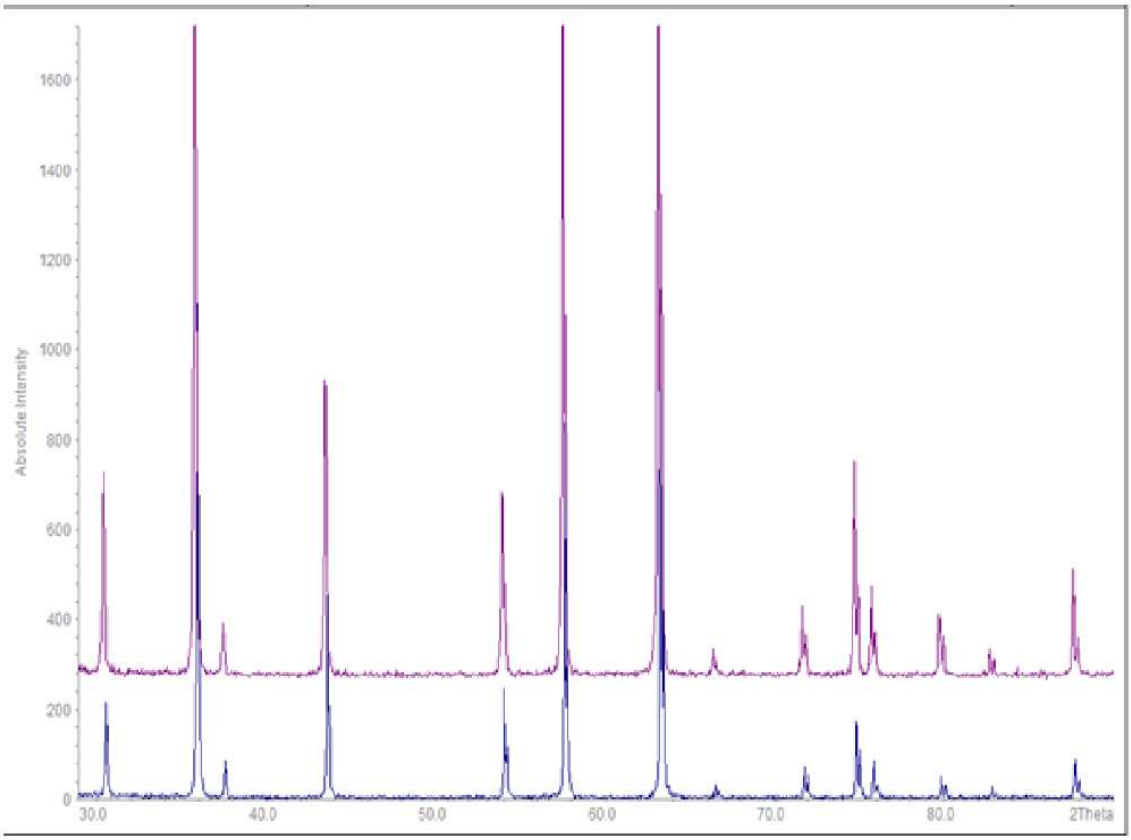

Fig.4.12: X-ray data for Cr_2CoO_4 Spinel pre (blue)and post (purple) evaporation

	A
Pre	8.3366(9)
Post	8.3331(6)
Change	0.04%

Table 4.6: unit cell parameter for $CoCr_2O_4$ spinel before and after evaporation

Of all 3 samples, the changes in spinel were the least significant. This is supported by the visual evidence of the lack of discolouration of the alumina boat, and minor decrease in mass, and minor changes in the colour compared to both other samples. Table 4.6 also supports this.

4.8 SEM ANALYSIS OF SAMPLES

Visual analysis of all three sets of pellets revealed that the biggest changes to colour happened at the surface of the pellet. Scratching or sanding the pellets returned them to their pre experiment status. In order to capture the changes at the surface SEM analysis

was performed with at voltages of 10Kv, small spot sizes of 9 and long sample times of around 600 seconds using the analyzer program in Oxford's Inca software for EDS of the surfaces. Below, some images reflect these settings, and some do not. Never the less, all EDS analysis results were gathered at 10Kv and spot size 9 and the EDS reports are for the field of view as per the analyzer routine.

4.8.1 CHROMIA PRE-EVAPORATION

Scanning electron microscopy revealed the pellets to be quite porous.

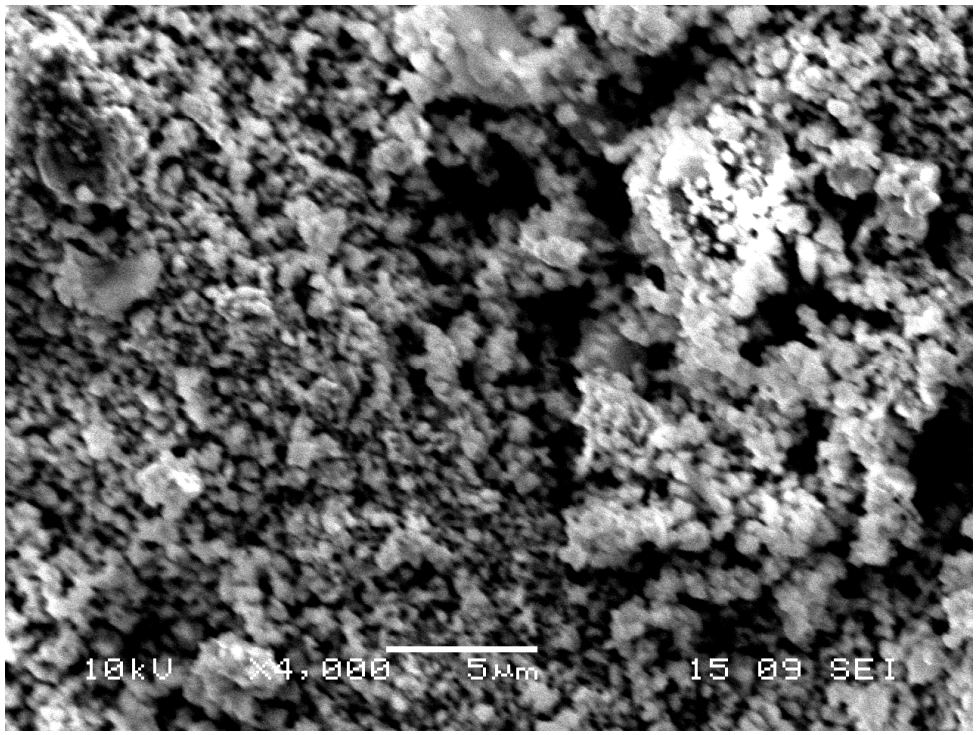

Fig.4.13: Surface of Chromia pellet prior to evaporation experiment

Element	Weight%	Atomic%
O K	28.18	56.03
Ti K	0.54	0.36
Cr K	71.28	43.61

Table 4.7 : EDS data for pellet surface in fig.4.13

4.8.2 CHROMIA POST-EVAPORATION EXPERIMENT

The chromia pellet was quite different after the evaporation experiment, with much larger agglomerations on the surface of the pellet. It was still quite porous.

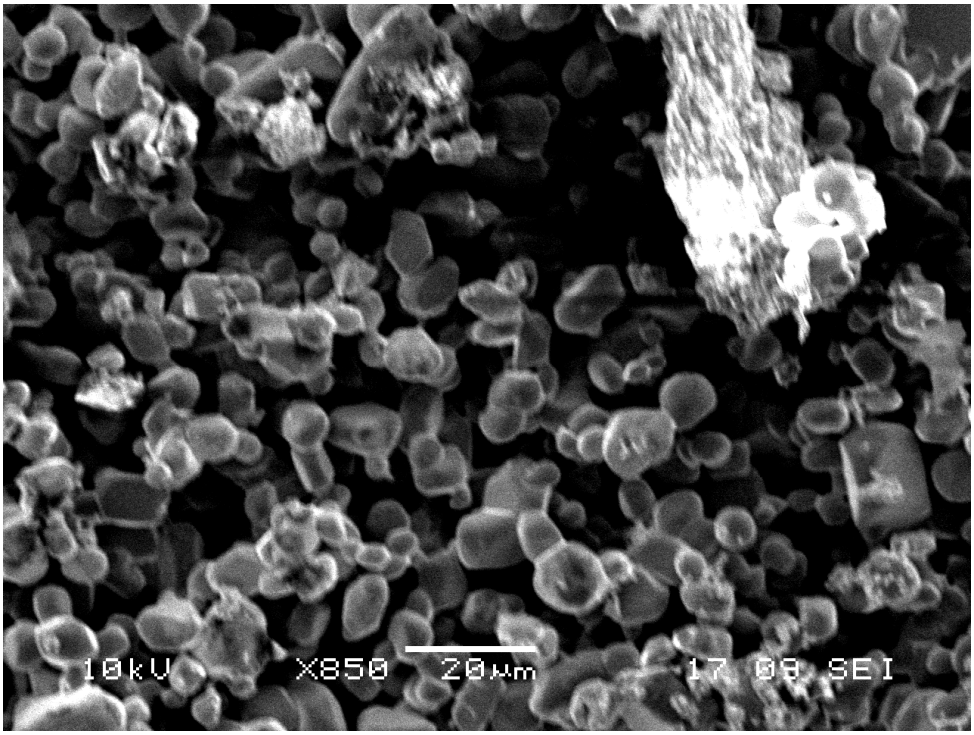

Fig.4.14: Chromia pellet post evaporation experiment

Element	Weight%	Atomic%
O K	22.43	48.44
Cr K	77.57	51.56

Table 4.8: EDS data for pellet surface in fig.4.14

The oxygen concentration appears to have decreased at the surface suggesting reduced oxidation states of chromium. This would support the dark colour of the post evaporation pellet.

4.8.3 CTO-PRE EVAPORATION EXPERIMENT

Below in fig.4.15 we see the surface of CTO prior to the evaporation experiment, and the EDS results in table 4.9. These will be compared to data in the next section.

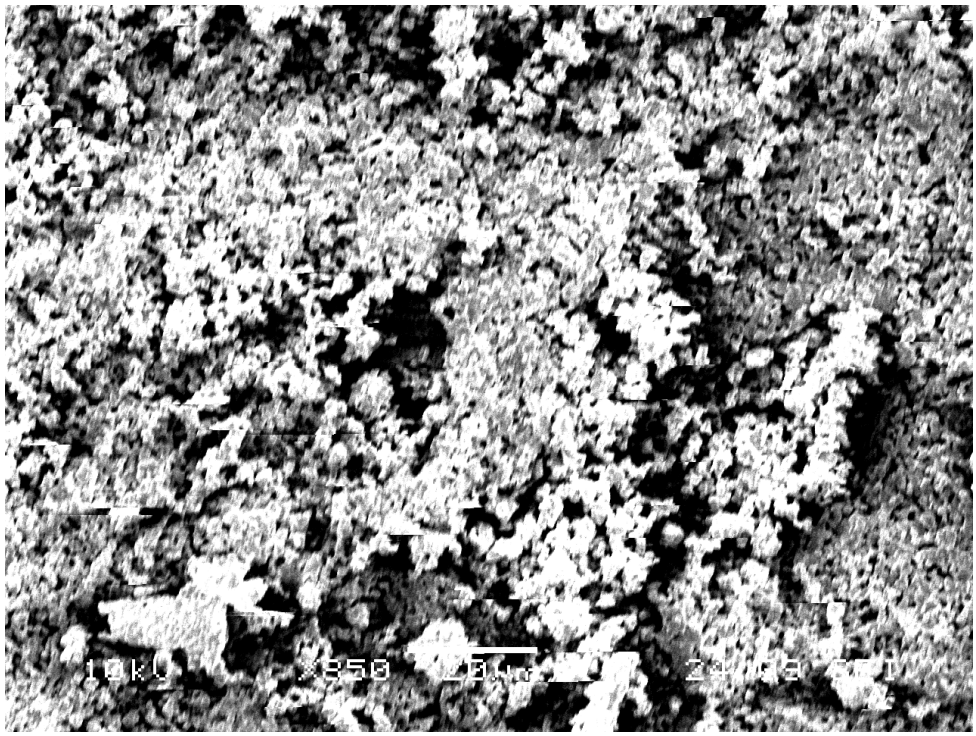

Fig.4.15:CTO pre evaporation experiment

Element	Weight%	Atomic%
O K	29.86	57.8
Ti K	8.62	5.57
Cr K	61.52	36.63

Table 4.9:EDS data for CTO pellet surface from fig..4.15

4.8.4 CTO POST EVAPORATION

Below in fig.4.1.6 is CTO after the evaporation experiment. Table 4.1.6 are the EDS results for the same sample.

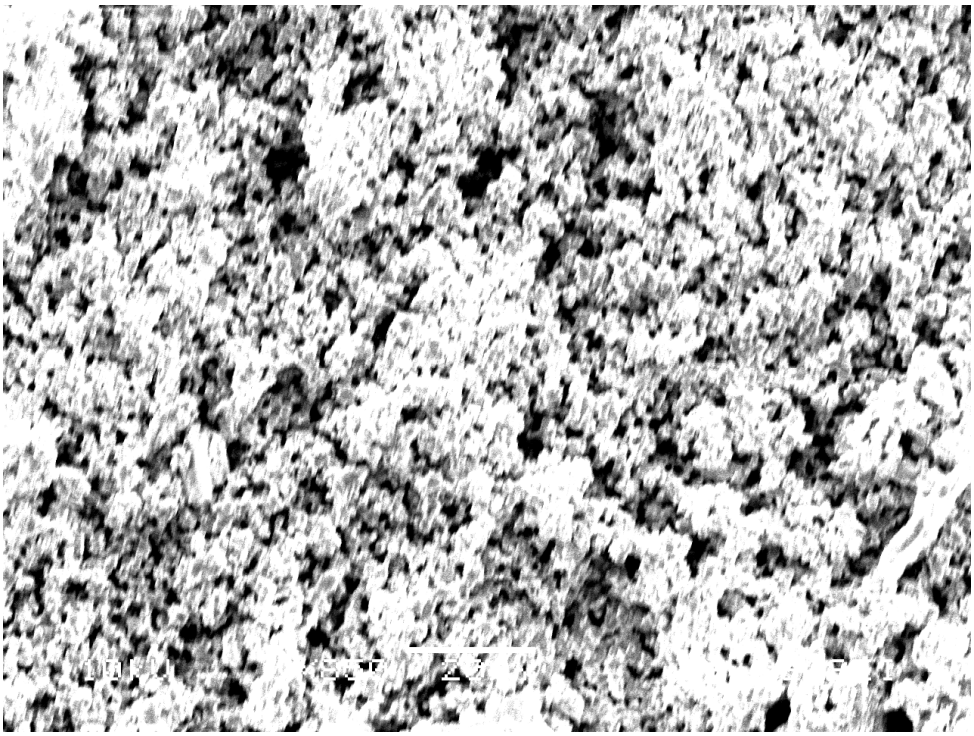

Fig.4.16: CTO post evaporation experiment

Element	Weight%	Atomic%
O K	32.58	60.56
Ti K	18.04	11.2
Cr K	49.38	28.24

Table 4.10:EDS data for CTO pellet surface from fig.4.16

For CTO,by comparing fig.4.15 and 4.16 we can see the micro structure did not change much, but the Ti concentration greatly increased as seen in tables 4.9 and 4.10, suggesting that perhaps chromium was lost from the surface, and that the enriched titanium layer was preventing further chromium evaporation. This would support the yellow tinge to the CTO post evaporation pellet.

4.8.5 COBALT CHROMIUM SPINEL PRE AND POST EVAPORATION EXPERIMENT

Below in fig.4.17 is an SEM image of the chromium cobalt spinel sample that will be compared to a post evaporation sample in the next section.

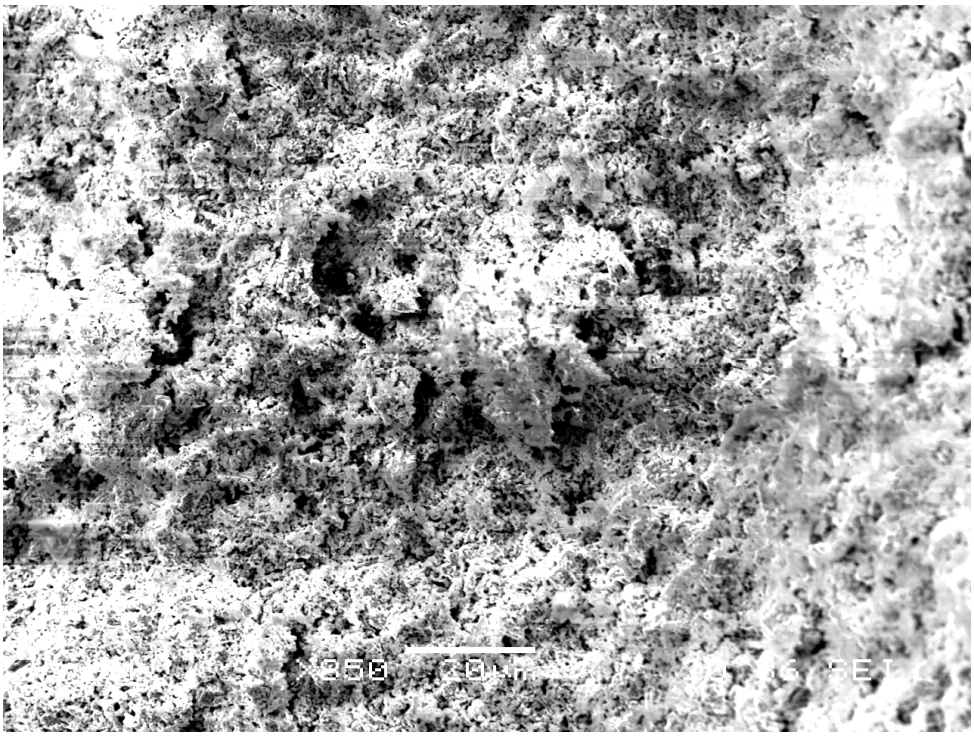

Fig.4.17: Cobalt chromium spinel pellet prior to evaporation

Element	Weight%	Atomic%
O K	15.54	38.04
Cr K	66	49.7
Co K	18.46	12.26

Table 4.11: EDS results for pellet surface from fig.4.17

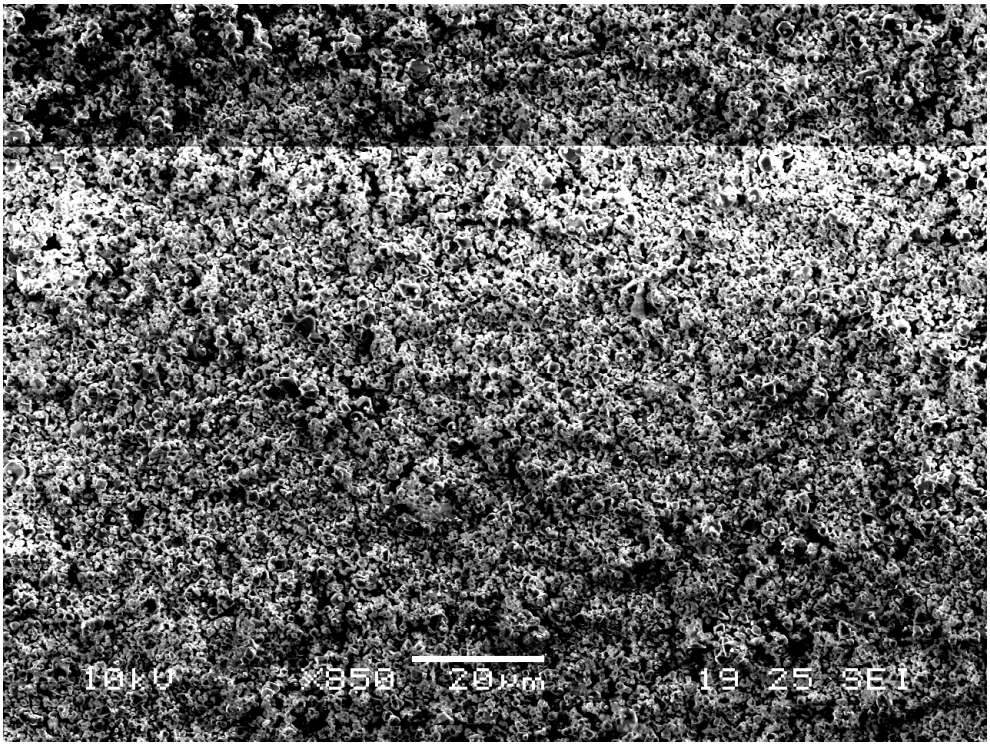

Fig.4.18: Cobalt chromium spinel block post evaporation experiment.

Element	Weight%	Atomic%
O K	23.18	50.39
Cr K	54.43	36.4
Co K	22.39	13.21

Table 4.12:EDS results for pellet surface from fig.4.18

As can be seen in fig.'s 4.17 and 4.18, of all the samples in the evaporation experiment, the spinel sample was the least affected by the evaporation experiment in colour, elements, or mass change. This is also demonstrated in the EDS result tables 4.11 and 4.12.

4.9 CONCLUSION

Adding a small amount of titanium to chromia reduces the high temperature moist atmosphere chromium evaporation rate by more than half. It would appear that the changes are most obvious at the surface, even for a relatively porous pellet, and that this layer may be protecting the deeper layers. Because this layer will have decreased chromium content it is likely to have lowered conductivity at the surface, however, it may be thin enough not to matter for SOFC interconnect duty. Optimization of the CTO layer and its resulting reduced chromium surface should be considered crucial if |chromium titanium eskolaites are to be used for coating SS430 for interconnect duty.

Creating the spinel phase by adding cobalt reduces evaporation even further by more than 4 times the evaporation of chromia. This is surprising considering that both cobalt and chromium are very likely to evaporate under these conditions alone, but together they are "fixed".

Although the chromia and CTO results did not agree with literature values, the sample preparation and exposure time can account for the differences. There are no published references for the evaporation rates of chromium cobalt spinels, which is also surprising considering the amount of activity surrounding these materials for solid oxide interconnect use.

As may be expected the evaporation of chromium has less to do with the mass of material than it does the surface area and density of the pellet. Large surface areas will clearly loose more material than smaller surface areas, and more dense pellets will lose less material as the surface area will be smaller. Caplan and Cohen did not discuss this relationship, as it may have been trivial to them due to the assumed density of chromia layers formed on steels. They also did not provide a discussion on the quality of their specimens, but to be fair, they must have all looked more or less the same afterwards considering the high density of their samples.

The samples used in this study were clearly only effected at the surface, which would suggest again that the density plays an important role, and that the surface area and not the mass are the critical parameters. Again in SOFC interconnect use, the assumption is that the chromia layers are fully dense. For these chromia pellets, the layer of material that was affected was only a few microns thick. On very dense pellets, this layer may not have been visible due to it being even thinner.

To find the exact relationship between surface area and evaporation, perfectly polished, non porous pellets would need to be manufactured. For the purposes of this experiment, a comparison between the materials manufactured under the same conditions (5 tonne pellet press, 1000^{o}C sintering) with similar surface areas (pellets were very similar in shape) should suffice to show the relationship between chromia, CTO and spinel and the evaporation of chromium from these samples.

Although these experiments do not necessarily show the material performance as coatings on steel for corrosion protection and chromium evaporation, it could be argued that low emittance of chromium form a material could equate to low transmission given a source on one side and a sink on the other. This is especially true when we consider the changes to the very surface of these samples during exposure to wet oxygen and the relatively unchanged bulk under the immediate surface. The particle sizes of all samples bar the post treatment Cr_2O_3 sample were similar according to the microscopy results. This coupled with the density data would suggest that the samples were similar in porosity and that mass loss would not be controlled by these factors. Although this data does not compare very well with Caplan and Cohen's data, there is a shortage of detail around their experiments regarding preparation and the effects of density. These key details may not have seemed relevant in 1962, but become crucial today.

The test was successful because it was demonstrated that adding a small amount of Ti or Co reduced the amount of Cr that evaporated. These experiments are repeatable and could be used to show performance of other chromium containing barrier layers for interconnect duty. There is little data on the evaporation rates, however, more data is useful and now that a framework for the data has been laid out, hopefully more workers in the file will contribute to this area so that the chromium retention can be modelled based on empirical data.

REFERENCES

1 Cohen, D.C.M., *The Volatilization of Chromium Oxide.* Journal of the Electrochemical Socieny, 1961. **108**(5): p. 438 442.

2. K. Hilpert, D.D., M. Miller, D. H. Peck, R. Weiss, *Chromium Vapor Species over Solid Oxide Fuel Cell Interconnect Materials and Their Potential for Degradation Processes.* Journal of The Electrochemical Society, 1996. **143**(11): p. 3642-3647.

3. Krumpelt, M.C., T.; Ingram, D, *SOFC Research and Developement in Support of SECA*, U. DOE, Editor. 2007, DOE: Argone, IL.

4. Konysheva, E.S., U.; Besmehn, A.; Singheiser, L.; Hilpert, K., Chromium vaporization of the ferritic steel Crofer22APU and ODS Cr5Fe1Y₂O₃ alloy. Journal of Materials Science, 2007. **42**(14): p. 5778-5784.

5. Konysheva, E.P., H.; Wessel, E.; Mertens, J.; Seeling, U.; Singheiser, L.; Hilpert, K., Chromium Poisoning of Perovskite Cathodes by the ODS Alloy Cr5Fe1Y[sub 2]O[sub 3] and the High Chromium Ferritic Steel Crofer22APU. Journal of The Electrochemical Society, 2006. **153**(4): p. A765-A773.

6. Konysheva, E.M., J.; Penkalla, H.; Singheiser, L.; Hilpert, K., *Chromium Poisoning of the Porous Composite Cathode.* Journal of The Electrochemical Society, 2007. **154**(12): p. B1252-B1264.

7. Konysheva, E., Influence of different perovskite interlayers on electrical conductivity between La0.65Sr0.3Mno3 and Fe/Cr-based steels. Solid State Ionics, 2005. **177**: p. 923-390.

8. Deng, X., *Cobalt plating of high temperature shainless steel inteconnects.* Journal Of Power Sources, 2005. **160**: p. 1225-1229.

9. Singh, P.Y., Z.; Viswanathan, V.; Stevenson, J., *Observations on the structural degradation of silver during simultaneous exposure to oxidizing and reducing environments.* Journal of Materials Engineering and Performance, 2004. **13**(3): p. 287-294.

10. Yang, Z.G.X., G. G.; Stevenson, J. W.; Singh, P., CORROSION BEHAVIOR OF INTERCONNECT CANDIDATE ALLOYS UNDER AIR//SIMULATED REFORMATE DUAL EXPOSURE CONDITIONS, in Advances in Solid Oxide Fuel Cells Iii, N.P. Bansal, Editor. 2008, Amer Ceramic Soc: Westerville. p. 279-288.

11. Zeng, Z.N., K., *Corrosion of metallic interconnects for SOFC in fuel gases.* Solid State Ionics, 2004. **167**(1–2): p. 9-16.

12. Lashtabeg, A.C.-V., J.; Irvine, J. T. S.; Bradley, J. L., Structure, Conductivity, and Thermal Expansion Studies of Redox Stable Rutile Niobium Chromium Titanates in Oxidizing and Reducing Conditions. Chemistry of Materials, 2009. **21**(15): p. 3549-3561.

13. Holt, A.K., P, *Electrical conductivity of Cr_2O_3 doped with TiO_2.* Solid State Ionics, 1999. **117**(1-2): p. 21-25.

14. Somiya, S.H., S.; Kamiya, S., *Phase Relations of the Cr2O3-TiO2 system.* Journal of Solid State Chemistry, 1978. **25**: p. 273 - 284.

15. Holt, A.K., P., Electrical conductivity and defect structure of Cr2O3 I. High temperatures (>1000^{o}C). Solid State Ionics, 1994. **69**(1994): p. 127-136.

5 TITANIUM AND CHROMIUM TITANATE COATINGS ON STEEL

5.1 BACKGROUND

CTO, chromium titanium oxide $Cr_{(2-x)}Ti_xO_{(3-y)}$, is a doped corundum type structure that has been identified as a potential coating for SS430 for several reasons. Firstly, it is a material that is structurally similar to chromia Cr_2O_3, and as such will have good adhesion to chromia that would be created by corrosion of steel due to compatible crystallinity and thermal properties. Secondly, conductivity is similar to chromia, depending on the amount of Ti present. Chromium retention is improved over chromium alond as demonstrated in chapter 4. Lastly it can be used as a gas sensor for reducing gases, meaning the electrical properties have been well studied in various atmospheres. It contains titanium which has been identified in SS441 as helping to control formation of dense layers of chrome oxide by suppressing chromium carbide formation in the grain boundaries. However CTO has not been tried as an interconnect coating for SOFC's

The general formula of CTO is $Cr_{(2-x)}Ti_xO_{(3-y)}$ where x varies between 0 and 0.4 and y varies between 0 and 0.5 [1] and has shown increased stability over SnO_2 for gas sensor duty. Above the solubility limit of Ti the material is no longer a single phase doped eskolaite and begins to take on additional chromium doped rutile crystallinity. At high x values a rutile structure appears. Both the Cr-doped rutile and Ti-doped eskolaite forms have higher conductivities than TiO_2 and lower than Cr_2O_3. The eskolaite phase material properties were studied extensively by Holt and Kofstad in the late 1990's. They discovered that CTO is an n-type conductor in reducing conditions and a p-type conductor in normal atmospheric conditions [2]. These properties make it well suited as a gas sensor for reducing gasses. They found that CTO cannot be distinguished from Chromia by x-ray diffraction. Recent work has suggested this is not the case [3] and it has shown that varying the concentration of Ti affects the both the A and C parameters of the unit cell. Below is a plot of Ti concentration vs. lattice parameter C for x between 0 and .3 for several isotherms. This data is compiled from Pai, Dash, Mukerjee, and Venugopal [3] .

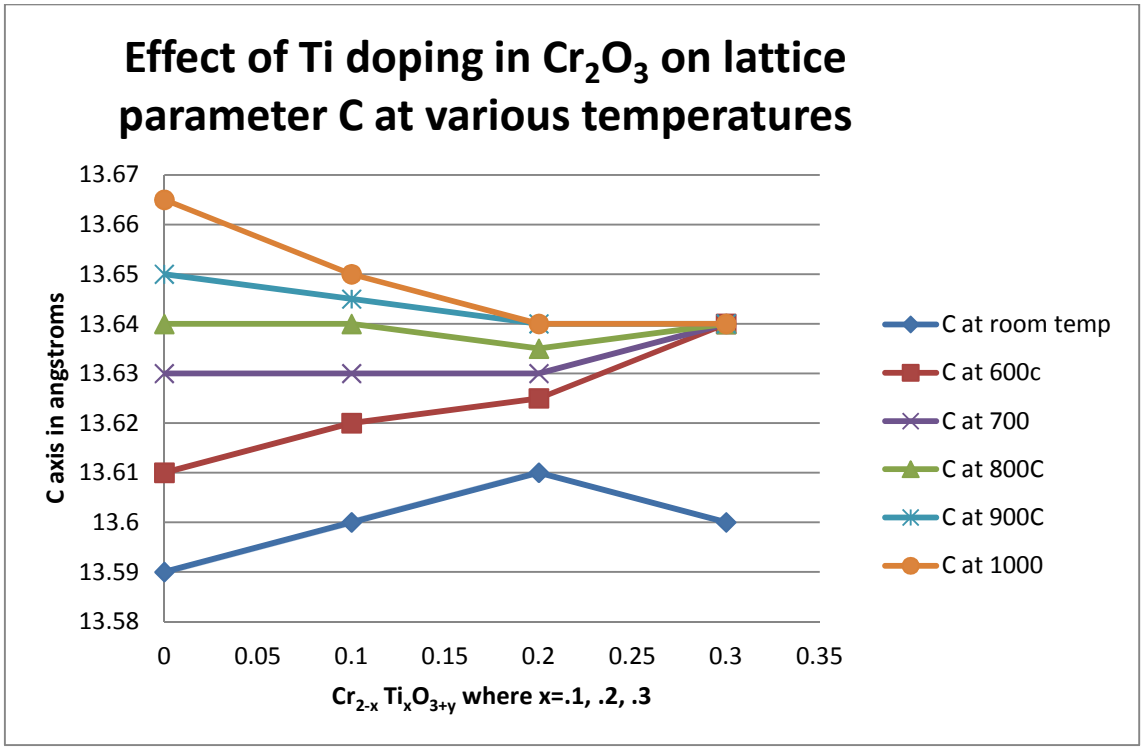

Fig.5.1: Plot of cell parameter C vs. Ti doping in CTO at various isotherms

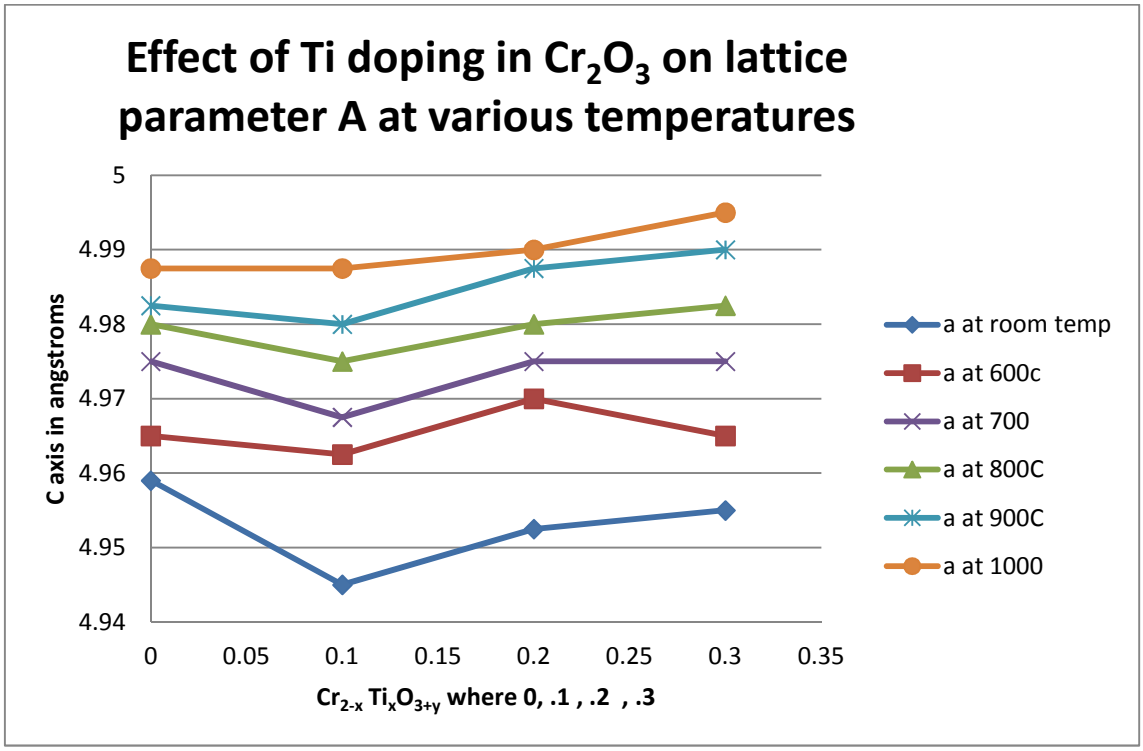

Fig.5.2: Plot of cell parameter A vs. Ti doping in CTO at various isotherms.

Using fig.5.1 and fig.5.2 it may be possible to distinguish values of X for materials manufactured, however, there are not constant changes to the parameters. A constant

increase or decrease in a unit cell parameter would be more useful than the behaviour of unit cell parameter A at the isotherms of anything other than 1000^{o}C. The C parameter is likely more useful especially at high doping concentrations. In both cases, room temperature doping isotherms could give the same results for different doping levels, making identification by comparing to this data impossible.

5.2 PROJECT AIM: CTO AS A COATING FOR SS430 FOR SOFC

The aim of this project is to coat SS430 with CTO, and evaluate its performance as a coating on SS430. The criteria for a coating are physical bonding to the surface, low electrical resistance, high oxidation resistance. In order to meet these criteria, the coating needs to be thin enough that electrical losses be minimal, but thick enough to protect the steel from further oxidation, and retain chromium (vi) species known to evaporate in SOFC cathode environments. Work on the evaporation of chromium from chromia, CTO, and Cr/Co spinel in the previous chapter highlighted CTO's potential in the evaporation arena. Literature reviews indicated CTO as having conductivity similar to chromia. Metallurgy reviews suggested that chromia does indeed bond to the surface of steel at intermediate temperatures and accounts for the corrosion protection of the alloy. With these factors in mind, a system of depositing CTO onto SS430 was sought.

5.3 SOL-GEL COATINGS

5.3.1 SOL-GEL FOR POWDER SYNTHESIS

Sol-gel coatings were identified as a way to put the stoichiometric correct forms of CTO on to SS430. Initial attempts to coat SS430 with CTO used the basic sol-gel process as outlined in the experimental chapter. This method works very well for production of fine powders, and was used in chapters 4 to produce CTO pellets for evaporation experiments. Ingredients in the sol-gel mixture are chosen due to availability, reactivity, miscibility, wetting and other factors. However, this sol-gel was originally developed for pure powder combustion synthesis and not for coatings and is incompatible with metal coatings for several reasons. The ingredients of this particular sol-gel mixture are chromium (3) nitrate, titanium tetrabutoxide, ammonium citrate and glycine as fuel, and dispersing agents. The reasons for incompatibility are:

The mixture has a high wetting angle on stainless steel so it does not dry with a single film but instead several blobs. A small amount of detergent was added which helped coat more uniformly, but it was still not ideal.

The conversion of material from gel to powder is very exothermic due to the resulting ultrafine mixture of containing glycine fuel NH_4NO_3. As the mixture is heated the solvents evaporate leaving highly volatile mixture of fuel, very finely dispersed metals and oxidizer behind. Once the reaction starts, it is over very quickly due to the high dispersion, fine mixing and rapid kinetics.

In the laboratory this usually takes place in a beaker on a hot plate. Because of the uncontrollable and often unmonitored nature of this type of synthesis, peak temperatures and durations cannot be measured. Temperatures may get high enough for sintering to take place in situ, making future grinding and further densification difficult. When fired directly onto stainless steel a CTO coating was not found. Attempts to coat other substrates with thicker versions of sol-gel gave the same results: coatings did not form and powder was found near the reaction site. This can be seen in fig.5.3.

Fig.5.3: Stainless steel pipes and rod coated with CTO sol-gel and fired at 900C. The resulting CTO powder can be seen on the alumina plate below. Powder that remained in the pipes and rod brushed off with ease.

5.3.2 SOL-GEL CTO INK

Powder and pellets made from CTO synthesized by the powder synthesis sol-gel were used to make ink. Unfortunately any hard CTO formed on the surface of SS430 from this technique cracked off during cooling. This is because the temperature required to sinter CTO into a dense layer is in a temperature range where corrosion layer growth is so rapid in Steel that there is nothing to attach the CTO to. This is readily visible in fig.5.4

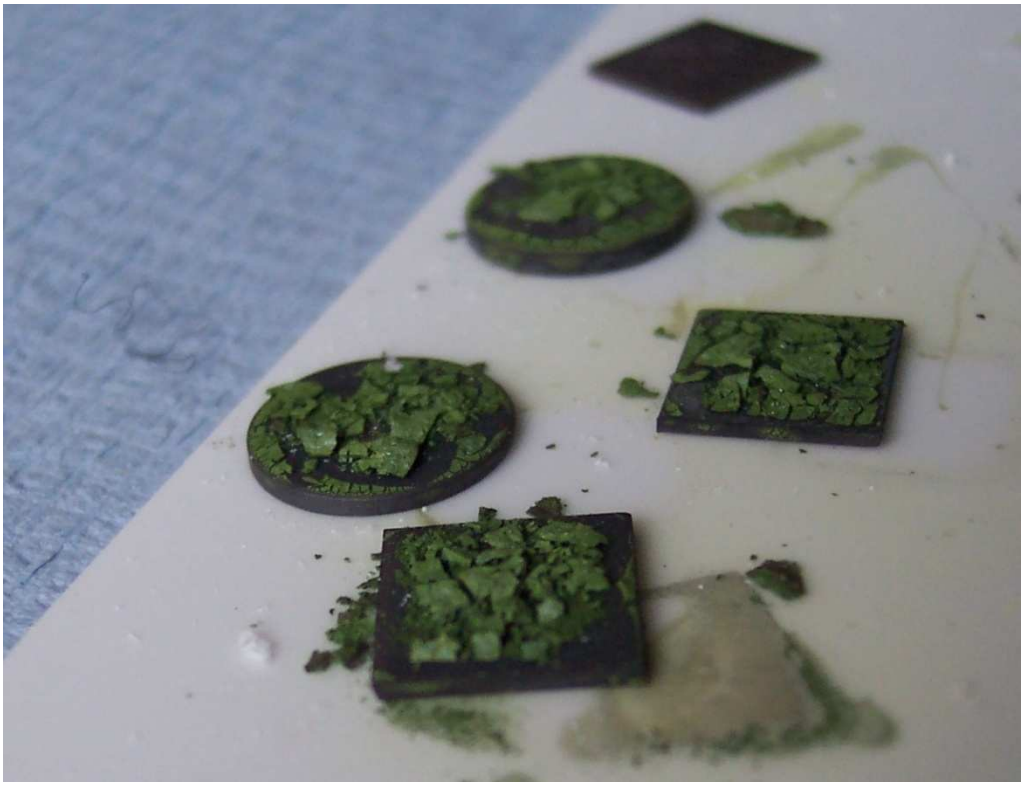

Fig.5.4: Stainless steel coated with CTO ink and fired. All the CTO crumbled off.

5.3.3 INSITU SOLID STATE SYNTHESIS FROM POWDER

Making the desired range of compounds by adding their mixed or unmixed oxides as an ink to SS430 also proved to be a failure. It was hoped that the process would be similar to silicon oxide glazing on metals. However, the high melting points of rutiles and eskolaites, and the corrosion resistance of the steel are not in the same temperature range

5.3.4 ALCOHOL BASED SOL-GEL

A second sol-gel was prepared using an ethanol solution of $Cr(NO_3)_3$ and $Ti(OC_3H_7)_4$ that did not contain ammonium citrate. The recipe by Neri recommends $CrCl_3$ however, none was available. This solution was painted onto various substrates and fired at 450^0C [4].

5.3.4.1 ALCOHOL SOL-GEL CHARACTERIZATION BY X-RAY DIFFRACTION

Compared to previous attempts, this recipe did produce powder on the surface of the substrates. Steel substrates appeared to be changed to dark blue. Sol-gels from section 5.2 formed powders that did not stay on the surface of the substrates, and the resulting surface was unchanged. Unfortunately, the powder was not adhered to the surface. These results are clearly visible in fig.5.5.

Fig.5.5a and b: Alcohol based sol-gel before and after brushing. The CTO did not adhere.

X-ray diffraction showed a strong eskolaite pattern from the surface of the SS430, although the layer was very thin and the pattern was dominated by the steel.

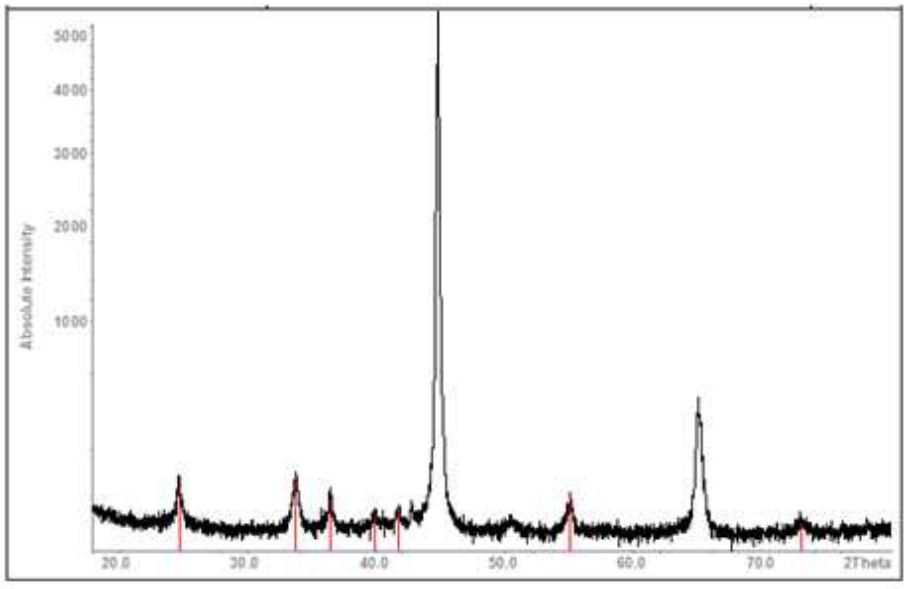

Fig.5.6: X-Ray diffraction pattern of SS430 coated with alcohol based CTO sol-gel and Cr_2O_3Peaks

Refinement of the non Steel peaks with added hkl's from the eskolaite card is presented below. CTO data was obtained from figs. 5.1 and 5.2, Cr_2O_3 unit cell parameters were taken from PDF card 38,1479. %CTO and % Cr_2O_3 represent the deviation from the standard if CTO (%CTO) or chromia (%Cr_2O_3) had been used.

	CTO Standard	Cr_2O_3 Standard	Sample	%CTO	% Cr_2O_3
A	4.952	4.958	4.990(21)	0.77	0.63
C	13.61	13.59	13.65(3)	0.3	0.4

Table 5.1: Unit cell parameters for Alcohol sol-gel heated on SS430 for 2 days at 450^oC

The parameters in table 5.1 did not agree with Pia's work, but also did not agree with the standards for chromia. Pia's work was characterizing pure materials, and not very thin coatings formed on stainless steel at 450 C and then cooled. They also found that variations in the unit cell parameter were not constant as discussed in section 5.1

5.3.4.2 SEM AND EDS CHARACTERIZATION OF ALCOHOL BASED SOL-GEL COATING

EDS of the surface of SS430 with alcohol based sol-gel did not find any Ti, even at low acceleration voltages and small spot sizes with very long capture times. The SEM image is below as fig.5.7.

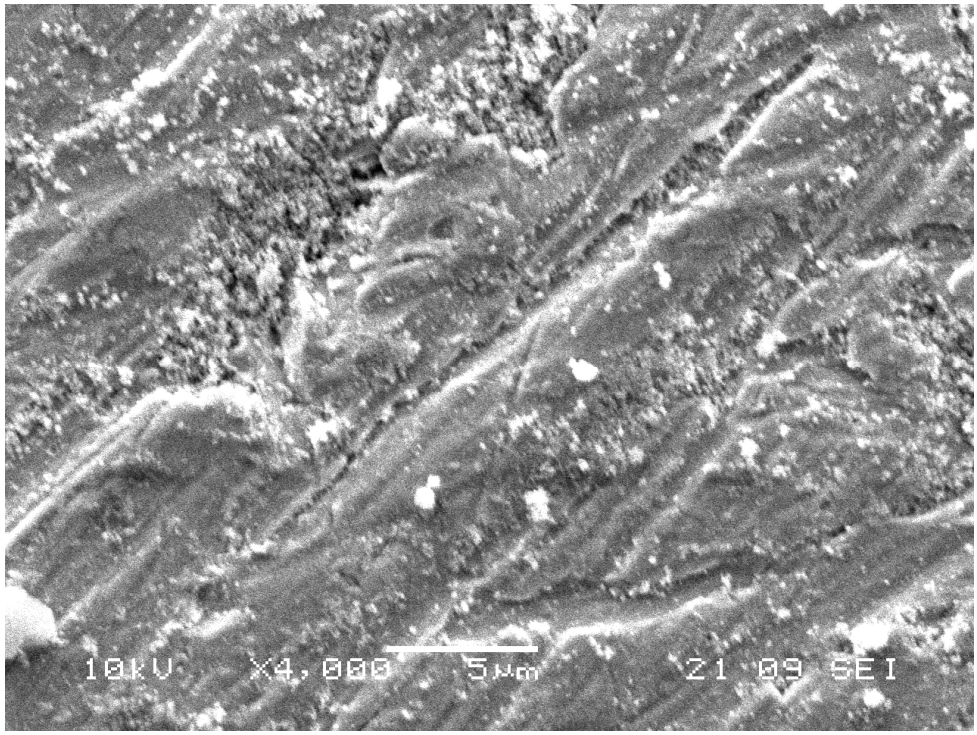

Fig.5.7: SEM image of SS430 coated with alcohol based CTO sol-gel and fired at 450C for 24 hours.

Element	O	Ti	Cr	Fe	Total	Ti:Cr
Weight%	42.72	0.9	19.85	36.33	100	1:22
Atomic%	71.75	0.51	10.26	17.48	100	1:20

Table 5.2: EDS data for area of fig.5.7

As can be seen from the above table 5.2, Ti was detected at a very low level, possibly below the limit of the EDS's reliable reading abilities. This may indicate that Ti was there, perhaps the very bottom surface of the sol-gel had deposited a layer of CTO. However, assuming this happened, then further corrosion of the SS430 drove the Cr concentration up. Evidence for this comes from the Ti:Cr ratio, which was set at 1:9 in the sol-gel, but is closer to 1:20 in the EDS report. The entire sample was used in the analyzer program to obtain these results which uses the field of view for analysis. The acceleration voltage was 10kv and the spot size was 9. Duration of the analysis was 600 seconds. These values are comparable to the settings used to detect Ti from the surface of evaporated and heated samples of SS430 in other sections.

Compared to the ammonium nitrate based sol-gel solution, where green powder appeared everywhere but on the substrate, the alcohol based sol-gel formed powder stayed on the surface of the substrate, but mostly did not bond. The blueing of the surface is most likely to have been caused by the temperature spike of combustion, as SS430 left for 2 days at 450^{o}C does not form such a dark colour. There may not by any thin film bonding of CTO to the surface. Compared to the EDS data from sections 5.4 and 5.5 it can be concluded that this particular system of sol-gel cannot form coatings on SS430. The back side of this sample was also discoloured, to a gold or copper colour, consistent with corrosion of SS430 under these time and temperature conditions.

It is therefore concluded that this Sol-gel did not stick to SS430, the change in colour was due to the heat spike caused by combustion of the sol-gel.

5.4 SURFACE COATING WITH A SINGLE ELEMENT

In order to make titanium doped chromia from stainless steel, titanium would be the only additional element needed. It is widely known that in moderate temperature ranges SS430 corrodes to form predominately Cr_2O_3. As noted in Chapter 4, chromium is also known to evaporate from steels in the presence of atmospheric water. At higher temps up to 800C Cr/Mn spinels start to become apparent as an upper layer capping the eskolaite and iron/iron-chromium oxides. This would suggest that if titanium or titania can be bonded to the surface at low temperature and then reacted with the chromium in or coming out of the substrate, it could be possible to make CTO on the surface of stainless steel.

5.4.1 MECHANISM

For this production to take place under heating Ti would need to be added. If Ti is added in its elemental form it will oxidize to form TiO_2 upon the addition of heat. The other option is to deposit TiO_2.

For the production of CTO by this method, either Ti would need to diffuse into Cr_2O_3, or Cr would need to diffuse into TiO_2 until the structure would change from rutile to eskolaite.

As Ti oxidizes, the resultant TiO_2 layer allows further oxidation by transport of oxygen in to the interface between the Ti metal and the oxide layer. For eskolaite this mechanism is different, as chromium migrates from the metallic layer through the oxide layer and the further growing occurs on the interface between the oxide and the atmosphere. This would suggest that it's more likely for Cr to diffuse into TiO_2 than for Ti to diffuse into Cr_2O_3.

In support of this preference, studies have shown that TiO_2 can absorb other metals onto its surface and diffuse them into the bulk at moderate temperatures. [5]
For CTO to be formed from deposited Ti or TiO_2 onto SS430, Cr doped rutile would have to be an intermediate phase before chromium saturated rutile would convert to CTO.

The intermediate rutile phase materials have been shown to be conductive, especially after reduction. [6-7] and may have some commercial value as coatings on SS430 for other electrochemical systems.

It may not be possible to form the exact materials $Cr_{(2-x)}Ti_{2x}O_3$, where x is a fixed value, by the diffusion of chromium into titania. Unlike most laboratory based solid state diffusion, where fixed amounts of elements are added in stoichiometric quantities, the diffusion of chromium through corrosion layers is dynamic: its heat and time dependant. In the system of a thick steel sheet with a thin titanium cap there is a disproportionate over abundance of chromium, and a finite and small amount of titanium. It's more likely that over time there would be gradients of Cr through the Ti. Therefore, the concentration of Ti will continue to decline as the corrosion layer increases in thickness over long periods of time. For thicker layers of Ti that are reacted this way, there will be a concentration gradient of increased chromium at the metal/corrosion layer interface and increased titanium at the air/corrosion layer interface. After either depletion of the chromium reservoir or infinite time, the Ti concentration will be orders of magnitude lower than the starting concentrations.

5.4.1 RUTILE INKING

Attempts to make CTO by adding TiO_2 powder or paint to the surface of SS430 and allowing chromium to react with it proved unsuccessful. To slow the production of eskolaite the inks needed to be sintered to make them continuous and bond to the steel. Unfortunately at the various temperatures tried, the resultant layer cracked off and production of eskolaite continued unhindered. Additionally, the inked layer was too thick to survive heat cycles and simply cracked off upon cooling.

5.4.2 TITANIA SOL-GEL

Sol-gel for Titanium was made by following the alcohol CTO sol-gel recipe but without $Cr(NO_3)_3$. The ingredients were mixed for 3 hours, then painted onto SS430, ss316 and alumina. After drying overnight, these samples were heated in a muffle furnace to 450^{o}C at a rate of 1^{o}C/min and held at that temperature for 24 hours, then cooled at the same rate. Upon removal from the furnace the samples had white powder upon them.

Fig.5.8a and b: SS430 with alcohol based Ti sol-gel after firing at 450^{o}C for 24hours(left) and same sample after brushing (right)

As can be seen in fig.5.8 above, the sol-gel appears to have made TiO_2 but it has not adhered to the surface of the steel. Where the sol-gel paint has not covered the surface, normal corrosion has taken place. Where the sol-gel paint was on the surface blueing has occurred. Assuming that adhesion did not take place, the blueing is likely due to a temperature spike during the synthesis of TiO_2.

5.4.3 Acidified alcohol SOL-GEL 450 24 hours

The sol-gel solution from above was modified by adding a few drops of nitric acid, which converts some of the OH to water, and reduces the available oxygen content during combustion, which in turn slows the combustion kinetics and lowers the combustion temperature. The solution was then painted onto SS430 and SS316 coupons which were then heated to 450^{o}C for 24 hours.

Fig.5.9: SS430 and SS316 with acidified alcohol sol-gel solution painted and fired at 400^{o}C for 24 hours. Scratch mark denoted by white arrow.

As can be seen infig.5.9, this solution did adhere and survived the firing process. The scratch test showed good adherence compared to previous sol-gel's. The scratch was examined by SEM in Fig.5.13

5.4.3.1 X-RAY CHARACTERIZATION OF ACIDIFIED ALCOHOL BASED TITANIA SOL-GEL COATING ON SS430

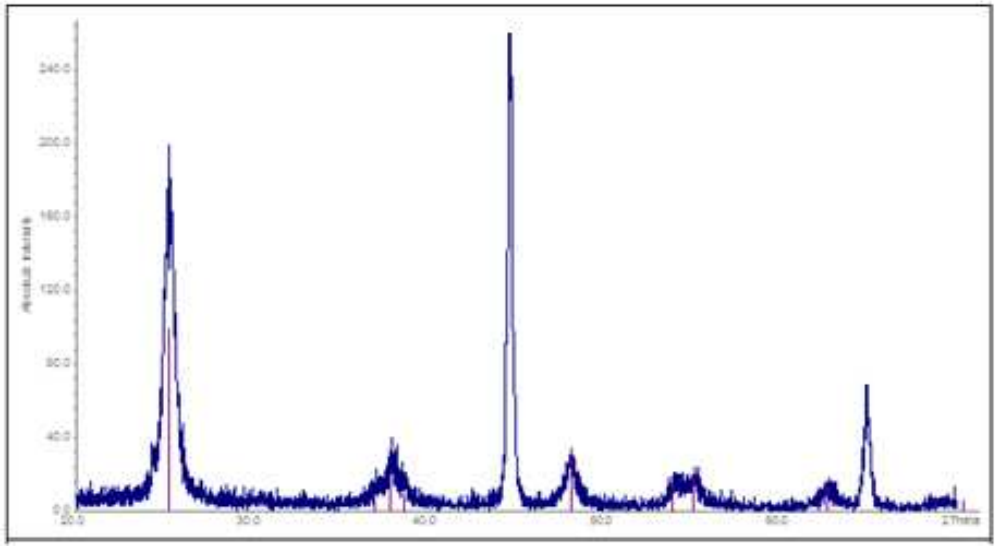

Fig.5.10: X-Ray diffraction pattern of acidified alcohol sol-gel and peaks for anatase (purple).

In fig 5.10, of note is the lack of rutile peaks. This particular formulation of sol-gel formed anatase. The two extra peaks are the steel substrate. The previous sol-gel formulas all formed rutile phase.

5.4.3.2 SEM ANALYSIS OF ACIDIFIED ALCOHOL SOL-GEL COATED SS316

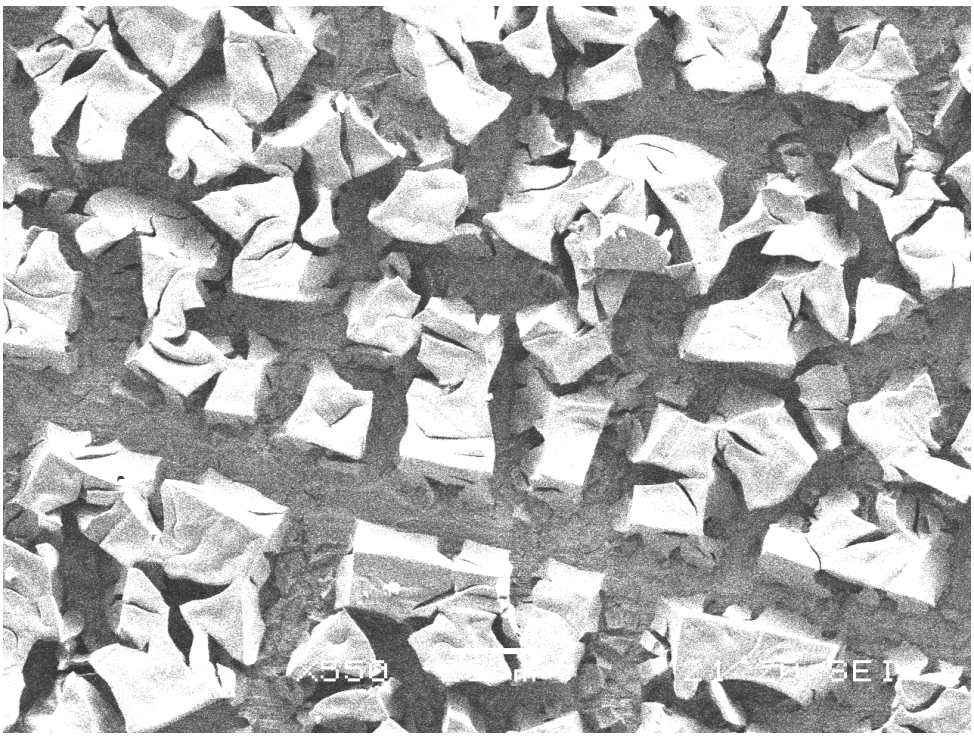

Fig.5.11: SEM of acidified alcohol based Ti sol-gel

As can be seen in fig.5.11, the sol-gel appears to have a dried mud, discontinuous appearance. Line scans show that the surface of the steel in the channels between the “mesas” of anatase.

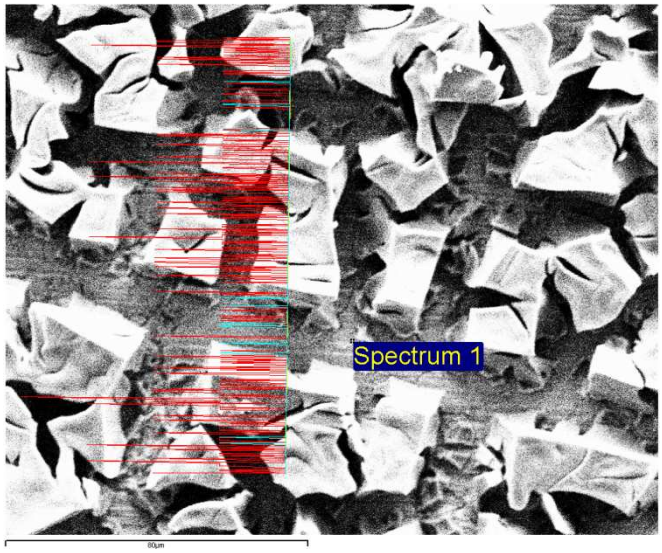

Fig.5.12: line scans EDS of fig.15. Red scans lines are Ti, blue scan lines Cr.

In an effort to check the adherence of the anatase phase, a section was rubbed. The towers came off, leaving the anatase foundations firmly stuck to the surface of the SS430. The appearance of cracks on the SS430 is chromia scale.

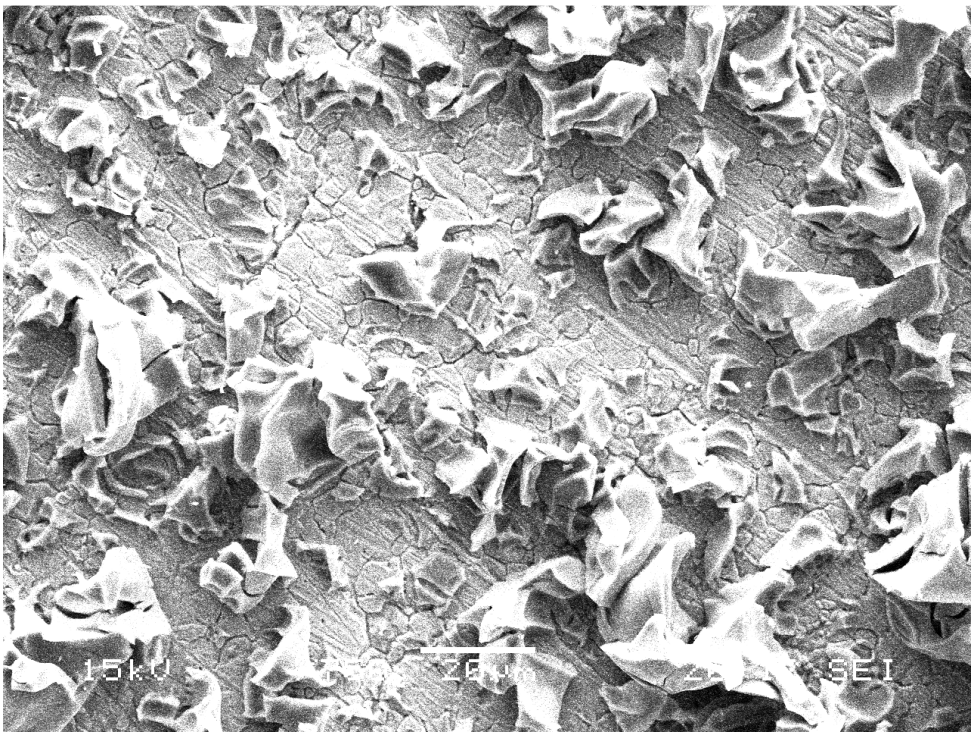

Fig.5.13: SEM image of rubbed acidified alcohol sol-gel coating on ss316

As can be seen in fig.5.3, the steel layer is visible between the foundations of the anatase towers. Although this was a major improvement from previous attempts, it demonstrates

that the sol-gel could not form a continuous layer, and would not be suitable for coating interconnects for SOFC use without much further optimization.

5.5 THIN LAYER TI EVAPORATION TO PROMOTE CTO OR SUBSTITUTED RUTILE ON SS430

As mentioned above, Ti is the only missing element required for CTO to be produced on the surface of SS430. Although simply putting rutile powder onto SS430 and firing at various temperatures proved unsuccessful, there are other routes to deposit elemental Ti onto other materials, and these can be later oxidized. These include evaporation, various forms of sputtering, organometallic evaporation and others.

Unfortunately at the present time there are no practical low temperature laboratory or industrial electrochemical deposition routes for titanium. The same is not true for cobalt, nickel, or copper for instance. If such an economical route for Ti were available it would be a highly desirable and commercially successful industrial process with a multitude of applications including aerospace.

A metals evaporator was available which was generally used for depositing gold onto epoxy samples for use in SEM. Although no experience existed regarding its use for sputtering other elements other than gold or silver, a trial and error program was started to deposit Ti with the metals evaporator. The parameters were: heating element thickness (W wire thickness), contact surface area between heating element and target (number of coils which also dictates total length), titanium thickness, and heating current. By trial and error a system of reliable Ti coating was achieved. Please see Experimentation chapter for a full discussion.

5.5.1 THEORETICAL THICKNESS CALCULATION

Based on the calculation $T = m/(4\rho * \pi * r^2)$ where T is thickness, m is mass of target, ρ is the density of the target, and r is the distance between target and substrate as set out in the chapter 3 the thickness was calculated. Each sputtered piece of Ti was approximately 30mm by 3 mm by .0005mm thick. Based on these values and a distance between target and substrate of 40mm the thickness was calculated to be 1.2×10^{-8} m. This Ti layer will make a rutile layer that is 2.3×10^{-8}m thick. It is hoped that the TiO_2 layer will become impregnated with Cr by evaporation and/or solid state diffusion from the chromia layer to form $(Cr_{.9}Ti_{.1})_2O_3$ which has a density of 0.00522g/mm^3. The stoichiometry is 9:1, meaning 1 mole of Ti makes 9 of CTO. Based on these values the thickness after corrosion is calculated to be 3.1×10^{-7}m per target of Ti. These are theoretical values and do not take into account the possibility of other stoichiometric intermediate products.

5.5.2 CHARACTERIZATION OF EVAPORATED TITANIUM

5.5.2.1 LAYER ON ALUMINA

Ti was evaporated onto a short section of alumina tube. The evaporated titanium changed the colour of the tube from white to metallic. The whole tube was tested with a multi-meter to test for resistivity. The multi-meter showed that the metallic layer was conductive, suggesting that elemental Ti had been deposited. Below is an image of the sample. The heating element and target were positioned above the tube with a distance of 20mm. As can be seen, as the tube curves away from the targets position, less metal is deposited.

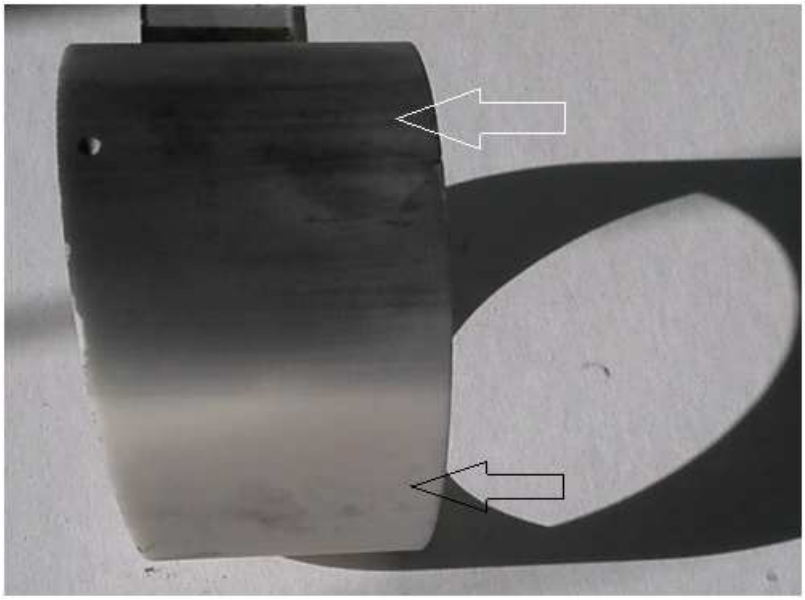

Fig.5.14: Alumina tube with titanium metal evaporated onto it. White arrow shows Ti layer, black arrow shows un coated area.

As can be seen in fig.5.14, as the tube curves down away from the top (white arrow) where the target was positioned the titanium layer becomes thinner. This is also evident with the multi-meter which shows increasing resistance as the probes leave the thick layer at the top. Ti is not known as a particularly good conductor as far as metals go (resistivity of Ti is 4.2×10^{-5} Ωcm, compared to copper at 1.6×10^{-6} Ωcm), yet most Ti oxides that are not reduced Magneli phases are insulators. Magneli phases usually appear as a black or very dark grey-blue colour, depending on the phase. Generally speaking, Magneli phases have higher resistivities than metallic titanium at 0.0016 Ωcm.

Further samples of Ti sputtered onto alumina also appeared metallic. Upon heating to 450^{o}C for durations of 48 hours these samples lost their metallic colour and left behind a slightly yellow hue on the white background of alumina.

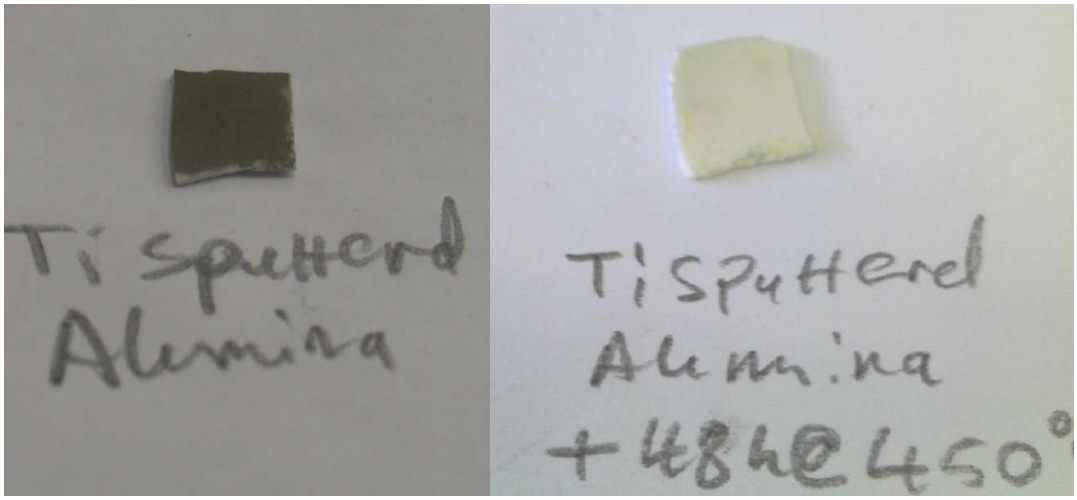

Fig.5.15a and b: Samples of alumina with Ti evaporated onto surface. Ti, pre heat treatment (left), and after 2 days at 450^{o}C in air (right)

The sample fragments in fig.5.15 above are two pieces of the same sputtered sample of alumina. The sample on the left was not heated, the sample on the right was heated to 450^{o}C for 48 hours.

Using a 4 point probe with various currents and voltages the resistance of the inner terminals was found to be 18.70Ω. Using a multimeter, the resistance was found to be 4.3KΩ. The multimeter gave open circuit for the sample on the left, and no current could be passed through the sample on the left using a 4 point probe. It can be concluded that when Ti is evaporated it is in its metallic form, and upon heating, it oxidizes.

5.5.2.2 X-RAY DIFFRACTION OF PRE-HEATED SAMPLE ON ALUMINA

X-Ray diffraction was performed on the above samples. Below are the results, including the peak file generated for refinement.

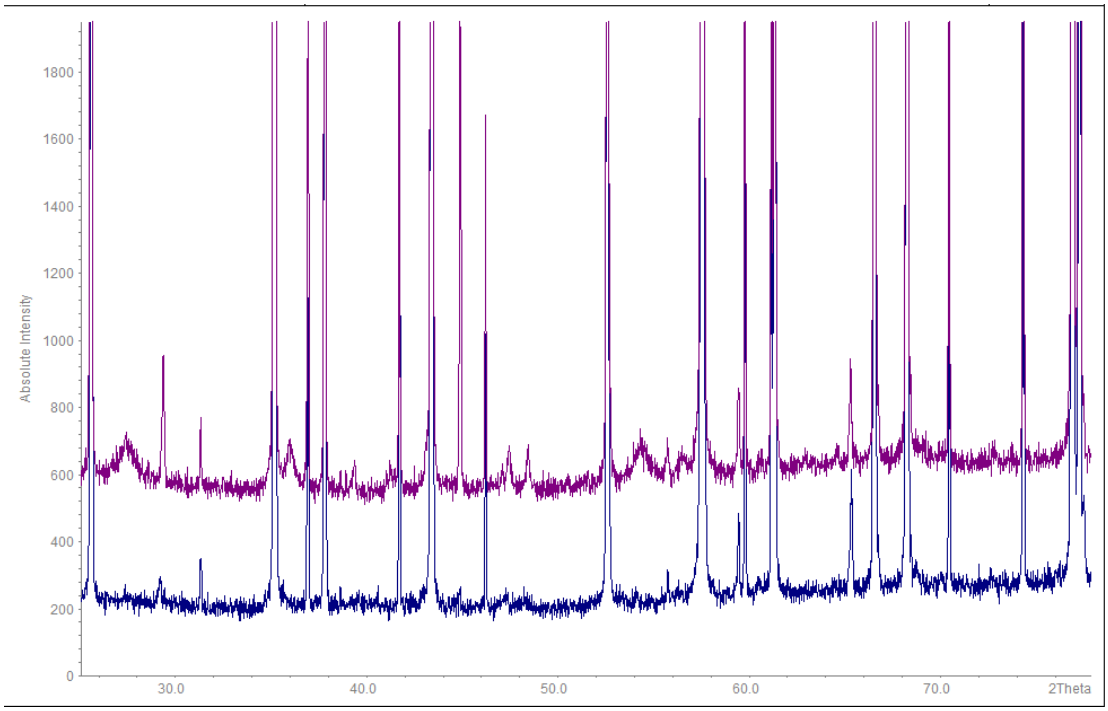

Fig.5.16: X-Ray diffraction pattern of Ti coated alumina (blue) oxidized Ti coated alumina (purple)

Refinement using hkl data from the PDF card for rutile number 12, 2176 is presented below.

	TiO_2		
	Standard	Sample	%
A	4.59	4.604(18)	0.31
C	2.9592	2.953(10)	0.21

Table 5.3: Refined unit cell parameters for rutile on alumina.

In fig.5.16 no metallic titanium was found on the unheated sample, represented by the blue line in Fig.5.16 and the above graph and the metallic coloured sampled in Fig.5.15a. The purple curve in Fig.5.16 represents the sample that was heated to 450^{o}C for 48 hours, which is the white/yellow coloured sample in the Fig.5.15.b. Based on these results, it would appear there is no rutile on the metallic sample. This agrees with the with the conclusions from section 5.5.2.1 that titanium is deposited as a metal, but oxidizes upon heating, in this case, to rutile, and not anatase.

5.5.2.3 SEM OF TI EVAPORATED ONTO ALUMINA PRE HEAT TREATMENT

The sample from Fig.5.15a, alumia with a coating of metallic titanium, was examined with SEM and appears in fig.5.17 below.

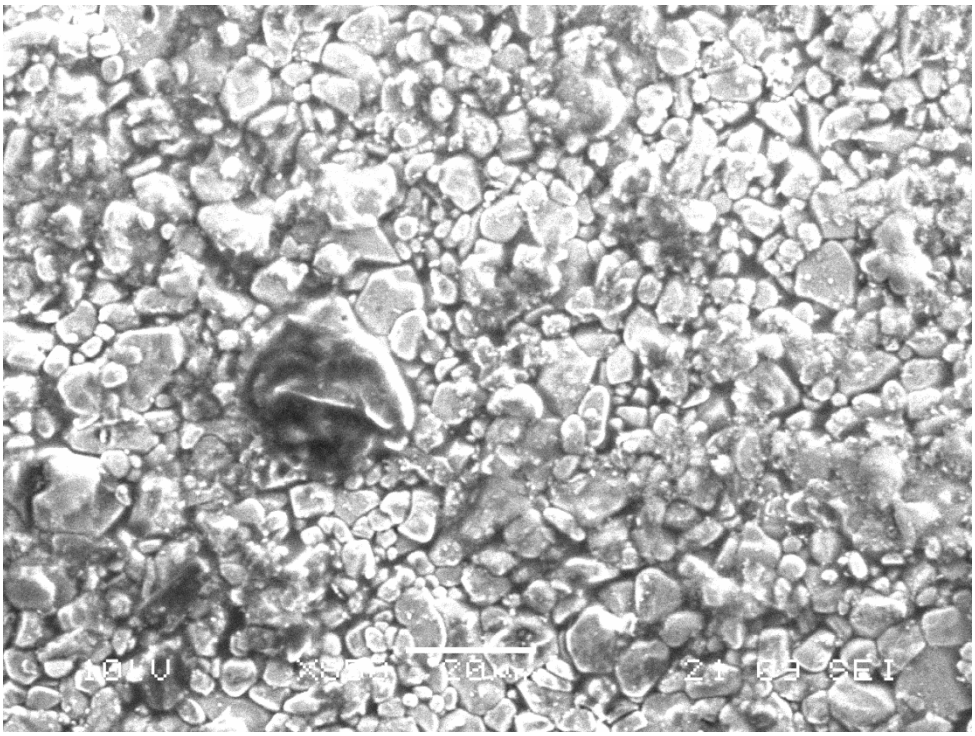

Fig.5.17: SEM of Sample from Fig.5.15a, Ti metal on Alumina.

EDS for the sample above revealed titanium, aluminium, and carbon.

Element	Weight%	Atomic%
C K	18.97	26.7
O K	54.77	57.88
Al K	22.47	14.08
Ti K	3.79	1.34
Totals	100	

Table 5.4: EDS results from fig.5.17. 10kv, spot size = 9, WD = 21

Below in fig. 5.18 is SEM image of rutile on alumina.

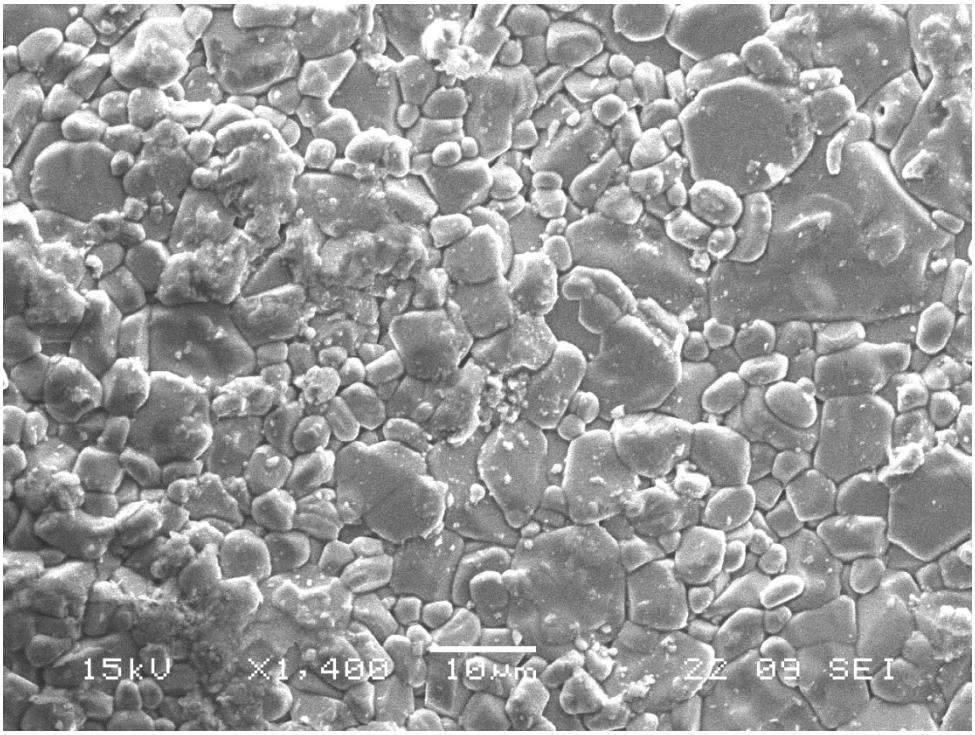

Fig.5.18: Rutile on alumina from the sample from Fig.5.15b by oxidation of Ti at 450, 48 hours.

The grains are as they appear on alumina. Although EDS showed clear Ti peaks for this sample, quantization was not possible, probably due to the flaring due to the lack of conductivity. This was the case for SEM acceleration voltages of 10kv and 15 kv, both with spot sizes of 9, and sample times of 600 seconds in the analyzer program of the Inca software. It could be assumed that there would be no loss of Ti by any means. Flaring was not obsereved on the un-oxidized sample, which would support the conclusion that Ti is metallic as sputtered, but oxidizes upon heat treatment.

5.5.3 EVAPORATION OF TI ONTO SS430

Initial visual analysis showed a browning of the metal substrate after evaporation of 2 slivers of titanium metal. Further evaporations onto SS430 lead to darkening of the brown colour and eventually a coffee like hue. Tools are not currently available to show these subtle changes, but the coating is visible in fig.5.19.

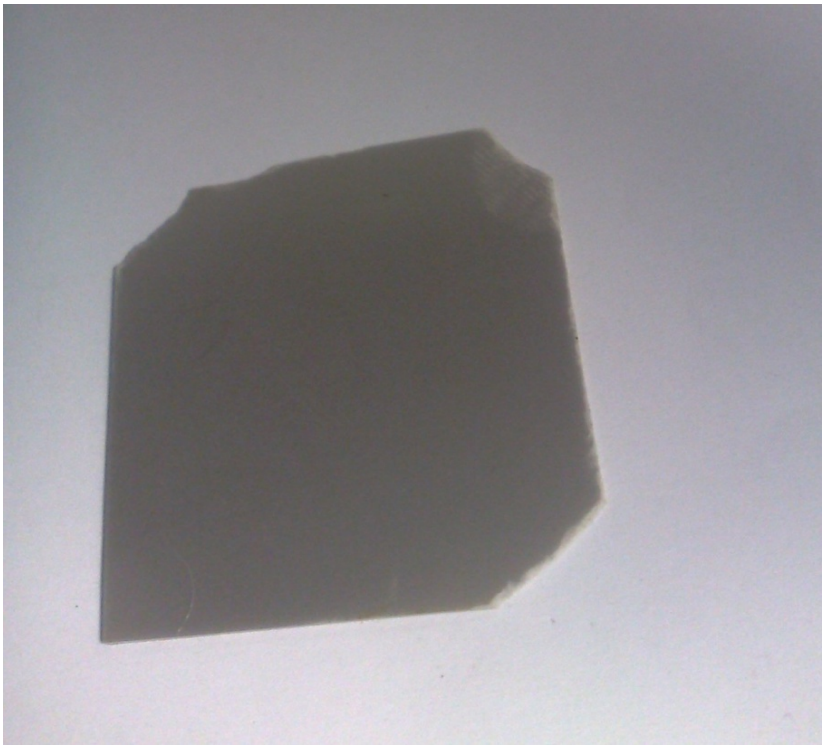

Fig.5.19 SS430 with Ti evaporated onto the surface

Fig.5.20 below shows samples of SS430 with coatings of titanium with increasing temperature and duration firings. First, all samples were fired at 300^{o}C for 24 hours, then all but the first sample were fired at 350^{o}C for 24 hours, then the two right samples were fired at 400 ^{o}C for 24 hours, then just the right sample was fired again at 450^{o}C for 24 hours. As the temperature and duration increased the colour changed from just metallic, to gold, to yellow and then toward green. The back side of these samples were all brown in varying degrees, characteristic of SS430 corrosion at low temperatures.

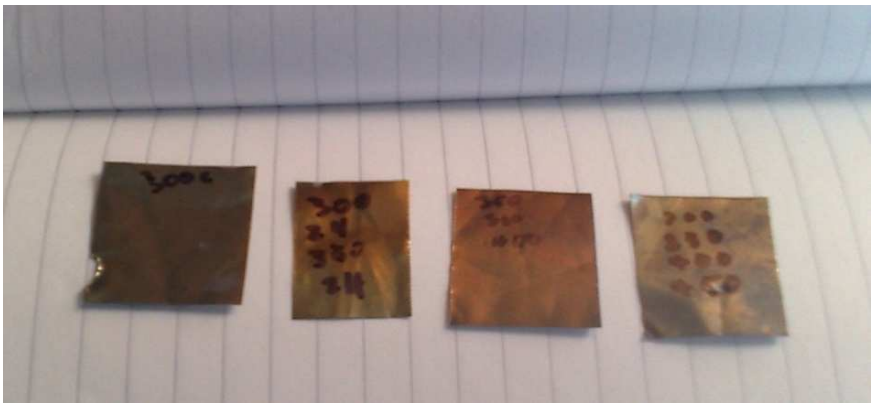

Fig.5.20: SS430 samples coated with titanium by sputtering fired for increasing durations at increasing temperatures.

5.5.4 SUMMARY OF TEMPERATURE DEPENDANT CORROSION OF TITANIUM COATINGS

The following sections concern the corrosion behaviour of SS430 both uncoated and coated with Ti. The X-Ray patterns of both are presented below. Detailed descriptions follow starting with section 5.5.5.

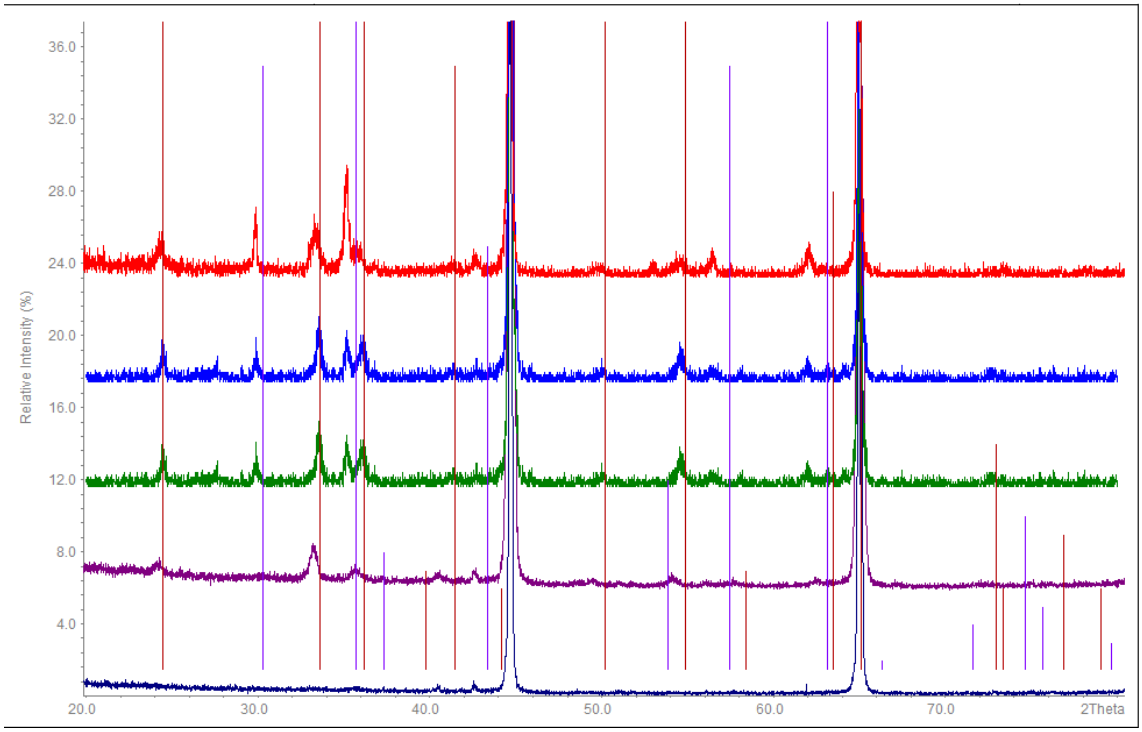

Fig.5.21: SS430 with increasing temperature treatments of 400°C(dark blue), 450°C(purple), 500°C (green) 600°C(light blue), 700°C(orange) and peaks for eskolaite(brown) and spinel (purple line)

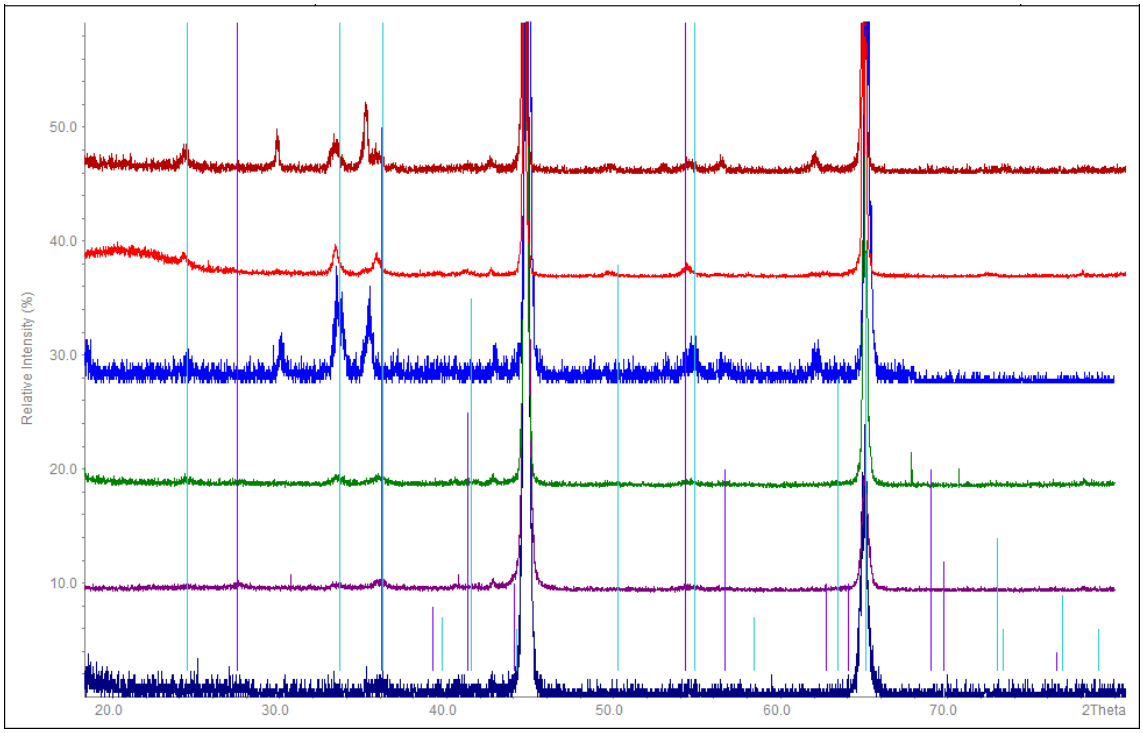

Fig.5.22: Ti coated SS430 with increasing temperature treatments 400°C(dark blue), 450°C (purple), 500°C (green), 600°C(blue) 650°C (orange) and , 700°C(brown) with rutile peaks (purple line) and eskolaite peaks (light blue)

In fig.5.21 we can see that corrosion is eskolaite typ at lower temperatures until around 500°C when spinel phase starts to form. At 700°C both the eskolaite and spinel peaks are shifting to the right due to changes in the unit cell parameters due to incorporation of other elements such as iron.

In fig.5.22 we can see faint rutile peaks, even at 400°C until 550°C. At 600 and above the corrosion is similar to uncoated samples with spinel phases aprearing and eskolaite peaks shifting to the right.

5.5.5 TITANIUM COATED SS430 HEATED TO 650°C FOR 48 HOURS

After coating with Ti and heat treatment to 650°C for 48 hours the sample looked very different to previous temperatures. There is no single continuous coating, and as can be seen, there appears to be a layer of clumps coating another layer of crystals. There are no eskolaite or spinel type crystals.

.

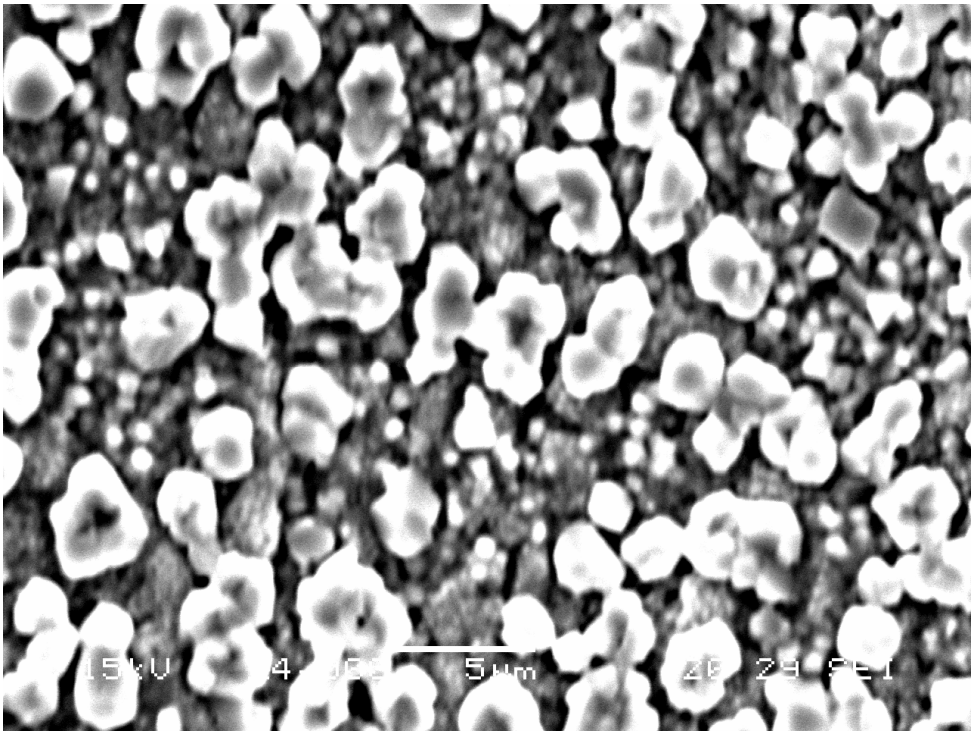

Fig.5.23: Ti coated SS430 heated to 650^{o}C for 48 hours

Below are the EDS results in table 5.4 for the above area.

Element	Weight%	Atomic%
O K	32.38	61.54
Ti K	0.14	0.09
Cr K	35.94	21.02
Mn K	18.66	10.33
Fe K	12.89	7.02
Totals	100	

Table 5.4: EDS results for coated and heated sample from fig.5.23

After heating at 650^{o}C Ti is hard to detect in this sample. Of interest are the amounts of Cr and Mn which at these temperatures are quite volatile. Below is data for the uncoated sample in table 5.5.

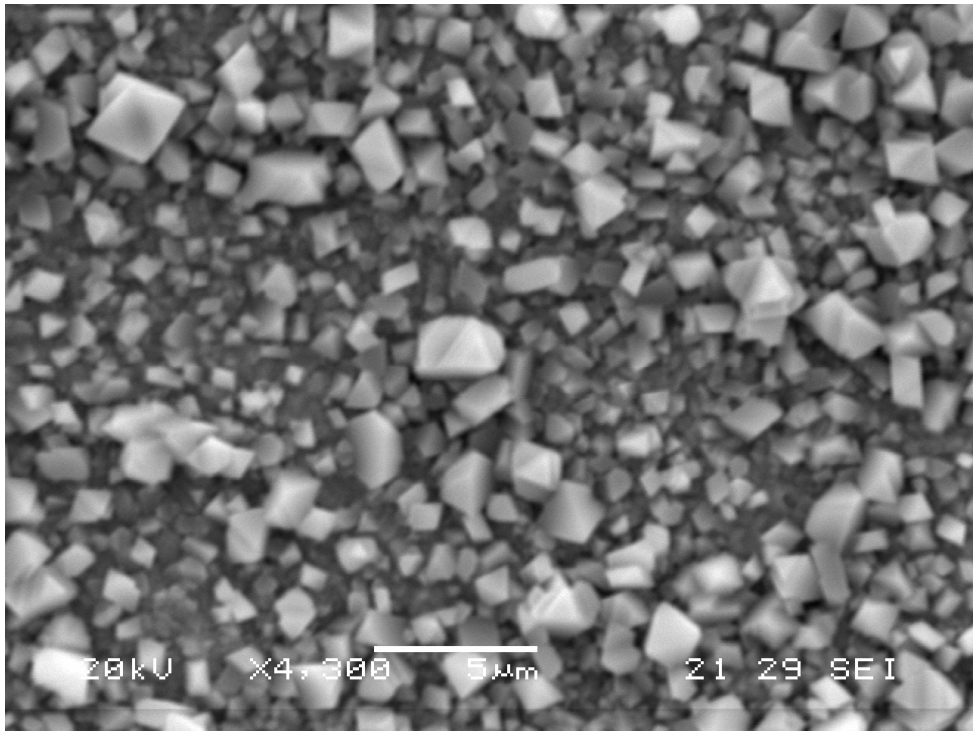

Fig.5.24: Uncoated SS430 heated to 650^{o}C for 10 days

As can be seen in fig.24, spinels are forming under the same conditions where Ti prevents it.

Element	Weight%	Atomic%
O K	29	57.98
Ti	---	----
Cr K	29.9	18.39
Mn K	10.19	5.93
Fe K	30.91	17.7
Totals	100	

Table 5.5: EDS results for the whole surface of Fig.5.22

Comparing table 5.4 to table 5.5 there are small decreases in Mn and Cr without the Ti layer, and large increase in the amount of Fe detected. It should be kept in mind that these are very thin layers on stainless steel, and depending on the acceleration voltage, spot size and capture time, different penetration depths with the microscope will register different amount of elements. Working distances were the same for both samples, spot sizes were 29, however, acceleration voltages were different, with 15kv the maximum without flaring achieved for the Ti coated sample, and 20kv for the uncoated sample. The flaring of the coated layer would suggest lower conductivities, due to the presence of rutile. The higher acceleration voltage for the uncoated layer would explain the increase in Fe due to higher penetration depth. Finding the exact amounts of elements in the thin corrosion layer on the surface of stainless steel can be difficult and tedious work. However, from the evidence

provided from the sources of SEM visual inspection, EDS data, it would appear clear that Ti coatings are preventing spinels from forming, by taking away at least one reactant, either Mn or Cr and also by limiting the surface of the steel for production of these products.

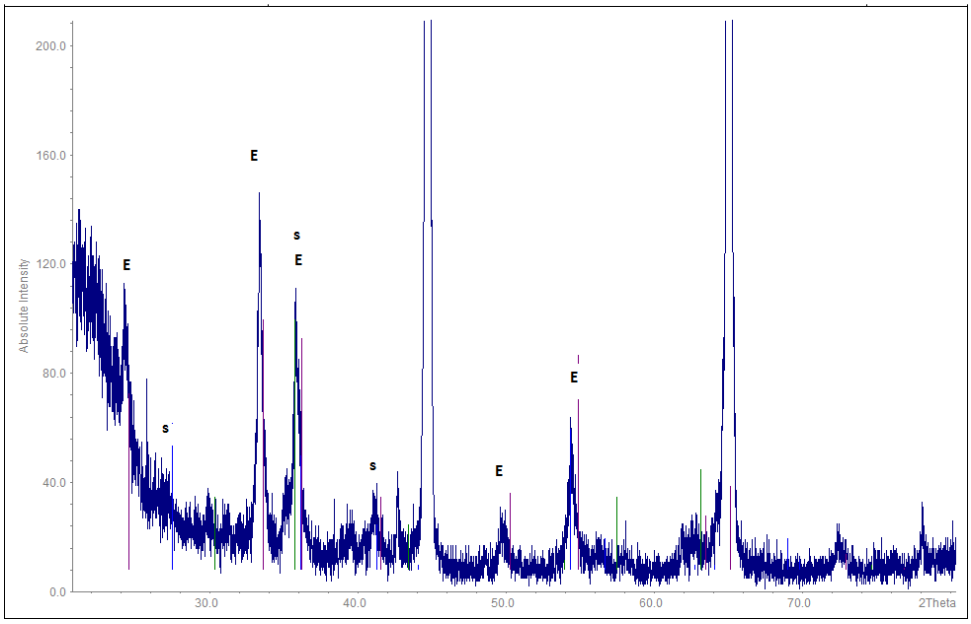

Fig.5.25: X-Ray diffraction pattern of SS430 with Ti heated to 650^{o}C with possible eskolaite peaks (E) and spinel peaks (S)marked

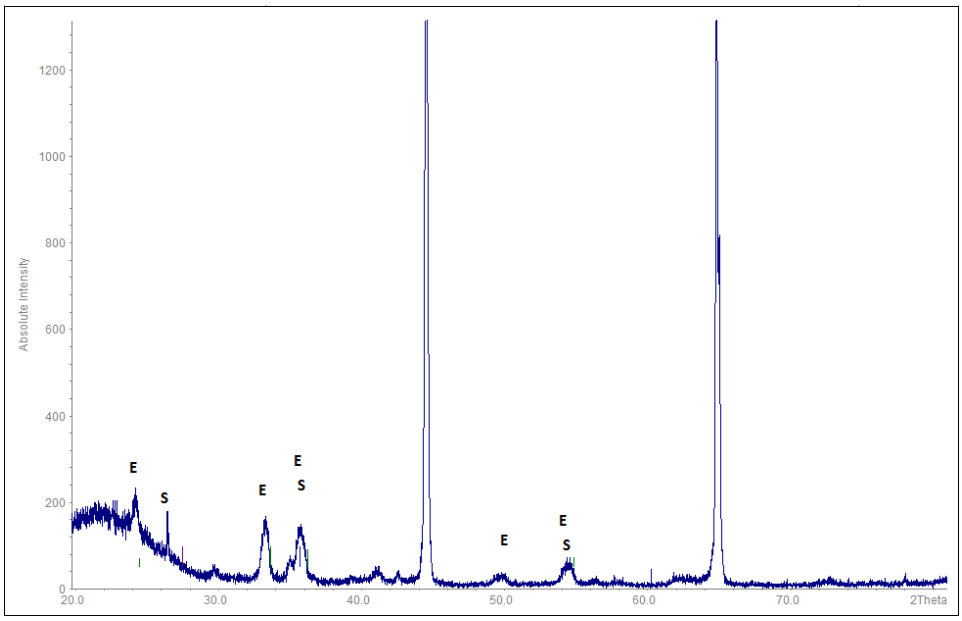

Fig.5.26: X-Ray diffraction pattern of SS430 heated to 650^{o}C with possible eskolaite peaks (E) and spinel peaks (S)marked

There is not much to differentiate between fig5.25 and fig.5.26. This would indicate that at this temperature the titania layer is quicky over run by corrosion products which advance unhindered.

5.5.6 SS430 COATED WITH TI AND HEATED TO 600^{O}C FOR 10 DAYS

The two parameters to manipulate for production of CTO by deposition of Ti onto SS430 are temperature and time of heating. Temperature will control the thermodynamics of what is can be produced, and time will allow for slow kinetics. Because the temperature has been lowerd, extra will be needed for mas transfer through the rutile phase.

Following on from previous section, samples of SS430 were coated with thin layers of Ti and heated to 600^{o}C. The sample was analysed with SEM and using X-Ray diffraction.
Below is the X-Ray diffraction pattern recovered from this sample.

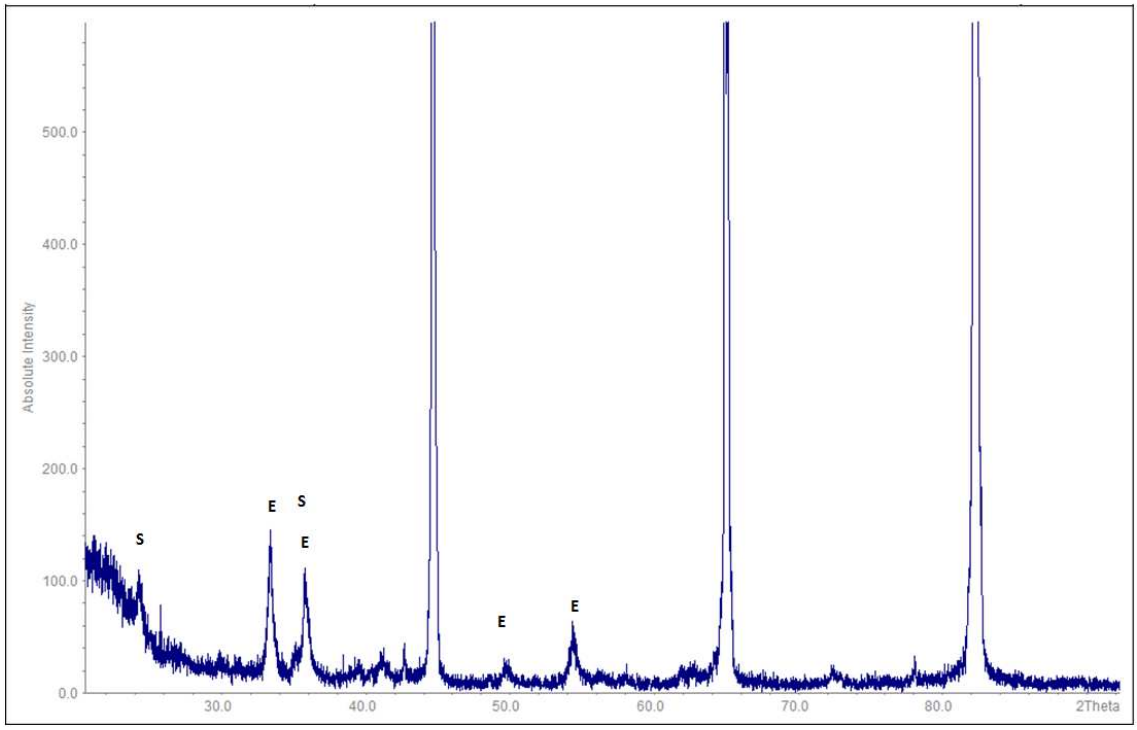

Fig.5.27: SS430 coated with Ti and heated to 600^{o}C with possible eskolaite peaks (E) and spinel peaks (S)marked

The major non steel peaks were determined to be eskolaite in nature and were indexed using hkl values for generic eskolaite Unit cell parameters were found to be 5.4 for A and 13.3 for C, too large to be considered eskolaite, therefore a table of results is not presented.

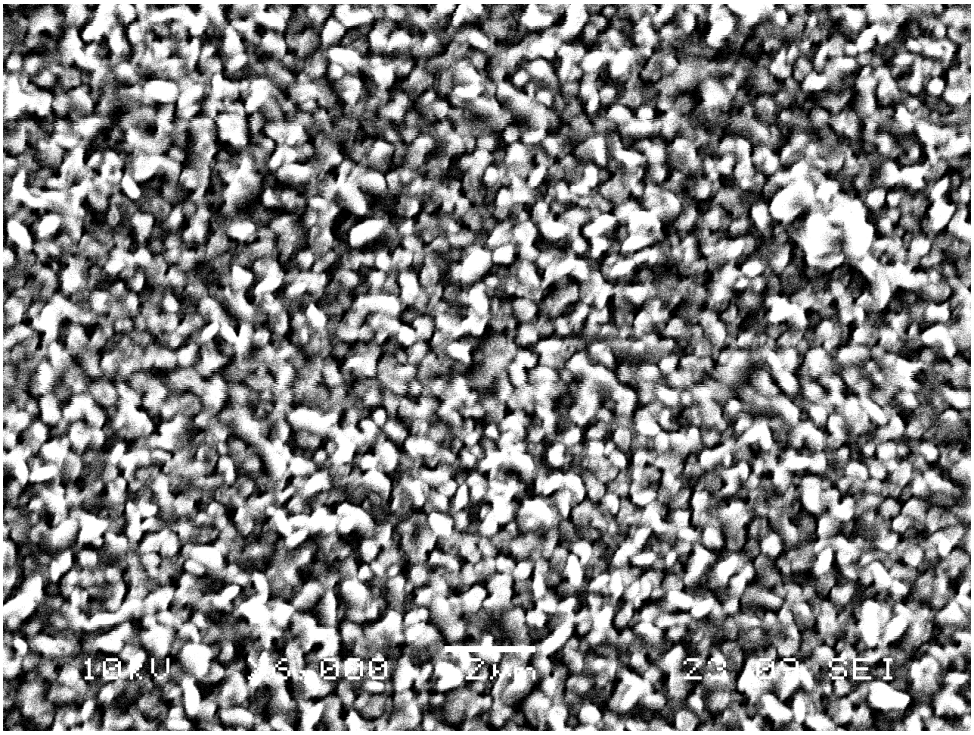

Fig.5.28: SS430 coated with Ti and heated to 600^{o}C for 10 days

Again, the TiO_2 layer is no longer continuous. Below is the EDS data for the above image. The acceleration voltage was 10k, spot size 9 and working distance 20 as used in previous samples.

Element	Weight%	Weight% variance	Atomic%
O K	42.26	3.95	70.05
Ti K	11.2	3.5	6.2
Cr K	46.55	4.7	23.75
Totals	100		

Table 5.7 : EDS results for fig.5.28 area scanned with analyzer routine.

SS430 heated to 600^{o}C without coating is examined below.

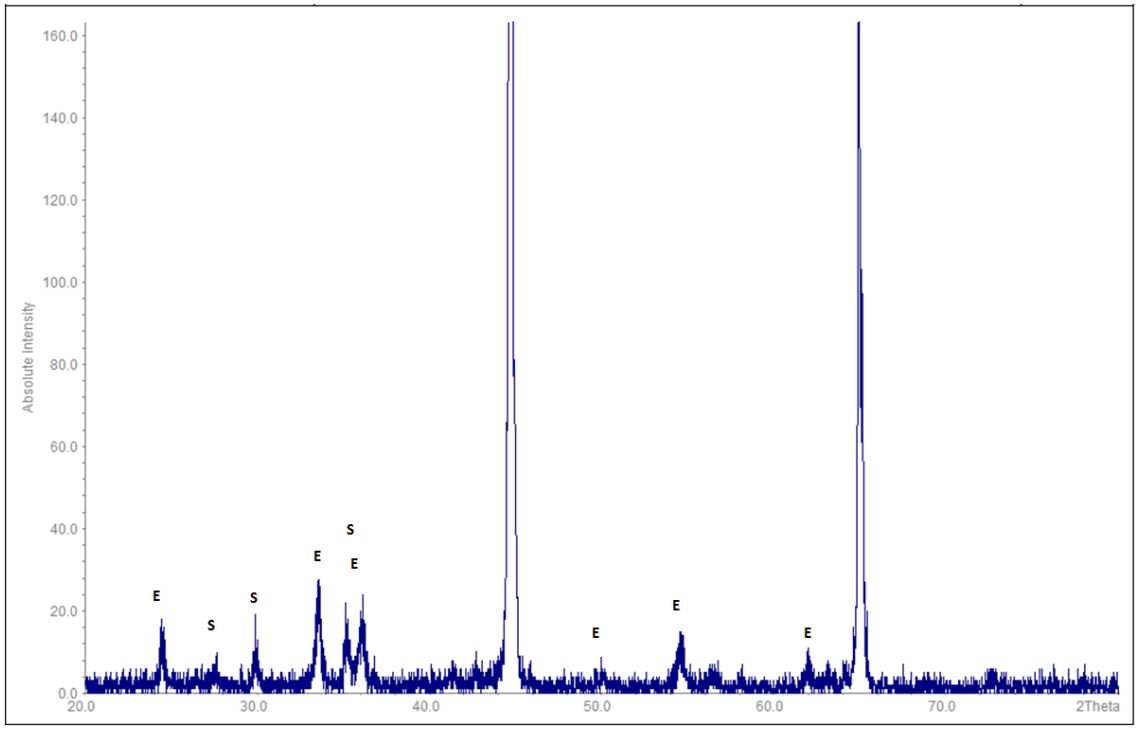

Fig.5.29: X-Ray pattern of SS430 heated to 600 for 10 days.

For the above pattern in fig.5.29 two non steel peak sets were found. These were determined to be $FeCrO_3$ and $Cr_{1.5}Mn_{1.5}O_4$, a spinel from space group Fd3m.

	$FeCrO_3$				$Cr1.5Mn1.5O4$		
	Standard	sample	%		Standard	Sample	%
A	5.01	5.09	1.5	A	8.455	8.51	0.651
C	13.63	13.8	1.5				

Table 5.8: Refined indexed peaks for non steel peaks from fig.5.29

No peaks were un-indexed, but some were shared. The refinement is relatively poor compared to other refinements in this section. The eskolaite phase is most likely a mixture of iron, manganese, and chrome oxide combinations. Following is an SEM analysis of the un-treated sample.

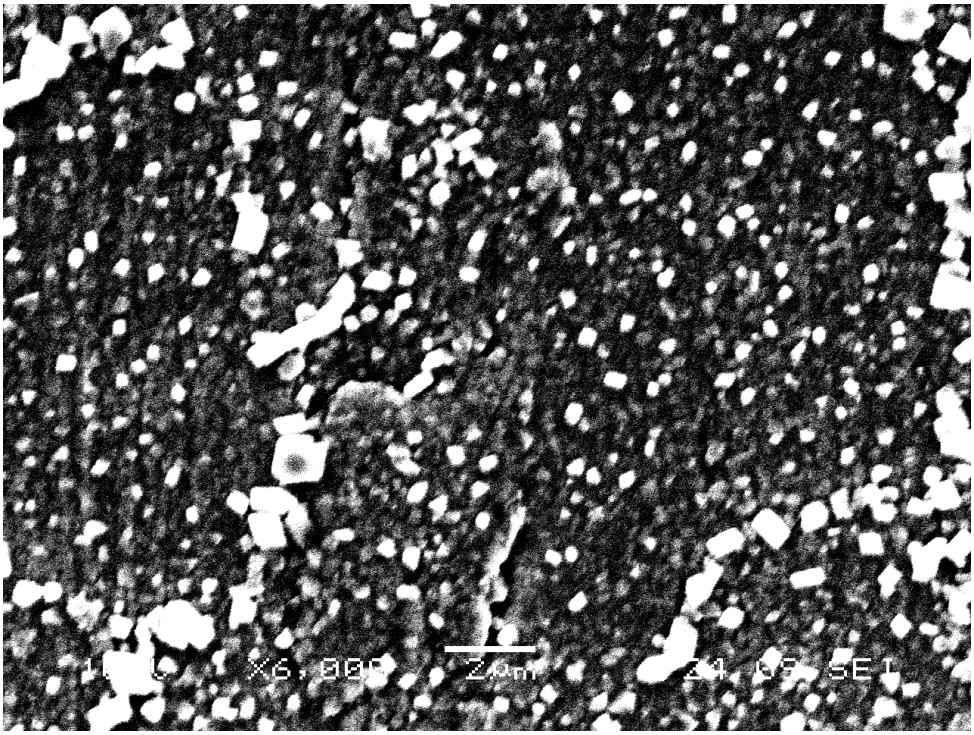

Fig.5.30: SS430 un-coated and heated to 600^{o}C for 10 days

As might be expected from X-Ray analysis, spinel crystals are beginning to form inn fig 5.30. When we compare fig.5.30 wwith fig.5.28, it would appear that at this temperature, Ti is prohibiting the production of spinels. To do this, either Mn or Cr need to be "mopped up" as they migrate from the steel. Even though the Ti layer at 600^{o}C is no longer dense, it is still preventing, or may have prevented whilst still dense, spinel formation that would normally go on unhindered as seen in fig.5.30 and fig.5.24.

Element	Weight%	Weight% error	Atomic%
O K	33.27	6.8	61.81
Ti K	0.93	8.15	0.58
Cr K	65.8	8.37	37.61

Table 5.9: Inca results for scan from fig.5.30

The above EDS results ignored Mn and Fe, and were intended to show that Ti was below the effective reading limits.

5.5.7 SS430 COATED WITH TI HEATED TO 550^{O}C FOR 10 DAYS

Similar samples to the previous sections were prepared and heated to 550^{o}C for 10 days. Below are the results.

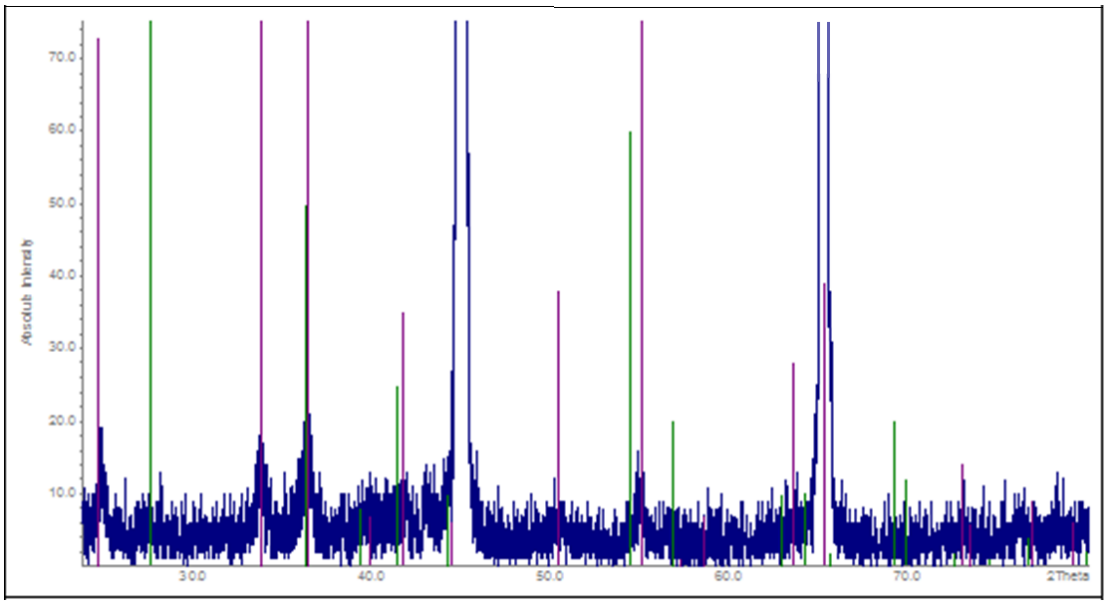

Fig.5.31: X-Ray pattern for SS430 heated to 550^{o}C for 10 days with Cr_2O_3(purple)representing eskolaite and rutile (green)

As can be seen by the above pattern in fig 5.31 Cr_2O_3 is now the predominant phase, with sloping to the left of these peaks caused by $FeCrO_3$.

	Eskolaite		
		Sample	%
A	4.9587	4.98(3)	0.43
C	13.594	13.59(4)	0.03

Table 5.10 : unit cell parameters for fig.5.31

The values in table 5.10 are much closer agreement with eskolaite than for lower temperature samples. This is partly due to the quantity and quality of peaks found in the chromia range. The values in table 5.10 were compared to those in 5.1 and 5.2 at the beginning of the chapter. The results are below.

		CTO(x=.1)		CTO(x=.2)	
	Sample	Standard	%	Standard	%
a	4.98	4.945	0.70	4.952	0.56
b	13.59	13.6	0.07	13.61	0.15

Table 5.11 unit cell parameters compared to standards from fig.5.1and 5.2

It would appear that un-doped chromia is a better fit for the unit cell parameters from the sample, even though all are quite poor. At these temperatures the minor elements of steel are contributing interesting doping fractions, however, the subsequent peaks are very hard to determine. This is because the peaks generated are so small, and because there are so many, and because there are so many elements. Many of these structures are not characterized by the ICDD because they are not pure phases. Below is the SEM micrograph of the same sample in fig.5.32.

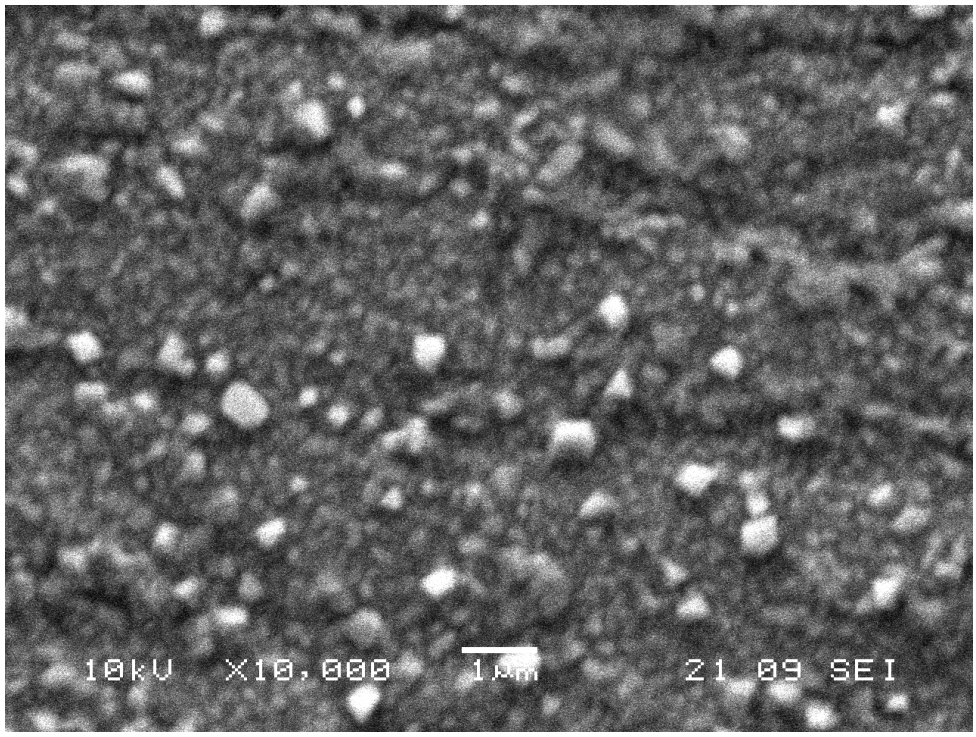

Fig.5.32: SS430 coated with Ti and heated to 550^{0}C

Unlike previous samples, there appear to be small lumps of something that is less conductive than the background. The above image area was used in the "analyser" routine of the Inca software, below is the table of results.

	A			B	
Element	Weight%	Atomic%	Element	Weight%	Atomic %
O K	24.85	52.61	O	40.99	69.11
Ti K	3.62	2.56	Ti	5.970	3.363
Cr K	32.16	20.95	Cr	53.04	27.52
Fe K	39.37	23.88			
Totals	100	100		100	100

Table 5.12 : EDS results for fig.5.32 (A) above and corrected table excluding iron (B)

Of interest were the white areas seen in the image. These parts were sampled with the point and ID routine in the Inca software. Below are the results.

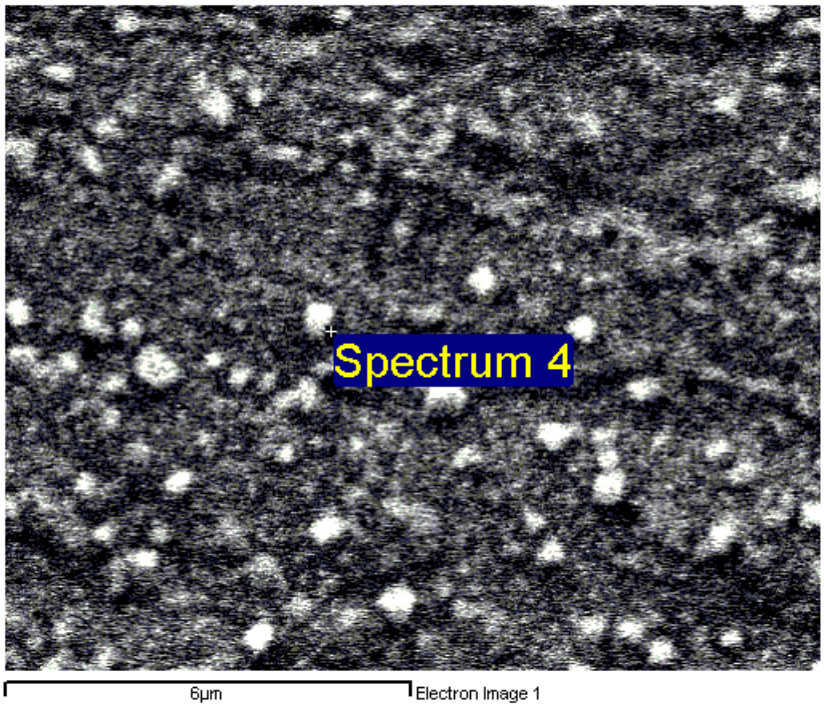

Fig.5.33: SEM of SS430 coated with Ti showing sample point for below EDS data

Element	Weight%	Atomic%
O K	59.63	82.45
Ti K	10.5	4.85
Cr K	29.87	12.71
Totals	100	100

Table 5.13: EDS data for spectrum 4 in fig.5.33.

Compared to table 5.12b, it would appear the white areas have increased titanium and decreased chromium concentrations.

5.5.8 ANALYSIS OF SS430 WITH TITANIUM HEATED TO 500^{O}C FOR 10 DAYS

Following from the above experiments, a new sample was created and heated to 500^{o}C for 10 days. Below is the X-Ray diffraction pattern for titanium coated SS430 heated to 500^{o}C for 10 days. Lowering the temperature slows the corrosion rate of the steel. The goal is to create a coating from the Ti deposited and the Cr evaporation from the steel. Previous sections show that at higher temperatures the growth of corrosion is faster than the ability of the titanium to allow chromium to diffuse into it.

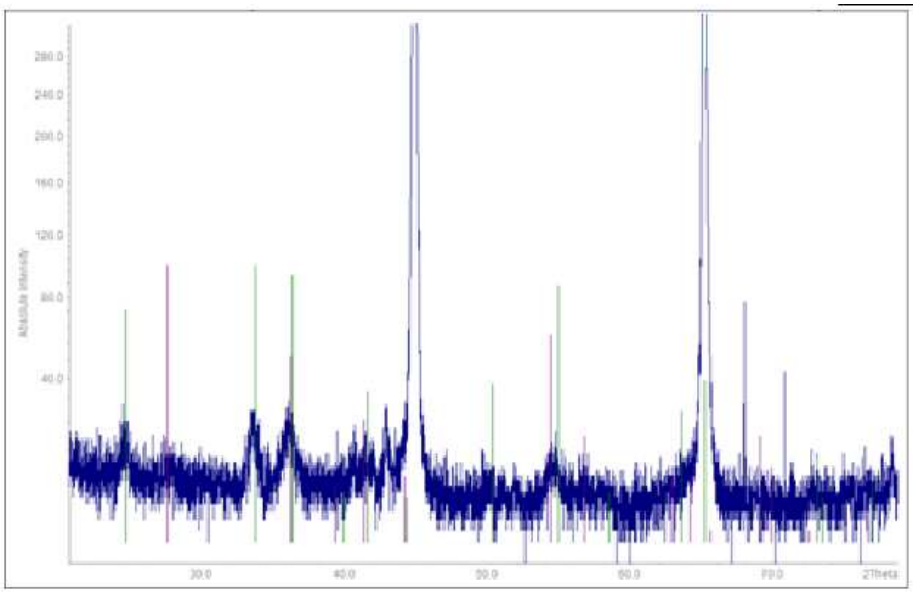

Fig.5.34: X-Ray patterns of SS430 coated with Ti at 500^{o}C for 10 days with Cr_2O_3 (green) and Rutile (purple) peaks

Refinement of unit cell parameters had large error. The pattern was similar to samples heated to 550^{o}C but with lower intensities.

The above samples used for X-Ray analysis were also used for scanning electron microscopy as seen in fig.5.35.

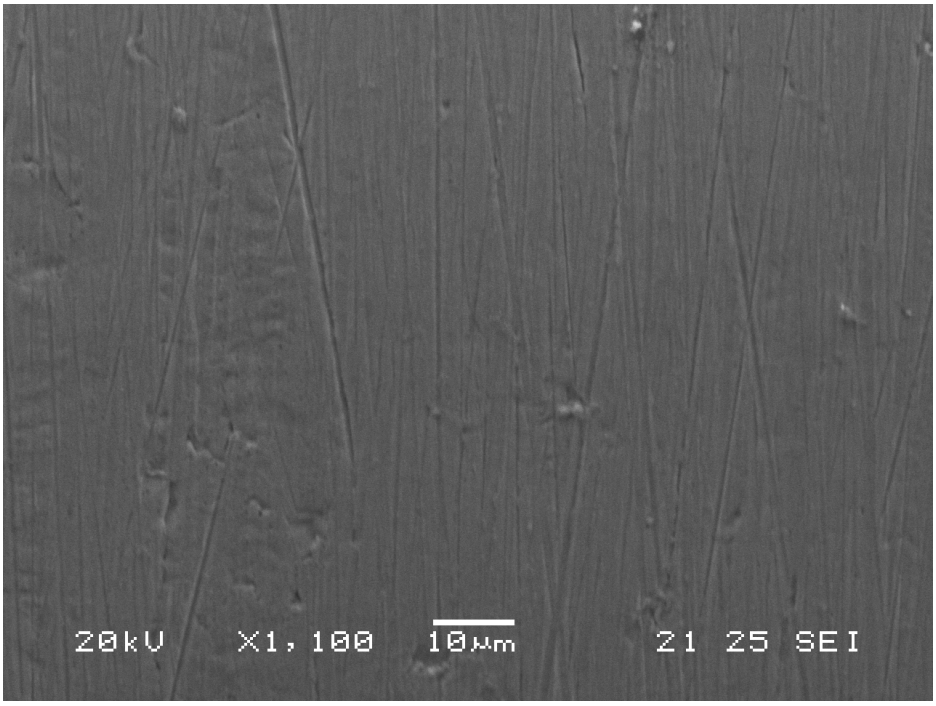

Fig.5.35: SS430 coated with Ti and heated to 500^{o}C for 10 days. 20kv, spot size 25

Element	O	Ti	Cr	Fe	Total
Weight%	40.44	3.39	19.26	36.91	100
Atomic%	69.63	1.95	10.21	18.21	100

Table 5.14 of results for EDS. Field of view from fig.5.35 is the source.

As can be seen from the EDS in tables 5.14 and 5.13, for similar amount of evaporated Ti, the proportion of Ti present in EDS analysis is getting larger compared to the higher temperature samples. This is because as the reaction temperature is decreased the amount of iron, chromium and oxygen is also decreased, with a corresponding increase in apparent titanium.

The back of this sample was not coated with Ti, and it was apparent that chromia was beginning to spall from this surface. This would suggest that at the 500^{o}C temperature range the titanium coating was slowing oxygen transfer into the corrosion layer.

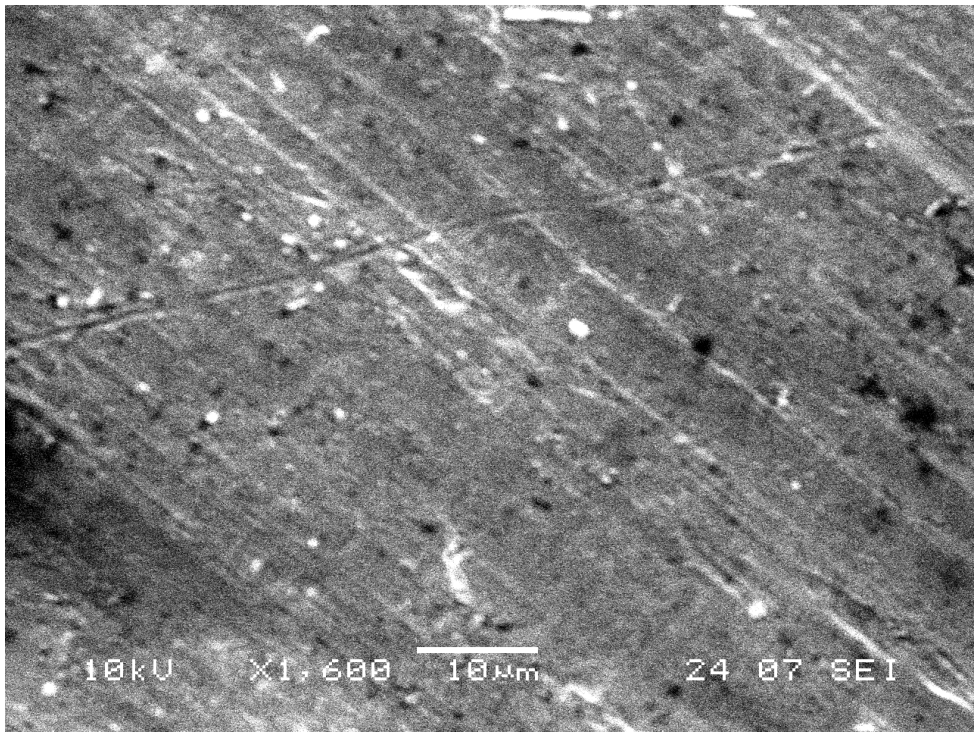

Fig.5.37:SS430 heated to 500^{o}C for 10 days

5.5.9 SS430 WITH TITANIUM COATING HEATED TO 450^{O}C FOR 15 DAYS

With 50^{0}C decrease in temperature for the same duration an SS430 sample with the same amount of Ti evaporated onto it showed similar visual characteristics to the lower temperature version. However the X-Ray pattern was quite different.

Whereas the sample heated to 500^{o}C displayed no rutile peaks, the sample heated for the same duration at 450^{o}C had steel peaks and began to exhibit both rutile and chromia peaks.

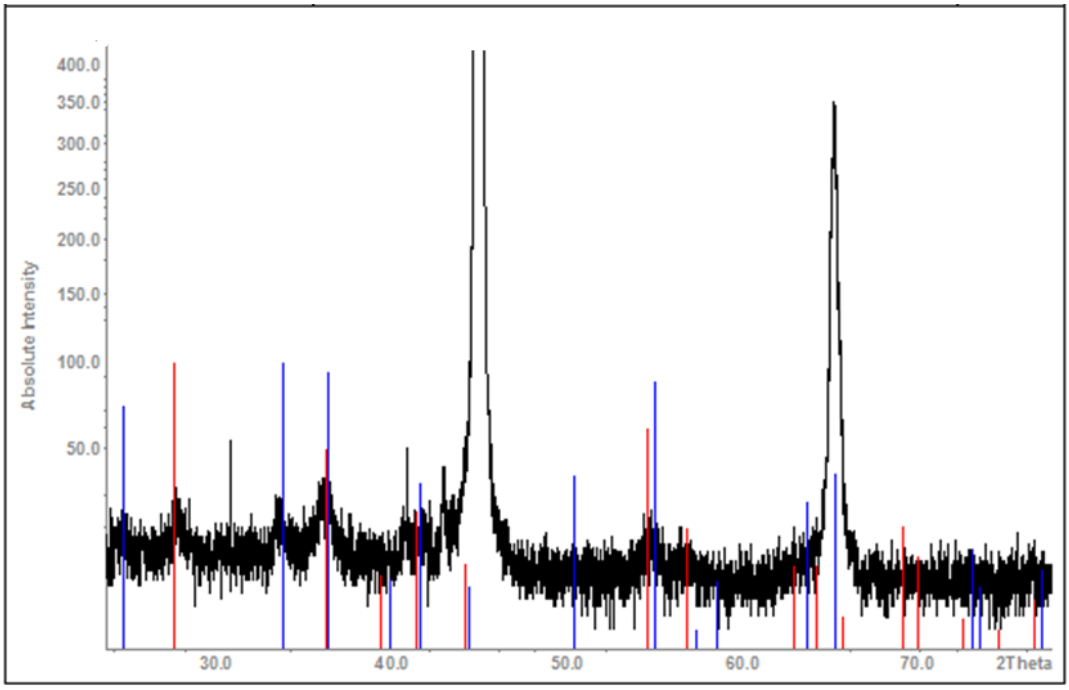

Fig.5.38: X-Ray diffraction pattern from SS430 heated to 450^{o}C for 15 days withCr_2O_3(Blue) and rutile(red)

Refinement was performed on peaks considered to be rutile and peaks that were considered to be chromia.

	TiO_2				Cr_2O_3		
	Standard	sample	%		Standard	Sample	%
A	4.59	4.6(3)	0.22	A	4.95876	4.9(1)	1.2
C	2.9592	3.0(2)	1.4	C	13.5942	13.6(1)	0.04

Table 5.15 : Refined unit cell parameters from indexed peaks from fig.5.38

In table 5.15 T there is a large deviation for the C parameter for TiO_2 and the A parameter of Cr_2O_3 which is likely due to incorporation of other elements into the structure.

As the temperature of reaction is decreased the rutile phase is remaining in place. Increases in duration are used to ensure reaction completion at lower temperatures.

5.5.10 SS430 with Titanium coating heated 400^{O}C for 15 days

After heating for 15 days at 400^{o}C the Ti coated side changed colour with purples, blues and other colours. The backside of the same sample turned slightly brown tinged.

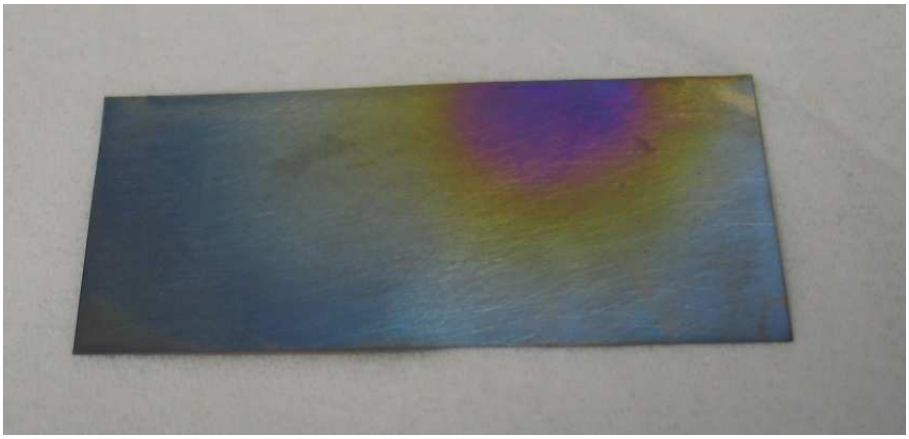

Fig.5.39: SS430 with Ti after 15 days at 400^{0}C

Fig.5.38: Back side of sample from fig.25 showing corrosion.

X-Ray analysis of the sample from fig.5.37 showed that rutile could possibly be forming. Unfortunately the rutile peaks were very wide, and very few, making refinement problematic.

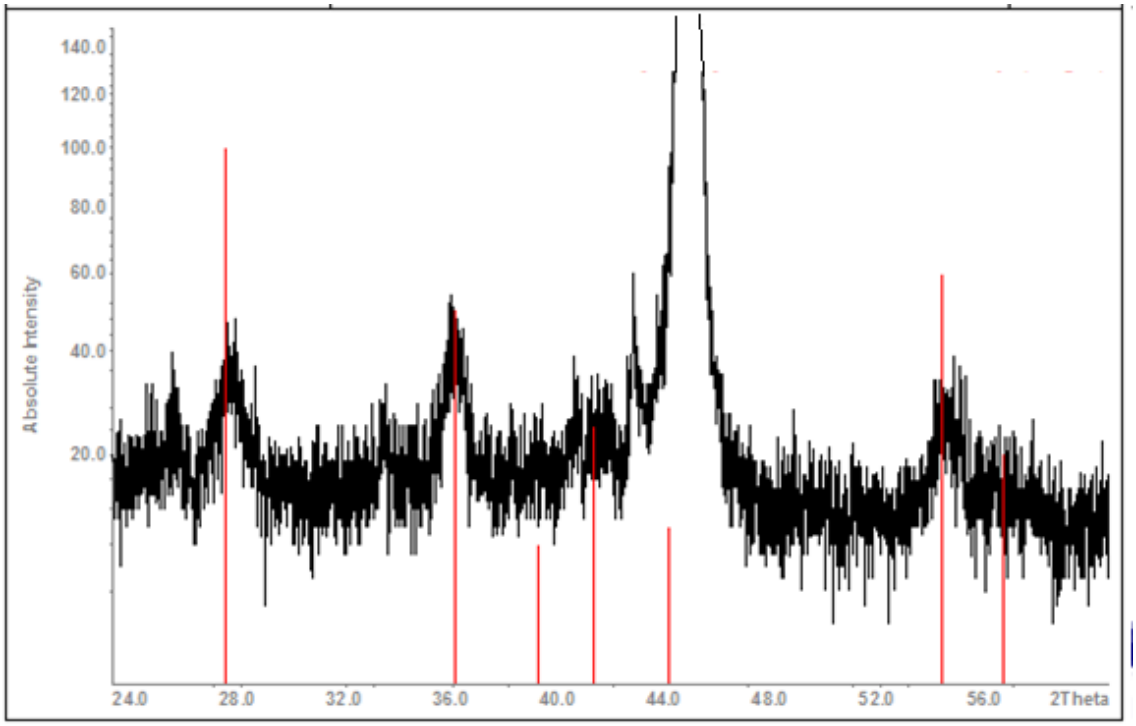

Fig.5.39: X-Ray diffraction pattern for SS430 with Ti evaporated and heated to 400^{o}C for 360 hours with rutile peaks (red).

Refinement of the unit cell parameters for the rutile peaks of this sample was performed using Stoe software and hklHKL values from rutile card 21,1276

Rutile is in space group P 42 /m n m. The few hills that could be construed as peaks that were clearly not stainless steel when combined with corresponding HKL values from the rutile card are reported below. Interestingly, no eskolaite phases were found.

	TiO_2		
	card	sample	%
A	4.59	4.6(332)	0.22
C	2.9592	3.0(231)	1.4

Table 5.16: Refinement of unit cell parameters for rutile on SS430 with Ti evaporated and heated to 400^{o}C for 15 days.

Large deviation from rutile indicates that at 400^{o}C the rutile is being doped by some other element, most likely Mn or Cr. The rear of the sample was also sampled with X-ray diffraction.

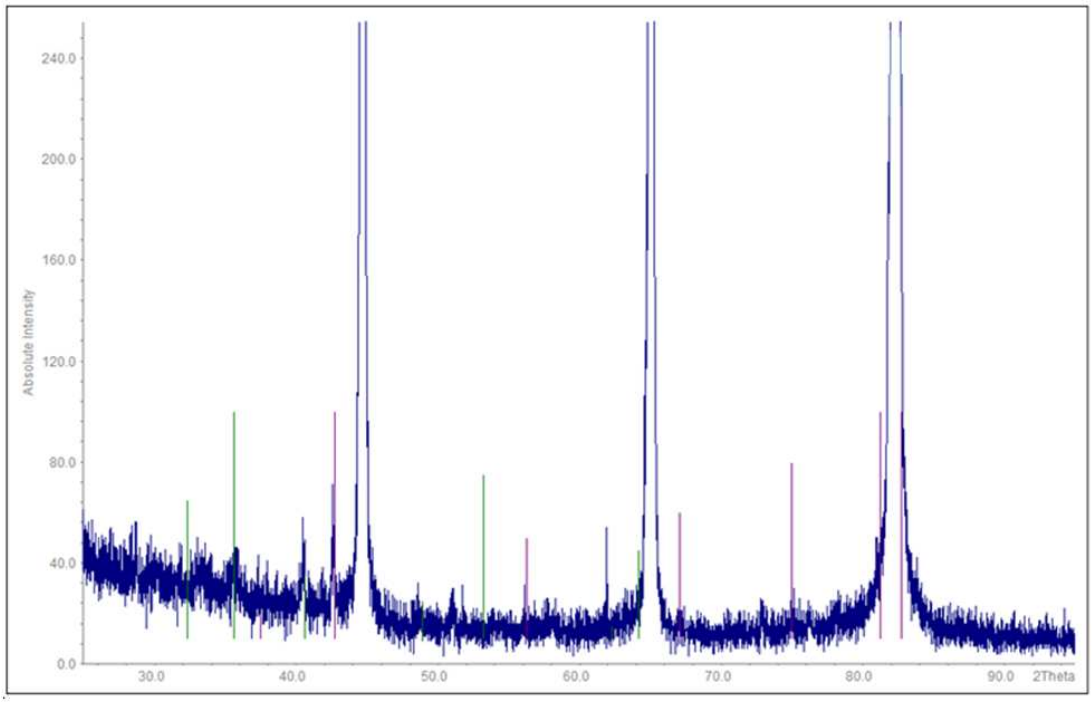

Fig.5.40: X-Ray diffraction of pattern for bare SS430, 15 days at 400^{o}C with Cr_2O_3 (green) and rutile (purple) peaks. Three large unindexed peaks are Steel.

Separation and refinement of peaks from corrosion layers at these temperatures is very difficult. The peaks were not refinable.

SEM images of the Ti coated side of the sample show a thin coating on the surface of SS430. Slight flaring is visible. The back side of this sample did not have the same flaring at high voltages, suggesting that something non conductive was at the surface of this sample. This would be expected for a rutile coating.

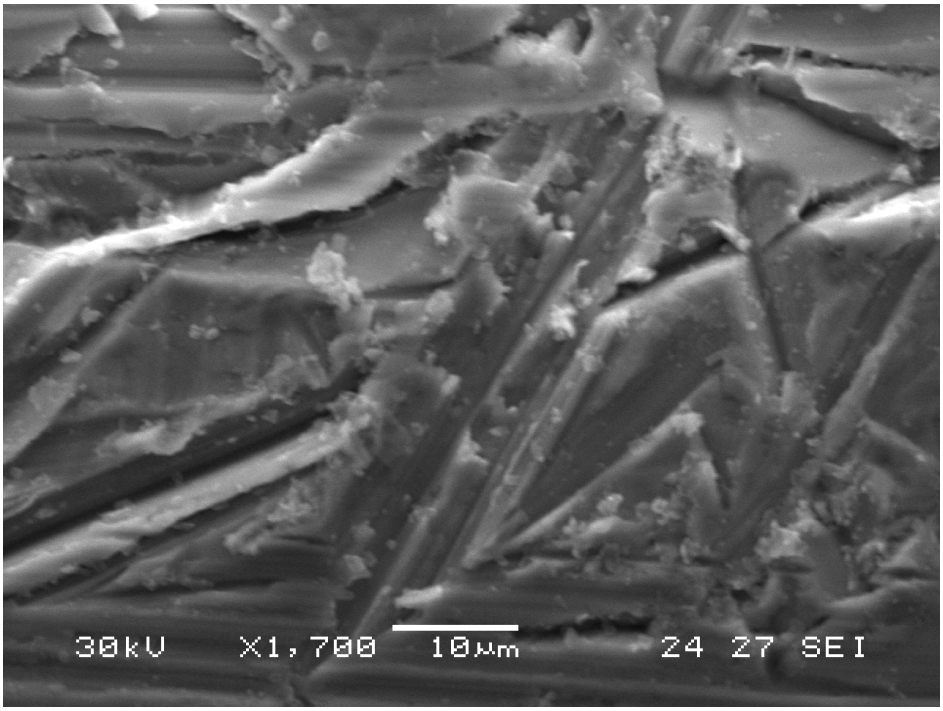

Fig.5.41: Micrograph of SS430 coated with Ti and oxidized at 400^{o}C for 15 days.

In fig.5.14 we see clear evidence of a rutile layer on the surface of ss430. This is highlighted by the white areas suggesting the beginning of flaring. EDS was used to find the elements on the surface, with the acceleration voltage set at 10kv and spot size set to 7, sample time was set to 600 seconds. The entire surface in the image below gave comparative evidence of the presences of Ti at or near the surface. The analyzer program was used.

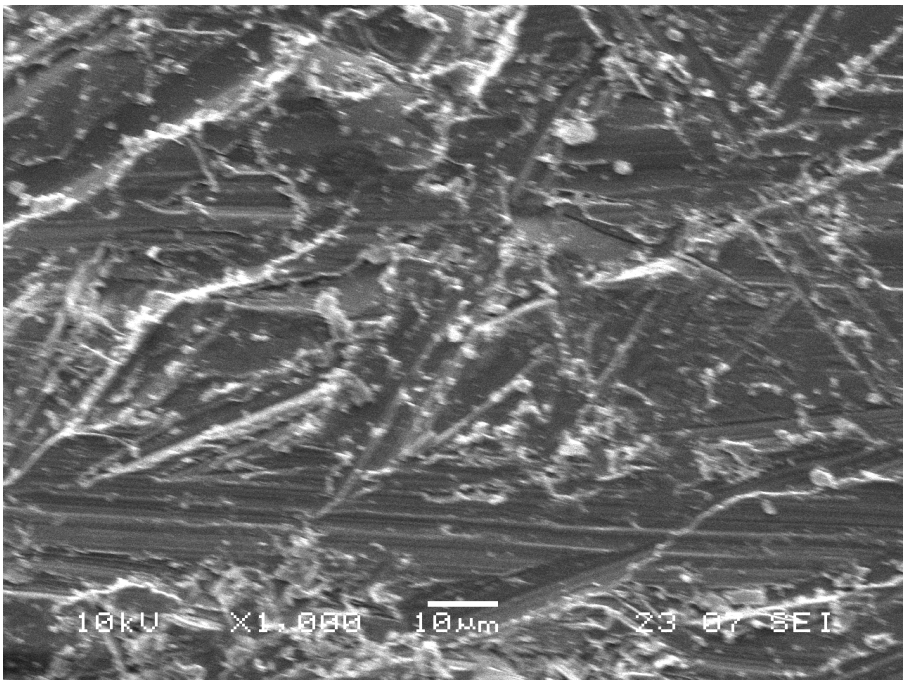

Fig.5.42: SEM scan for data below. 10kv, wd=23, spot size = 7.

Element	O	Ti	Cr	Fe	Total	Ti/Cr
weight%	31.23	25.21	4.99	38.57	100	0.19794
Atomic%	59.779	16.130	2.939	21.152	100	0.18222

Table 5.17: EDS results for surface scan of fig.5.42

The opposite side of the same plate analyzed at 10kV with a spot size of 7 yielded the following results

Element	C	O	Ti	Cr	Fe	Total
weight%	13.31	26.11	0	10.6	50.37	100
Atomic%	28.88	42.52	0	5.312	23.50	100

Table 5.18: EDS results from sample Fig.5.43

Although the penetration depth was not known to exact measurements, based on tables 5.17 and 5.18 it is clear that EDS can be used to detect the Ti layer after steel has been heat treated to 400^{o}C. As noted in earlier sections this was not the case for higher temperatures.

5.6 CONDUCTIVITY TESTING

The geometry of titanium coated steel samples, very thin coatings on highly conductive substrates, not only makes X-Ray diffraction and Electron Microscopy difficult, but also makes electrical readings and their meanings difficult to interpret by standard techniques. The difficulty lies in separating the contributions to conductivity from the coating layer and the substrate. Under normal circumstances, it would be advisable to create the layer without the substrate and apply measurement techniques to this layer. However, because this is a corrosion layer, by its very nature it requires the substrate for its production, as the substrate is the source of one or more of the reactant elements. Replacement of the substrate with a surrogate would not produce the desired materials.

5.6.1 FOUR POINT PROBE MEASUREMENTS

4 point probe techniques were attempted, but the results were widely dependent upon placement of the power source and the sensor wires. This is because the majority of the current was carried by the substrate, with very little passing through the corrosion layer for sensing.

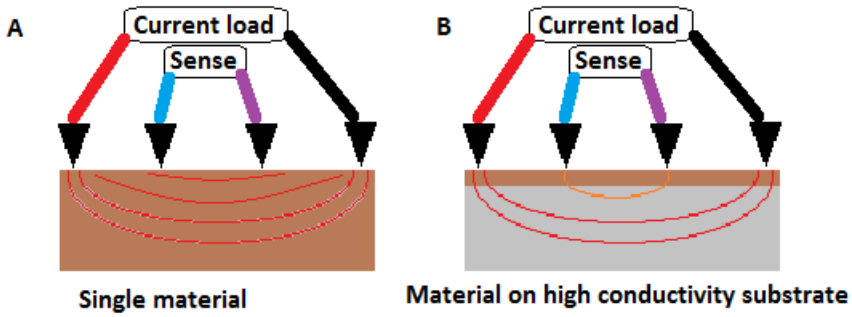

Fig.5.45 a and b: Current paths for 4 point probe layouts

As can be seen in the above fig.5.45a, if the material is single consistent material, voltages collected between the current load can be used to calculate the resistance of the material. In fig.5.45b it can be seen that electrons taking the path of least resistance would not be sensed as they would continue through the highly conductive substrate and ignore the resistive area. This would make the reading of voltage drop across the inner terminals not useful for calculating the resistance of the top layer. Fig.5.45b is an accurate representation of the system created when functional layers on steel are created by corrosion.

5.6.2 SYMMETRICAL TESTING SCENARIOS

In order to test Ti coated interconnects in real world applications, symmetrical testing was attempted. Many failures were encountered. A summary of data and conclusions follows.

5.6.2.1 SYMMETRICAL TESTING WITH PELLETS WITH ELECTROLYTES

Initial design of the symmetrical experiments consisted of coated or uncoated steel disks with long tangs extending out, and LSM/YSZ/LSM pre fired symmetrical disks. The tangs acted as leads making measurement or current connection possible. Unfortunately, the resistivity of this system was very high due to the high resistance of the LSM/YSZ/LSM pellets and poor contact at the surface. The layout is shown in fig.5.46. Readings from this series of experiments were not used due to inconsistent results from run to run, and from cell to cell within a single stack.

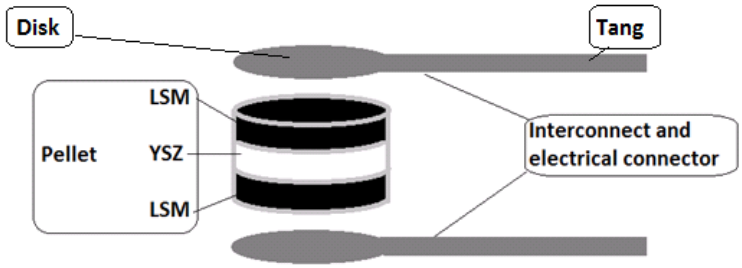

Fig.5.46: Initial system for symmetrical testing incorporating a single 3 phase pellet of LSM/YSZ/LSM and the interconnects with electrical tangs.

5.6.2.2 PELLETS WITHOUT ELECTROLYTES

The system was changed to remove the YSZ phase from the pellet to reduce the resistance of the overall system. In these experiments the resistance decreased compared to the 3 phase system, however, resistance was still very high due to uneven contact pressure and poor contact surface area, and there was large variance from cell to cell. This was due to the solid and uneven nature of the surface of the LSM pellets causing poor contact. This data was also not usable.

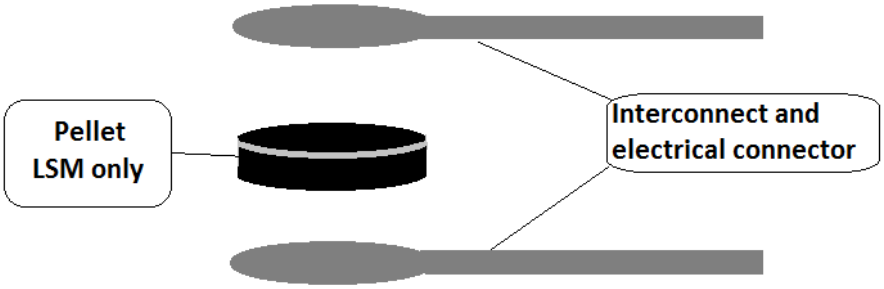

Fig.5.47: Single symmetrical cell with LSM only pellet.

5.6.2.3 WET TAPE SYSTEM

In order to increase contact surface area it was decided to use unfired tapes instead of pre-fired. These tapes were placed between the interconnects and pressure from the push rod was applied. The intention was for LSM to conform to the surfaces before cooking. At first, too much clamping pressure squeezed LSM out meaning that interconnects were touching interconnects directly. Very high conductivity was recorded, however, these values were not useful for obvious reasons because they were due to shorts between the interconnects.

In order to stop the squeezing out of LSM a new method was used where the system was assembled with wet tape but minimal pushrod pressure was applied. The rig was then placed in the furnace and fired at 700^{o}C , then cooled. The system was then run as normal with current going between the outer most interconnects and readings taken in between. This system yielded the most useful results.

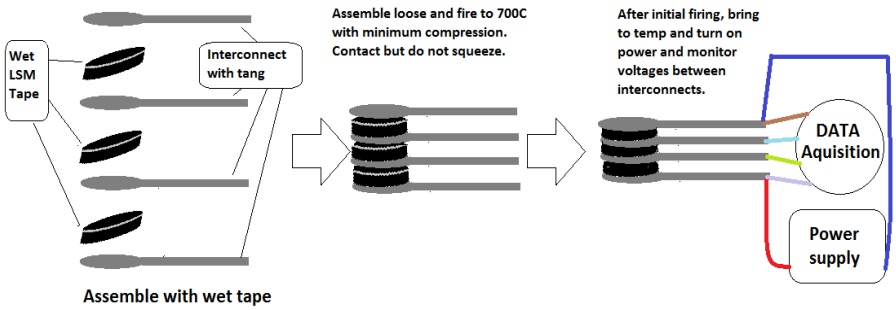

Fig.5.48: Wet Tape system

Using the close placement thermocouple and the wet tape system, Ti coated SS430 interconnects were compared to uncoated SS430 interconnects. Data is presented below. Res1 is the resistance calculated from the current supplied and voltage read between the brown and blue terminals on the "DATA Acquisition" module in the above figure, Res 2 is the calculated resistance from the current and voltage read between the blue and green terminals, and Res 3 is the resistance calculated from the voltage read between the green and grey terminals.

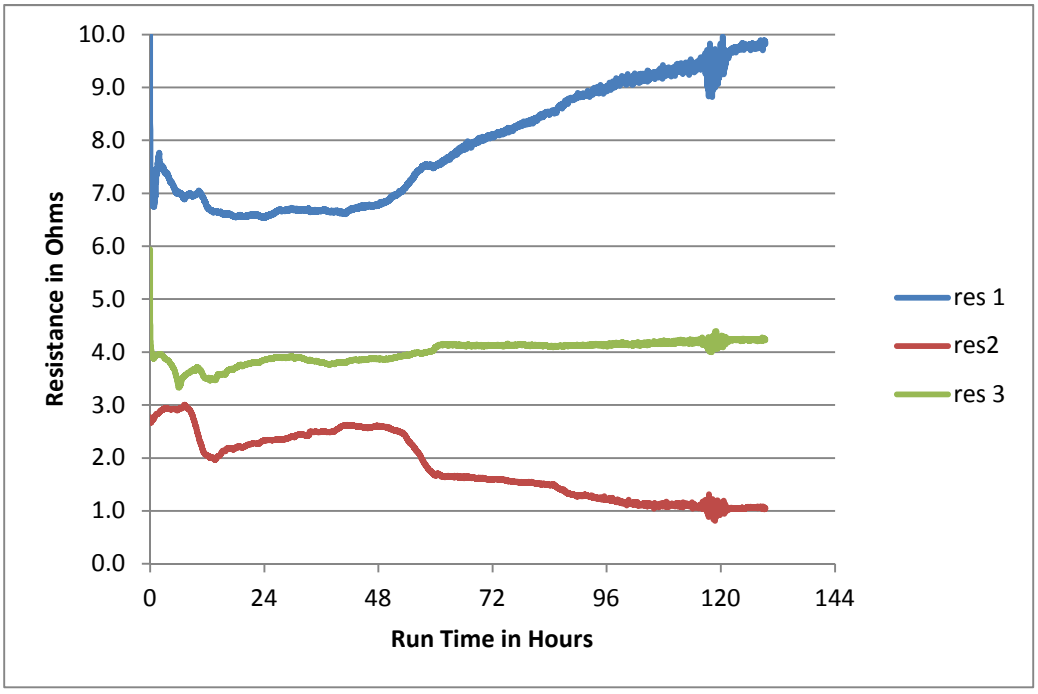

Fig.5.49: Ti interconnects with in situ sintered LSM tapes at 700^{o}C

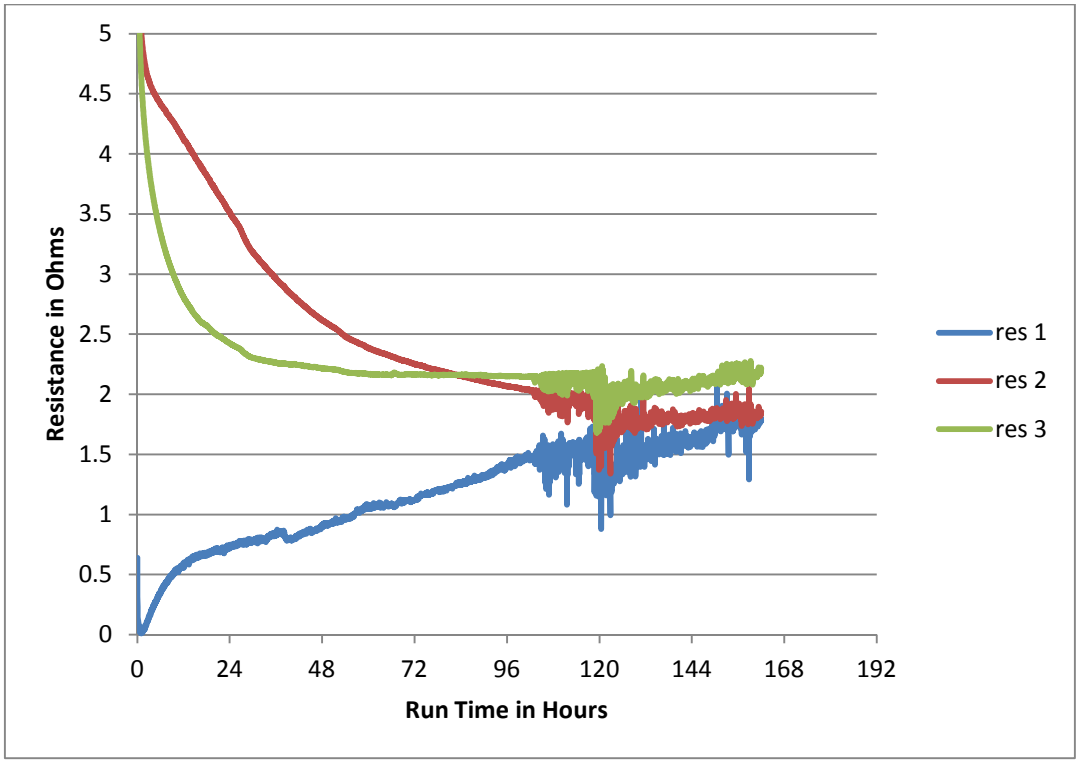

Fig.5.50: Uncoated interconnects pre-heated at 700^{o}Ct.

These experiments were performed before those from section 5.5, before an understanding of the rutile layer's behaviour at elevated temperatures was attained. In these experiments, the rutile layer would have been over-run by the corrosion layer, and become non continuous at these operating temperatures. These experiments do however demonstrate the higher resistances associated with Ti coatings on SS430 at 700^{o}C

5.6.3 IMPEDANCE SPECTROSCOPY

In order to grasp the various contributing factors to conductivity in the entire system, impedance spectroscopy was employed. SS430 foil samples with Ti evaporated onto both surfaces were heated to 400^{o}C. The resultant layer was then covered with 1cm^{2} area of gold on each side and placed in a jig between two platinum spheres at the end of alumina rods. The current, voltage and frequency were controlled by a Hewlet Packard spectrum analyzer.

The first run consisted of 2 layers of Ti on each surface that was then heated to 450^{o}C for 4 days. The thickness of these layers was calculated using equations from section 5.5.1 to be about 2 x 10^{-8} m thick on each side. This sample was heated to 450^{o}C in stages of 50^{o}C, 200^{o}C, 350^{o}C, 400^{o}C, and 450^{o}C and dwelled at each temperature for 30 mins whilst spectroscopy was performed between 1Hz to 10^{6}Hz with A.C. amplitude of 5mv. Although no cooling run was performed for this particular experiment, data is presented below. System resistance values were corrected by dividing total resistance by two to get the resistance of one layer, then subtracting the appropriate lead resistance for that temperature. Lead resistances were found by performing EIS without a sample at various

temperatures. Lead resistance was found to run from 1.56 Ω at 300°C to 2.00 Ω at 900°C. The graph showed linearity, and a trend line was used to find resistances at lower temperatures.

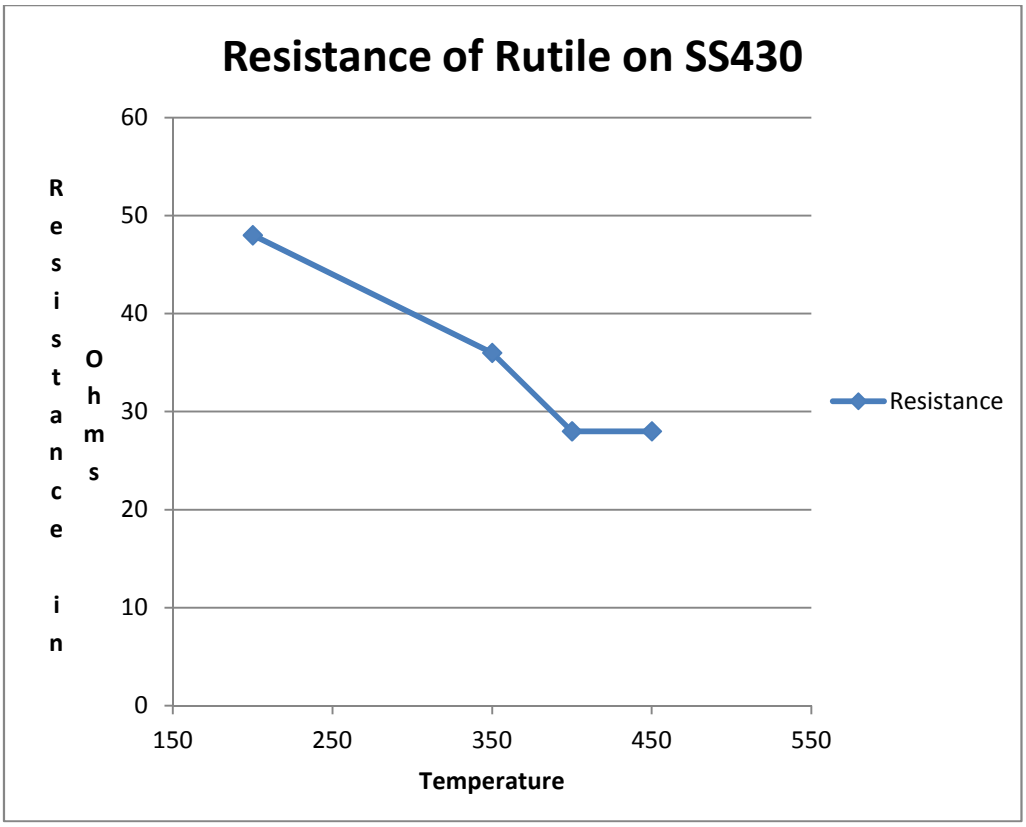

Fig.5.51: EIS resistances vs. temperature for rutile produced at 450°C on SS430

This sample was prepared by evaporating Ti onto SS430, heating to 400°C for 7 days. It was intended to show that As noted in sections 5.5.10, at 400°C rutile is the only corrosion product found on this type of specimen, however, at 450°C eskolaite starts to form as seen in section 5.5.9. The contact area was just the platinum spheres, which are on the order of a millimetre in diameter.

A second sample was prepared using samples that were heated to higher temperatures to promote the eskolaite phases. This sample was then coated with 1cm^2 of gold before insertion into the jig. The resistance values were corrected by dividing by 2 and subtracting lead resistance. Results are presented below

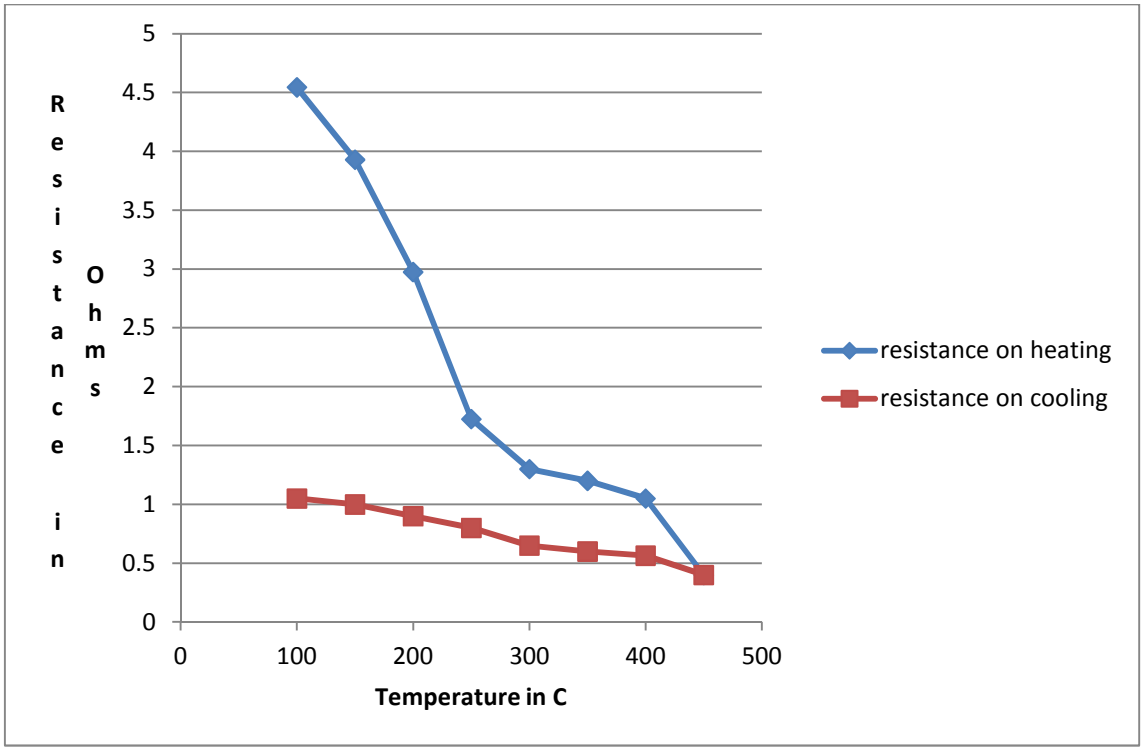

Fig.5.52:SS540 coated with Ti with increased temperatures to 450^{o}C EIS resistance results

As seen in fig.5.52 above, the Ti layer resistance steadily decreased with increasing temperature, and did not return to the cold temperature resistance on cooling. The steady increase in resistance on cooling would point to semiconductor behaviour because heating metals increases resistance, heating semiconductors such as LSM decresases resistance. At the maximum temperature and duration of this run additional corrosion is not expected to be significant. The difference between start and finish resistances for the same temperatures is due to the increased surface area of contact between the platinum spheres and the sample during the run. This is often termed “bedding in.”

A third sample was tested, this time with thicker Ti deposited, and heated to 400^{o}C. The thickness was calculated to be 4 x 10^{-8}m thick as per calculations in section 5.5.1. 1 cm^{2} of gold was evaporated onto each side, and the sample was mounted into the jig. The final temperature was 700^{o}C in steps of 50^{o}C. Resistances were adjusted to give just the produced rutile layer and steel layer resistance as described in previous sections. Below are the results.

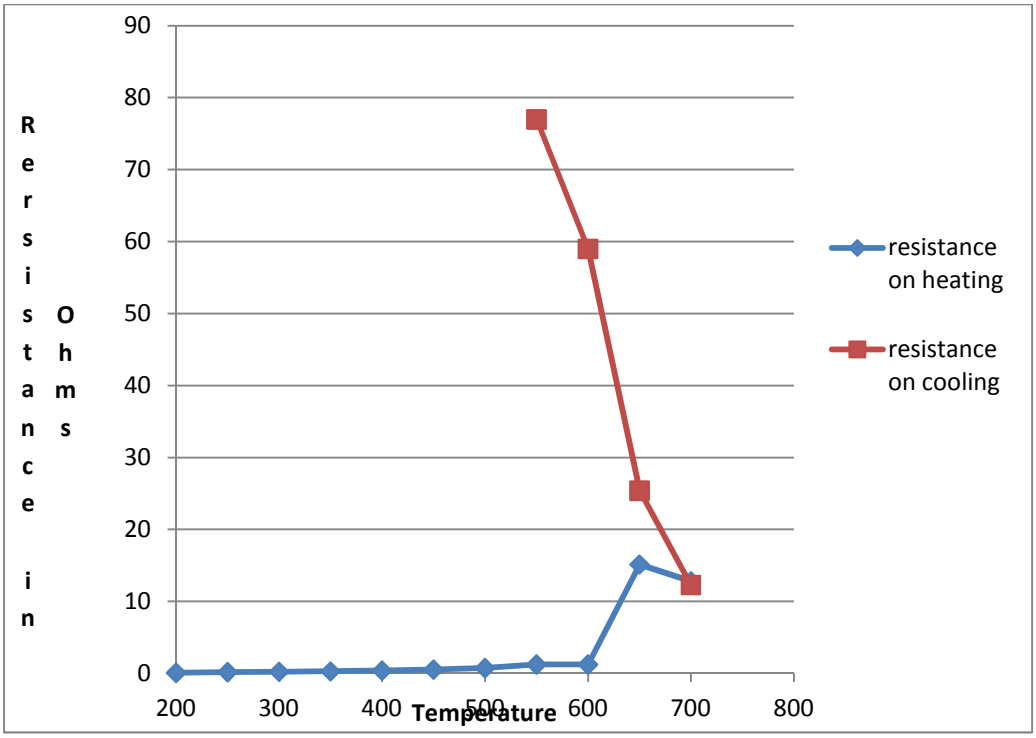

Fig.5.53 : Resistance vs. temperature SS430 with Ti heated to 400°C recorded with EIS

What can't be seen from the graph above are the initial resistances. Low temperature resistances ranged from 0.2Ω at 50°C to 2Ω at 600°C on heating. However, at 650°C the resistance jumps to 15Ω and continues up. Penetration of the platinum spheres through the Rutile layer into the Steel layer would not be expected with the thicker Ti deposit. Resistance steadily increases even on cooling. At the higher temperatures the Ti layer is ruptured by the rapidly growing eskolaite layer. This is expected at 600°C and is noted in section 5.5. The cause is rapidly the forming corrosion layer that displaces the rutile layer. From this we can conclude that although the rutile layer is thin enough to pass current with low resistance at low temperatures, it is no sufficiently protective enough to stop or slow the corrosion of steel and growth of a corrosion layer that will eventually displace the rutile layer.

5.7 REDUCTION OF LOW TEMPERATURE RUTILE FORMED ON SS430

The clear image of dense rutile on the surface of SS430 in fig.5.41 opens the door to another series of possible products for this technique. Reduced TiO_2 Magneli phases ($Ti_{(x)}O_{(2x-1)}$) have been studied at great length since the late 1970's when Hayfield discovered and studied the electrical properties. Previously to that, Arne Magneli [8], the Swedish chemist and crystallographer who discovered the crystallographic shear plane, and his students discovered non stoichiometric structures in Ti-O and V-O systems which gave rise to the term Magneli phase.

For some 30 years the standard form of production for these suboxides usually starts with TiO_2 powder, casting it into shapes with binders, firing it as TiO_2 Shapes, and then reducing these structures at 800°C for extended periods to remove some of the oxygen.

Unfortunately this production route makes materials that are not fully dense, and that are difficult to connect electrically using standard techniques. In most cases, when used as a wet electrochemical electrode, although the material has excellent oxidation resistance as an anode, the porosity causes wicking of electrolytes between the ceramic and whatever metal is used to connect it. This attack usually results in the disintegration of the metal connector and failure of the electrode system. In addition, no physical deposition technique has been perfected, meaning that at present, there are limited markets for reduced titania as an electrode.

Based on the quality of the of the TiO_2 layer created in section 5.5 on both Al_2O_3 and SS430 at 400^{o}C a program of reducing this layer in situ on SS430 was begun.
There are several routes to reduce rutile. Magneli's team used ground elemental Ti mixed with TiO_2 and reacted in a vacuum furnace. Hayfield set the standard with H_2 reduction, but other techniques are yet to be discovered. {Smith, 1998 #616}

For the preliminary set of experiments, it was decided to use SS430 coated with Ti and heated to 400^{o}C as these formed the most obvious and dense rutile as a precursor. These samples were then reduced in 5% H_2/95% Ar. As the thickness of this layer is very thin, it was decided that short durations of 2 days would be adequate. The thickness was calculated to be 1x10^{-6}m thick based on the calculations in section
Below is an image of two samples: The top sample was heated to 600^{o}C in flowing 5%H_2, the bottom was heated to 700^{o}C in the same gas. The background is Al foil. Unreduced samples appear as in section 5.5.9.

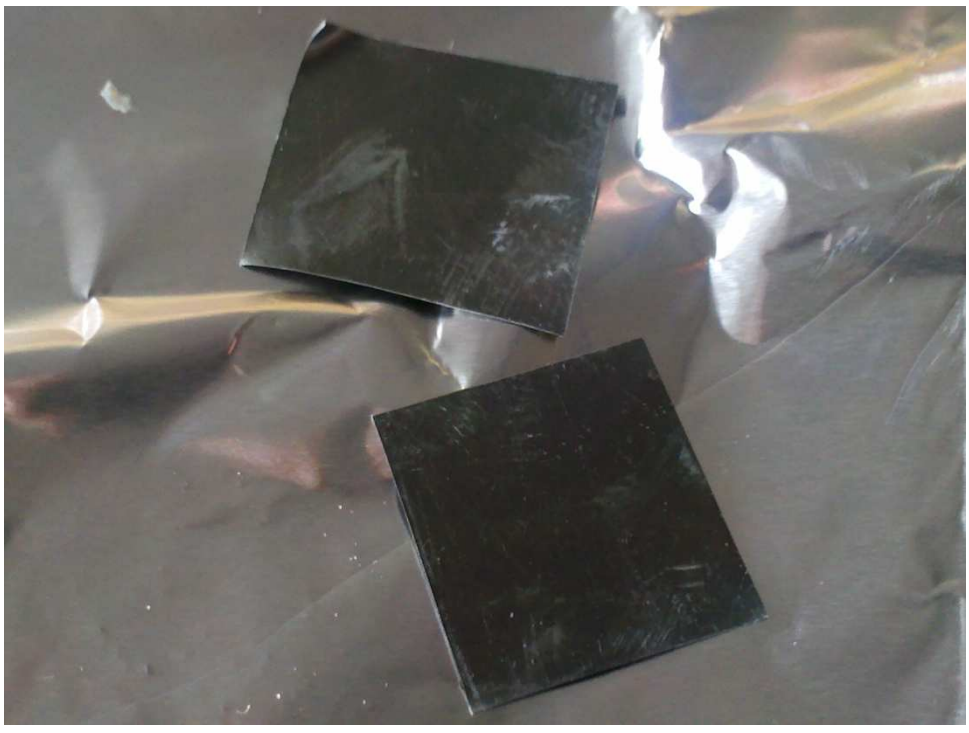

Fig.5.54: SS430 heated to 600^{o}C (top) and 700^{o}C (bottom) in 5% H_2

As can be seen the samples have turned the characteristic black of reduced TiO_2. X-Ray analysis was performed. Below are the patterns for both scans and an additional reduction at 800°C.

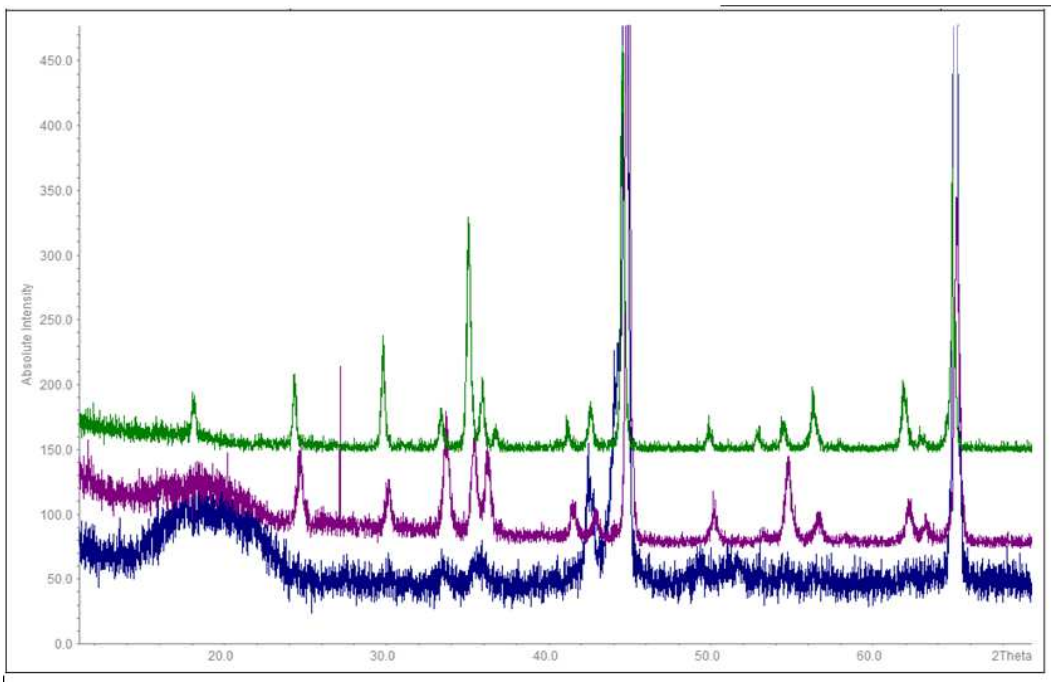

Fig.5.55: X-Ray patterns for SS430 coated with Rutile, reduced in H_2 at 600°C(blue) and 700°C (purple)and 800°C(green)

Unfortunately, none of the reduced $Ti_xO_{(2x-1)}$ peaks were found in any sample. The non steel peaks from the 800°C sample were subjected to a search, and the cubic structure $CrMn_{1.5}O_4$ was found to be the best match for all the peaks. Below is the refined index result.

	$CrMn_{1.5}O_4$		
	standard	sample	%
A	8.479	8.14(8)	3.998

Table 5.19: Refined unit cell parameter for sample from peaks from fig.5.55

These peaks are not a good match. It is probable there are many phases of material on the surface of SS430 after this type of treatment, and peaks attributed to this particular cubic structure are actually due to a multitude of other reduced corrosion products. Lower temperature and longer duration reductions may shed more light on what is happening with these materials.

Below Scanning electron microscopy was performed on the same sample.

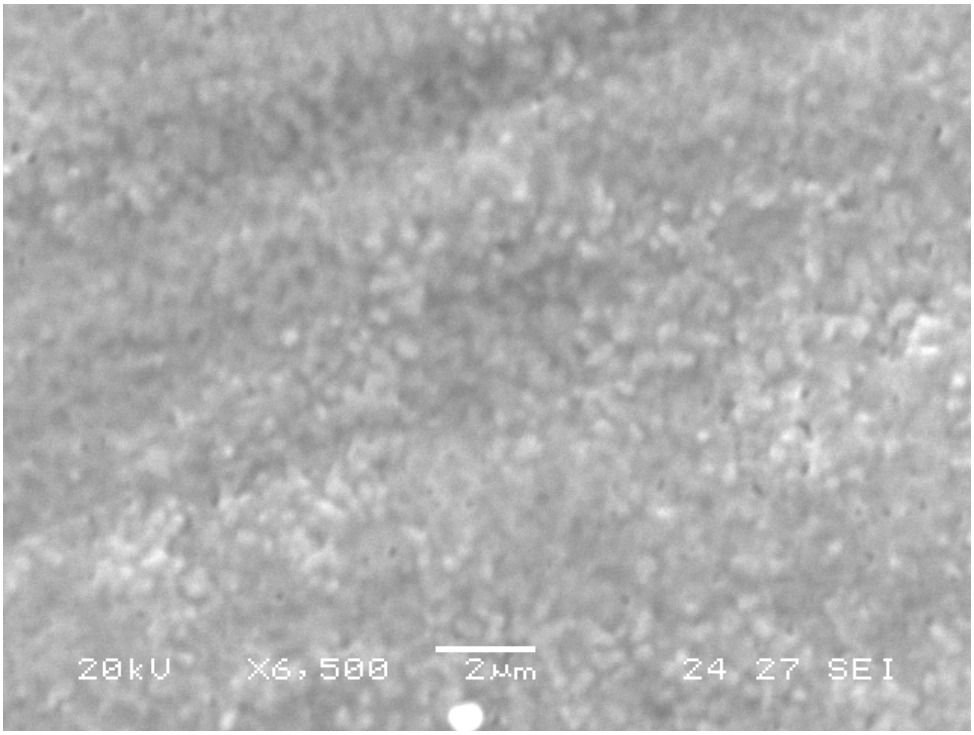

Fig.5.56: surface of SS430 with rutile after reduction at 800^{o}C

Element	Weight%	Atomic%
O	35.86 +/- 0.74	64.98
Cr	37.56 +/- 0.67	20.94
Fe	12.70 +/- 0.55	6.59
Mn	11.86 +/- 0.53	6.26
Ti	2.03 +/- 0.18	1.23

Table 5.19: EDS results for surface scan of fig.5.56

Fig.5.56 looks quite different from fig.5.41, the same sample prior to reduction. Where there was a continuous sheet of rutile coating there now appear nodules with very fine microstructure. This could be due to materials diffusing into the rutile layer and forming other products that cluster.

5.7.2 ELECTROCHEMICAL IMPEDANCE SPECTROSCOPY OF REDUCED RUTILE ON SS430

Similarly to section 5.6.3, samples were prepared by evaporating 4 Ti targets onto each side of a SS430 foil, which was then oxidized to rutile, to form layers calculated to be approx 10^{-7} m thick based on the calculations from section 5.5.1. These materials were then reduced in a hydrogen furnace at 600^{o}C with 5% hydrogen in argon for 4 days.
The sample was then coated with a 1cm^2 square of gold on each side, and put in the jig described in section 5.6.3 and impedance spectroscopy was performed at temperature

intervals increasing from 50°C to 400°C then decreasing down to 50°C in 50°C intervals. Assuming no change in surface contact resistance the difference between the heating and cooling resistances can show re-oxidation of the sample.

The results were circular in nature suggesting a large capacitive component to the behaviour. The circular fit was used to find the real axis intercepts so that resistance only could be found. Below the data is presented with green representing heating resistances, and blue representing cooling resistances.

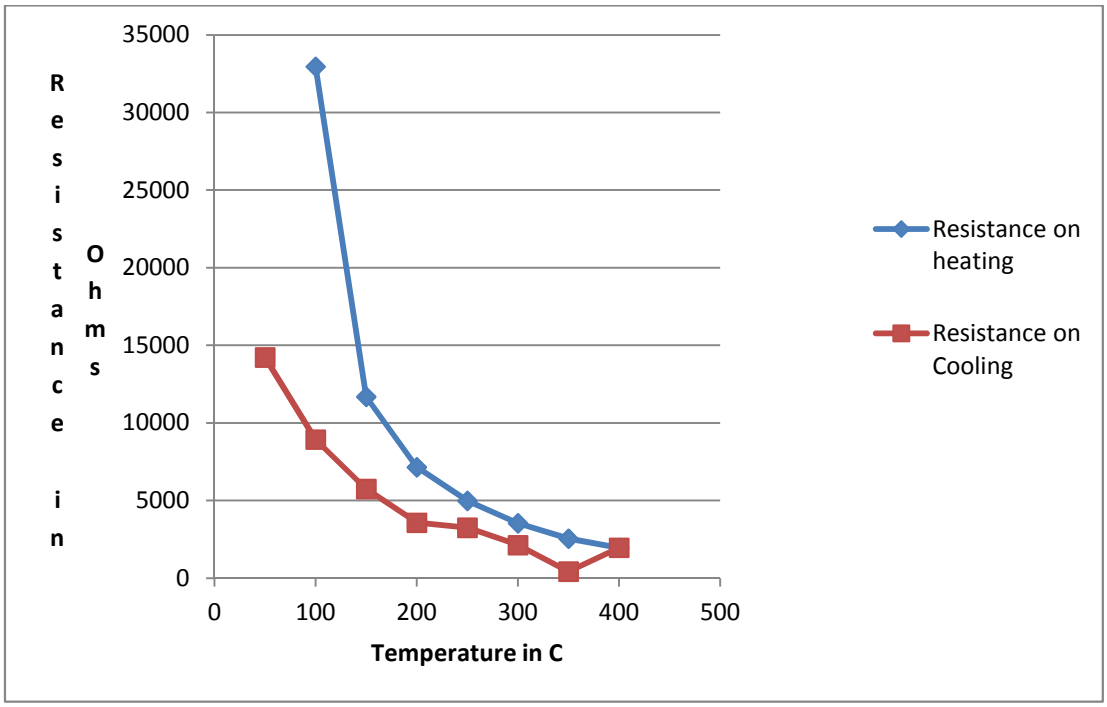

Fig.5.57: Resistance results for impedance spectroscopy of reduced rutile on SS430

The resistances were considerably higher than expected for reduced rutile, higher than for just rutile. It is not clear why this should be, but as expected re-oxidation seems to have played a role with resistance increasing after peak temperatures reached, and staying in that region even after cool down. As the curves were semicircular, curves fit also gave estimated capacitance values. These can be used to discover the thickness of the layers.

As each side was coated with 1cm^2 of gold and because the samples were planar, the gold coatings are essentially parallel plates in a capacitor. Below is the equation that relates capacitance and area and thickness [9].

$$C = \acute{\varepsilon}\, e_o \frac{A}{L}$$

In the above equation, C is the capacitance, έ is the permittiviy between 2 plates, generally assumed to be 10, A is the area, in this case, 1cm^2 e_o is the permitttivity of free space at 8.85x10^{-14} F/cm, l is the thickness of the layer. Using capacitance and the known values of

area, thickness of the layer can be calculated by rearranging the above equation to the one below.

$$L = \acute{\varepsilon}\, e_o \frac{A}{C}$$

The thicknesses are reported below.

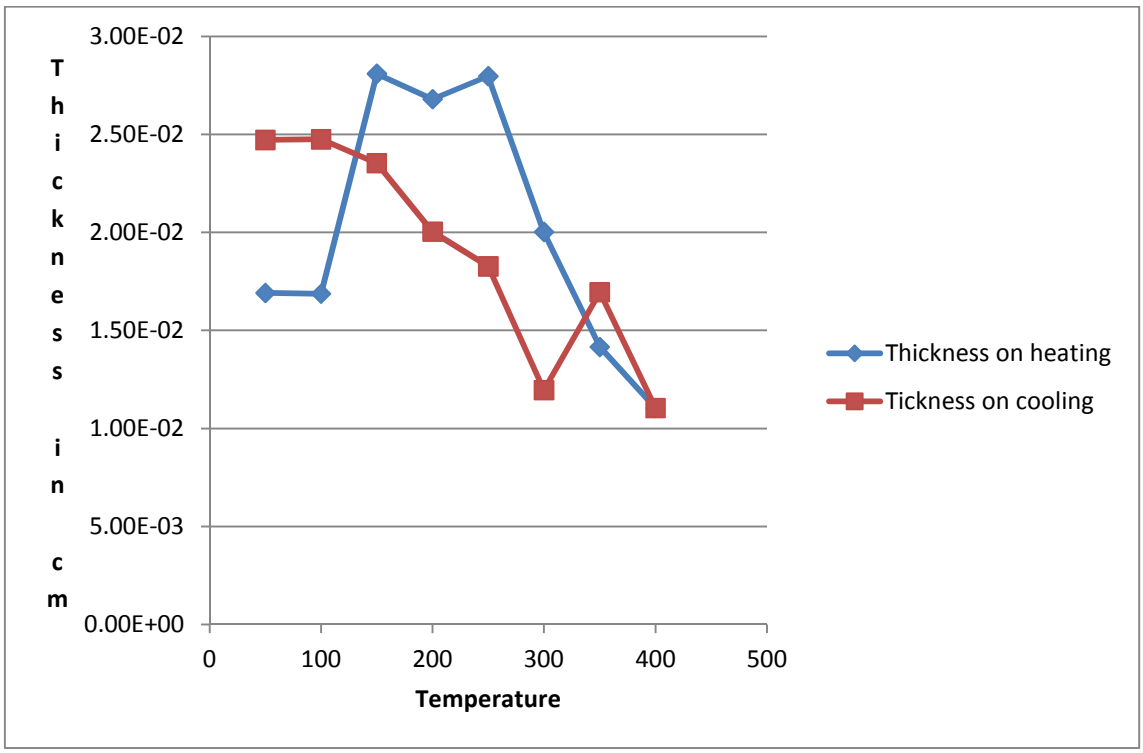

Fig.5.58: Thickness of one layer on a sample in cm during the impedance scan of reduced rutile on the surface of SS430

The values of thickness calculated from the capacitance were 4 orders of magnitude higher than calculated in previous sections, suggesting an error in one of the assumptions. The sample was examined in the SEM, for both the actual thickness and for changes to the surface.

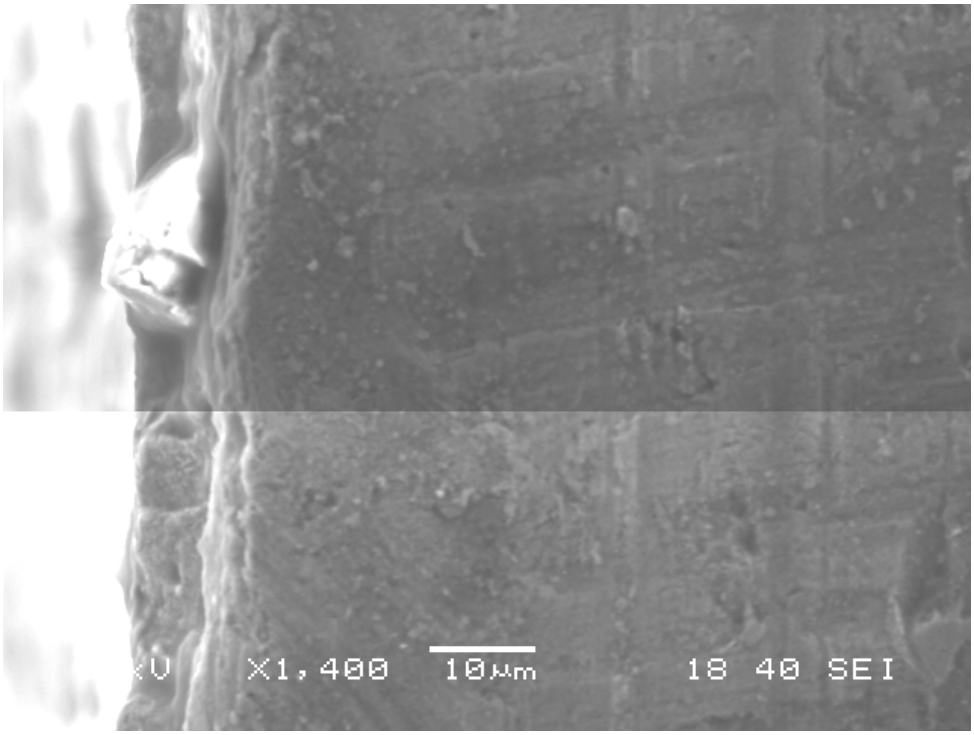

Fig.5.59: Edge of SS430 with reduced rutile layer showing to the left of image

The presented face of this sample in fig.5.59 is the edge and it is corroded. It should be kept in mind that this sample has been heated in air, reduced, and heated in air again, so corrosion on the edge surface should be expected. The thickness of the layer to the left is approximately 10^{-6}m. This compares to approximately 10^{-4}m from fig.5.58 and calculated thickness of 10^{-7}m calculated from section 5.5.1. The surface was examined below. This variation would suggest that either the gold is no longer continuous or some other assumption is invalid.

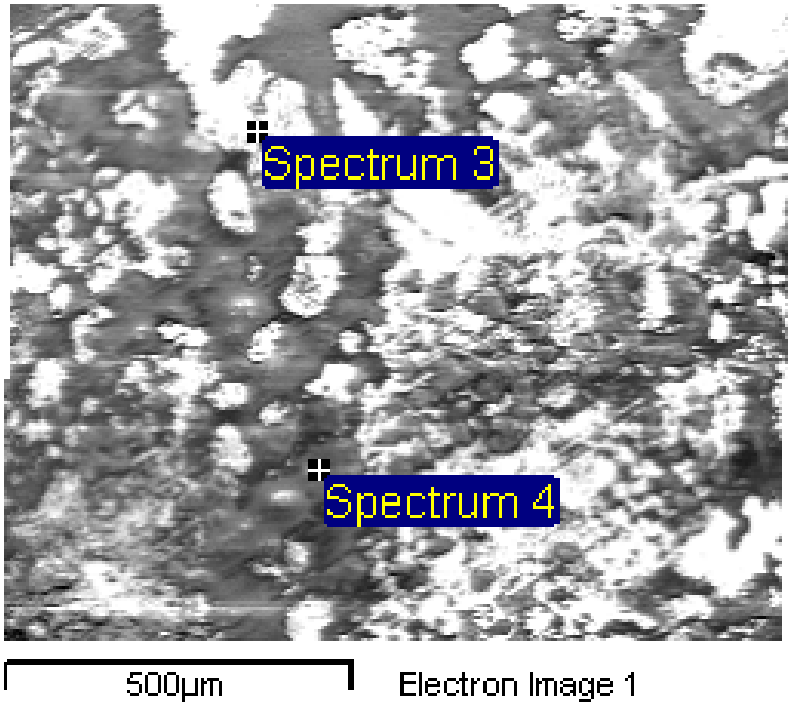

Fig.5.60: Surface of SS430 with reduced rutile and a sputtered gold layer showing points of analysis for EDS

	Spectrum 3			Spectrum 4	
Element	Weight%	Atomic%	Element	Weight%	Atomic%
O K	22.4	56.5	O K	31.9	78.5
Ti K	6.92	5.82	Ti K	4.93	4.0447
Cr K	33.3	25.8	Cr K	8.11	6.13
Mn K	7.79	5.72	Mn K	0.622	0.447
Au M	29.5	6.05	Au M	54.4	10.9

Table 5.12: EDS results for spectrum 3 and 4 in fig.5.60

The differences in Mn, Cr, and gold suggest the gold layer is not continuous and therefore the contact area is most likely not $1cm^2$. Working from the thickness of the sample as found the contact area was found to be $2x10^{-5}cm^2$. This would suggest that although the area of gold is decreasing during an impedence run, the conductivity of the sample system is increasing with a final resistance roughly half the value of starting resistance as observed in fig.5.57. It would be expected that the conductivity of a reduced rutile coating would decrease through oxidation. An increase in conductivity would suggest some other mechanism is contributing to the conductivity of the sample system. As the coating layer is the thinnest and most susceptible layer in the system, then changes to conductivity are directly related to changes in the coating. The most likely change to occur in the sample system would be solid state diffusion of other elements into the coating layer.

5.8 CONCLUSIONS

Because stopping corrosion on steels is actually neither desirable nor thermodynamically possible, a good way to create coatings on steel from elements in the steel is by also adding limiting reagents to the surface. Many products for coatings have been flagged and in some cases adding a single element to the surface may mean that elements in the steel and the element on the surface can produce a desirable coating.

Ti is limited in its deposition techniques due to thermodynamically favourable production of rutile that make certain steps difficult without going through the rutile phase. To form CTO we are relying on chromium to migrage through the rutile layer. Ti is used as a minor alloying element in stainless steels as a preferential carbide former to promote the production of chromia over chromium carbide in the grain boundaries.

Evaporation of elemental Ti was shown to produce a thin and dense rutile layer upon heating to 400^{o}C. Higher temperature heating was not shown to produce CTO definitively, but circumstantial evidence by several techniques support that CTO can be manufactured by transport of Cr from the steel into the rutile phase, saturating this phase to make Cr doped rutile, and then conversion of this Cr doped rutile to CTO. However, as with all corrosion, even with an additional coating, the behaviour is dynamic, time and temperature dependant.

Higher temperature corrosion fractured the Ti layer. There are two drawbacks to this

1 The separated layer will cause higher resistance will remain as evidenced by stack runs, and EIS.
2 The broken layer will not slow the evaporation of chromium as much as a layer in tact.

As time is a key factor in the growth of corrosion layers, future work should take into account longer heating times at lower heating temperatures. These conditions are much more likely to form CTO.

Combined with the information from chapter 4, it can be shown that Ti layers on SS430 will slow the evaporation of chromium from the SS430 in the temperature ranges of 500^{o}C and below. This may well become important as operating temperatures in SOFC's become lower. There is an electrical resistance penalty, especially at short durations where the Cr has not migrated into the TiO_2 layer enough.

There is a "sweet spot" of temperatures where X-Ray and SEM analysis can be used effectively to find the layers created by evaporating Ti onto SS430. These seem to be between 400^{o}C and 550^{o}C. Above 550^{o}C corrosion has either displaced, cracked, or absorbed the Ti layer.

Ti should not be investigate in the current operating conditions of SOFC, however, as a coating for steels used in MCFC this thechnique is beginning to show some promise. If operating temperatures of SOFC are to come down significantly, Ti coatings should be revisited.

REFERENCES

1. Naisbitt, S.C.P., K. F. E.; Williams, D. E.; Parkin, I. P., A microstructural model of semiconducting gas sensor response: The effects of sintering temperature on the response of chromium titanate (CTO) to carbon monoxide. Sensors and Actuators B: Chemical, 2006. **114**(2): p. 969-977.
2. Holt, A.K., P, *Electrical conductivity of Cr2O3 doped with TiO2.* Solid State Ionics, 1999. **117**(1-2): p. 21-25.
3. Pai, R.V.K., K.; Dash, S.; Mukerjee, S. K.; Venugopal, V., *Synthesis, characterization and thermal expansion of Cr2−xTixO3+δ.* Journal of Alloys and Compounds, 2010. **507**(1): p. 267-272.
4. Neri, G., Low temperature Sol-Gel synthesis and Humidity sensing porperties of Cr2-xTixO3. Journal of European Ceramic Society, 2004. **24**: p. 1435-1438.
5. Egerton, T.A.H., E.; Lawson, E.J.; Brynmor, M.; Rowlands,C.C., *An EPR study of diffusion of chromium into rutile.* Physical Chemistry Chemical Physics, 2000. **2**(14): p. 3275-3281.
6. Chen, G.W., C. C.; Cho, H.; Macdonald, D. D.; Mallouka, T. E., *EIS Studies of Porous Oxygen Electrodes with Discrete Particles.* Journal of The Electrochemical Society, 2003. **150**(9): p. E423-E428.
7. Lashtabeg, A.C.-V., J.; Irvine, J. T. S.; Bradley, J. L., Structure, Conductivity, and Thermal Expansion Studies of Redox Stable Rutile Niobium Chromium Titanates in Oxidizing and Reducing Conditions. Chemistry of Materials, 2009. **21**(15): p. 3549-3561.
8. lars Kihlborg, I.O., *Obituary* Acta Crystallographica, 1996. **a53**: p. 103-104.
9. Irvine, J.T.S.S., D.C.; West, A.R, *Electroceramics: Characterization by impedance spectroscopy.* Advanced Materials, 1990. **3**: p. 132 - 138.

6 COBALT EVAPORATION TO PROMOTE PROTECTION LAYERS

As was discussed in Chapter 4, it has been shown that the cobalt chromium spinels release much less chromium in wet oxidizing conditions than chromia. The formation of such spinels on interconnects can act as a barrier layer to slow the evaporation of chromium from interconnects used in SOFC's. It has been well documented that chromium containing spinels form not only on the surface of SS430 naturally, but also in the triple phase boundary of SOFC's [1] . Many workers now believe that instead of stopping these spinels, promoting spinels to form in a more desirable location is a better option. To this end, many are depositing spinel phases directly, whilst others are depositing cobalt and/or manganese on the surface or in the bulk of SS430 in order to grow the spinel phase from the coating, atmosphere, and chromium contained in SS430 in situ as a barrier late [2-4].

The possible routes for depositing cobalt onto SS430 include electroplating, the various forms of sputtering, electroless plating and others. However, many of these application techniques are costly, time consuming, and environmentally un-friendly. In the case of electroplating, although deposited layers can be very thin and control can be quite precise, the conditions of removal of the substrate from the plating bath is crucial, as the surface can re-dissolve in an aggressive plating bath as soon as the current is removed. Using the evaporation technique from Chapter 5, cobalt coatings on SS430 were deposited using the metal evaporator and spinels were grown on the surface.

The validity of this technique was confirmed in Chapter 5 as chromium is readily available from SS430 to form chromium doped rutile, and eventually titanium doped eskolaite. As a target cobalt has the advantages of ease of handling and low melting point compared to titanium. Additionally there is a wealth of data available for cobalt chromium spinel, and it is not considered a doped material, although other stoichiometries are possible including Co_3O_4 $Cr_{1.5}Co_{1.5}O_4$ and Co_2CrO_4, as well as combinations of Co, Mn, and Cr, as well as other elements. These other spinels are sometimes easier to identify than titanium products and relatively easy to separate from each other.

6.1 PRODUCTION OF FUNCTIONAL LAYERS BY CORROSION

The production of self limiting corrosion layers is studied for corrosion products that consist of elements only taken from the substrate and the atmosphere in cases such as steel, aluminium and titanium[5-6] , but not as well understood for functional layers created by corrosion from both elements deposited and elements in a substrate. With such layers, the deposited layer becomes a limiting reagent. This does not always produce desired products, as the products are not only a function of deposited materials, but as seen in Chapter 5, but also of corrosion temperature and time. This is because there is a finite amount of the limited reagent, but vastly more of the other elements in the substrate, and an infinite amount of oxygen.

As the two governing factors are time and temperature, it is important to approach the limits as a function of temperature. This is due to the thermodynamics of corrosion. Fewer

products are possible at lower temperatures, larger quantities are available after longer times.

In this study an attempt was made to characterize produced layers under the influence of temperature.

In Chapter 5 finding deposited layers proved to be a function of temperature. In order to properly characterize the cobalt layers and their oxide product layers, temperature was increased in steps of 50^{o}C or 100^{o}C. After 600^{o}C time was manipulated between 3 and 9 days at 700^{o}C, and a thicker layer was also incorporated at this temperature. Al_2O_3 surrogate substrates were used at a few specific temperatures to determine products that would be made from the deposited layer only. This technique was useful in Chapter 5. For the following work a metal evaporator was used for several reasons. Firstly, it was an available and well studied technique due to its use for depositing titanium. Secondly, the coating thicknesses are very thin and quite controllable as was demonstrated in Chapter 5, which means that diffusion lengths are short and desired products are more likely to be produced in less time.

6.2 THIN COBALT EVAPORATION

To avoid contamination from previous experiments, new heating elements were wound around a stainless steel mandrel of 3 mm O.D. from tungsten wire of 0.5mm thickness. Each heating element had approx 3.5 turns. A 2 cm length of cobalt from Advent stock number CO508709 which is 0.25mm in diameter of 99.95% purity was wrapped around each heating element. The current was set to maximum and the switch turned after the pressure had decreased to 5x10^{-5} millibar. The substrate was a strip of SS430 foil stock number FE6961 also from Advent which was 0.1mm thick and approx 2.5 cm wide by 10 cm long. After the heating elements were engaged a greyish shiny hue was seen to be left on the surface of the SS430 and inside the evaporator

6.2.1 CALCULATED THICKNESS

The theoretical mass of the target to be evaporated was 8.74x10^{-3} grams. Based on the calculation in Chapter 2 for the thickness$T = m/(4\rho * \pi * r^2)$, the density value of 8.9g/cm^3 for cobalt, and a distance between target and substrate of 40mm, the theoretical thickness is 4.88 x 10^{-8} m. During heating this pure Co layer will react with chromium and oxygen to form spinel. Using the volume and molecular weight of a mole of the specific spinel Cr_2CoO_4 of 557.99 A^3 and 229.92 g/mole respectively for, and Avogadro's number, the layer will grow to 2.48x10^{-6} m thick theoretically depending on the stoichiometry of the spinel, and assuming no other elements are involved. If the Spinel were $CrCo_2O_4$ the layer would be approximately half that thickness.

These results can be directly compared to those for Ti sputtering in that Chapter based on those thickness calculations.

6.3 OXIDATION OF SAMPLES

6.3.1 ROOM TEMPERATURE

As SS430 would be used as the substrate for most experiements, a reminder of its properties is below.

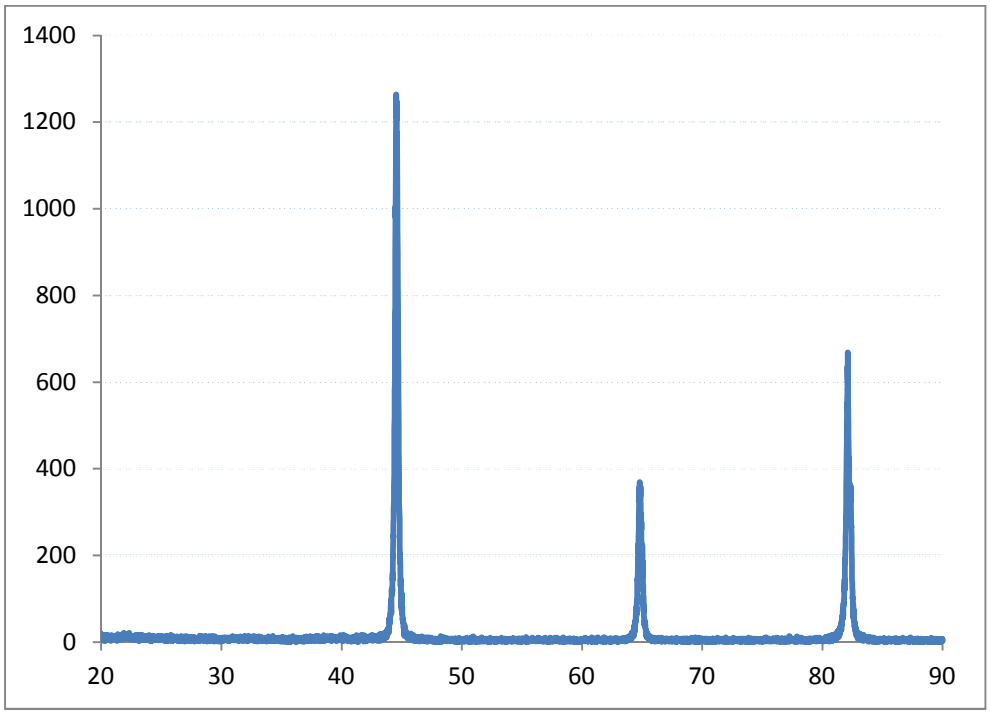

Fig.6.1: X-Ray diffraction pattern of SS430 as delivered.

A sample of SS430 was examined with SEM (fig.6.1) and EDS (table 6.1). Below are the EDS results for unheated, uncoated SS430. It should be noted that although Mn is present as a minor element, EDS did not find it.

Element	Weight%	Atomic%
O K	2.64	8.53
Cr K	17.69	17.62
Fe K	79.67	73.85
Totals	100	

Table 6.1: Results for EDS of results for untreated SS430

SS430 was coated with a thin layer of cobalt calculated to be about 5 x 10^{-8} m thick. This sample was studied with X-Ray diffraction and SEM. Below are the results.

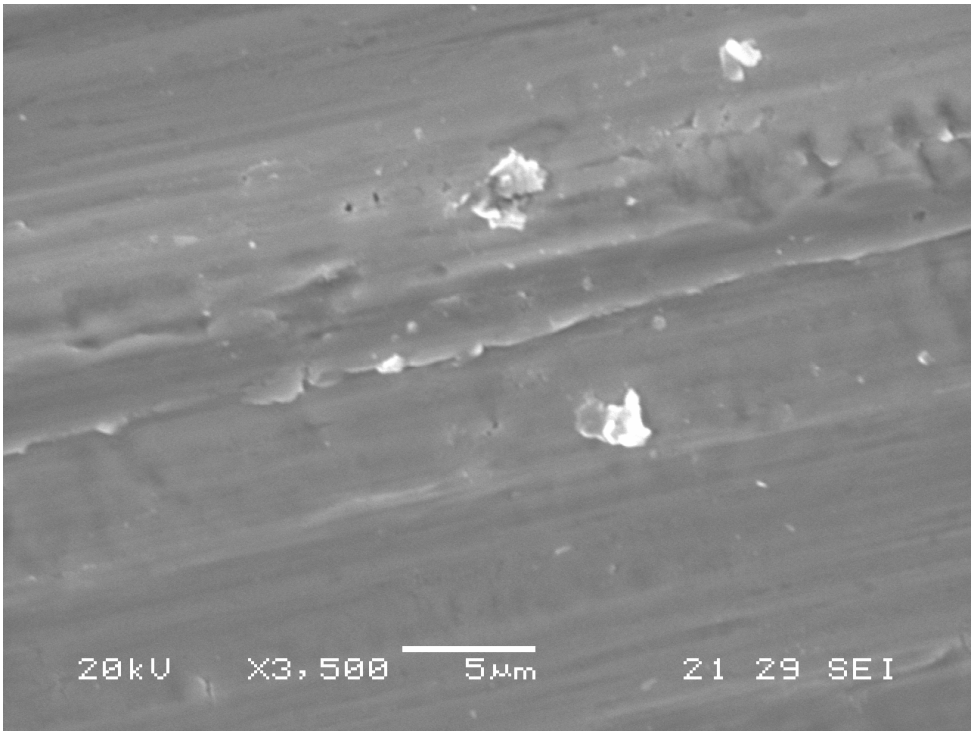

Fig.6.2: SS430 coated with Co without heat treatment

The Cobalt layer was not visible to the naked eye in fig.6.2, nor was it found to be that dissimilar from the steel as delivered. It is much easier to detect than Ti for similar amounts sputtered onto SS430, even at large spot sizes and high acceleration voltages. For Ti, small spot sizes and low acceleration voltages, combined with very long detection times are required. For Co, similar conditions to those required for best images are adequate for detection.

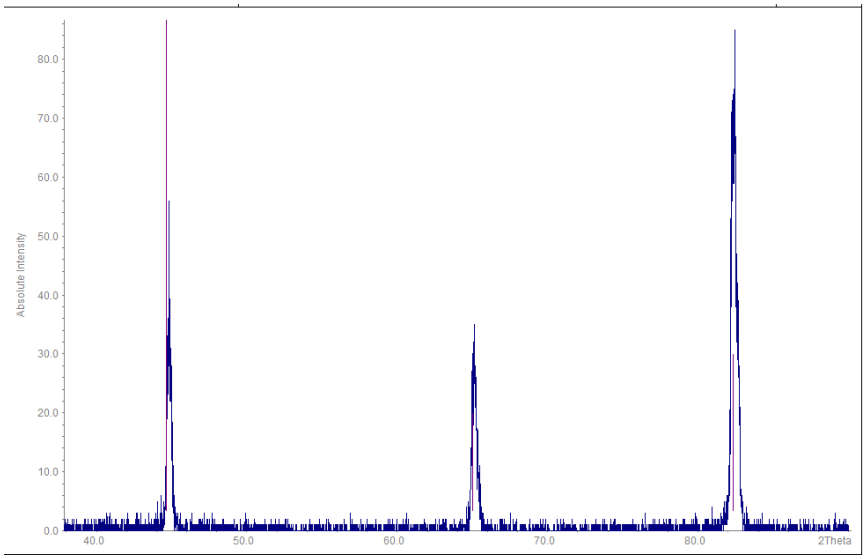

Fig.6.3: X-Ray diffraction pattern of SS430 coated with cobalt

X-Ray diffraction on this sample did not show any signs of material other than SS430, which would be expected for a sample with a thin layer of Co on SS430 that has not been heat treated. Indexing was not necessary as no extraneous peaks were found that could not be explained by elemental cobalt or steel.

6.3.2 SS430 COATED WITH COBALT HEATED TO 400^{O}C FOR 7 DAYS

A sample of cobalt coated SS430 was heated in air for 7 days at 400^{o}C. The thickenss of the coating was 5 x 10^{-8} m before oxidation. Belowin fig 6.4 is the X-Ray diffraction pattern for this sample.

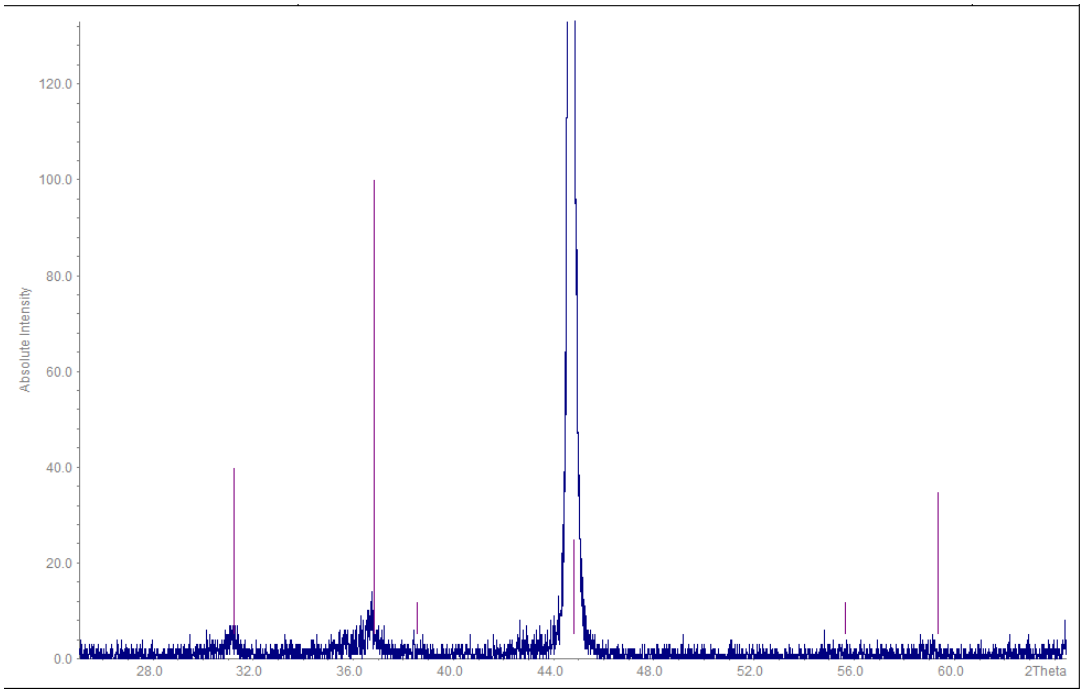

Fig.6.4: SS430 coated with cobalt and heated to 400^{O}C with Co_3O_4 peaks (purple)

As can be seen in the above X-Ray diffraction pattern, after heating to 400^{o}C in air for 7 days, the cobalt appears to have converted to cobalt spinel. Refinement was not possible due to width and low quantity of peaks. The pattern was dominated by iron peaks. No other peaks were determined to be present. Refinement was not performed as only two real peaks were found.

This sample turned slightly grey.

6.3.3 ALUMINA AND SS430 COATED WITH COBALT HEATED TO 450^{O}C FOR 7 DAYS

A sample of SS430 and alumina were both coated with 5 x 10^{-8} m of cobalt. Below is the X-Ray diffraction pattern for alumina with cobalt and heated to 450^{o}C for 7 days.

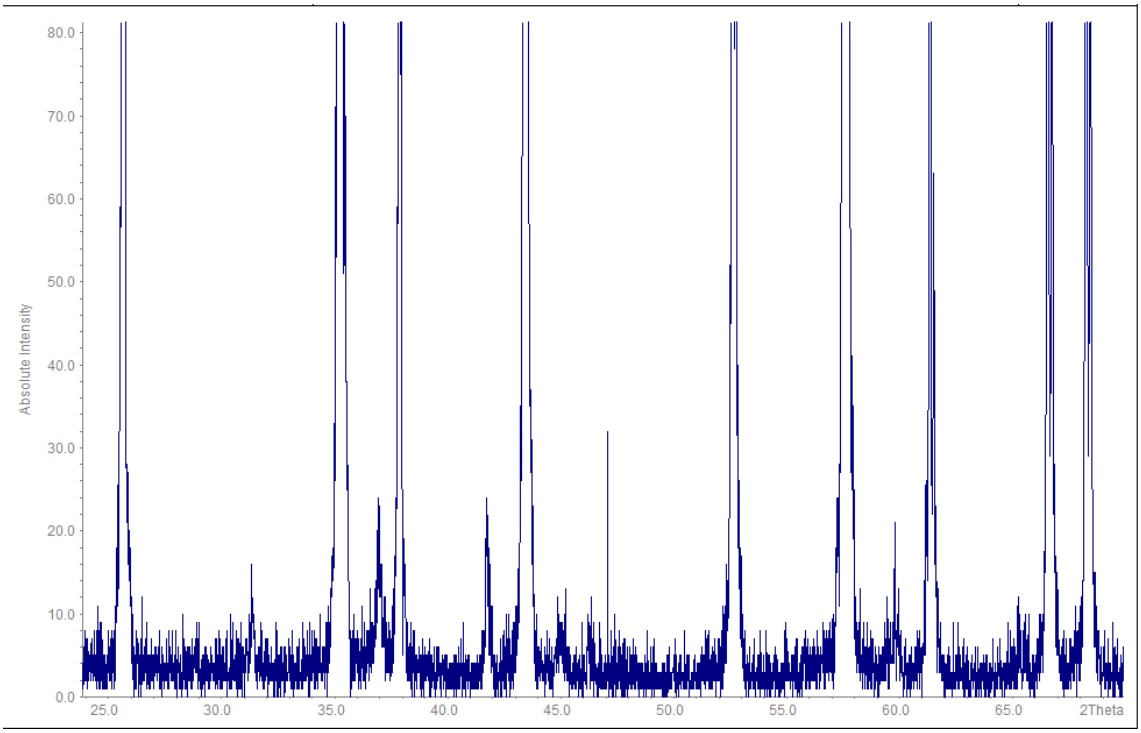

Fig.6.5: X-Ray diffraction pattern of cobalt on alumina heated to 450^{o}C

Alumina has many peaks compared to spinel as can be seen in fig.6.5. The cobalt on the alumina sample had converted to Co_3O_4 with nonalumina peaks at about 2theta= 37^{o} and 42^{o}. The peaks were refined using the spinel hkl values for Co_3O_4 from card number 43,1003. The unit cell parameter is listed below in table 6.2.

	Co_3O_4		
	Standard	sample	%
A	8.08(6)	8.020	0.74

Table 6.2: Unit cell parameter Spinel peaks formed by Co on Al_2O_3 at 450^{o}C for 7 days

This is a small difference considering only 4 cobalt oxide peaks were found on alumina at this temperature that could be positively identified. As no steel or any other chromium containing material was present, no chromium spinels were expected or found.

A sample of SS430 was also coated with the same thickness of Co and heated to 450^{o}C for 7 days. Below is the X-Ray diffraction pattern for this sample.

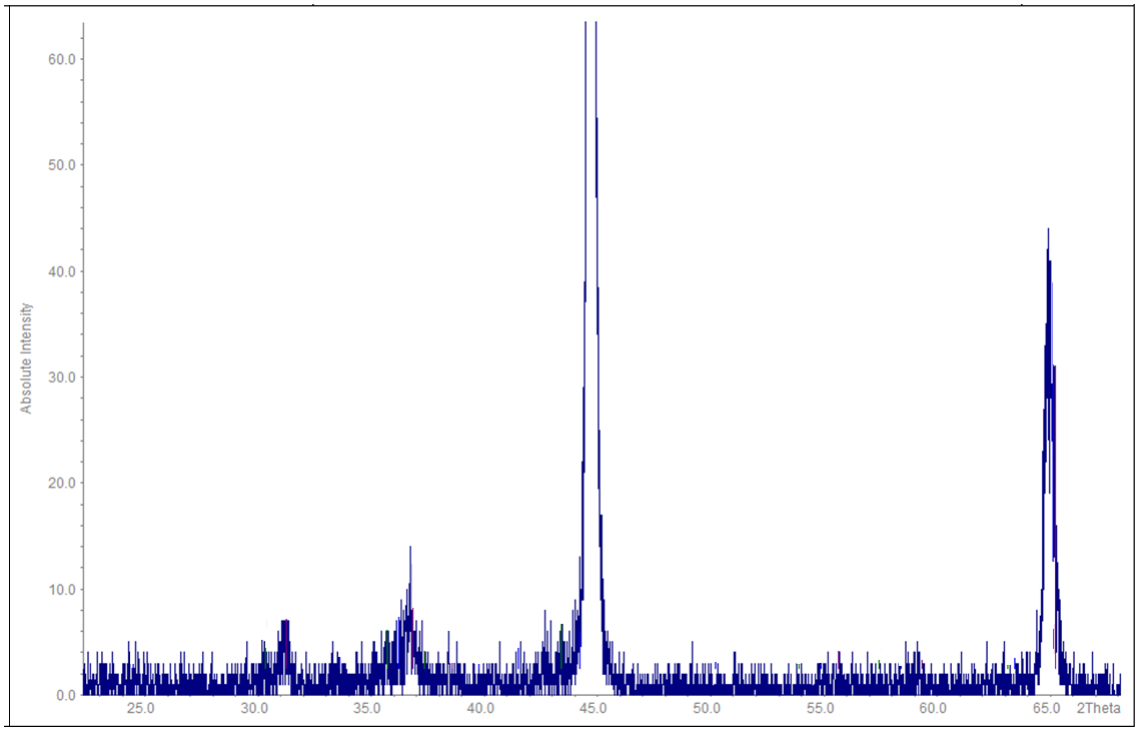

Fig.6.6: X-Ray graph of SS430 coated with cobalt and heated to 450^{o}C

Cobalt that was evaporated onto SS430 and heated to 450^{o}C was forming multiple peak systems as cab been seen in fig.6.6, however, two shared peaks coincided with the steel peaks making refinement difficult. Below is the refinement data for cobalt spinel only in table 6.3.

	Co_3O_4		
	Standard	sample	%
A	8.084	8.10(6)	0.20

Table 6.3 : Unit cell parameters for cobalt spinel from fig.6.6

At this temperature there is no spinel other than Co_3O_4 forming, and little to no chromia. No other peaks could be found other than Co_3O_4 and the steel background.

6.3.4 SS430 COATED WITH COBALT AND HEATED TO 500^{O}C FOR 7 DAYS

Cobalt of the same thickness from previous sections was again evaporated ont ss430 and heated, this time to 500^{o}C for 7 days. below is the X-Ray diffraction pattern.

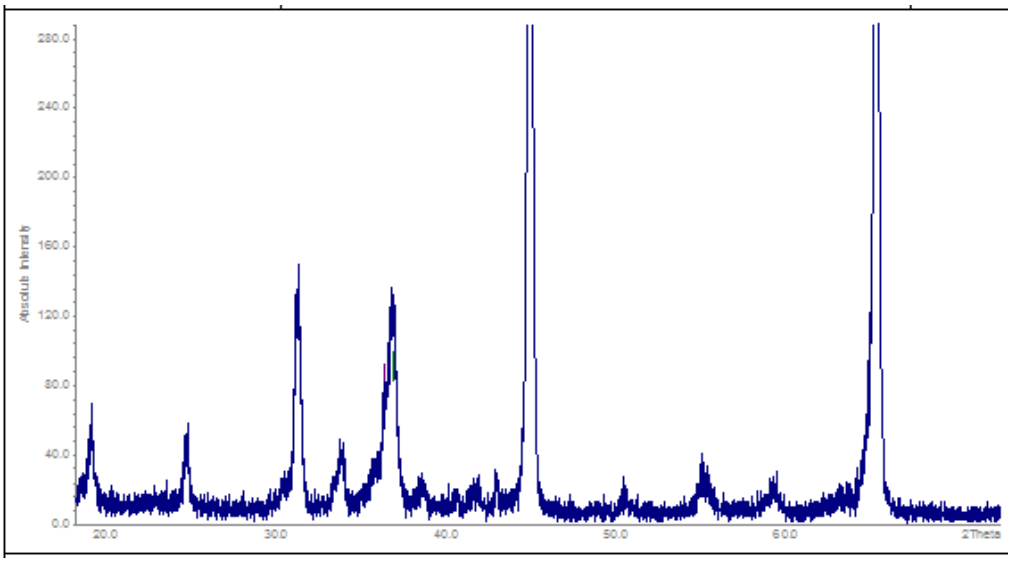

Fig.6.7: X-Ray diffraction pattern for SS430 coated with cobalt and heated to 500℃

The corrosion layer on SS430 heated to 500^{o}C was considerably different than the samples heated to 450^{o}C. Eskolaite could be seen at 500^{o}C, where as it was not detectable at 400^{o}C or 450^{o}C. Eskolaite and two possible spinels were determined to be the corrosion products. These peaks were separated into those for eskolaite and those for spinel, and refinement was performed using hkl values from the relevant PDF cards. The unit cell parameters are presented below.

	Cr2O3				Co3O4				Co2CrO4		
	Standard	Sample	%		Standard	Sample	%		Standard	Sample	
A	4.95876	4.91(6)	0.98	A	8.084	8.120(1)	0.4	A	8.17	8.120(1)	0.6
C	13.5942	13.55(6)	0.33								

Table 6.4 : unit cell parameters for peaks found on Co coated SS430 heated to 500^{o}C

When comparing the previous tables and figures It would appear in these preceding temperature ranges cobalt and steel corrosion is following a similar pattern of behaviour to Ti corrosion at 400-450^{o}C, where the evaporated corrosion layer is forming first (rutile for Ti, Co_3O_4 for Co), then at elevated temperatures an underlayer of eskolaite is forming.

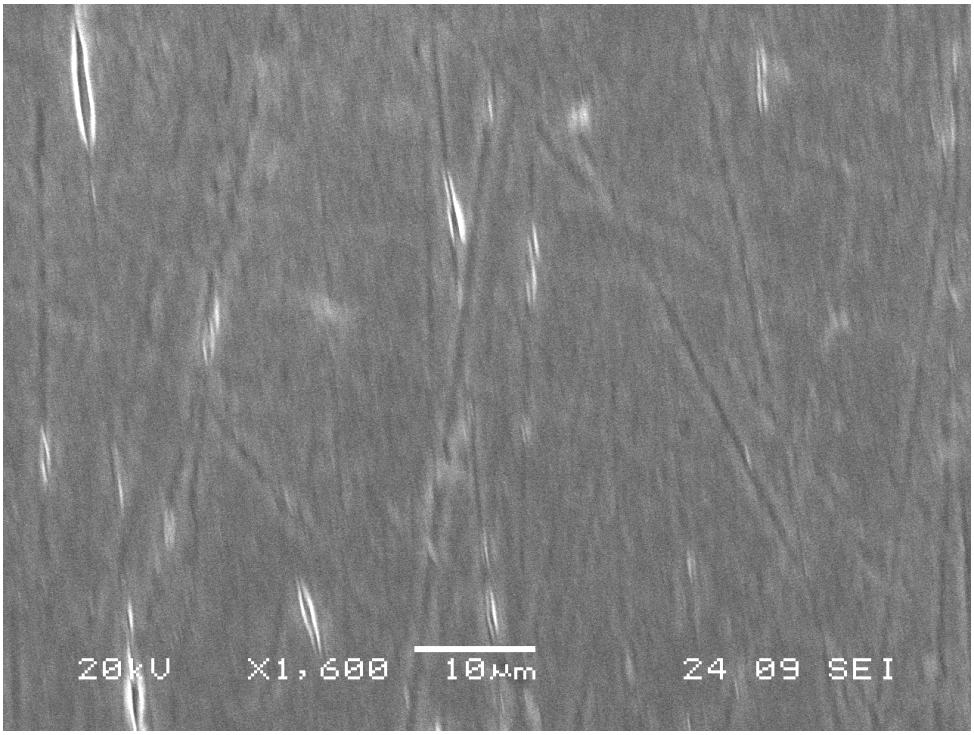

Fig.6.8: SEM OF COBALT ON SS430 HEATED TO 500℃ FOR 7 DAYS

No crystals of spinel were formed at this temperature that could be seen with the SEM.

6.3.5 SS430 coated with Co and heated to 600^{o}C for 7 days

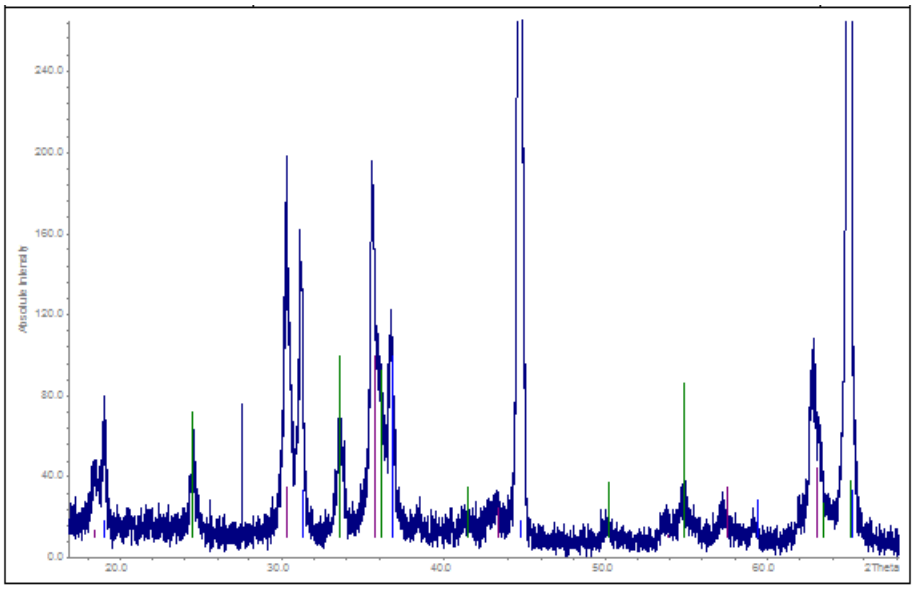

Fig.6.9: SS430 coated with cobalt fired at 600℃ fo r 7 days with peaks for Cr_2O_3(blue) Co_3O_4 (purple) and Cr_2CoO_4(green)

The above X-Ray diffraction pattern had 4 major peak sets. The first peak set were all related to the base layer of steel, and were ignored. There were also 2 spinel sets, and a chromia set.

The first spinel peak set was for Co_3O_4, which was present in all the previous temperature samples. The second set was determined to be Cr_2CoO_4 and not $CrCo_2O_4$ as the peaks did not match closely. The refined unit cell parameters are presented below.

	Cr_2O_3				Co_3O_4				Cr_2CoO_4		
	Standard	Sample	%		Standard	Sample	%		Standard	sample	%
A	4.95876	4.92(9)	0.78	A	8.084	8.132(1)	0.59	A	8.3299	8.32(4)	0.11
C	13.5942	13.60(2)	0.04								

Table 6.5 : Unit cell parameters of non steel peaks from fig.6.9.

Scanning electron microscopy did not show any defined spinel crystals forming on the surface of this sample after 7 days, however, a dense blanket was appearing that was made of grains.

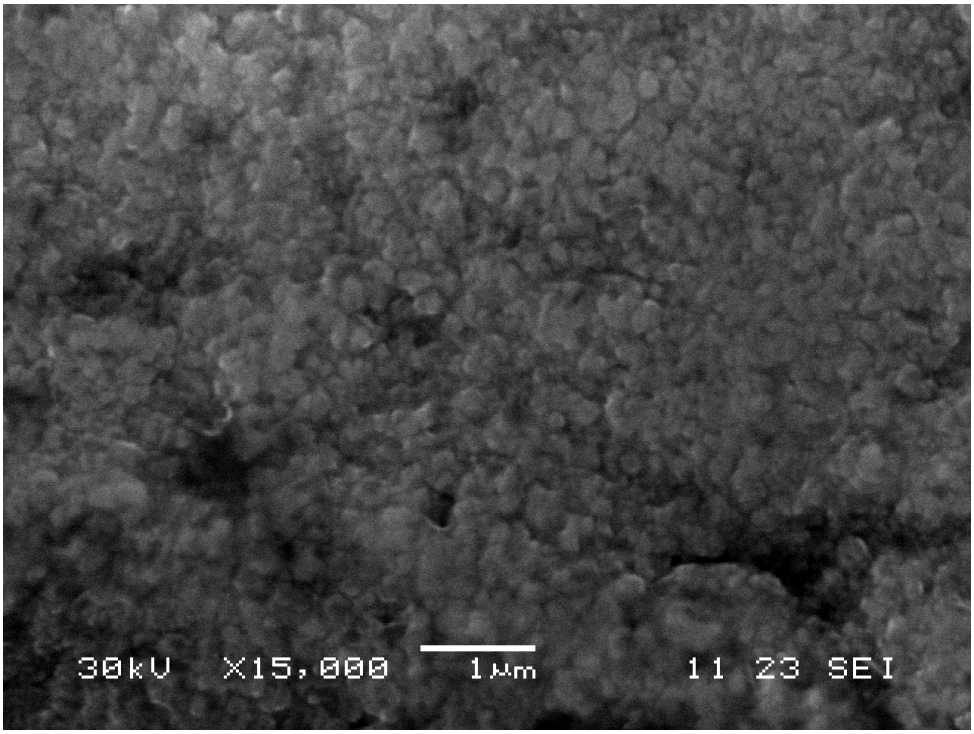

Fig.6.10: SEM SS430 with Co evaporated, heated to 600^oC .

6.3.6 SS430 COATED WITH COBALT AND HEATED TO 700^OC FOR 3 DAYS

Following the lines of the above experiments, a similar sample was prepared with the same initial thickness of cobalt of $5x10^{-8}$m thick, and heated to 700°C for 3 days. Below is the X-Ray diffraction pattern for the sample.

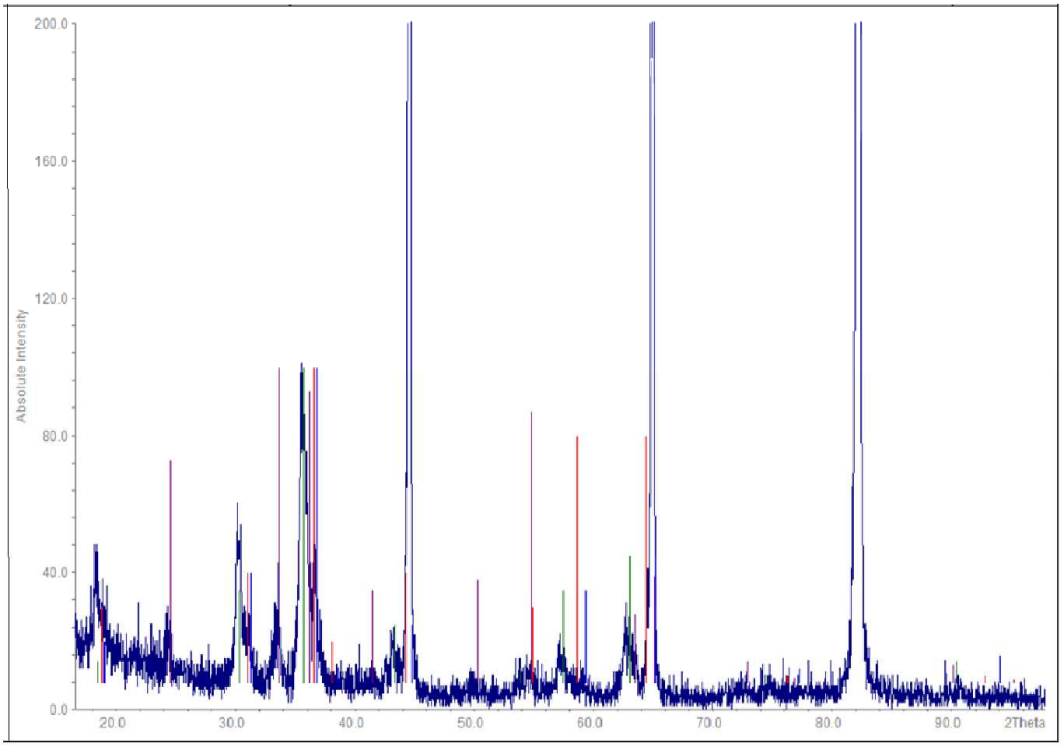

Fig.6.11: X-Ray diffraction pattern of SS430 with cobalt heated to 700°C 3 for 3 days with Cr_2O_3(purple) $CoCr_2O_4$ (Green),Co_3O_4,(blue) and Co_2CrO_4(red) peaks

Refinement of the above peaks was performed with 4 non steel peak sets found. However, as can be seen from fig.6.11, Co_3O_4 and Co_2CrO_4 have very close peaks.

	Cr_2O_3				Co_3O_4		
	Standard	sample	%		Standard	sample	%
A	4.95876	4.87(7)	1.79	A	8.084	8.122(11)	0.47
C	13.5942	13.2(3)	2.90				
	$CoCr_2O_4$				Co_2CrO_4		
	Standard	sample	%		Standard	sample	%
A	8.3299	8.08(6)	3	A	8.17	8.125(24)	0.6

Table 6.6: Unit cell parameters for indexed peaks from fig.6.11

The parameters had large deviations for the one major reason: (as discovered in Chapter 5), in this temperature range, manganese and iron will become much more involved in the corrosion layer.

For comparison, untreated SS430 was also heated to the same conditions. Below is an SEM of the resultant corrosion layer. Uncoated samples of SS430 at lower temperatures were discussed in Chapter 5.

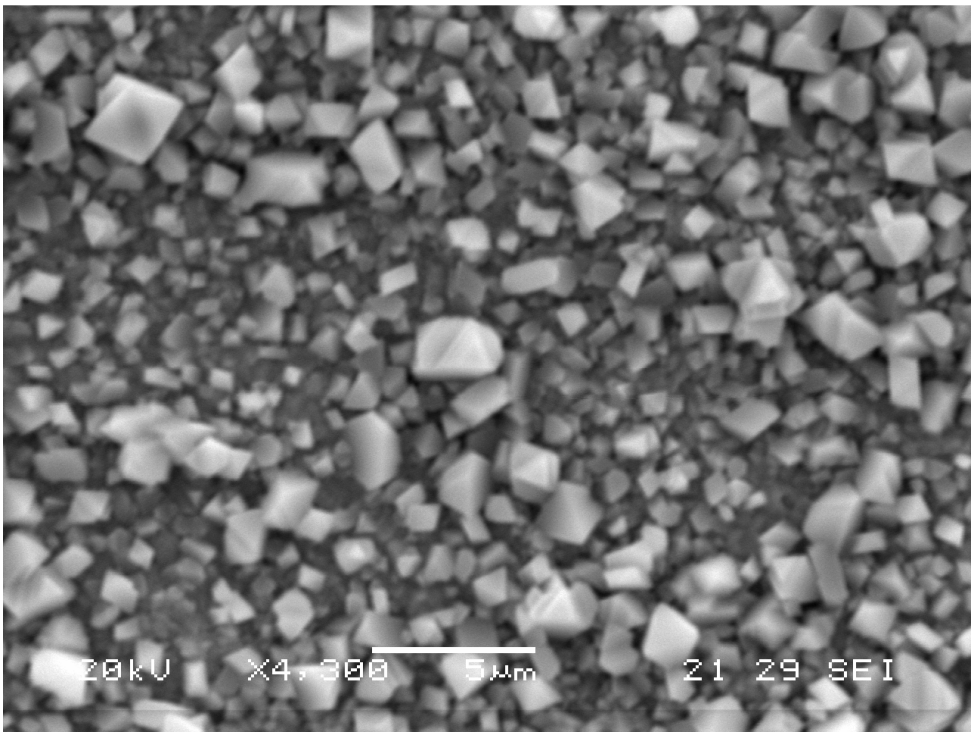

Fig.6.12: SEM of SS430 uncoated heated to 700^{o}C for 3 days

Some spinel and eskolaite crystals can be seen in fig.6.12. This is consistent with corrosion of SS430 at this temperature. The spinel is likely Cr/Mn spinel.

Element	Weight%	Atomic%
O K	29	57.98
Cr K	29.9	18.39
Mn K	10.19	5.93
Fe K	30.91	17.7
Totals	100	

Table 6.7: EDS of SS430 post oxidation for 3 days at 700C

EDS results confirm that Mn is becoming enriched in the corrosion layer. Manganese is a minor constituent of SS430, at about 0.4% by weight [7]. We can conclude that Mn is enriched in the surface layer, and must be contributing to the corrosion products.

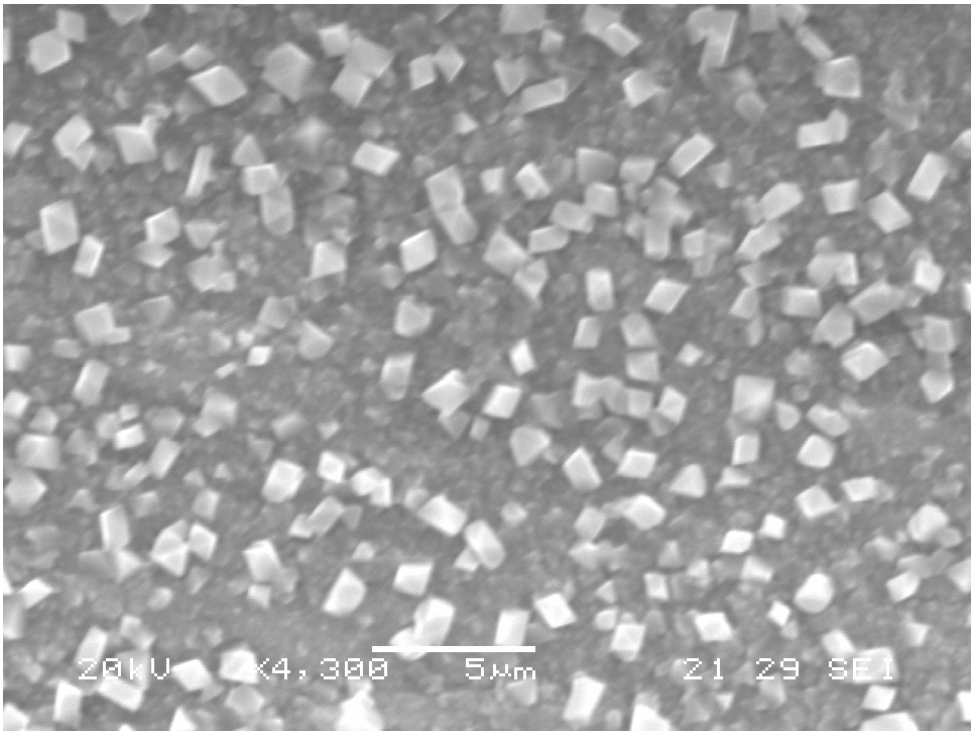

Fig:6.13. SS430 coated with cobalt post oxidation 700C for 3 days

Element	Weight%	Atomic%
O K	28.79	58.08
Cr K	22.13	13.74
Mn K	11.72	6.89
Fe K	23.28	13.45
Co K	13.04	7.14
Totals	100	

Table 6.8: EDS results of SS430 coated with cobalt post oxidation

Although SS430 makes some spinels or other cubic structures and a lot of eskolaite when it oxidizes at higher temperatures, it would appear that the addition of a very small amount of cobalt promotes smaller spinel crystals and subdues the production of eskolaite. When we compare the sample heated at 700 for 3 days to the sample heated to 600 for 7 days, we can see that the spinel crystals in fig.6.13 are actually lying on a blanket similar to the blanket in fig.6.10. In addition, Mn is beginning to make a strong showing in the EDS results, confirming its involvement in the corrosion process and suggesting a more complex spinel formation.

6.4 THICKER COBALT LAYER

A longer target of cobalt at 4cm was used to coat the next samples. The theoretical mass of the target to be evaporated was 0.00011 grams. Based on the calculation in Chapter 2 for the thickness $T = m/(4\rho * \pi * r^2)$, the density value of 8.9g/cm^3, and a distance between target and substrate of 40mm, the theoretical thickness is 2.4 x 10^{-7} m. Using the volume and molecular weight of 557.99 A^3 and 229.92 g/mole respectively for Cr_2CoO_4 spinel, and Avogadro's number, the layer will grow to 1.2 x10^{-8} m thick theoretically.

6.4.1 SS430, THICK COBALT, 700^{O}C, 3 DAYS

A sample of SS430 was coated with a thicker layer of cobalt that was about 1.5 x 10^{-7} m. Below is the X-Ray diffraction pattern of that sample after heating at 700^{0}C for 3 days.

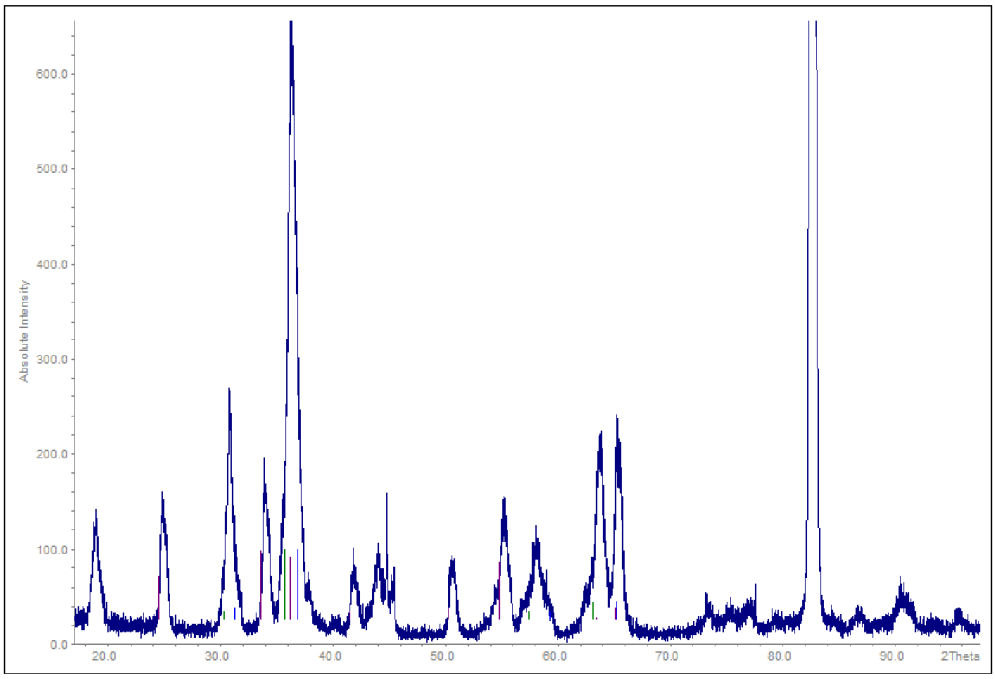

Fig.6.14: Thick cobalt on SS430 heated to 700^{o}C for 3 days with Cr_2O_3(purple) Cr_2CoO_4 (green)and Co_3O_4(blue) peaks

Four peak sets could be determined; steel, Cr_2O_3,and Co_3O_4, and Cr_2CoO_4,from fig 6.14. Below are the refined unit cell parameters for the indexed peaks for assumed materials.

	$FeCrO_3$				Co_3O_4		
	Standard	sample	%		standard	sample	%
A	5.0115	5.06(6)	1.9	A	8.084	8.08 (3)	0.05
C	13.6232	13.52(10)	.76				

	$CoCr_2O_4$	
	Standard	Sample
A	8.3299	8.39(4)

Table 6.9: Unit cell parameters for assumed compounds from fig.6.13

The eskolaite phase had the largest deviation in table 6.9, probably due to mixing of iron, manganese, and other elements. However, the spinel phase Co_3O_4 was quite close to standard. This is to be expected with a thicker layer of cobalt as it will take longer for the layer to become oxidized and then altered by elements migrating from the steel.
Electron microscopy showed that there was a layer forming encrusted with crystals that was beginning to separate from the substrate.

Fig.6.15: SS430 coated with thick cobalt and heated for 3 days at 700℃

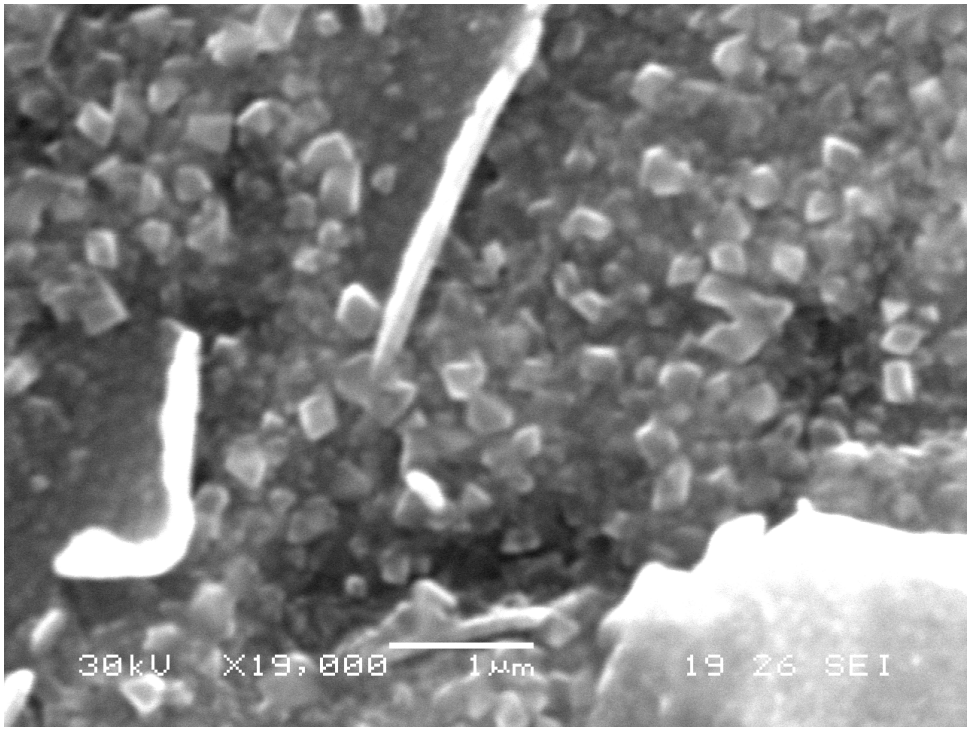

Fig.16: Close up of fig.15 showing film edges

SEM images showed that there could possibly be spinel crystals forming. This sample was reheated for longer for a total of 9 days.

6.4.2 ADDITIONAL HEATING FOR SAMPLE FROM 6.4.1

The same sample from 6.4.2 sample was heated for an additional 6 days at 700^{o}C and X-Ray diffraction was performed again. Peaks became much taller and narrower, and eskolaite phases had a much lower showing than at other thicknesses or temperatures. SS430 peaks had similar positions to corrosion products but were not so recognizable by the hight of their peaks as in previous sections. This is due to the thickness of the corrosion layer transmitting far less steel peaks back to the detector.

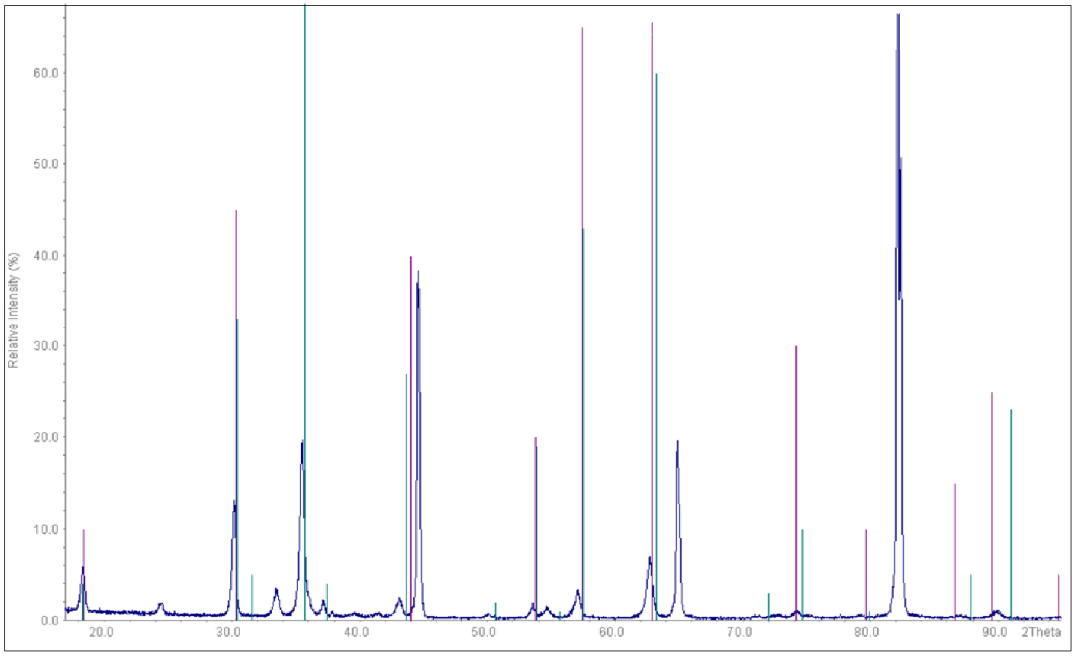

Fig.6.17: X-ray diffraction pattern of SS430 with Co heated for a total of 9 days at 700℃ with Cr_2O_3 (purple) and Cr_2CoO_4(green) peaks

Although none of the peaks matched well, it was determined that Cr_2CoO_4 and Cr_2O_3 were the two most likely corrosion products. Refinement of the indexed peaks is below.

	$FeCrO_3$				$CoCr_2O_4$		
	Standard	sample	%		standard	Sample	
A	5.0115	5.15(7)	3	A	8.3299	8.64(5)	3.7
C	13.632	14.0(3)	3				

Table 6.10 : Unit Cell parameters of indexed non steel peaks for fig.6.17

The peaks found were consistent with a background of SS430 and spinel and the eskolaite phase, however, the deviations were quite large. This is because of mixing of the many elements and undefined ratios. The difference in the layer after 6 days of additional heating would suggest that there were concentration gradients of elements throughout the corrosion layer.

Below are a series of images of the resultant layer.

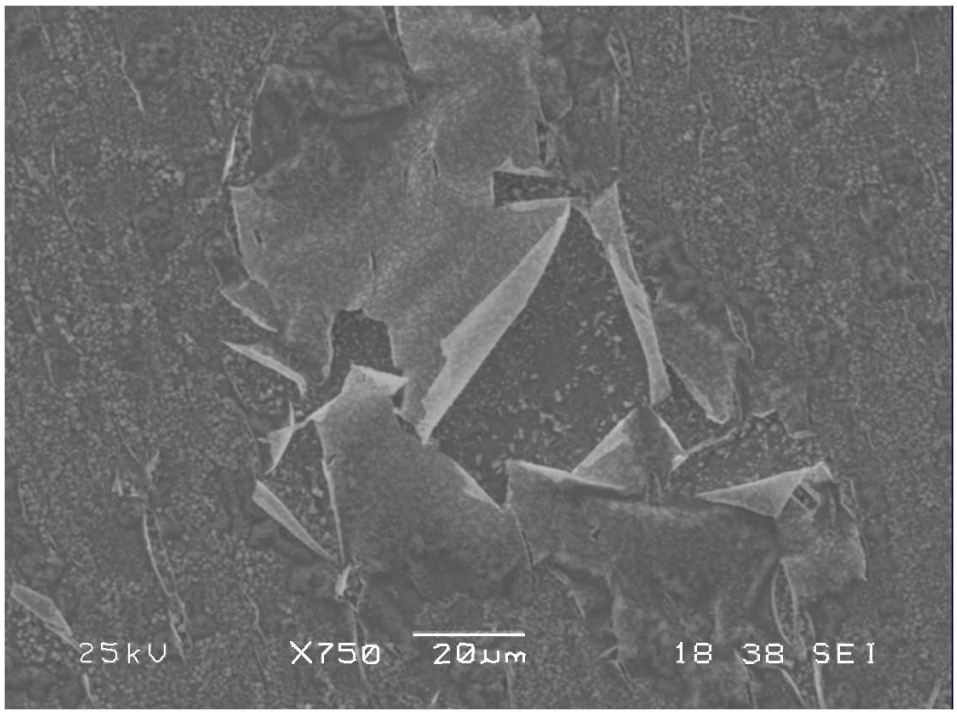

Fig.6.18: Long view of transparent layer with break in it

After 9 days of heating a thin transparent foil appeared in the images. The foil appeared to be covering and containing crystals that had defined facets. Using higher magnification, the crystals and their facets became clearer. The thickness of the film is discussed further in this section.

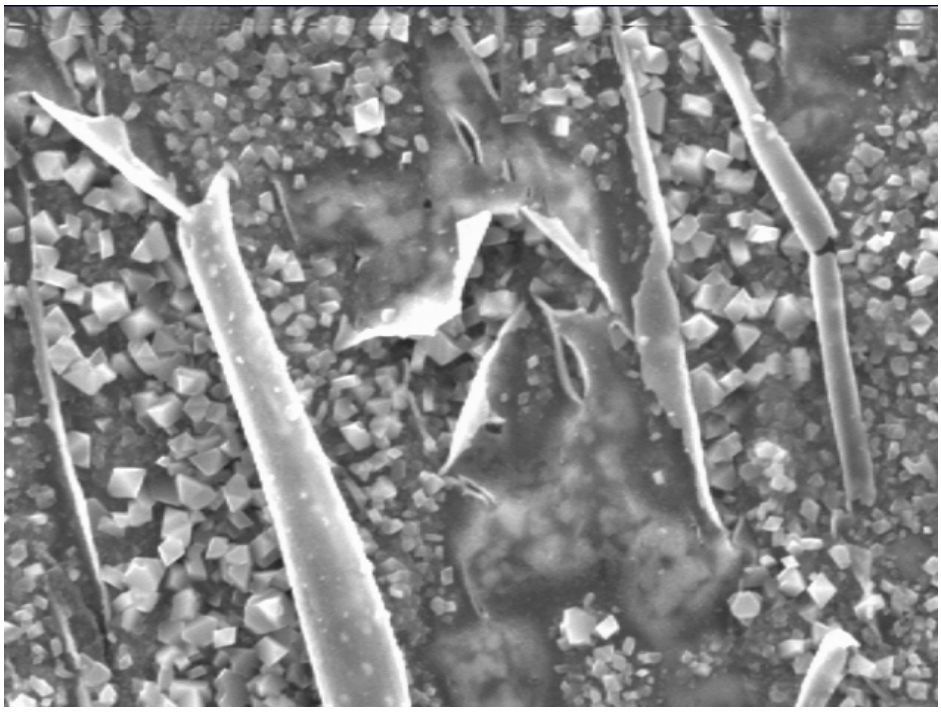

Fig.6.19: Close up of fig.6.18

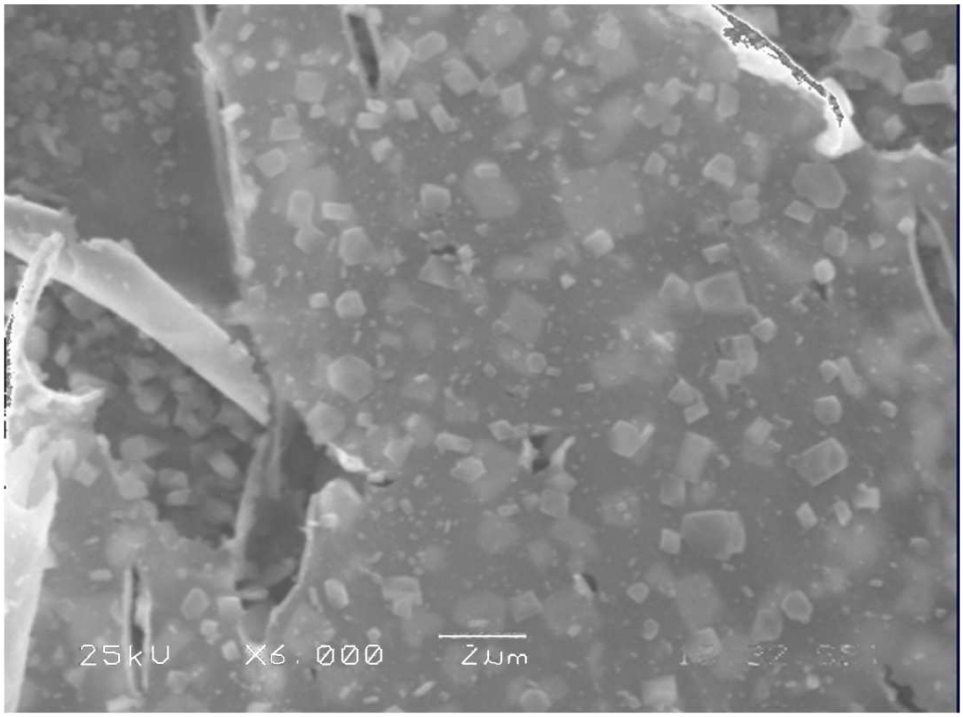

6.20: Close up of transparent film

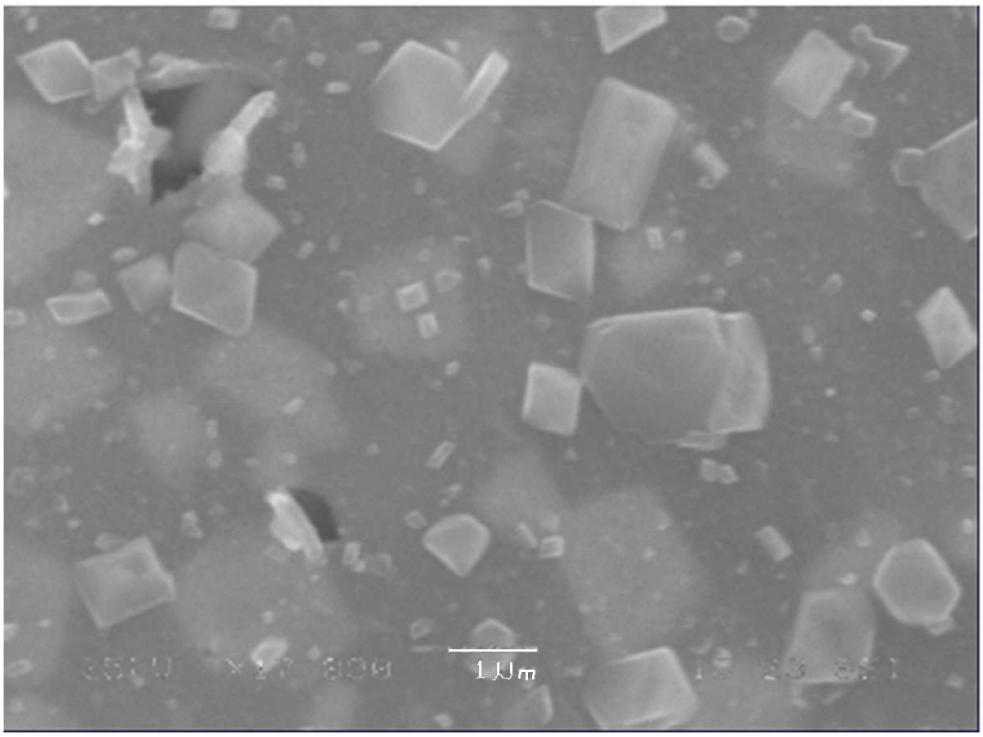

Fig.6.21: Higher magnification of same area

As can be seen above, crystals could be seen under and through this layer.

The layer is most likely to be Co_3O_4 that is allowing some oxygen through but holding back Cr and other elements. As oxygen continues to pass through the layer either through the film or through the cracks, corrosion products are continuing to form. Clear spinel facets are seen through the film.

Examination of the film by its self is not possible using SEM and X-Ray diffraction on SS430 substrates.

In areas that were no longer covered due to breakage of the film, spinel crystals were found. From fig.6.21 we can determine the thin layer to be about .1um thick. This layer is not the total corrosion layer however, but is most likely produced by evaporated cobalt that has come free of the substrate and oxidized prior to the formation of the crystals below.

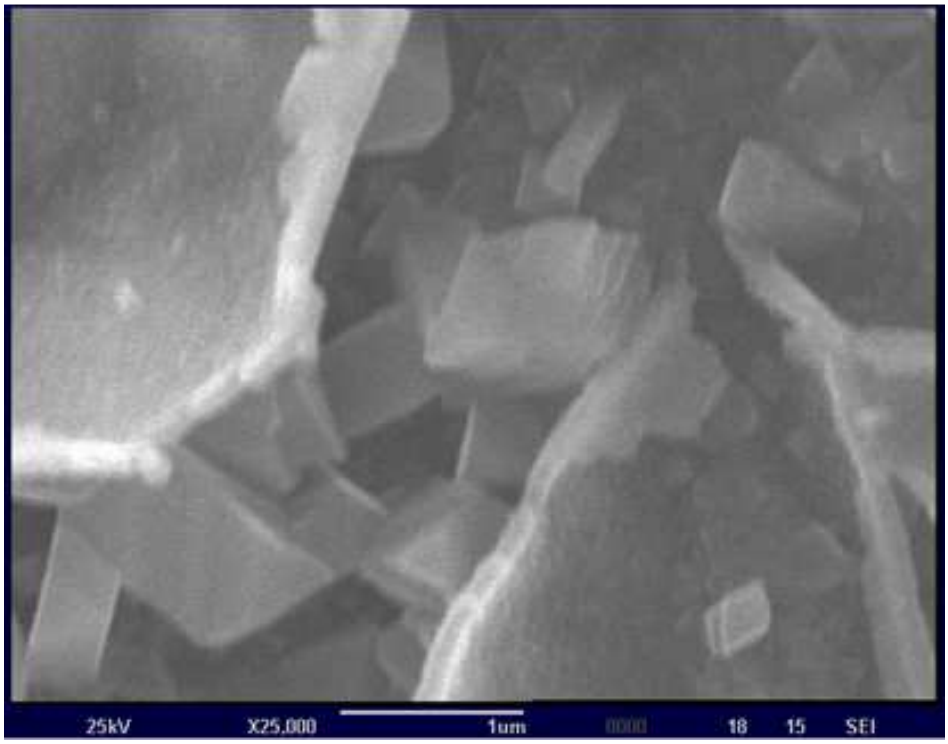

Fig.6.22: Close up of crack in layer and crystals underneath. A good estimate is that the layer is about .1µm thick. Crystals are about 5µm wide

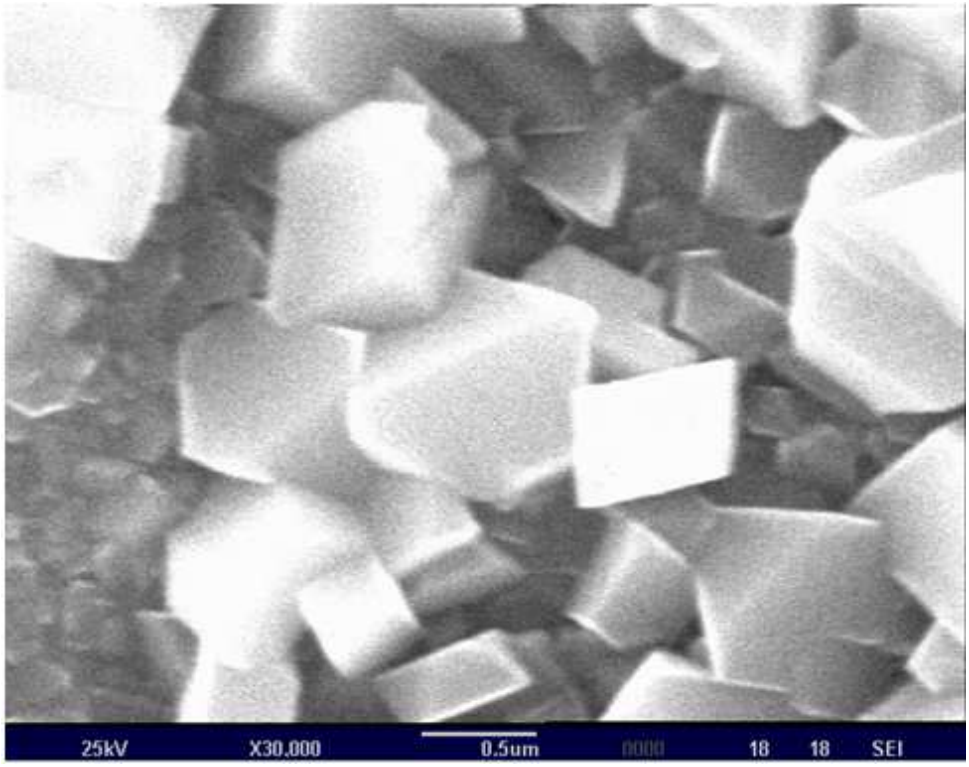

Fig.6.23: Close up of crystals showing defined facets and width of ctystals

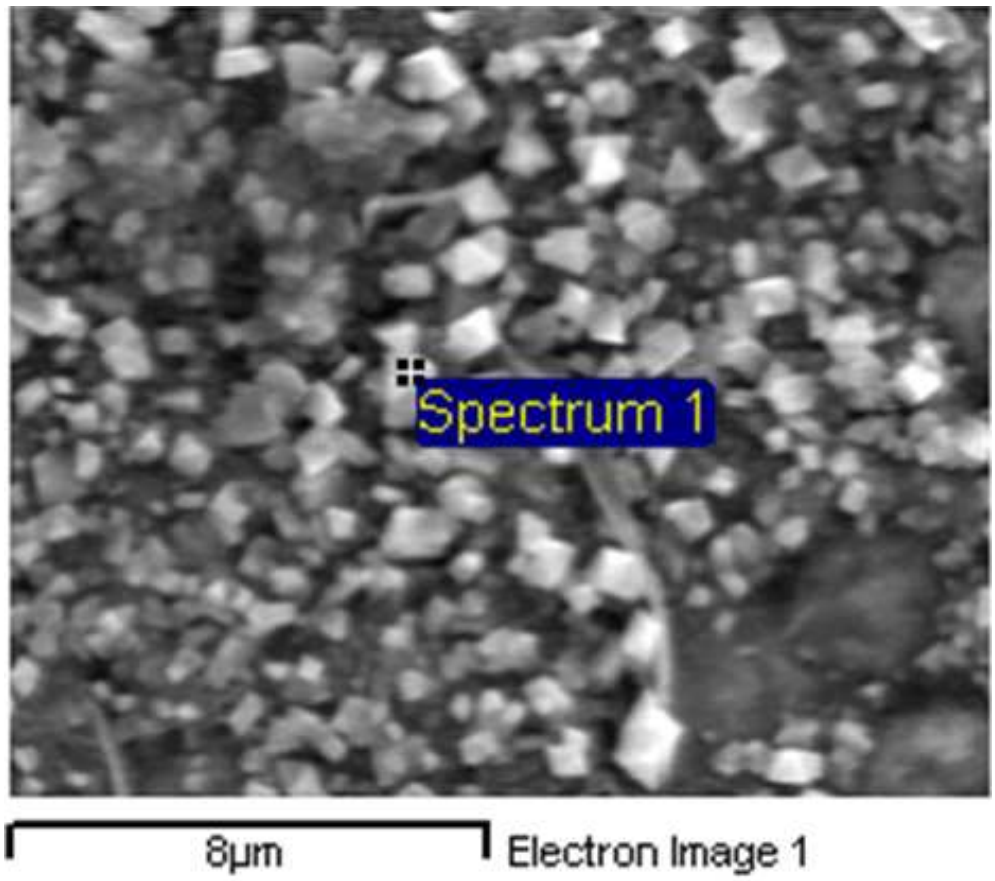

Fig.6.24: Close up of crystals in an area where film is no longer continuous. Spectrum 1 is the position of EDS analysis below

Element	Weight%	Atomic%
O K	37.79	67.67
Cr K	20.32	11.2
Mn K	11.3	5.89
Fe K	13.71	7.03
Co K	16.89	8.21
Totals	100	

Table 6.11: EDS results for fig.6.24

Results from table 6.11 show that Mn,Fe are Co becoming more involved in the corrosion layer and are involved in spinel formation. Increases in Co would be expected over previous sections as more Co was deposited than in previous sections. Below is a table of the nominal composition of SS430[8].

Element	Mole %
Fe	82.81
Cr	16.3
Mn	0.45
Si	0.4
C	0.04

Table 6.12 : Reference Composition of SS430

Mn is a minor element, but clearly contributes to the corrosion layer confirming its high mobility.

6.4.3 SS430 HEATED TO 700^{O}C FOR 9 DAYS

The back of this sample showed much fewer spinel crystals, which is consistent with SS430 corrosion in these conditions. The image is quite similar to fig.6.12. The corrosion on the back is likely to be chromium manganese spinel, mixed with eskolaite. There was a lack of the thin film layer observed in Fig. 6.19 to Fig.6.22, confirming that the film is due to the evaporation process.

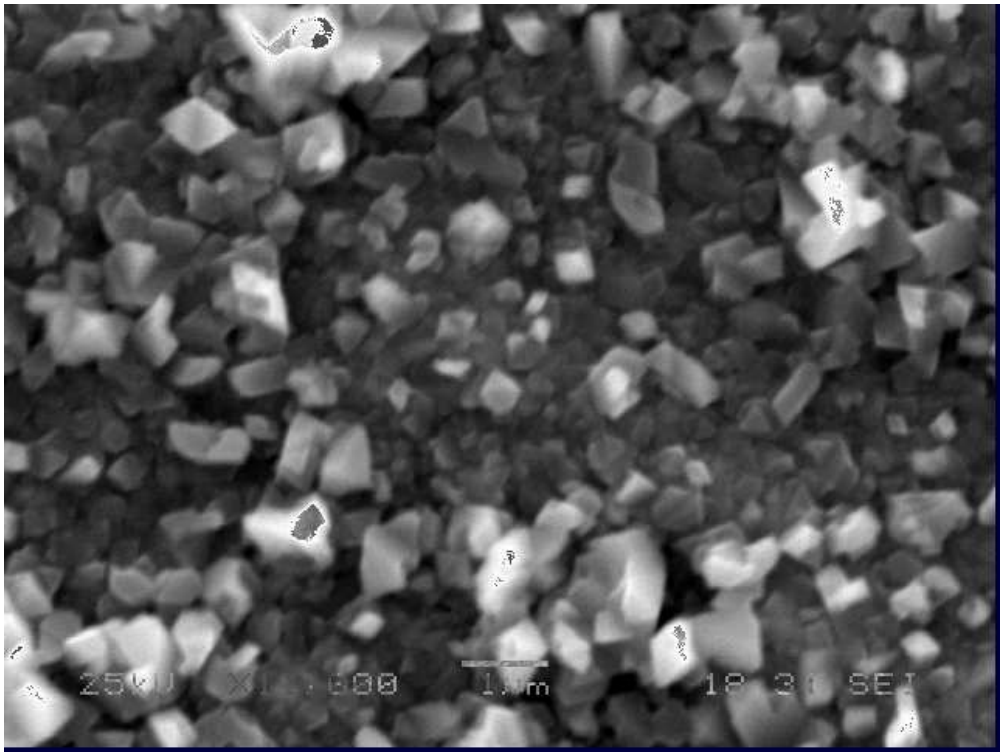

Fig.6.25: Back of sample

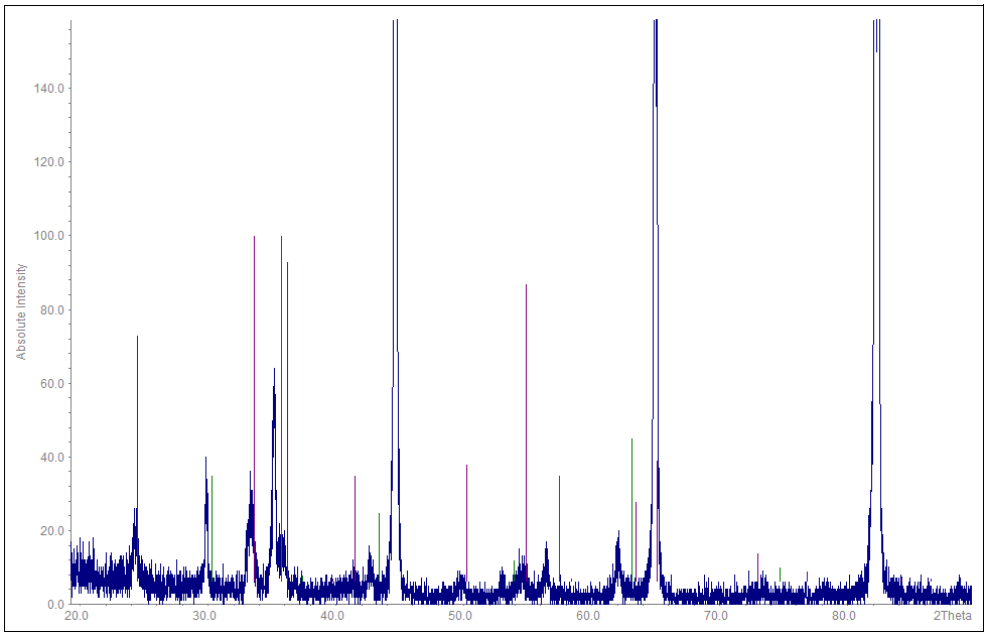

Fig.6.26: X-Ray pattern for SS430 heated to 700^{o}Cwith eskolaite(purple) and spinel(green)

The non steel or eskolate peaks were found to be $Cr_{1.5}Mn_{1.5}O_4$. Below are the indexed unit cell parameters for these materials. As no cobalt was added, non would be expected.

	Mn1.5Cr1.5O4		
	Standard	Sample	%
A	8.455	8.465	0.118133

Table 6.13: Unit cell parameters for the two best fit corrosion products on SS430 at 700^{o}C

$CrMnO_3$ has peaks very close to Cr_2O_3 and could be considered a doped eskolaite type phase but is reported in ICCD database as triclinic. There were not enough peaks to refine the 3 lattice parameters and 3 angles. For steel without coatings, this would suggest that at elevated temperatures, ternary spinels and substituted eskolaites are starting to form, making positive identification of the materials difficult. This is the case for most corrosion layers; the higher the temperature, the more possible combinations are thermodynamically possible.

6.4.4 EDGE ANALYSIS

A section of the sample from 6.4 was cut and mounted at 90 degrees in epoxy. However, no useful information could be gained from viewing in SEM. As with Ti samples, the layer was too thin to see an edge in this way. This is probably caused by the curing conditions with the epoxy that can peel the layer off as it shrinks/cools/cures. Fig.6.22 suggests that whatever the transparent layer is, it may not be distinguishable from the rest of the corrosion layer when viewed edge on.

6.5 VERY THICK COATING COBALT SPUTTERING AT 800^{O}C FOR 9 DAYS

A fresh sample was prepared using SS430 and approximately 3 times the previous amount of cobalt to be sputtered. To accomplish this, 10 cm of cobalt wire was bent into loops about 1cm long and inserted into the heating element. The mass of cobalt would be 0.00011g. The layer was calculated to be 6.1 x 10^{-10} m as deposited. The thickness of this layer after oxidation was calculated to be 3.1 x 10^{-8} m.

After deposition, the sample was heated for 9 days at 800^{O}C. The surface appeared black and flaky. SEM examination of the front surface can be seen as a series of images zooming in below.

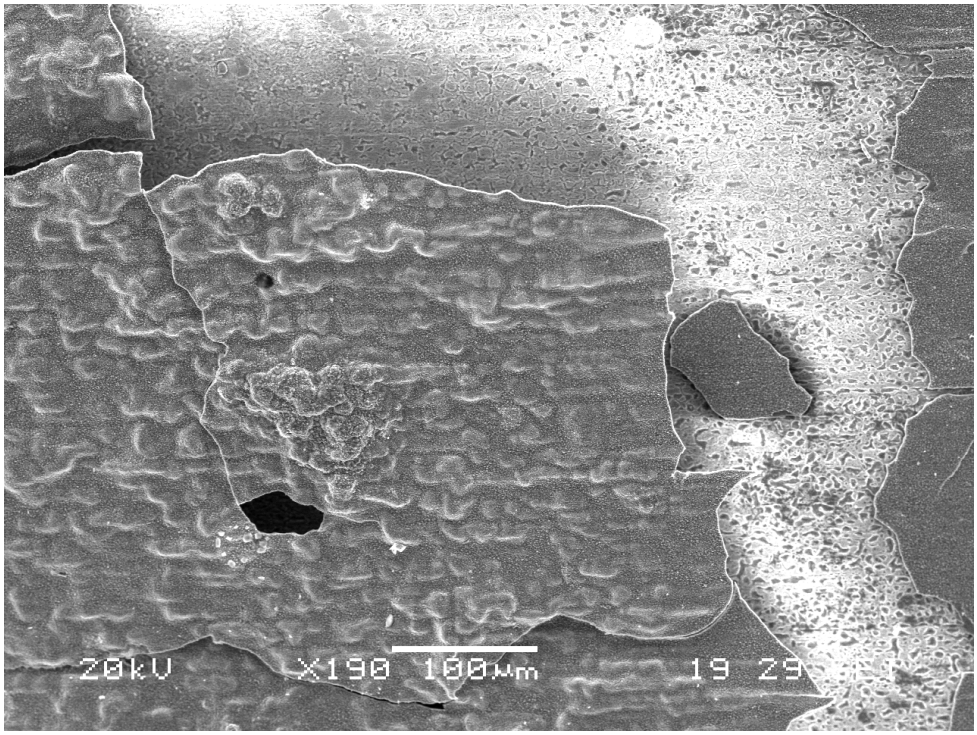

Fig.6.26: Cobalt coated SS430 with thick cobalt oxidation layer heated to 800^{o}C for 9 days.

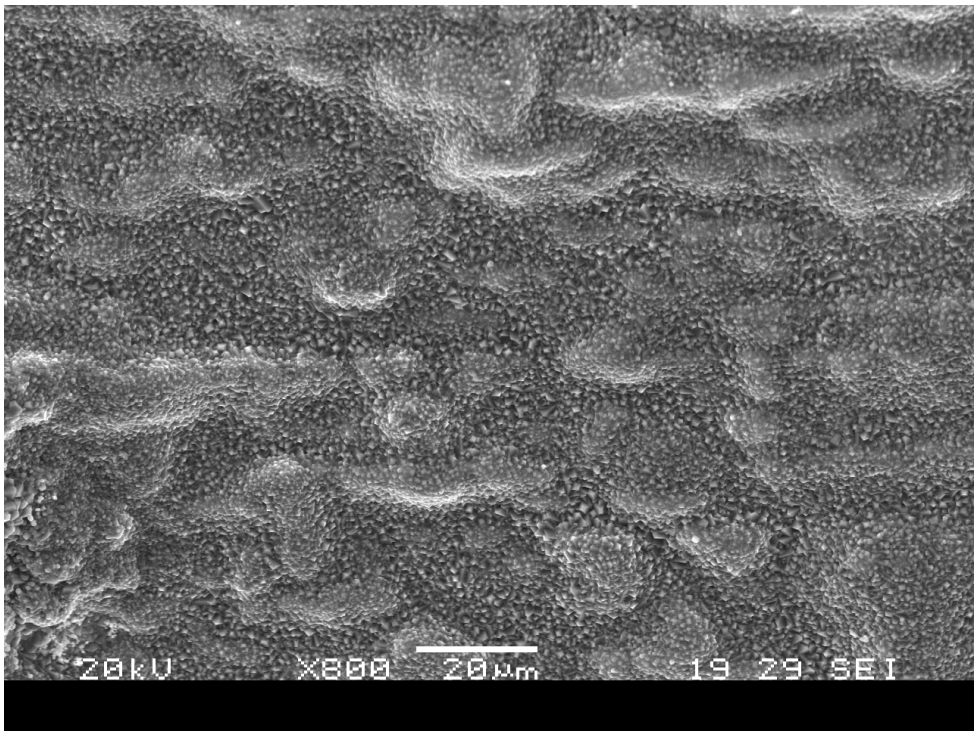

Fig.6.27: Zoom in of oxidation layer from fig.6.26

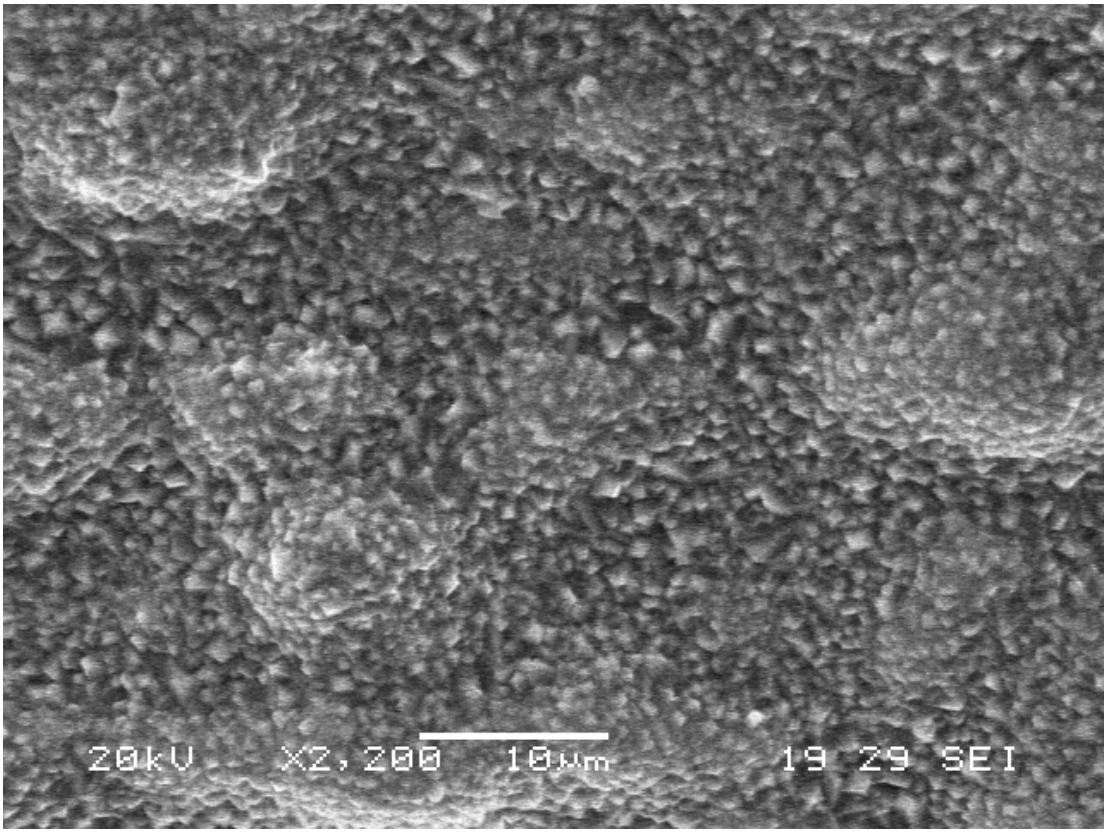

Fig.6.28 further zoom of thick cobalt oxidation layer

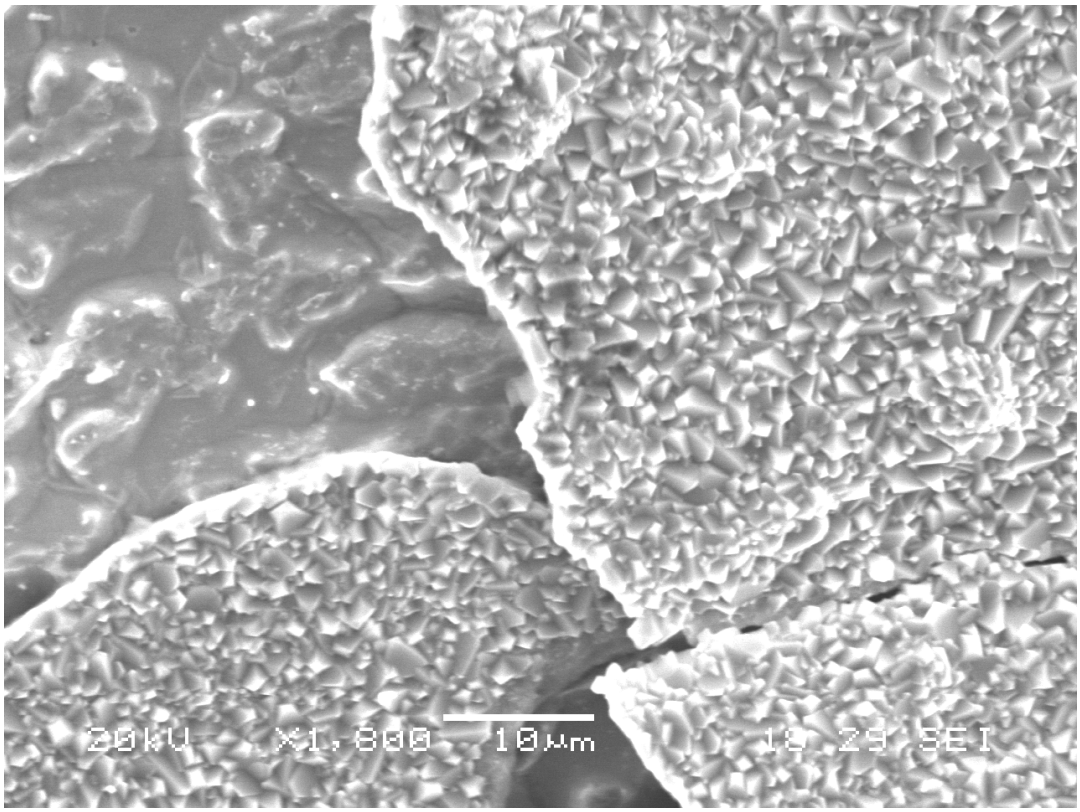

Fig.6.29: Close up of cracks in thick cobalt oxidation layer

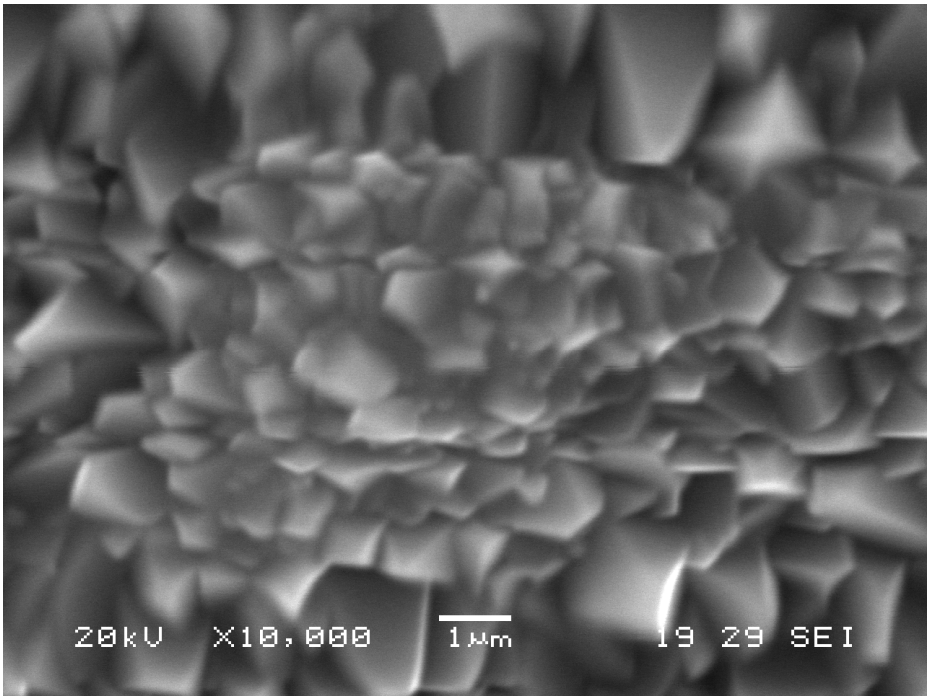

Fig.6.30: Close up of facets on thick oxidation layer

6.5.2 ELEMENT ANALYSIS

EDS was performed on a part of the sample where the two surface conditions met.

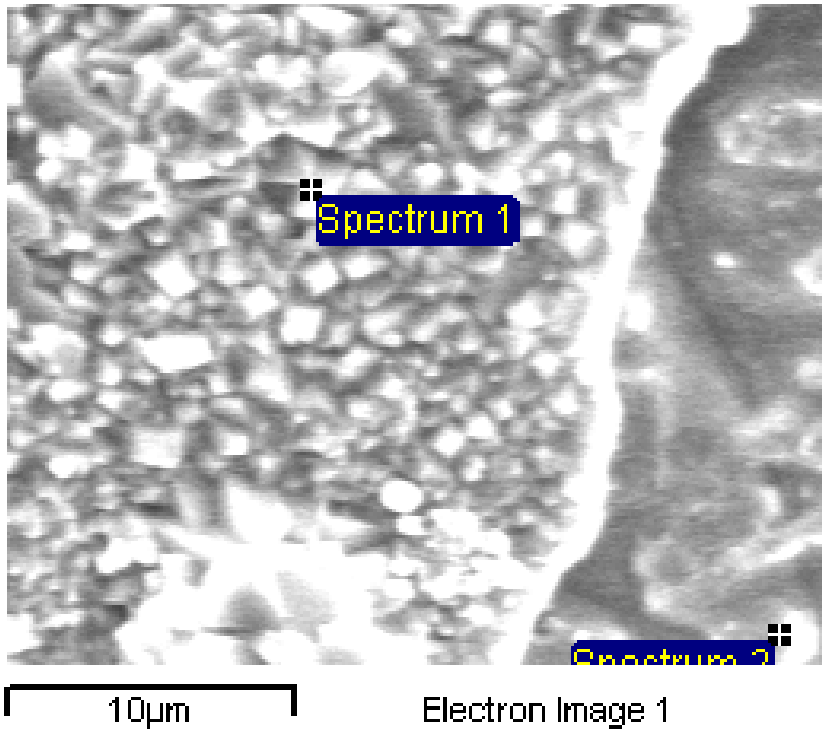

Fig.6.31: sites of EDS analysis

Spectrum	O	Cr	Mn	Fe	Co	Total
Spectrum 1	24.77	25.94	22.56	4.01	22.72	100
Spectrum 2	7.98	14.11		77.91		100

Table 6.14: EDS analysis of thick cobalt layer

Due to the thickness of the layer, it is assumed that the values are correct and that not much background is picked up from the substrate. The cobalt layer, as noted from spectrum 1, is rich in chromium, manganese and cobalt, but not rich in iron. Iron is detected in the crack at the bottom right hand corner of fig6.31. Spectrum 1 shows that there are almost equal amounts of Cr, Mn and Co in the spinel layer, suggesting complex spinels are forming.

6.5.2 THICK SAMPLE EDGE

The second sample was mounted in epoxy at 90 degrees in epoxy. Below is the micrograph of this sample.

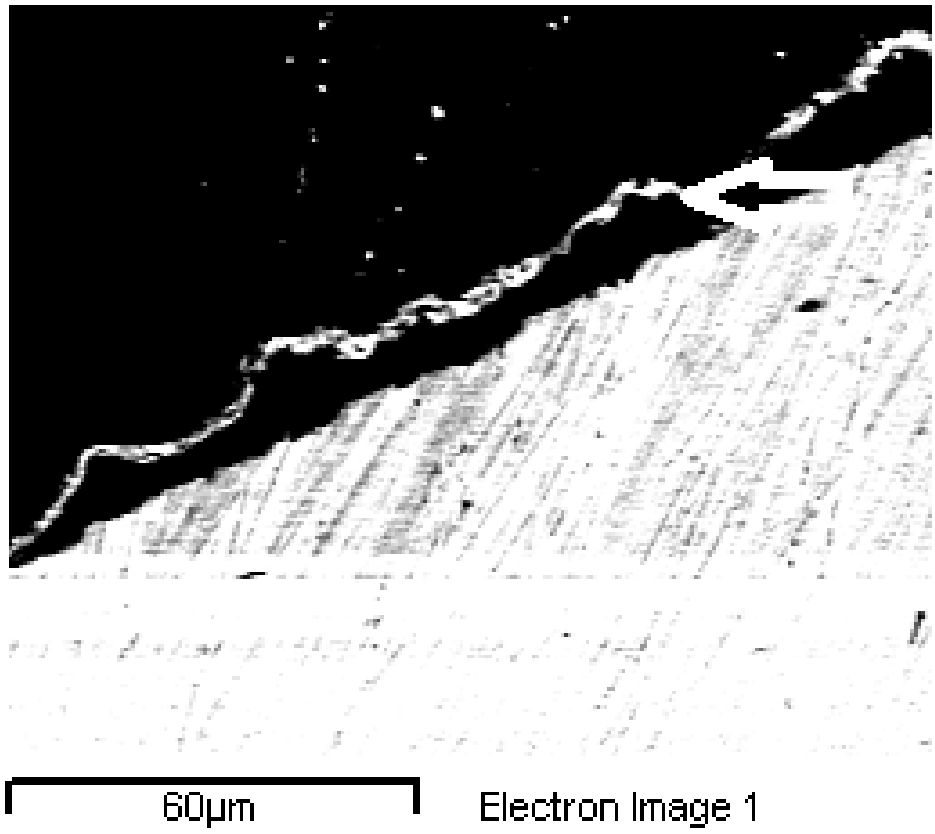

Fig.6.32. SEM edge image of SS430 with cobalt corrosion layer denoted by small arrow

Results of EDS from the point of the arrow from fig.6.32 are in the table below.

Spectrum	Cr	Mn	Fe	Co	Total
Spectrum 4	50.09	28.4	6.26	15.25	100

Table 6.15: EDS results of thick layer spalling from fig.6.32

This image in fig.6.31 shows that the thicker coating at higher temperature has spalled, either before or after the epoxy process. It is visible, and shows elements consistent with spinel. Additionally, the thickness appears to be consistent with previous calculations. That is, if this layer is about 3 micron, then samples from the 4cm of sputtered cobalt would be about a micron, and from 1 cm of cobalt would be .3 of a micron. There is no gold coating or flaring of these samples, even at 30kv. This would suggest the materials are somewhat conductive.

6.4 ELECTRICAL RESISTANCE MEASUREMENTS

For the same reasons that Ti and TiO_2 and reduced TiO_2 layers on SS430 are difficult to characterize electrically using 4 point probes and multimeters, cobalt chromium spinels are also difficult to characterize. For this reason, the same Eelectrochemical Impedance Sectroscopy (EIS) techniques used in Chapter 5 were employed for cobalt evaporated and oxidized layers.

Samples were taken from section 6.3.5, thin layers of cobalt that were evaporated onto SS430 on both sides and heated to 600^oC for 7 days. Each side was coated with $1cm^2$ of gold to increase contact surface area. Compared to ESI studies in Chapter 5 where the reduced TiO_2 samples displayed semicirular curves meaning the layer was capacitive, the curves recovered for the spinel sample were straight lines only, suggesting the sample was a simple resistor. The total resistance was divided by 2 because there were two layers, and then the appropriate lead resistance as a function of temperature was subtracted to give the layer resistance. Below the resistance is graphed against temperature for heating and cooling.

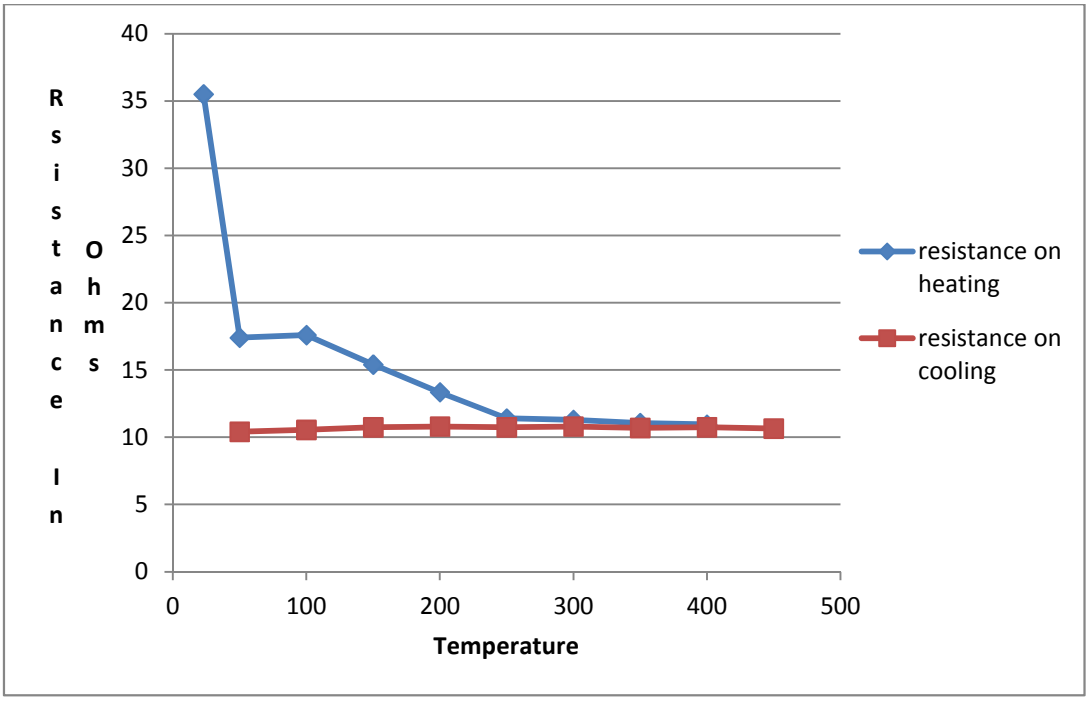

Fig.6.33 Resistance v.s temperature for cobalt coated SS430 heated in air

Similar to the Ti EIS results from Chapter 5, the curve for heating does not match the curve for cooling, however, resistance is not increasing suggesting the layer is not growing, and that about 10Ω can be reported for the resistance. High resistance at low temperatures on heating suggests poor contact at low temperatures, and a bedding in behaviour at higher temperatures. The temperatures and durations used for EIS are not expected to form many additional corrosion products.

6.7 CONCLUSIONS

The use of cobalt layers to slow the evaporation of chromium from SOFC interconnect steels and alloys has been well documented in the past, however, the simple evaporation technique has not been tried. Following on from Chapter 4 which showed that chromium cobalt spinels lost 1/4th the mass of chromium oxide at high temperature, it was shown that clear evidence is available of the spinel layer. Very thin layers were produced. Thicker layers were shown to spall off at modest temperatures. In support of the literature review, it is clear that cobalt can “fix” chromium and perhaps “get” chromium and manganese that are often evaporating from steels and then forming spinels at the triple phase boundary.

Not only is cobalt easier to deposit then titanium, but it is also better at fixing chromium than titanium, and the produced corrosion layers are much more conductive than the corresponding chromium titanium eskolaite layers.

1. Konysheva, E.P., H.; Wessel, E.; Mertens, J.; Seeling, U.; Singheiser, L.; Hilpert, K., Chromium Poisoning of Perovskite Cathodes by the ODS Alloy Cr5Fe1Y[sub 2]O[sub 3] and the High Chromium Ferritic Steel Crofer22APU. Journal of The Electrochemical Society, 2006. **153**(4): p. A765-A773.

2. Chou, Y.S.S., J. W.; Xia, G. G.; Yang, Z. G., Electrical stability of a novel sealing glass with (Mn,Co)-spinel coated Crofer22APU in a simulated SOFC dual environment. Journal of Power Sources, 2010. **195**(17): p. 5666-5673.

3. Copperthwaite, R.G.G., F. M.; Sangiorgio, T.; Hutchings, G. J., *Cobalt Chromium Oxide: A Novel Sulphur Tolerant Water-Gas Shift Catalyst.* Applied Catalysis, 1990. **63**(1): p. L11-L16.

4. Deng, X., *Cobalt plating of high temperature shainless steel inteconnects.* Journal Of Power Sources, 2005. **160**: p. 1225-1229.

5. Sedriks, A.J., *Corrosion of stainless steel, 2. edition*. Other Information: PBD: 1996. 1996. Medium: X; Size: [200] p.

6. Schutz, R.W.T., D E, *Corrosion of titanium and titanium alloys.* ASM Handbook, 1987. **13**: p. 669-706.

7. Hamilton Precision Metals, H.P., *Technical Data Sheet SS430*, Hamilton Precision Metals 1780 Rohrerstown Road, Lancaster, PA 17602

8. http://www.ameri-source.com/stainless_steel_strips/sssspecs.html. Available from: http://www.ameri-source.com/stainless_steel_strips/sssspecs.html.

7 CONCLUSIONS

7.1 CORROSION OF STEEL INTERCONNECTS

The problem in general with all steel interconnects will always be the same: in the absence of an inexpensive material that will always conduct and never corrode, and for the protection layer to grow, thermodynamics must dictate corrosion will occur. For the layer to stay thin, we hope kinetics will hamper growth beyond a certain layer thickness. The two mechanisms that control kinetics of corrosion are the transport of oxygen or ions and the transport of electrons or holes. The easiest mechanism to control is the flow of electrons, and most protective corrosion layers (Silicon, titanium, aluminium) are non conductive. For interconnects, this is not an option, leaving only chromium as the protective element that will migrate outward from the alloy and form at the air/oxide interface, instead of oxygen migrating in. This is also the only conductive corrosion layer that is further corrosion limiting. Unfortunately, for all SOFC with wet environments this then throws up chromium poisoning as a major problem. The only way to combat this and still have a chromium layer for conductivity on the steel is to react the chromium with something more stable at operating conditions than chromia.

7.2 EVAPORATION STUDY

Although there has been much study in the area of chromium retention of cobalt spinels for SOFC interconnect use as documented and referenced in chapter 6, there has been no direct study to compare the evaporate of chromium form the resultant barrier layers. The assumption that if a barrier layer can retain chromium then it will be a poor chromium transmitter seems a valid one. Unfortunately, due to surface area differences, this study was not directly comparable to the other chromium evaporation studies. However, this study now sets the ground work for further work in this area. Any other data regarding the retention of chromium at high temperatures with wet environments will be welcomed.

The major focus of this work has been on forming a corrosion layer with chromium and some additional single element layer to form a stable corrosion product layer. As such potential layer materials were tested and compared to chromia for chromium retention. From this work it was found that replacing 10% of the chromium with titanium significantly decreased the evaporation of chromium by about 62% at 1200^{o}C. This was calculated from data in fig.4.6.

Replacing 33% of the chromium with cobalt reduces the chromium loss to 74% the loss of chromium oxides alone again at 1200^{o}C. Other works have shown that this provides acceptable life spans for steel interconnects.

With titanium as a replacing element, because it is a doping of eskolaite, a range of titanium proportions can be used from very low to 30%. With cobalt, because the crystal structure is not a doped eskolaite but a true spinel, only fixed amounts of cobalt can be used. However, although fixed amounts of each element were tested in the evaporation study, it's still clear that there is plenty of room for more elements and different proportionalities in the spinel

structure. This is useful if varying amount of chromium, iron, and manganese will be emanating from the steel interconnect into the barrier layer.

As the characterization of coating layers in the area of chromium evaporation was a project goal from chapter 2 section 2.13, it can be seen that this was achieved.

7.3 CHROMIUM TITANATE PRODUCTION

CTO was found to reduce chromium evaporation, but proved very difficult to deposit onto SS430. It's possible that there is a sol-gel recipe that will deposit CTO directly onto SS430 and remain fully dense and perfectly bonded. Unfortunately a solution with such characteristics was not found in this study. Additionally a sol-gel to deposit just titanium oxide that remains fully dense was not found, although a sol-gel to deposit the anatase phase was found that bonded very well, but was not fully dense.

Had time and funding permitted, further characterization of this alcohol based titanium oxide sol-gel should have been performed for completeness. However, thermally converting elemental Ti to rutile and then doping this layer with Cr proved to be much more adherent and robust a system. Unfortunately characterization of this layer also proved very difficult due to the signal ratio of other products and the background steel. Characterization was much clearer at lower production temperatures.

The search for a CTO or Ti sol-gel that will bond to SS430 should not continue due to the nature of the layers density. previous work in this area did not discuss the density of these layers for gas analysis, as was discussed in chapter 5. Nec unless In addition, if a fully dense Ti sol-gel cannot be found, it's possible a single layer of Ti evaporated onto the surface of SS430 followed by the existing acidified anatase forming sol-gel could be the basis of a dense, but high surface area Ti coating as the basis for a reduction program to form a high surface area electrode for wet electrochemistry.

For corrosion layers on steel, without an entire PhD's worth of work to characterize changes in unit cell parameters for most possible combinations of Fe, Cr, and Ti, as rutiles and eskolaites, characterization will remain problematic.

7.4 TITANIUM EVAPORATION, RUTILE, ANATASE, AND REDUCED LAYERS

The discovery of dense rutile on SS430 at lowered temperatures came relatively late in the research. Had it been discovered earlier, the work would have taken a different direction, and reduction of these layers would likely have commenced earlier with more results of this work to report.

Although the application of titanium to SS430 surfaces may not be advantageous for interconnects at high temperature due to poor conductivity and poor higher temperature properties, there is room for further investigation of these materials at the lower temperature ranges. There may also be many other uses for thin film titanium in the areas of aerospace and automotive systems. A very thin layer of Ti can protect SS430 from further corrosion by

adding a passivation layer that otherwise would never exist. The system can be further manipulated in several ways.

Although it was a project goal to coat SS430 with titanium with a view to production of chromium titanate, this was not achieved. No difinitve evidence that chromium titanate was produced was found. Although many deposition techniques were tried, only evaporation proved successful. Although this may prove advantageous in other areas, for intermediate to high temperature solid oxide fuel cells, it can be shown that protection of the steel was not adequate for this service.

7.5 COBALT EVAPORATION AS A DEPOSITION TECHNIQUE

Very thin layers of cobalt were demonstrated to be evaporated onto SS430 using the evaporation technique. These layers appeared to be capable or capturing spinel forming elements, and forming spinels, underneath, in, and on top of the resultant oxide layer.

Thicker cobalt evaporation showed poor thermal expansion properties, with spalling at all temperatures and generally poor adhesion. However, Cobalt showed the best chromium retention, and was relatively easy to characterize due to the limited unit cell parameters for the chromium/ manganese/ cobalt spinel range. It was much easier to evaporate than titanium, and the operating temperature range was higher than that of Ti layers. It was also the easiest to characterize with electron microscopy. Further work should focus on the very thin layers that were transparent in SEM. This may be possible with different substrates, and TEM.

The electrical properties of the spinels were superior to those of the chromium titanium oxide layers that were deposited on SS430 from chapter 5.

It can be shown that as a project goal from section 2.13 of using deposition techniques developed for titanium with cobalt, although only evaporation as tried, it was quite successful.

7.6 FURTHER WORK

Not studied in this work but of particular interest are Ti/cobalt combinations. The rutile layer was so surprisingly adherent to the steel that it offers a potential layer as a sub layer for cobalt. This study showed that all layers of cobalt spinel spalled and peeled, and that thick layers cracked off in sheets. A potential solution to this could be a combination of layers starting with a layer of Ti that is reacted to rutile, followed by a very thin layer of cobalt that would act as a getter for whatever chromium were to make it through the Ti layer. It is possible that a pre layer of TiO_2 delays the evaporation of chromium and manganese enough at lower temperatures that smaller amounts of both Ti and Co would be needed than otherwise would be used alone.

Another consideration would be additional work into reduction of rutiles in situ on SS430 for other electrochemical electrode products. Other substrates might be considered for this

work other than SS430, with the focus in inexpensive and easy to manipulate, and a reduced coating performing the role of functional layer.

For the evaporation studies the effect of manganese should be investigated in much more detail. Although manganese is a minor element in SS430, it is a major constituent of corrosion layers of SS430 according to EDS studies in this work. The evaporation study did not take into account small amounts of manganese in pellets in either Ti or Co chromium materials, however as there had been no comparison this is still a good place to start.